Powder Build-up in Detergent Packing Lines

by

Christopher David Hewitt

A thesis submitted to

The University of Birmingham

for the degree of

Engineering Doctorate

School of Chemical Engineering

University of Birmingham

23/01/2015

Abstract

Powder build-up is a fouling process in which a small fraction of a powder becomes a non-porous film adhered to a surface. Build-up within powder packing processes is a significant problem for the detergent industry, leading to equipment downtime for cleaning, drives tripping due to high torque and reduced powder quality. More specifically, build-up has a tendency to form in auger fillers where agglomerate particles undergo plastic deformation, leading to the formation of build-up on the internal surface of the tube within which the auger is housed.

To develop understanding regarding the process by which build-up is formed, a combination of macro scale auger filling experiments (with the auger/tube clearance maintained constant at 0.3 mm) and laboratory scale characterisation of the virgin powder has been undertaken. This involved a comparison of results obtained via uniaxial compaction followed by tablet diametric compressions, with the results of macro scale auger filler experiments. From this work it has been determined that the build-up forming powders have Kawakita b^{-1} parameters of 0.5 MPa or less, and form disc-shaped tablets with strengths below 0.5 MPa following compaction to 58 MPa.

This may result from powders containing agglomerates failing via plastic deformation, with the Kawakita b^{-1} parameter being related to the agglomerate particle's plastic yield stress [10]. Based on the work of Maugis and Pollock [31], it is proposed that the adhesive forces existing between agglomerate particles and the tube surface are a function of the agglomerate particle's plastic yield stress. The fact that build-up-forming powders have low tablet strengths may result from the constituent agglomerate particles being formed from soft plastic materials, which agglomerate into tablets which are also soft and plastic. It seems probable that the cohesive forces within the tablets formed by build-up-forming powders are a function of their ability to undergo plastic deformation, with low yield stresses leading to low adhesive forces.

Based on the work of Crutchley and Bridgwater [29] and Calvert *et al.* [30], it is proposed that powder build-up forms as agglomerate particles pass through the clearance existing between the auger and the tube wall. They then experience large MPa scale stresses which are functions of the ratio of the powder's particle size (quantified via the D_{90} measured via gravimetric sieving) and the magnitude of the auger/tube clearance C. To confirm this hypothesis experiments have been performed using an auger filler, varying clearances between 0.3 and 10.0 mm. This showed that build-up formation did not occur once C/D_{90} was greater than 3.5.

This thesis is dedicated to my wife and parents

“Time is the school in which we learn.”

Delmore Schwartz, “Calmly We Walk Through This April’s Day”

Acknowledgements

I would like to thank my supervisors Andrew Ingram and David Smith, who have supported me through the course of this project with both the experimental work and the organisation of two Institution of Chemical Engineers (IChemE) Particle Technology Subject Interest Group (PTSIG) meetings. Andrew consistently challenged my ideas and encouraged me to consider each item of work in sufficient detail, while David encouraged me to consider the real world implication of my findings, converting academic learnings into real work cost savings for industry.

I would like to thank Richard Greenwood, Mark Ridyard, Andrew Patton, Andrew Dorset, Mojtaba Ghadiri, Hossein Ahmadian, Graham Calvert and Charley Wu for their periodic reviews of my work, giving some longer term perspective to the project and keep us on track to complete the project within the time allotted and to the required standard. I would like to thank Richard in particular for nominating me to edit an editorial for The Chemical Engineer magazine titled “The IChemE’s Secret Formulation Engineers”, discussing formulation engineering and the need for greater levels of research in this area.

I would like to extend special thanks to Procter and Gamble (P&G) and the Engineering and Physical Sciences Research Council (EPSRC) for funding the expenses associated with travel undertaken as part of this project visiting P&G plants in London, China, the USA, Egypt, Saudi Arabia, and Spain, as well as conferences in China, Germany, Switzerland, Glasgow, Leeds and Birmingham. I would also like to acknowledge All-Fill International Ltd. and Mateer Burt Co. Inc. who have kindly supplied some of the figures within this thesis.

Finally I would like to thank my wife and parents and friends for their continuing support throughout the course of this project.

Contents

List of Figures

List of Tables

Nomenclature

Roman Symbols:

Symbol	Definition	SI Units
a	Kawakita parameter	
A	Heckel parameter	
A’	Cross section area of a column fracture plane	m^2
A*	Total cross sectional area of fracture planes	m^2
A_0	Bed cross sectional area	m^2
AR_t	Tablet aspect ratio	
b	Kawakita parameter	Pa^{-1}
B	Relative density	
C_x	Auger/Tube clearance, when present subscripts are the magnitude of the clearance in millimeters	m
D_{90c}	Count based D_{90} particle size	
D_{90m}	Mass based D_{90} particle size	
De	Deformation number	
DF	Dimensionless force	
D_t	Tablet diameter	m
e	Porosity	
E*	Defined by Eq. (2-38)	
e_0	Initial porosity at σ = 0	
E_i	Young’s modulus for particle i	Pa
e_{min}	Minimum porosity	
eRH	Equilibrium relative humidity	
F	Failure force of a column	N
F*	Total force	N
$f_{0.5}$	The number of fills at which the last auger torque reading of 0.5 Nm was recorded	
$f_{1.0}$	The number of fills corresponding to first auger torque reading of 1.0 Nm	
$F_{90\ Rollers}$	The 90^{th} percentile force from the roller simulation	N
$F_{90\ Shear\ cell}$	The 90^{th} percentile force from the shear cell simulations	N
F_a	Applied force	N
F_b	The adherence/pull off force relevant to a brittle separation	N
F_d	The adherence/pull off force relevant to a ductile separation	N
F_m	The adherence/pull off force relevant to a separation without reduction of the final contact area or ductile failure of the contact	N
F_t	Tablet breaking force	N
F_{vdW}	van der Waals force	N
H	Plastic hardness	N
h	Powder bed height	m
h_i	Initial powder bed height	m
h_s	Separation distance	m
h_σ	Powder bed height at a given value of σ	m
K	Heckel parameter	Pa^{-1}
K’	Defined by Eq. (2-35)	
K’’	Defined by Eq. (2-43)	Pa^{-1}
k_1 k_2 & k_3	Proportionality constants	
k_{Hi}	Defined by Eq. (2-31) and Eq. (2-32)	Pa^{-1}
M	Hamaker constant	J

n	Number of columns	
P	Applied load	N
p_l	Density of the liquid binder	kg m^{-3}
P_l	Effective applied load including surface forces	N
p_m	Mean pressure	Pa
p_{pl}	The plastic yield pressure of a sphere	Pa
P_{vdW}	van der Waals pressure	Pa
P_y	Mean yield pressure	Pa
P_{Y1}	K^{-1} at low stain rate	Pa
P_{Y2}	K^{-1} at high stain rate	Pa
r	Contact radius	m
r_0	Contact radius in the absence of an applied load	m
r_c	The reduced value of contact area prior to brittle failure of a contact	m^2
r_f	Final contact area	m^2
R_i	Radius for particle i	M
s_{max}	Maximum saturation number	
SRS	Strain rate sensitivity	
t	Tablet thickness	m
U_c	Impact velocity	m s^{-1}
w	The ratio of liquid to solid on a mass basis	
x	Spinner plate gap	
y	Horizontal distance from tube wall to edge of spinner plate	
Y	Yield Strength	N
Y_g	Dynamic yield stress	Pa
x	Contact zone diameter	m

Greek symbols:

Symbol	Definition	SI Units
α	Coefficient of friction	
α’	Apparent coefficient of friction	
$\alpha\sigma_l$	Frictional stress	Pa
$\gamma_{i,ii}$	The interfacial energy acting between particle i and particle ii	
γ_i	The surface energies of particle i	
ε	Strain	
ε_N	Natural strain	
ϑ_i	Poisson ratio for particle i	
θ	Angle of repose	
λ	The ratio of adherence to the applied load	
μ	Dimensionless parameter indicating the extent to which forces outside the contact area influence adhesive forces	
ρ_g	Granule density	kg m^{-3}
ρ_s	Density of the solid particles	kg m^{-3}
σ	Stress	Pa
σ_0	Yield strength	Pa
σ_l	Lateral compressive stress	
σ_r	Single particle failure stress	Pa
τ	Shear failure stress	Pa
τ_0	Cohesive strength	Pa
τ_0'	Apparent strength of single particles	Pa

ω_A	Thermodynamic work of adhesion	J m^{-2}
x	Contact zone diameter	m
$\mathrm{h}\omega$	Lifshitz–van der Waals constants	J

1. Introduction

1.1 Introduction

This thesis will focus on build-up or fouling of laundry detergent powders in packing machines and has been undertaken as an Engineering Doctorate (EngD) in Formulation Engineering at the School of Chemical Engineering, University of Birmingham with Procter and Gamble (P&G) as the industrial sponsor. Build-up is a thin film of smeared material found on equipment surfaces formed from only a small fraction of the powder flowing through an item of process equipment. Build-up is typically found in items of process equipment where high levels of shear are present, such as auger fillers, carton rotary fillers, loss in weight screw feeders, rotary valves *etc.*

Figure 1-1 shows a Scanning Electron Microscope (SEM) image of a sample of build-up taken from a rotary carton filler. These fillers utilise a series of flasks to volumetrically measure a quantity of powder, with powder entering these flasks under the influence of a scraper. It is hypothesised that particles experience high stresses as they pass through the small clearance which exists at the fillers scraper, however, definitive evidence for this hypothesis is currently lacking. In terms of the powder formulation P&G have found that build-up typically contains significantly more surfactant than the powder passing through the filler and as can be seen in Figure 1-1 the build-up is coherent and non-porous suggesting plastic deformation is required for its formation. Also P&G have found that build-up tends to form more rapidly when powder formulations have high levels of surfactant within them.

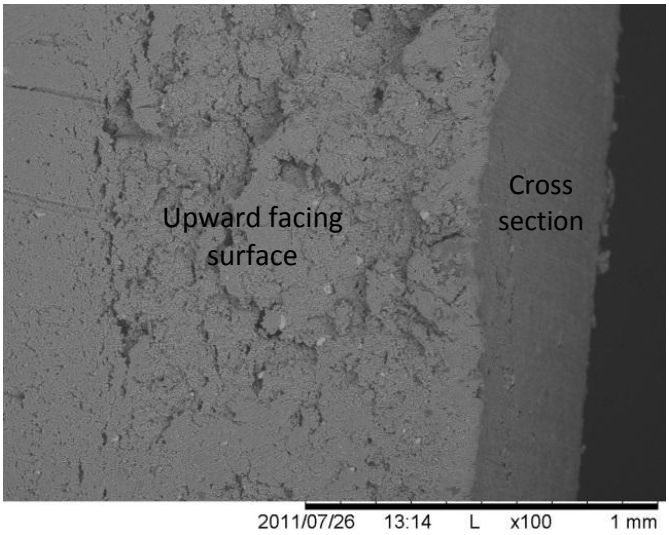

Figure 1-1: SEM image of build-up taken from a carton rotary filler.

1.2 Laundry Detergents

Laundry detergents are products containing surfactants and other ingredients which are used to wash fabrics. Laundry detergents are available in many physical forms such as powders, liquids as well as unit dose forms such as tablets and liquitabs (liquid encased in a soluble membrane), however, the focus of this thesis will be laundry detergent powders [1].

Laundry detergent powders are complex materials typically made via the manufacturing process described in Figure 1-2. The process starts with slurry being formed which contains three phases: undissolved inorganic particles, an organic liquid phase (surfactants and polymers) and an aqueous phase containing water and dissolved inorganic particles [2]. This slurry is then spray dried and then blended with various solid granular materials such as sodium carbonate, sodium percarbonate, sodium sulphate, coloured beads, encapsulated enzymes, anti-foaming powders, polymers which release stains, polymers that prevent new stains etc. Liquids not suited to spray drying due to their high volatility and/or flammability, are then sprayed onto the powder in a continuous mixer.

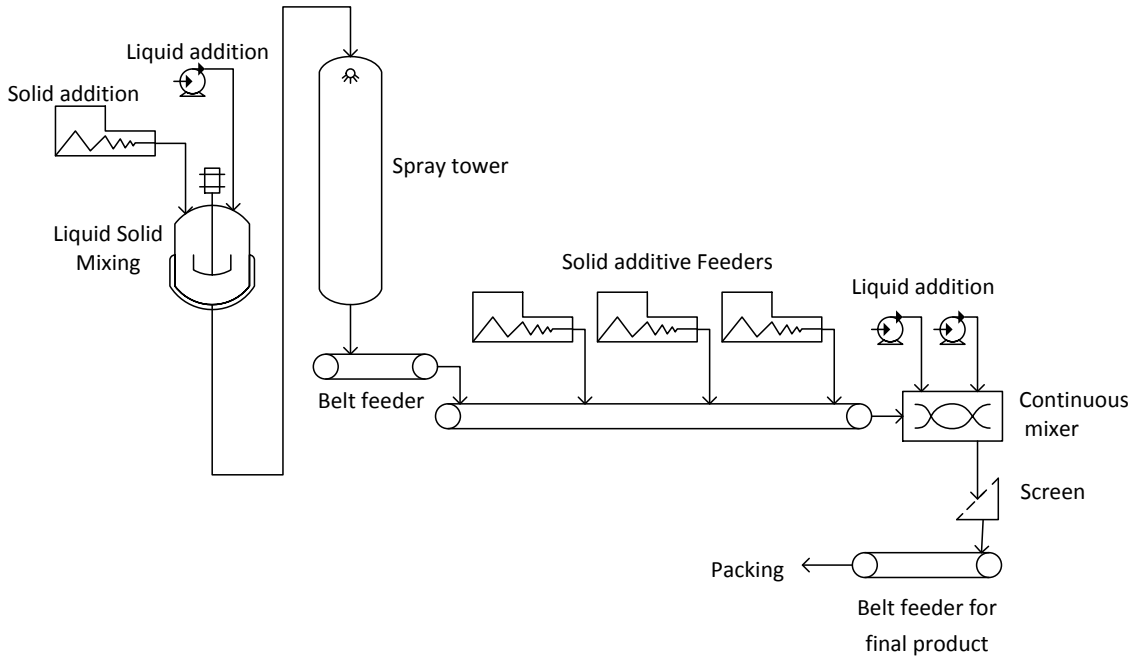

Figure 1-2: Typical Production Process for Laundry Detergent Powder [3].

1.3 Packing

Once all the solid and liquid components have been blended, the finished powder product is transferred to storage bins, before being transferred to a pack machine. These machines transfer a given mass of powder (30 g to 10 kg) into either flexible bags or boxes. In many cases and particularly in the case of small (<500 g) flexible bags auger fillers are used. These packing machines often have significant issues with powder build-up and because of this they will be the focus of this thesis.

1.3.1 Auger fillers

Auger fillers are volumetric powder packing machines used by the detergent, food, and pharmaceutical industries to fill powders into various types of packaging *e.g.* bags, boxes, tubes *etc.* They operate by turning a vertically mounted auger through a number of revolutions at a given speed (see Figure 1-3). As the auger turns powder is fed into the auger from a hopper

and is then conveyed through the auger. Powder then passes through the clearance between the spinner plate and the funnel and then leaves the spinner plate under the influence of centrifugal force. The powder then falls though a collector funnel designed to channel the powder into the relevant receptacle.

When operating an auger filler the following parameters have to be considered:

I. Auger revolutions per fill

II. Auger rotational speed

III. Spinner plate/tube clearance

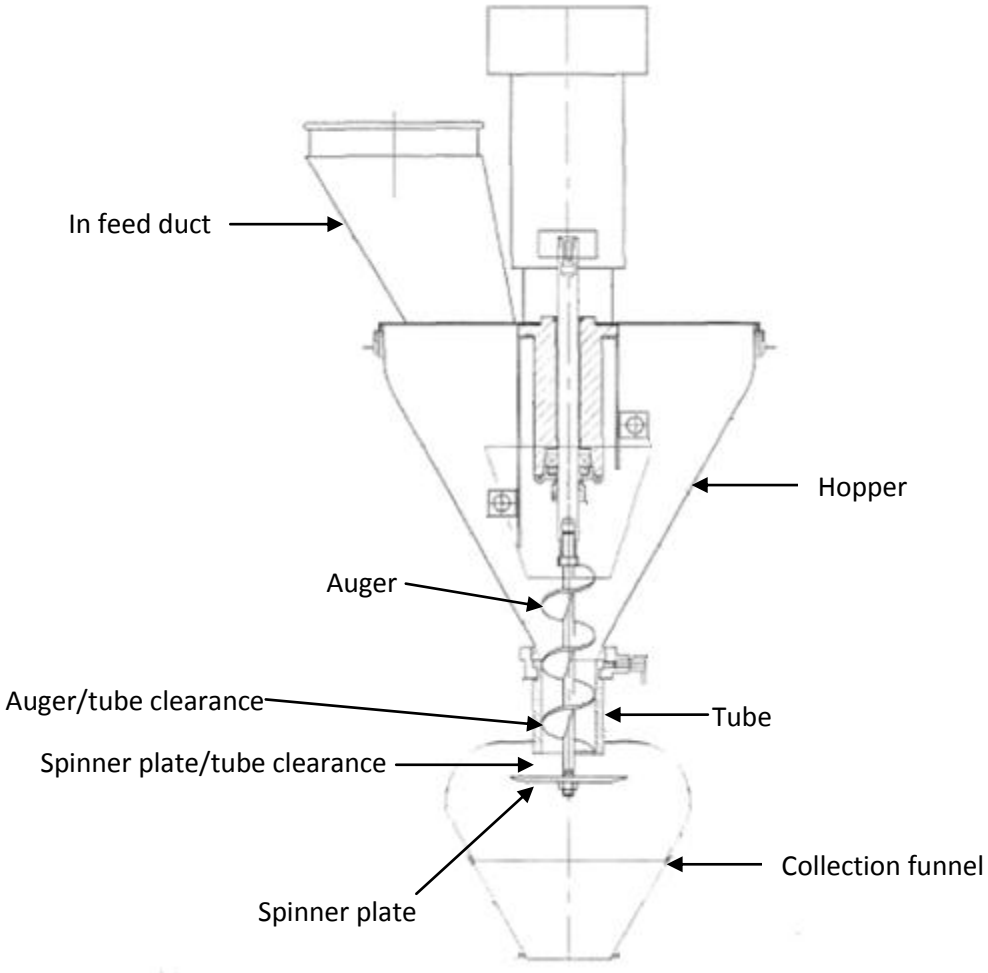

Figure 1-3: Mateer Burt Co. Inc. Bespoke P&G 1900 Series Auger Filler [4].

I. Auger revolutions per fill

The mass of material transferred is expected to increase linearly with the rotation of the auger. This is because the auger is known to be a positive displacement device similar to a loss in weight screw feeder. The number of revolutions will therefore be used to control the filled weight either via operators weighing packs and manually modifying auger revolutions to achieve a target pack weight or via a control loop, where a check weigher automatically weighs every pack and feeds back to the auger filler to modify revolutions accordingly. Auger revolutions per fill are a key factor in determining the accuracy of filling: auger filler vendors typically advise that fillers should operate at a minimum of three revolutions per fill and augers should be sized to allow this.

II. Auger rotational speed

The speed at which the auger turns is an important factor which dictates the rate at which the auger filler operates, typically running at higher rotational speed would allow for a higher packing rate. However in cases where auger fillers are of a clutch break design, wear on the breaking system can lead to significant errors in the position at which the auger is stopped and thus the number of revolutions achieved. In this case increasing rotation speed of the auger can act to reduce packing accuracy and thus a balanced approach of packing accuracy vs. packing rate must be taken.

III. Spinner plate / tube clearance

Because the auger filler stops between fills it is essential that powder stops flowing between fills and yet allows powder to flow when the auger and spinner plate are rotating. As can be seen in Figure 1-4 this is achieved via the use of the spinner plate and adjustments to the spinner plate gap.

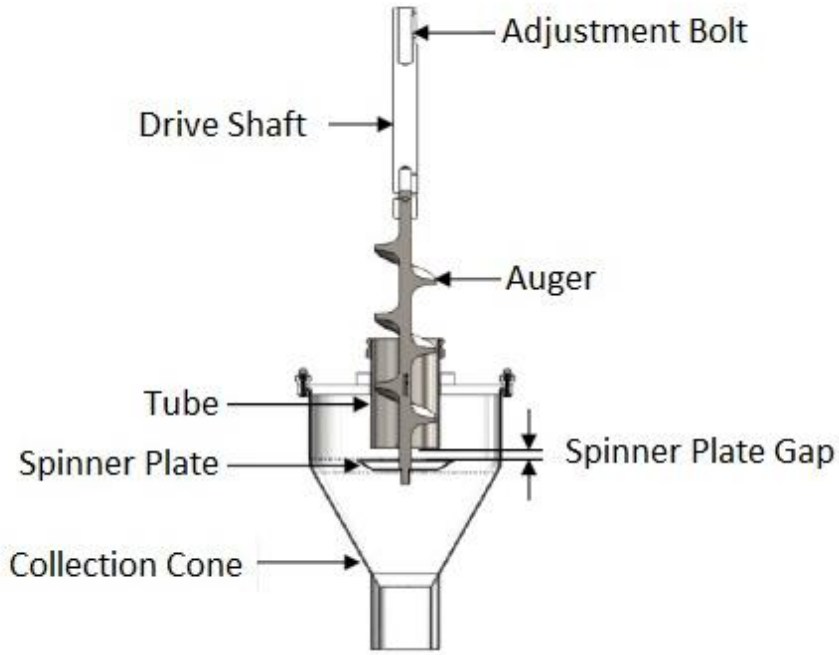

Figure 1-4: Schematic of ALLFILL auger filler tooling [5].

The spinner plate utilises a powder's internal friction to hold powder within the auger, while the auger is stationary. Figure 1-6 shows a right angle triangle extracted from Figure 1-5 showing the relationship between powder angle of repose θ, spinner plate gap x and spinner plate size y. For a powder to cease flowing while the auger is stationary this triangle must be formed allowing the powder's internal friction to ceases flow while the auger is stationary. If a powder does not cease flowing when the auger is stationary either reducing the spinner plate gap or installing a larger diameter spinner plate i.e. increasing y or reducing x, will enable this to occur (as defined by Figure 1-6). Modification to the spinner plate gap must always be performed with caution as small gap sizes can lead to bulk powder jamming events and in case of plastic powders compaction of the material within the auger leading to the formation of a dense solid mass no longer able to undergo flow.

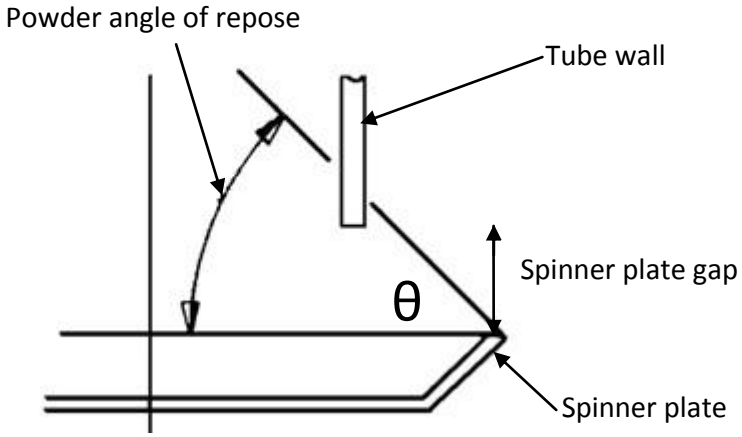

Figure 1-5: Powder sitting on spinner plate while stationary [5].

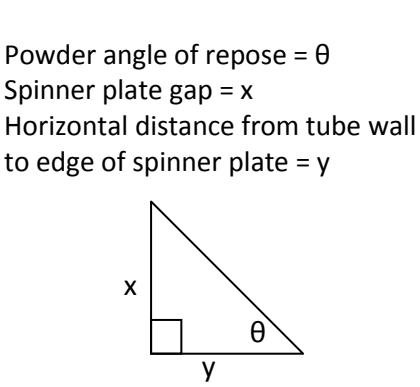

Figure 1-6: Right angle triangle extracted from Figure 1-5.

To further illustrate the relationship between x, y and θ Figure 1-7 shows three spinner plate gap settings. The smallest gap setting labelled 'good' gives the greatest resistance to powder flow and thus the powder's transition to a non-flowing state is more rapidly and consistently achieved while allowing powder to flow while the auger rotates.

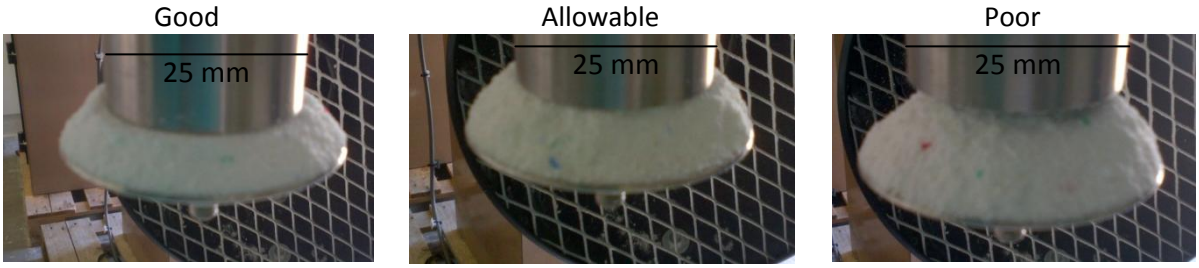

Figure 1-7: Three spinner plate gap settings.

Angle of repose is known to be a measure of a powder's ability to flow, with powders having high angles of repose exhibiting poor flowability [6]. Auger fillers containing the tooling shown in Figure 1-4 are designed to work with free flowing powders [5] with angles of repose below approximately 45^{o} [6].

1.3.2 Powder Build-up in Auger Fillers

Auger filler build-up is a fouling process involving the transformation of solid discrete particles to a coherent non-porous smeared film adhered to the tube. The formation of build-up can be thought of as a form of pressure agglomeration process involving the amalgamation of solid particles into a continuous and coherent solid mass. The compact disc (CD) accompanying this thesis contains two videos showing build-up observed in a pilot plant auger filler and a manufacturing plant auger filler. Figure 1-8 shows build-up on tube surfaces in a number of pilot plant and manufacturing plants. In all cases build-up forms a film covering the internal surface of the tube and then in most cases begins to drop out of the auger.

In a manufacturing plant the potential consequences of this are:

I. The need to clean the auger filler to remove build-up.
II. Unplanned downtime due to equipment break downs and trips.
III. Reduced packing accuracy leading to compensatory overfill and associated costs due to reduced efficiency.
IV. A reduced packing rate due to build-up consuming the cross sectional area available for powder flow. If the rate is reduced by 10 % the consequence of this may be the need to install 10 % more packing lines which would require significant capital funding.
V. Reduced powder quality due to the presence of build-up in finished product, potentially this could lead to a 10 g lump of build-up being shipped in a small 55 g pack. Clearly this would negatively impact consumer experience as they inspect and make use of the laundry detergent and thus this is highly undesirable.

In some cases issues arising from auger filler build-up can lead to the need to shut down for cleaning at intervals of as little as 30 minutes [7], which is unlikely to be judged as acceptable given the large reduction in plant capacity this would lead to.

This formation of build-up in auger fillers is believed to originate from two main concerns; packing accuracy and packing rate. To facilitate these requirements auger filler manufacturers typically design fillers to rotate rapidly at high speeds (100 to 1000 RPM) with small auger/tube clearances (0.1 to 3.0 mm) similar in magnitude to the detergent particle size. It seems likely that this situation will lead to the generation of large stresses between the auger and the tube wall potentially leading to the formation of build-up. This perhaps explains why build-up will tend to grow to consume the clearance between the auger and the tube, but the remaining powder will tend to remain flowing due to it not passing through this clearance and thus not being exposed to the high stresses which exist with it. Also the non-porous coherent nature of the build-up suggests that these forces are similar in scale to those found in granulation processes such as roller compaction and tableting. However it should be noted that evidence is currently lacking for these concerns and an initial goal for this thesis is to determine if in fact varying these parameters has any appreciable effect upon build-up formation.

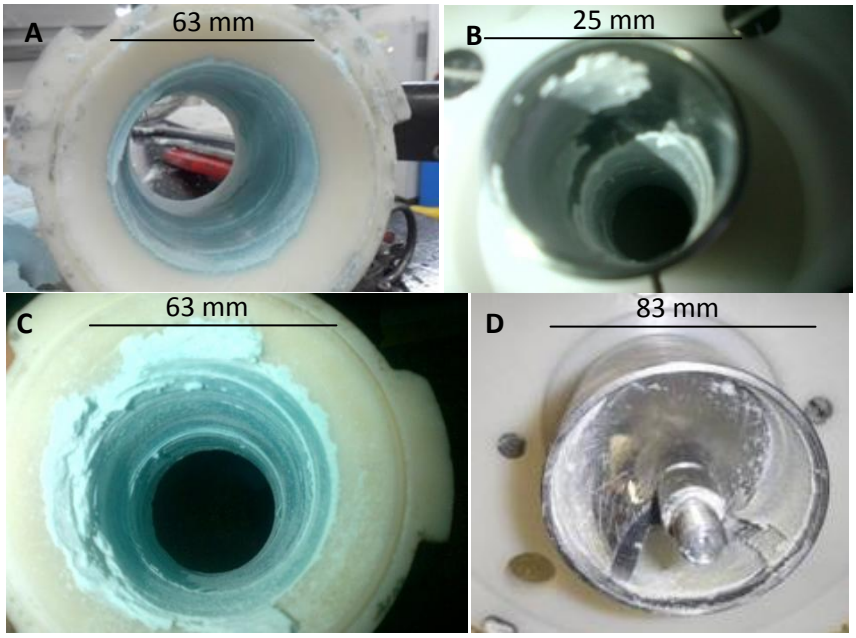

Figure 1-8: Auger filler tube wall Build-up (A and C; build-up in a manufacturing plant auger filler, B; build-up in a R&D auger filler packing powder for consumer testing, D; build-up during the experimental packing of a detergent raw material).

1.4 Trends in Laundry Detergent Formulation and their Impact on Powder Build-up

In the detergent industry and the consumer goods industry in general there is a drive towards compacting products and concentrating ingredients to reduce the manufacturing, packaging and transportation costs. This is generally achieved by concentrating active ingredients and removing components present only as fillers and/or processing aids. In the detergent powder industry this leads to powder formulations becoming higher in surfactant. This then leads to powders becoming comprised of low yield stress secondary particles susceptible to issues such as build-up formation [8].

1.5 Business case

The build-up of powders within powder handling processes is a significant problem for industry both in auger fillers and in other similar situations such as rotary valves, screw conveyors and the scrapers found in rotary carton packing machines. The formation of build-up often leads to equipment downtime for cleaning, drives tripping and reduced powder quality due to the presence of unwanted agglomerated lumps of powder. In some cases these issues can become so severe that it is not economically feasible to operate a given item of equipment with a given powder formulation. This then means that modifications have to be made to a powder formulation which can have cost implications and potentially limit the level at which a given component of the formation can be added. In the absence of reliable solutions to auger filler build-up formation this can have severe implications for P&G as projects may be delayed or scrapped, and the consumers perception of the product's performance can be negatively impacted potentially resulting in reduced sales.

The importance of powder build-up in powder handling is illustrated by the attention paid to it by equipment vendors. For example rotary value vendors such as Rota Val Ltd. offer scrapers

and a variety of polished surface finishes which they claim act to reduce the formation of build-up or allow for the operation in the presence of build-up [9]. However they offer no clear scientific reasoning for why this may or may not work, for example why will the scraper remove build-up while the vanes of a rotary valve will form it?

Currently there is no clear methodology available to predict the build-up of powders and decisions regarding the correct equipment configuration to purchase are made on the basis of engineering judgment and experience. Figure 1-9 serves to illustrate this point. A rotary valve was installed into an existing packing line, a vane was fitted with a 'saw tooth' scraper and the casing was mirror polished. However even with these measures in place build-up did form leading to a need to clean the valve every four hours. The soft plastic nature of the build-up meant that the saw tooth design of the scraper served only to form ridges in the build-up and did not effectively remove it. Presumably this saw tooth design is intended to bring about fracture of build-up facilitating its removal, however the presence of the ridges in Figure 1-9 suggest that in this case the scraper brought about plastic deformation which served only to allow the valve to run without tripping, but with very high levels of audible noise.

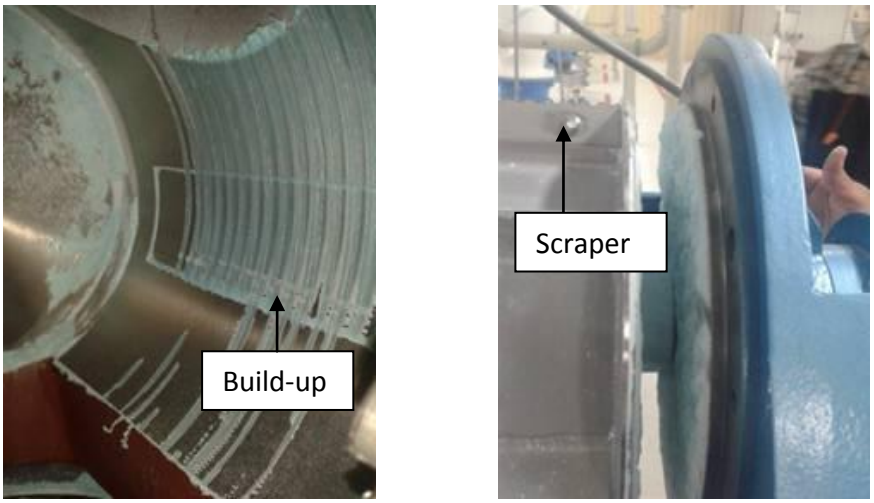

Figure 1-9: Rotary valve build-up and scraper.

In the case of the detergent industry this problem is made more complex as detergent formulations change frequently meaning that an item of equipment may be required to process many tens of different formulations during its life time. This leads to the need for a reliable means of predicting issues relating to powder build-up.

Currently assessments are typically made via running large scale trials which by their nature are expensive due to the volumes of raw material involved, the disruption to on-going manufacture and the travel costs for the individuals involved. Also large scale trials are essentially one-off experiments and it is often difficult to say definitively if the phenomena observed during a trial will be seen consistently during the detergent formulation's on-going manufacture.

For these reasons it is highly desirable to have a methodology which can be used to predict build-up based on laboratory scale measurements, avoiding the costs involved in large scale trials and allowing formulations to move more rapidly into full scale production.

1.6 Objectives

The objectives of this investigation were to develop:

I. Macro scale / pilot plant test methods which enable the tracking of build-up generation with time.
II. A means of predicting auger filler build-up based upon the properties of the powder flowing through the auger which is of practical use to industry.
III. Understanding of processes which lead to build-up generation in auger fillers.
IV. Equipment modifications which can then be used to reduce or eliminate powder build-up.

1.7 Outline of Thesis

Chapter two – Literature Review: In this chapter due to the lack of pre-existing literature specifically discussing build-up literature from other related fields such as tableting, uniaxial compaction and particle adhesion will be reviewed. Information within said literature will then be used to construct a hypothesis for the potential mechanisms by which build-up may form which will then give direction to the experimental investigation to follow.

Chapter three – Experimental methods and Materials: In this chapter the key experimental methods used within the thesis will be introduced giving details of the equipment used in the generation of the results presented in this thesis. The justification for the selection of each technique is discussed, with reasons given for the specific design of each method. In last section of this chapter the materials to be used in experimental investigations are discussed giving some background regarding the manufacturing processes used to produce them

Chapter four – Material Characterisation: In this chapter of the thesis, the mechanical properties of materials used in detergent formulations will be characterised via uniaxial compaction experiments.

Chapter five - Initial Experimental Investigation: In this chapter of the thesis the results of an initial experimental investigation will be discussed. This involved the testing of two powders at pilot plant scale using an auger filler and the manipulation of parameters within the auger to determine their impact on build-up formation. The results of this investigation will be used to firstly confirm the hypothesis from the end of Chapter two and to inform the experimental investigation to follow in Chapters 6, 7 and 8.

Chapter six - Linking Macro and Laboratory Scale Measurements to Develop an Auger Filler Build-up Operating Space Model: In this chapter the macro/pilot plant scale test method for

tracking build-up formation with time will be developed and its repeatability will be studied. This method will then be used to compare the behaviour of powders in the auger to laboratory scale measurements and thus provide the ability to predict the formation of build-up laboratory scale measurements.

Chapter seven - Development of an Operating Space Model for Screw Tester Build-up: In this chapter of thesis a Screw Tester will be used to determine if the approach to predicting auger filler build-up can be reapplied to other similar devices such as the Screw Tester. In addition to this the uniaxial method used in Chapter six will be subjected to additional scrutiny in order to determine the impact of phenomena such as die filling effects and initial powder bed aspect ratio.

Chapter eight – The Influence of auger/Tuber Clearance and Particle Size on auger Filler Build-up: In this chapter an experimental investigation will be discussed which focused upon determining the impacts of particle size and auger/tube clearance on auger filler build-up formation. The results of this investigation will be used to determine if it is possible to propose equipment modifications which would enable a reduction or elimination of build-up formation within the auger filler.

Chapter nine - Industrial Case Studies: In this chapter of the thesis a series of case studies will be discussed which illustrate the impact this EngD project has upon P&G's laundry detergent business.

Chapter ten - Conclusions: In this chapter the key conclusion from the preceding chapters will be pulled together and summarised. Also the degree to which the objectives laid out in section 1.6 have been achieved will be determined.

1.8 Publications Arising from this Work

- **Poster** C.Hewitt, D.Smith, M.Ridyard, A.Ingram, C.Y.Wu, Laundry Detergent Powder Build-up in Auger Fillers, 5th International Granulation Workshop, June 2011, Lausanne, Switzerland
- **Poster** C.Hewitt, D.Smith, M.Ridyard, A.Ingram, C.Y.Wu, Build-up of powders in auger fillers. 11 UK Particle Technology Forum University of Loughborough, April 2012, Loughborough, UK.
- **Oral presentation** C.Hewitt, D.Smith, M.Ridyard, A.Ingram, C.Y.Wu, Build-up of Powders in Auger Fillers, CHoPS 2012 7th International Conference for Conveying and Handling of Particulate Solids (CHoPS), September 2012, Friedrichshafen, Germany.
- **Oral presentation** C.Hewitt, D.Smith, M.Ridyard, A.Ingram, C.Y.Wu, Build-up of Powders in Auger Fillers, Powder fouling: Measuring, predicting and understanding reliability in powder handling, November 2012, Birmingham, UK
- **Editorial** C.Hewitt, IChemE's Secret Formulation Engineers, March 2013.
- **Poster** C.Hewitt, M.Ridyard, D.Smith, C.Wu, R.Greenwood, A.Ingram, An Experimental Investigation of the Build-up of Powders in Auger Fillers, PARTEC - International Congress on Particle Technology, April 2013, Nuremberg, Germany.
- **Conference paper and oral presentation** C.Hewitt, D.Smith, A.Ingram, Build-up of Powders in Auger Fillers, 5th International Granulation Workshop, June 2013, Sheffield, UK.
- **Oral presentation** C.Hewitt, D.Smith, A.Ingram, Build-up of Powders in Auger Fillers, Measuring, Predicting and Understanding Product Quality in Particle Technology, September 2013, Newcastle, UK.

- **Oral presentation** C.Hewitt, D.Smith, A.Ingram, Build-up of Powders in Auger Fillers, 7th World Congress on Particle Technology, May 2014, Beijing, UK.
- **Journal paper** C.Hewitt, M.Ridyard, D.Smith, C.Y.Wu, R.Greenwood, A.Ingram, An Experimental Investigation of the Build-up of Powders in Auger Fillers (in preparation).
- **Journal paper** C.Hewitt, M.Ridyard, D.Smith, C.Y.Wu, R.Greenwood, A.Ingram, An Experimental Investigation of the Effect of Equipment Geometry on the Build-up of Powders (in preparation).

2. Literature Review

In this chapter literature relating to the build-up of powders in auger fillers will be reviewed. As there is a lack of literature discussing auger filler build-up, the review will focus on literature from related fields such as tableting, uniaxial compaction and particle adhesion. The review will then be used to construct a hypothesis for the mechanisms by which build-up is formed.

2.1 Introduction

As discussed in section 1.3.2 the build-up of powders within powder handling processes has received little attention in the literature which has led to unreliable empirical approaches to solutions implemented by industry. However, literature has been published in other areas which can be used in conjunction with empirical observations as a starting point to gain a better understanding of the mechanisms by which build-up is generated. For example it is known that build-up is both coherent and non-porous and thus it is clear that some plastic deformation of particles is required for build-up to form. Also we know that build-up remains in contact with the tube surface in the absence of an externally applied load and thus adhesive forces must exist between the build-up and the tube surface. Additionally it is known that the clearance between the auger and tube is comparable to the size of the particles which form build-up and thus literature relating the particle attrition in small clearances is potentially also relevant.

2.2 Uniaxial Compaction

To gain understanding of the tendency of particles to undergo plastic deformation under the influence of forces experienced within the auger filler it is proposed that measurements of particle plastic yield stress is required. The measurement of particle yield stress can be achieved via the compression of single particles. However as was stated by Adams and McKeown [10], powders often comprise particles with a wide distribution of mechanical properties which leads to the need to compress a large number of particles in order to gain a statistically relevant

result. To enable the generation of results within a shorter time frame, an alternative technique is required. Generally the method by which this is achieved is uniaxial confined compaction of a bulk powder. This involves confining a powder bed within a cylindrical cell and then measuring the force applied to the top surface of the bed, as a function of punch displacement. A lumped parameter model is then typically applied to the experimental data to enable the extraction of parameters informative of the particles failure stress.

A key disadvantage of uniaxial compaction versus single particle compressions is that it is often not possible to definitively determine the failure mechanism. Because of this the parameters extracted are typically informative of a generalised failure stress and not specifically informative of parameters such as plastic yield stress. Additionally uniaxial compactions are performed with the bulk powder and thus it is possible that particle rearrangement, particle plastic deformation and particle fracture may occur and thus impact experimental results.

Denny [11] performed a review of the processes which take place during uniaxial compactions of granular materials:

- At low pressures particle rearrangement without deformation may occur, however, it is not clear to what extent this occurs. Nordstrom *et al.* [12] found via comparing tap density data with uniaxial compaction data that particle rearrangement is strongly influenced by mean particle size with fine powders undergoing more rearrangement than coarse powders. For the powder studied they found that a critical particle size of approximately 40 μm existed above which no significant rearrangement occurred.
- If particles are brittle, fracture will then occur, leading to an increase in density resulting from smaller particles occupying voids between larger particles. As the

applied force increases a critical particle size will be reached where a transition from compaction via fracture to compaction via plastic deformation will occur resulting from particle crushing strength increasing with reducing particle size [13].

- As pressures increase most powders ultimately undergo plastic deformation, which is considered to be the most common mechanism by which powders compaction [13].
- Ultimately plastic deformation will reach a maximum level where inter-particle porosity reaches a value close to zero. At this stage the compact acts as a single particle and volume reduction occurs primarily via elastic deformation. For hard materials compaction associated with this elastic deformation will be small compared to the associated plastic deformation. However, for softer materials significant levels of elastic deformation may occur.

The number of processes occurring during a uniaxial compaction experiment means that it is unlikely that any simple linear equation will be able to fit experimental data sufficiently well [11]. Furthermore in the case that an equation does fit the data the complex nature of the transformations may lead to the parameters being difficult to interpret. For example if compaction occurs via a mixture of plastic and elastic processes parameters derived may reflect both plastic and elastic deformation.

When performing uniaxial compaction experiments it is important to design the experiment considering the various mechanisms of compaction *i.e.* particle rearrangement, plastic and elastic deformation with reference to their consequential effect on experimental results:

- Die filling: when reporting results the method of die filling should always be stated particularly when working with fine powders, as it is known that in some

cases this can affect the initial bed height which features in many of models used to analyse uniaxial compaction data. Authors quote a variety of methods including simple pouring of powder [12] and pre-compaction via vibration [15] in order to minimise particle rearrangement during the early stages of compaction [11].

- Lubricants: some authors have made use of lubricants such as magnesium stearate in order to reduce the effect of wall friction [12]. Denny [11] commented that its use should be restricted to die walls to avoid impacting the particle's response to pressure.
- Particle size; particle size is known to have a significant effect upon particle yield stress and its measurement will always give context to results arising from uniaxial compaction experiments [11,13,14].
- Initial powder bed aspect ratio; many authors have studied the effect of varying aspect ratio by varying the mass of powder placed within the die, typically increasing the initial aspect ratio leads to particles appearing stronger due to the increasingly strong influence of friction at the die wall [10,11,14,15] (see Figure 2-1).

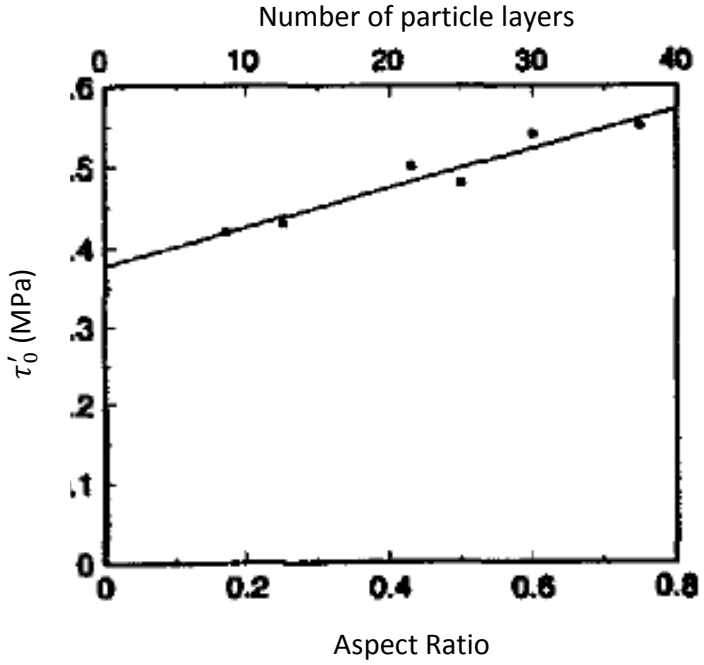

Figure 2-1: The apparent strength of agglomerate particles τ_0' as derived from uniaxial powder bed compaction data using Eq. (2-25) as a function of the initial aspect ratio of the powder bed, agglomerates are comprised of fine inorganic particles and a soft binder phase [10]

Atkins and Mai [13] stated that all solids will ultimately undergo brittle fracture when of sufficiently large size; also it is often difficult to comminute solids below a given size. These effects are known to be caused by changes in fracture stress with particle size whereas the plastic yield stress is independent of size for ideal homogeneous particles.

Samimi *et al.* [14] studied the effects of both particle size and aspect ratio on the uniaxial compaction of a soft plastic detergent powder; they found that particles showed a reduction in plastic yield strength with increasing particle size (see Figure 2-2). This contradicts Atkins and Mai [13] by showing that, for complex formulated materials, it cannot be assumed that plastic yield stress will remain constant with particle size variations. Samimi *et al.* [14] went on to show that aspect ratio effects reduced as particles became larger, with the largest particle studied (1.70 to 2.00 mm) showing no clear dependency of aspect ratio (see Figure 2-2).

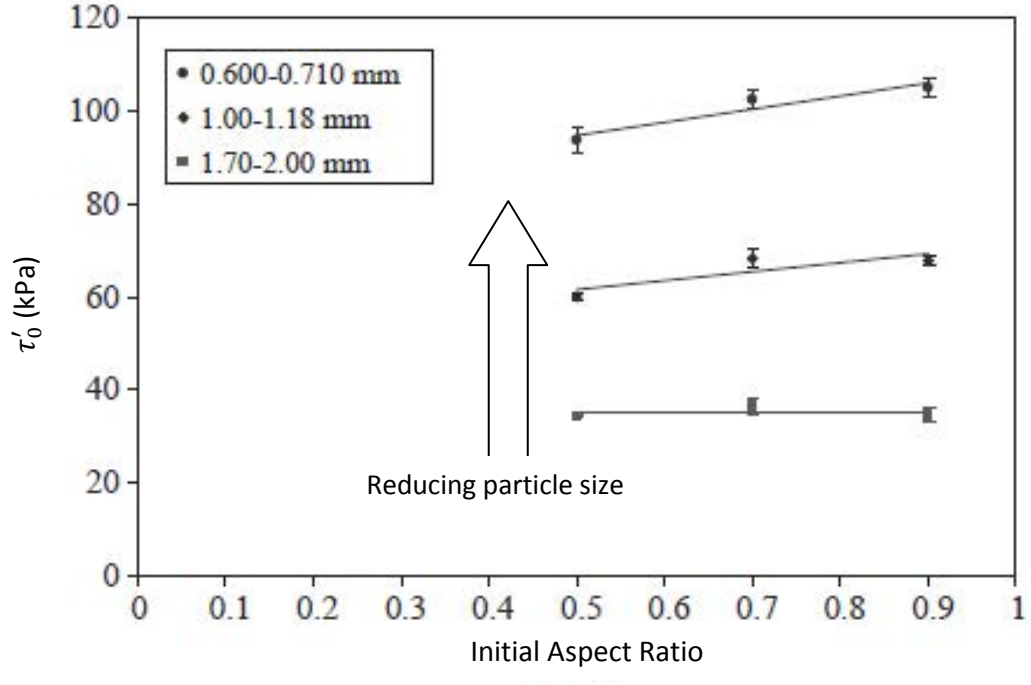

Figure 2-2: The apparent strength of single agglomerate particles τ_0' as derived from uniaxial powder bed compaction data using Eq. (2-25). Plotted as a function of the initial powder bed aspect ratio for beds comprised of size fractions of soft detergent based granules [14]

Also it should be noted that many authors have studied aspect ratio effects, however, this is typically achieved via altering the fill level with the compaction die. Evidence is currently lacking to show that the same behaviour would be observed if die diameter were varied and thus this should not be assumed to be the case.

2.3 Methods for Uniaxial Compaction Data Analysis

Uniaxial compaction testing of confined powder beds provides force displacement data, which is useful in determining the relative compactability of two powders. However, it is generally convenient to process this data in a manner which will yield a linear plot, making comparisons easier and allowing for the extraction of numeric parameters informative of specific powder properties such as plastic yield stress [11]. In the time since Walker [16] first obtained accurate compaction data, a large number of methods have been proposed for the analysis of uniaxial compaction data, however, the models proposed by Heckel [17], Kawakita and Ludde [18] and Adams *et al.* [19] have come to dominate.

2.3.1 The Heckel model

The Heckel model Eq. (2-3) relates the porosity of the powder bed to the applied pressure with the reciprocal of the K constant being termed the Heckel parameter. Heckel [17] assumed that porosity $\boldsymbol{e}$ reduced with increasing applied stress σ according to a first order equation Eq. (2-1). If Eq. (2-1) is then integrated with $\boldsymbol{e}$ equal to $\boldsymbol{e_0}$ at σ = 0 we arrive at Eq. (2-2). If it is then defined that $B = (1 - e)$ and $ln\frac{1}{e_0} = A$, Eq. (2-2) can be rearranged to give Eq. (2-3).

$$-\frac{de}{d\sigma} = Ke \quad \textbf{(2-1)}$$

$$ln\frac{1}{e} = ln\frac{1}{e_0} + K\sigma \quad \textbf{(2-2)}$$

$$\ln\frac{1}{1-B} = A + K\sigma \quad \textbf{(2-3)}$$

where: B is the bulk density relative to the absolute density (the fully compacted density when $e = 0$) i.e. B is equal to the solid fraction, σ is the applied stress, e is porosity and A and K are empirical constants with A being dimensionless and K having units of reciprocal stress.

Heckel [17] determined experimentally that K^{-1} was three times the yield strength of the individual particles σ_o (see Eq (2-4)). Roberts and Rowe [20] suggested that K^{-1} is related to the ability of the material to plastically deform and because of this the Heckel model could be utilized for materials which compact via plastic deformation. They also commented that as it is known that the mean yield pressure of a material is defined by Eq. (2-5), thus the reciprocal of the Heckel K parameter can be considered to be numerically equivalent to the mean yield pressure.

$$K = 1/(3\,\sigma_o) \quad \textbf{(2-4)}$$

$$P_y = 3\sigma_o \quad \textbf{(2-5)}$$

where σ_o is yield strength and P_y is mean yield pressure with both parameters having units of pressure.

Denny [11] commented that experimental data is often non-linear and not always a good fit to the Heckel model across a wide range of pressures. Denny suggested that this may be due to

the Heckel equation assuming that yield stress is constant with pressure which may not be the case since as axial pressure increases, increasing lateral forces will be transmitted to particles from their neighbours which may act in a confined bed to increase a particle's yield stress. This implies that particles which yield later in the compaction will yield at higher levels of stress. These comments are yet to be substantiated by experimental evidence and other explanations for the curvature may also exist such as a transition from particle rearrangement and/or elastic deformation to plastic deformation.

2.3.2 The Kawakita model

Kawakita and Ludde [18] proposed Eq. (2-6) as an empirical model for powder compaction:

$$\frac{\sigma}{\varepsilon} = \frac{1}{ab} + \frac{\sigma}{a} \qquad \textbf{(2-6)}$$

where σ is the applied stress, ε is strain defined via Eq.(2-7) and 'a' and b are constants. Adams and McKeown [10] stated that in Eq.(2-6) the 'a' parameter is related to the voidage in the initial powder bed, while b is related to the strength of the individual particles within the compaction die and has units of reciprocal stress.

$$\varepsilon = \frac{h_i - h_\sigma}{h_i} \qquad \textbf{(2-7)}$$

where h_i is the initial bed height and h_σ is the bed height for a given value of σ.

For a granular material composed of an incompressible material, when h_σ reaches its maximum value ε will be equal to 'a'. Eq. (2-6) can then be rearranged to give Eq. (2-8). If ε is then set to a/2 it can be seen that σ equals b^{-1} and, as can be seen in Figure 2-3, b^{-1} can be considered to be the stress required to reduce the initial bed porosity 'a' by half.

$$\left(\frac{1}{\varepsilon} - \frac{1}{a}\right) a\sigma = \frac{1}{b} \qquad \textbf{(2-8)}$$

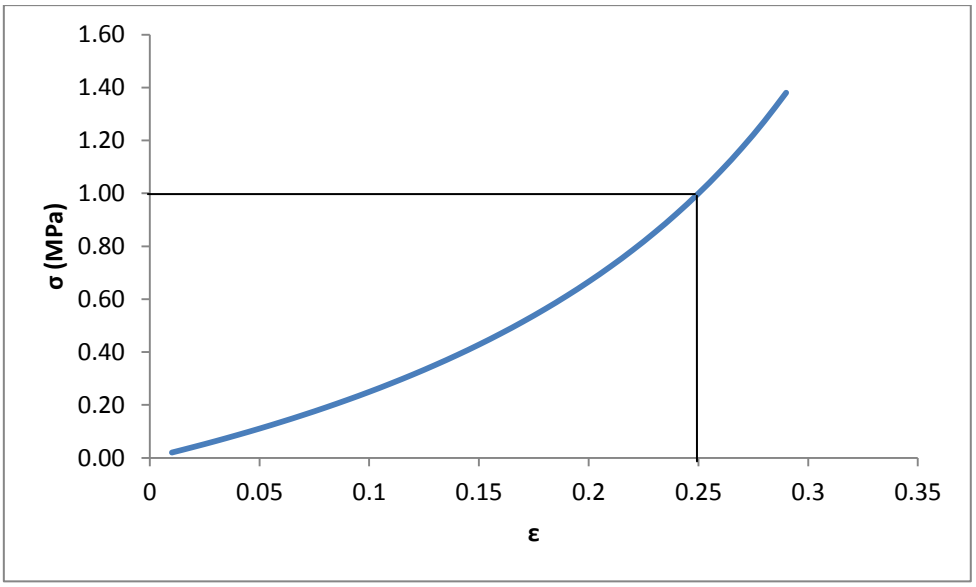

Figure 2-3: Theoretical stress versus strain plot based upon the Kawakita model when b = 1 and a = 0.5

A key issue with the Kawakita model is its sensitivity to the method of determining h_i. For example for powder with a high Carr's ratio (the ratio of the change in a powder volume due to tapping to the original untapped volume), if the compaction die is filled in a manner which leads to a small degree of compaction via particle rearrangement prior to compaction a low b^{-1} parameter may be recorded. However, if the same powder is placed within the die in a manner which leads to the powder being fully compacted prior the compaction a higher b^{-1} value may be recorded.

Denny [11] converted 'a' and ε in Eq.(2-6) to porosities (a = e_0 and ε = (e_0-e)/(1-e)) to give Eq. (2-9), which can be rearranged to give Eq. (2-10). If logarithms are then taken across Eq. (2-10) we then arrive at Eq. (2-11). With a special case existing where $b(1-e_0)\sigma$ is <0.1 Eq. (2-11) approximated to Eq. (2-12), allowing for a difference of 5% in the result.

$$\frac{\sigma(1-e)}{(e_0-e)} = \frac{1}{e_0 b} + \frac{\sigma}{e_0} \qquad \textbf{(2-9)}$$

$$\frac{e_0}{e} = 1 + \mathrm{b}(1-e_0)\sigma \qquad \textbf{(2-10)}$$

$$ln\frac{1}{e} = ln\frac{1}{e_0} + \ln\left[1 + b(1 - e_0)\,\sigma\right] \quad \textbf{(2-11)}$$

$$ln\frac{1}{e} = ln\frac{1}{e_0} + b(1 - e_0)\,\sigma \quad \textbf{(2-12)}$$

Eq. (2-12) can be differentiated to give a first order rate equation (see Eq. (2-13)), showing that both Eq.(2-6), (2-3) follow a first order lumped parameter model and that the Kawakita b parameter and Heckel K parameter can be related to each other via Eq. (2-14)

$$-\frac{de}{d\,\sigma} = b(1 - e_0)e \text{ when } b(1 - e_0)\sigma < 0.1 \quad \textbf{(2-13)}$$

$$K = b(1 - e_0) = b(1 - a) \quad \textbf{(2-14)}$$

2.3.3 The Adams model

Adams *et al.* [19] derived an alternative to the Heckel and Kawakita models. They considered the powder within the die as an assembly of parallel columns failing with all energy applied being dissipated during the compaction. In this model the columns are considered as isolated columns, failing in uniaxial compaction by tensile crack opening in a manner similar to that observed in the diametric compaction of tablets. In this 'column model' of confined uniaxial compaction, cracks initiate within a single column resulting from an axial major principal stress, constrained by a radial principal stress originating from the neighbouring columns and failing via oblique shear. This mode of failure was first recognised by Coulomb [21] who related the shear failure stress to the cohesive strength and a frictional stress $\alpha\sigma_l$ acting at the failure plane via Eq.(2-15).

$$\tau = \tau_0 + \alpha\,\sigma_l \quad \textbf{(2-15)}$$

where τ is shear failure stress, τ_0 is cohesive strength, α is the dimensionless coefficient of friction and σ_l is the lateral compressive stress.

Adams *et al.* [19] then consider the failure force F of a column measured in the axial direction to be proportional to the product of the failure stress τ, and the cross-sectional area of the fracture plane (see Eq. (2-16))

$$F = k_1 \tau A' \quad \textbf{(2-16)}$$

where k_1 is a dimensionless proportionality constant and A' is the area of the fracture plane.

If it is then assumed that the column will fail at its weakest point the failure force can be considered to be the failure force of the weakest particle within the column. The failure force will then be summed over all failing columns, where the total force F^* is defined by Eq. (2-17):

$$\sum_0^n F = F^* = \tau A^* \quad \textbf{(2-17)}$$

where $A^* = k_1 n A$ and n is number of failing columns.

It was then assumed that any increment in load will lead to an increase in n:

$$dF = \tau \, dA^* \quad \textbf{(2-18)}$$

And thus it follows that:

$$d\sigma = \tau \, dA^* / A_0$$

where $d\sigma$ is the change in bed pressure and A_0 is the bed cross sectional area. Adams *et al*. [19] then assumed that the increase in facture area and thus the change in pressure will be directly proportional to the change in bed height *i.e.* strain and thus bed pressure will follow the first order lumped parameter model shown in Eq. (2-19).

$$d\sigma = -k_2 \tau \frac{dh}{h} \quad \textbf{(2-19)}$$

where h is bed height and k_2 is a dimensionless proportionality constant. The lateral pressure σ_l in Eq. (2-15) was then assumed to be proportional to the applied pressure σ, and thus:

$\sigma_l = k_3\ \sigma$ **(2-20)**

where k_2 is a dimensionless proportionality constant.

Combining Equations (2-15), (2-19) and (2-20) yields:

$$d\sigma = -(\tau_0' + \alpha'\sigma)\ \frac{dh}{h} \quad \textbf{(2-21)}$$

where:

$$\tau_0' = \frac{k_2}{k_3}\tau \quad \textbf{(2-22)}$$

$$\alpha' = k_2\alpha \quad \textbf{(2-23)}$$

Eq. (2-21) can be integrated thus:

$$\int_{\sigma_0}^{\sigma} \frac{d\sigma}{(\tau_0' + \alpha'\sigma)} = -\int_{h_i}^{h_\sigma} \frac{dh}{h} \quad \textbf{(2-24)}$$

where $\sigma_0 = 0$

$$\ln\sigma = \ln\left(\frac{\tau_0^{'}}{\alpha'}\right) + \alpha'\varepsilon_n + \ln(1 - e^{(-\alpha'\varepsilon_n)}) \quad \textbf{(2-25)}$$

$$\varepsilon_n = \ln\left(\frac{h_i}{h_\sigma}\right) \quad \textbf{(2-26)}$$

where ε_n is the natural strain as defined by Eq.(2-26) and σ is the applied pressure, τ_0' should be considered to be the apparent strength of the single particles with units of stress, while α' is the apparent coefficient of friction. At high values of ε_n the final term in Eq. (2-25) tends towards zero and thus a plot of ln σ vs. ε_n can be used to determine values of α' and τ_0' via extraction of an intercept and gradient from the linear portion of the equation. Adams *et al.* [19] went on to show experimentally that the Adams $\tau_0^{'}$ parameter was strongly correlated to the Kawakita b^{-1} parameter with $\tau_0^{'}/b^{-1}$ on average being approximately 0.6 (see Figure 2-4). Similar relationships between $\tau_0^{'}$ and b^{-1} have since been shown by Adams and McKeown [10], Samimi *et. al.* [14] and

Yap *et al.* [15], showing that the Adams $\tau_0^{'}$ and Kawakita b^{-1} are equally informative of single particle failure stress.

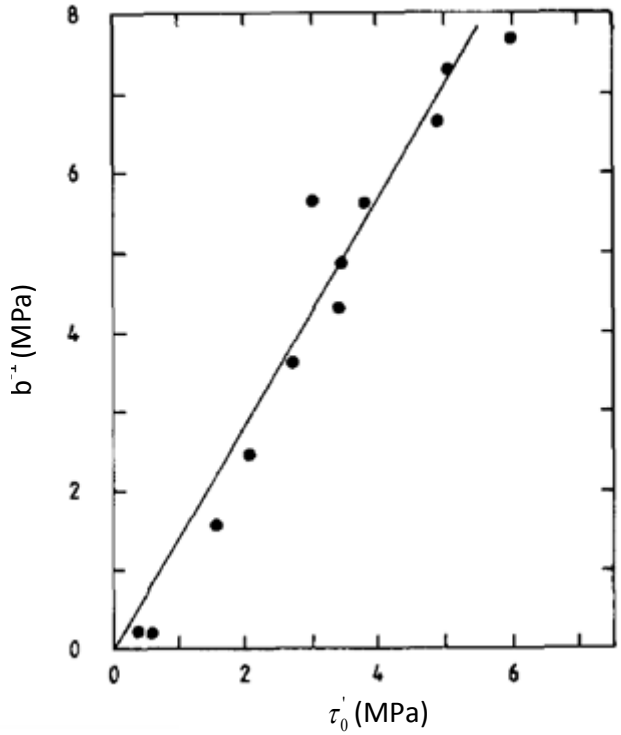

Figure 2-4: Comparison of Kawakita parameter b^{-1} with the Adams $\tau_0^{'}$ parameter for agglomerates formed from quartz sand and using varying amounts of a polyvinylpyrrolidone binder [19].

Yap *et al.* [15] performed a comparison of parameters derived from the Heckel, Kawakita and Adams models (Eq.(2-3), Eq. (2-6) and Eq.(2-25)), with results obtained via the compression of single particles (see Table 2-1). They determined that the Kawakita model was the only model able to achieve a good fit to experimental data ($R^2 > 0.98$) for all powders studied. It was also concluded that the Heckel parameter K^{-1} had significantly more scatter in its correlation with single particle yield stress than the Kawakita and Adams b^{-1} and $\tau_0^{'}$ parameters. The $\tau_0^{'}$ parameter and b^{-1} parameters gave reasonable indications of the single particle yield stress, but were unable to consistently differentiate particles with similar values of yield stress. However, as can be seen from the ratios quoted in Table 2-1 the Kawakita and Adams parameters were

consistently approximately equal to the single particle failure stresses while Heckel gave values significantly greater in magnitude.

Table 2-1: The ratio of Heckel, Kawakita and Adams parameters to single particle failure stresses σ_r [15].

	$\frac{1}{K\sigma_r}$ (−)	$\frac{1}{b\sigma_r}$ (−)	$\frac{\tau_o'}{\sigma_r}$ (−)
Eudragit® L100-55	2.7	1.3	1.7
Eudragit® L100	4.9	1.4	1.0
Eudragit® S100	9.7	3.2	2.8
Advantose™ 100	2.1	0.5	0.3
Calcium carbonate	5.1	1.2	1.0
Starlac™	2.9	0.7	0.5

Nordstrom *et al.* [12] proposed that the Kawakita 'a' and b parameters in Eq. (2-6) can be combined to form a rearrangement index ab which can then be used to indicate the level of particle rearrangement occurring in the early stages of compaction. This is based upon the assumption that as the 'a' parameter is related to the voidage within the die prior to compaction and the reciprocal of the b^{-1} parameter tends to increase with reducing particle size. Given that fine powders often contain high levels of voidage within the initial powder bed they will tend to undergo a higher level of particle rearrangement.

2.4 Particle Behaviour under the Influence of Shear Forces, and High Strain Rates

Auger fillers typically operate with values of rotational speed between 100 and 1000 RPM [4] and auger tube clearances between 1.6 and 3.2 mm [22], leading to the range of apparent shear rates given in Appendix 1 and summarised in Table 2-2. It should be noted that for a number of reasons the values of clearance quoted in Appendix 1 and Table 2-2 should only be taken as approximate guidelines. One reason for this deviation from quoted values is that tubes are typically manufactured from steel pipes which are specified based on their outside diameter and thus internal diameters will tend to vary [23] leading to clearances in some cases being as small

as 0.3 mm [24]. In some cases auger fillers have been purchased with Teflon tubes which are prone to wear often leading to large clearances up to 3 mm [25]. Furthermore these plastic tubes are initially accurately machined and thus prior to wear their associated clearances can be very small to the point where the auger can be initially in contact with the tube surface.

Table 2-2: Auger filler shear rates determined for operation at high and low shear rates, taken from data supplied by Auger Fabrication Inc. in Appendix 1.

	Low shear rate operation	High shear rate operation	
Rotational speed (RPM)	100	1000	1000
Auger Diameter (mm)	6.3	82.4	41.2
Tip speed (m/s)	0.03	4.31	2.16
Clearance (mm)	1.6	3.2	1.60
Apparent shear rate (s^{-1})	21	1348	1348

Examination of the values quoted in Table 2-2 leads to two conclusions:

I. Much higher levels of shear rate are present in the auger filler's auger/tube clearance vs. a typical uniaxial compaction experiment which would have shear rate below 1 s^{-1} (based upon a punch velocity of 50 mm/min and a bed height of 0.83 mm).

II. The tip speeds quoted in Table 2-2 are much higher than the typical punch velocities obtainable in laboratory scale physical testing machines [20] which are typically below 50 mm/min (0.00083 m/s).

This leads to the question: can yield stresses measured via uniaxial compaction be used to predict the formation of build-up in the auger filler given the differing levels of shear present in the two systems?

2.4.1 The Impact of Shear on Particle Deformation

Green [26] showed that shear forces were able to increase the contact area between two bodies more effectively than normal force alone. Duncan-Hewitt [27] suggested that this could be extended to ductile granular materials suggesting that movement of particles relative to one

another will lead to an increased contact area and thus potentially increase adhesive forces. However, experimental evidence for this is lacking and greater levels of understanding regarding the impact of shear forces on particle deformation is required [28]. This may mean that the properties of build-up generated in the auger filler will have different properties to compacts formed via uniaxial compaction.

2.4.2 The Impact of High Strain Rates

Clearly the tip speeds quote in Table 2-2 are much higher than the 0.05 to 5 cm min^{-1} punch velocities obtainable in typical uniaxial compaction experiments. Robert and Rowe [20] performed an experimental investigation into the effect of strain rate on mean yield pressure (via the Heckel K^{-1} parameter), compacting powders via uniaxial compaction at velocities of 0.033 mm s^{-1} and 300 mm s^{-1} and calculating a dimensionless strain rate sensitivity (SRS) index (see Eq. (2-27)). This leads to the generation of the results plotted in Figure 2-5, where P_y is equal to the reciprocal of the Heckel K parameter. They suggested that plastic deformation is sensitive to strain rate while fracture is not and thus brittle materials with high yield pressures such as calcium carbonate have low SRS indexes, while materials such as Maize Starch with low yield pressures have high SRS indexes.

$$\% \text{ SRS} = [(P_{y2} - P_{y1})/P_{y2}] \times 100 \quad \textbf{(2-27)}$$

where $P_y = K^{-1}$ and the subscripts 1 and 2 refer to low and high strain rates.

This suggests that for a powder of low yield pressure, accurate measurement of a mean yield pressure relevant to auger filler build-up formation must be performed at high strain rates. However, small scale equipment capable of achieving this task is not currently commercially available; also for many of the powders tested by Roberts and Rowe a reasonable correlation of SRS versus P_y (measured at low rate) was obtained within a range

of similar materials *e.g.* Drugs A, B, C and D. Thus it may be possible to relate mean yield pressures measured at low strain rate to the behaviour at high strain rate in the auger filler.

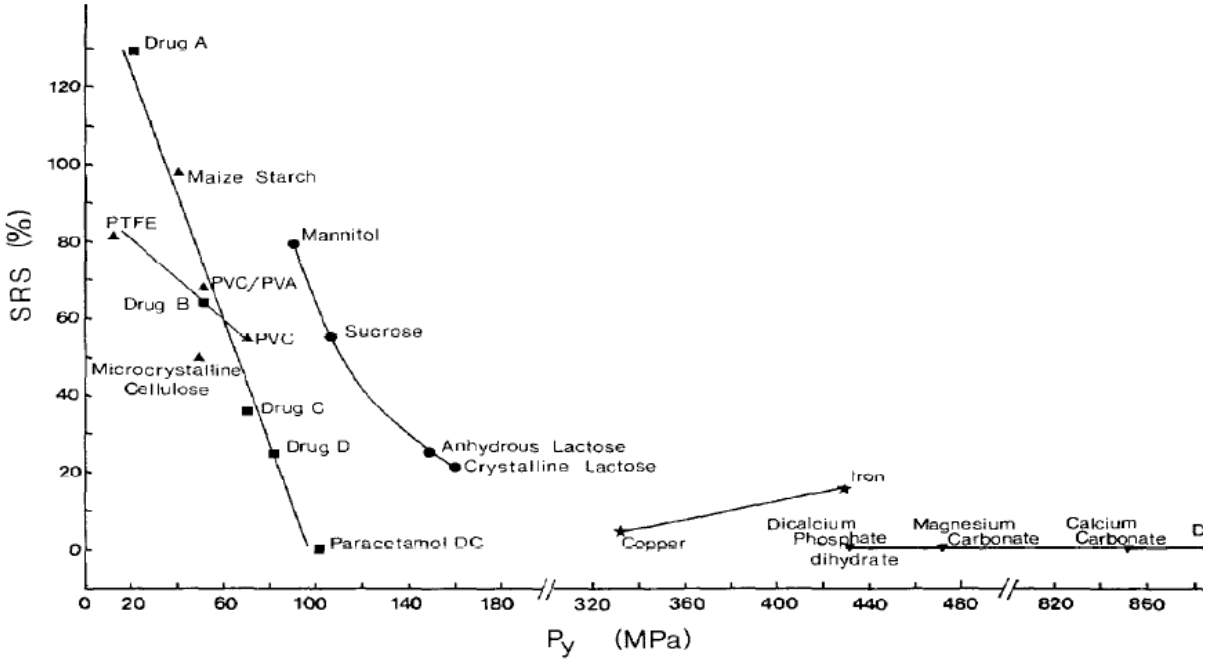

Figure 2-5: The relationship between low strain rate yield pressure (P_y) and the strain rate sensitivity index (SRS) [20].

2.5 Particle Behaviour in Small Clearances/Gaps

Detergent powders typically have a particle size distribution with a D_{10} of around 0.1 mm and a D_{90} of around 1.0 mm and auger fillers typically have auger/tube clearances on the same scale. This leads to the suggestion that the stresses particles experience as they pass through the auger/tube clearances may be similar to other situations where the clearance and particle size are comparable in magnitude. No prior work could be found discussing the behaviour of plastic/ductile particles in small clearances; however, literature is available for the behaviour of brittle particles in small clearances.

2.5.1 Crutchley and Bridgwater

Crutchley and Bridgwater [29] performed an experimental investigation of attrition of powders within small clearances, using powder containing particles with crushing strength ranging from

1.4 to 74 N and sieve fraction of 1.4 mm to 1.7 mm, 1.7 mm to 2.0 mm and 3.15 mm to 3.55 mm. They found that:

I. The stress acting upon the particles within the clearance was a function of the magnitude of the clearance expressed in particle diameters and not units of length.

II. In all cases percent breakage versus clearance gave plots similar to that shown in Figure 2-6 with breakage beginning at a gap of approximately half a particle diameter and a well-defined minimum between one and one and a half particle diameters. This possibly reflects break-up events involving one and two particles.

III. For all powders tested, no attrition was observed beyond a threshold of approximately 2.2 particle diameters. This potentially indicates that break-up events involving more than two particles are highly unlikely, due to the need for three particles to align within the gap as the blade passes.

IV. All powders underwent significant levels of attrition suggesting that the stresses generated were able to reach into the MPa range.

V. Larger particles tended to give rise to greater levels of break-up (accessed via sieving) for the same ratio of particle size to clearance [13]. This is potentially explained by the fact that for brittle materials particle strength reduces with increasing size.

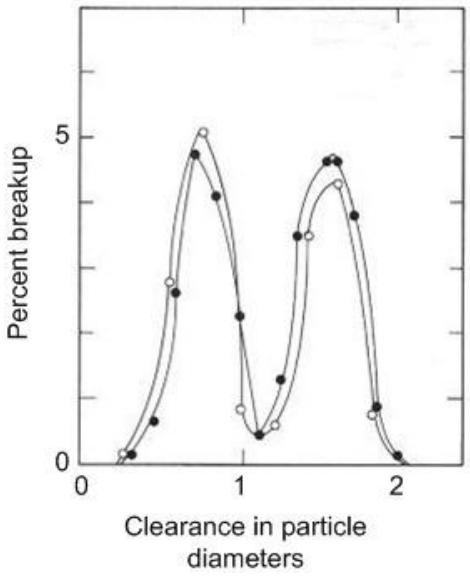

Figure 2-6: Attrition of Catalyst base particles taken from Crutchley and Bridgwater [29]

2.5.2 Calvert, Ahmadian and Ghadiri

More recently Calvert *et al.* [30] performed an evaluation of the performance of a testing device designed to shear particles as they moved between rollers turning at a differential velocity. The intention of the device was to subject assemblies of particles to shear deformation replicating levels of stress and strain experienced within a manufacturing plant. The Discreet Element Method was utilised in order to compare the normal force distribution in a shear box simulation (see Figure 2-7) under desired loading conditions to the normal force distribution generated in a roller simulation, with the aim being to decide on a value of roller gap width.

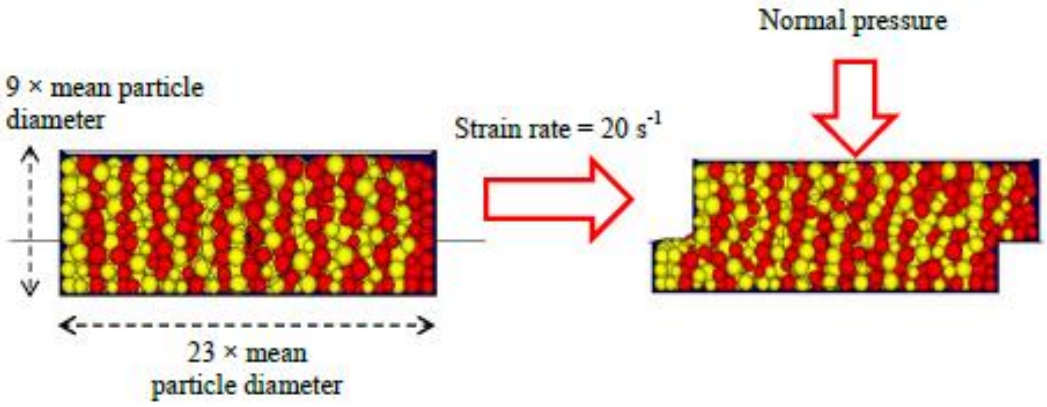

Figure 2-7: Shear cell simulation [30]

Simulations performed with a roller gap of 1.5 mm showed that the stress particles experience within the nip region (see Figure 2-8) increases with particle size (see Figure 2-9). This is in agreement with the findings of Crutchley and Bridgwater [29] that the force experienced by particles in a small nip region/gap is a function of the ratio of the gap size to the particle size. Fluctuations in force with varying strain and thus time seen in Figure 2-9 were attributed to jamming events.

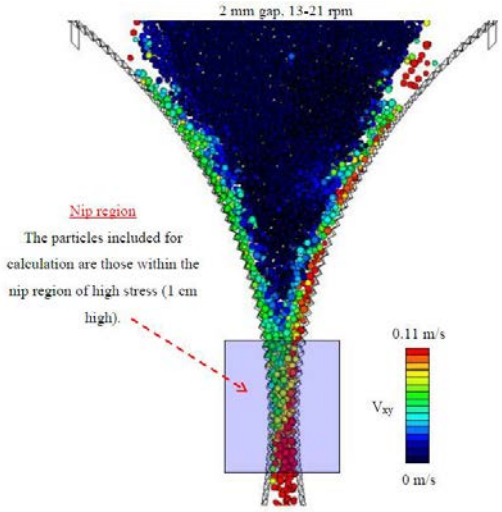

Figure 2-8: Illustration of the roller simulation, strain rate 20 s^{-1} [30].

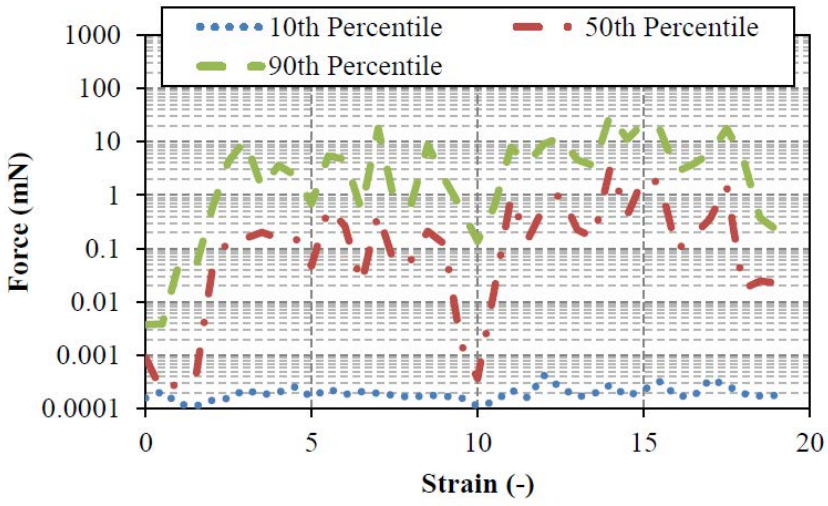

Figure 2-9: Force experienced in rollers as a function of strain for granule A (particle size = 0.30 to 0.51 mm, gap size = 1.5 mm) [30].

Calvert *et al.* [30] went on to perform simulations with varying normalised gap size as defined by Eq. (2-28). As can be seen in Figure 2-10 these simulations showed that a roller gap size of

approximately 3.5 times greater than the 90th percentile particle size, based on number distribution, was required to enable the stress experienced by particles within the nip region to be at unity with the shear box simulation *i.e.* DF = 1 where DF is defined by Eq. (2-29). Here it is assumed that the forces experienced in the shear box simulations are representative of stress experienced in the manufacturing process. In this case the manufacturing process involves processes such as hoppers and rotating drums in which the ratio of the particle size to the magnitude of a gap is not expected to be relevant. Based upon this it is assumed that once DF = 1 forces are now sufficiently low to be representative, however, in Figure 2-10 DF can be seen to continue to tend towards lower values beyond the point at which DF =1 and the normalised gap is equal to 3.5 suggesting a normalised gap of greater than 3.5 may be required.

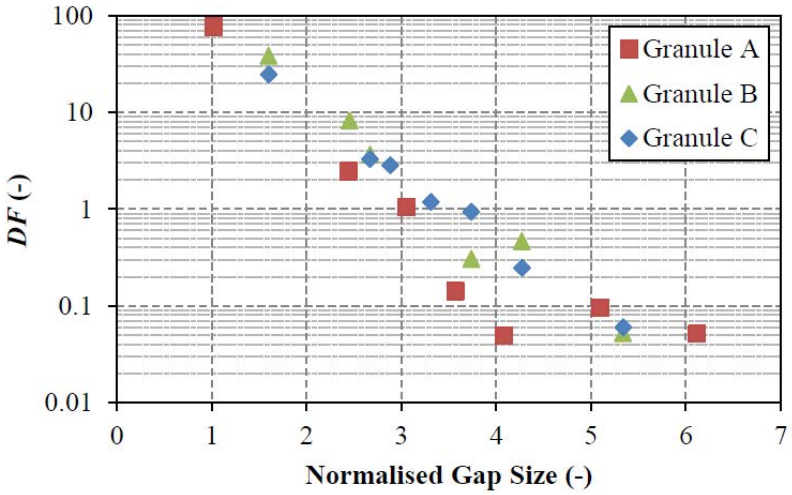

Figure 2-10: DF as a function of normalised gap size for all granules [30].

$$\text{Normalized Gap Size} = \frac{\text{Roller Gap Size}}{D_{90}} \quad \textbf{(2-28)}$$

$$DF = \frac{F_{90\ \text{Rollers}}}{F_{90\ \text{Shear Cell}}} \quad \textbf{(2-29)}$$

where $F_{90\ \text{Rollers}}$ is the 90th percentile force from the roller simulation and $F_{90\ \text{Shear cell}}$ is the 90th percentile force from the shear cell simulation.

In Figure 2-10 when calculating DF, $F_{90\ \text{Shear Cell}}$ was assumed to be constant between 8 and 20 kPa, however, as can be seen in Figure 2-11 this is not entirely true and thus is a source of error

in the determination of the gap size at which DF =1. Also the D_{90} used in Eq. (2-28) is used on the basis that the large particles will experience the greatest stresses, however, clearly 10% of the particles will be bigger than the D_{90} and experience larger stresses. Because of these two issues, a normalised gap size of 3.5 should be regarded as an approximate value at which DF = 1 with some reasonable margin of error associated with it.

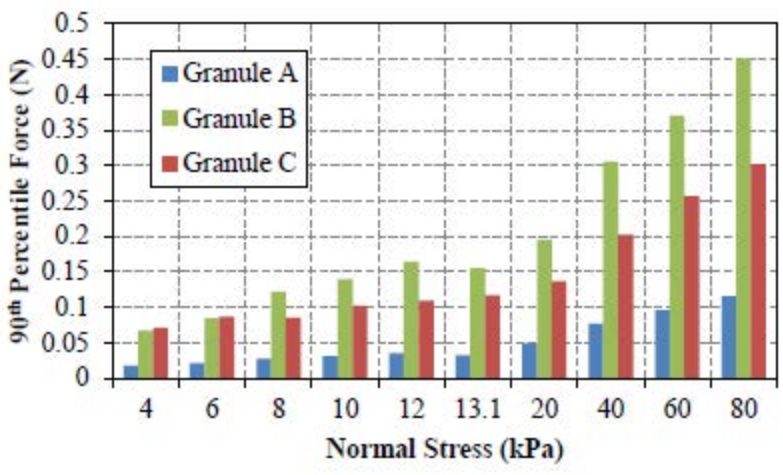

Figure 2-11: Shear cell 90th percentile normal contact force as a function of normal stress for granules A, B and C [30].

2.6 Particle Adhesion

Clearly the processes which lead to the formation of build-up involve adhesion of particles both to the original clean surface and to the subsequently built-up surface. The magnitude of the forces arising from adhesion and the underlying mechanisms are likely to be critical factors which determine both which particles within a blend are responsible for the formation of build-up and the ways in which other particles present within a blend are able to prevent build-up formation. The work required to overcome a given adhesive force is termed the thermodynamic work of adhesion. Typically it is not possible to measure the thermodynamic work of adhesion directly and thus various equations have been proposed to facilitate its calculation based on a given contact area arising from either plastic or elastic deformation. Work has typically focused on fine particles or large particles with low Young's modulus due to the fact that adhesive forces between substrates and large hard particles such as glass beads is

heavily influenced by surface asperities, and the deformation of these asperities in response to a given force [31, 36].

2.6.1 Elastic Deformation

The contact area existing between two smooth elastically deforming spheres was first studied by Hertz [32]. Hertz demonstrated how the size and shape of the contact zone arose from the elastic deformation of the bodies, with two spheres of radius R_1 and R_2 compressed together under an externally applied load P with units of force giving rise to a contact radius r as given by:

$$r^3 = \frac{3}{4}\pi(k_{H1} + k_{H2})\frac{R_1 R_2}{R_1 + R_2}P \quad \textbf{(2-30)}$$

where:

$$k_{H1} = \frac{1 - \vartheta_1^2}{\pi E_1} \quad k_{H2} = \frac{1 - \vartheta_2^2}{\pi E_2} \quad \textbf{(2-31), (2-32)}$$

where E and ϑ are the Young's modulus's and Poisson ratios for the two particles with E having units of Pressure and ϑ being dimensionless. However, the Hertz equation (Eq. (2-30)) takes no account of the influence of adhesive force on the contact area.

In the 80 years since adhesive forces were first studied by Bradley [33,34] and Derjaguin [35] great advances have been made. Johnson *et al.* [36] proposed Eq. (2-33) for a spherical particle contacting a planar substrate as a modified form of the Hertz equation (Eq. (2-30)) and went on to validate experimentally using rubber and gelatine particles via the use of a light microscope to measure the contact area directly. Rubber and gelatine particles were selected for the experimental validation based on the assumption that their low Young's modulus would ensure intimate contact with the surface and thus accurate assessment of the contact area. They were able to show that both compressive and tensile interactions were able to contribute to the radius of the contact according to the relationship described in Eq. (2-33) assuming that

materials deformed purely elastically and that interactions occur solely within the contacting region. Here tensile interactions arise from the particles tendency towards elastic recovery and compressive interactions arise from an applied load and adhesive forces.

$$r^3 = \frac{R}{K'}\{P + 3\omega_A \pi R + [6\omega_A \pi RP + (3\omega_A \pi R)^2]^{0.5}\} \quad \textbf{(2-33)}$$

where ω_A is the thermodynamic work of adhesion with units of Joules per meter squared, P is the externally applied load with units of Newtons, r is the contact radius and R is the particle radius with units of meters. The thermodynamic work of adhesion can then be related to the surface energies of the two materials via Eq. (2-34), where $\gamma_1$and γ_2 are the surface energies of the individual materials with units of Joules per meter squared. γ_{12} is the interfacial energy acting between them also with units of Joules per meter squared.

$$\omega_A = \gamma_1 + \gamma_2 - \gamma_{1,2} \quad \textbf{(2-34)}$$

K' is a constant describing the elastic mechanical properties of the particles via Eq. (2-35).

$$K' = \frac{4}{3\pi(k_{H1} + k_{H2})} \quad \textbf{(2-35)}$$

Setting the applied load to zero in Eq. (2-33) reduces to Eq. (2-36).

$$r_0^3 = \frac{6\omega_A \pi R^2}{K'} \quad \textbf{(2-36)}$$

The theory proposed by Johnson *et al.* [36] predicts that upon application of a tensile load, separation will occur at a contact radius of ~ 0.64 r_0, where r_0 is the contact radius when no external load is applied [37]. Examination of Eq. (2-36) shows that increasing Young's modulus and thus increasing values of the constant K will lead to lower values of r_0, and thus particles with a high Young modulus will detach at lower values of contact radius. This demonstrates that elastic tensile forces act to reduce contact area, while adhesive forces act to increase contact area.

Derjaguin *et al.* [38] proposed in contrast to Johnson *et al.* [36] that half of the interactions occur outside of the contact region. Tabor [39] compared the predictions made via the approaches proposed by Johnson *et al.* [36] and Derjaguin *et al.* [38] showing that the two approaches gave significantly different predictions of pull off forces. Muller *et al.* [40] performed an investigation of this effect showing that the contrasting conclusions derived from the two approaches arise from assumptions made regarding forces outside the contacting area, with both approaches being valid within a region defined by Eq.(2-37), which enable the calculation of dimension-less parameter μ. Values of μ > 1 indicate large particles, with low elastic moduli and high surface energy compliant with the approach of Johnson *et al.* [36]. This indicates that forces outside the contacting area can be neglected. Values of μ < 1 indicates the influence of forces outside the contact area and thus compliance with Derjaguin *et al.* [38].

$$\mu = \frac{32}{3\pi}\left[\frac{2R\omega_A^2}{\pi E^{*2} h_s^3}\right]^{1/3} \quad \textbf{(2-37)}$$

where E* is defined by Eq. (2-38) and h_s is the separation distance between the particle and the substrate, typically ~ 4 Å.

$$\frac{1}{E^*} = \frac{(1-\vartheta_1^2)}{E_1} + \frac{(1-\vartheta_2^2)}{E_2} \quad \textbf{(2-38)}$$

2.6.2 Plastic Deformation

Based upon empirical observations of the coherent nature of auger filler build-up (see Figure 1-8) it seems reasonable to assume that this involves plastic deformation. Maugis and Pollock [31] investigated the adhesive forces existing between metallic micro contacts. They determined that stresses induced by surface forces as derived from the theory of Johnson *et al.* [36] can in some cases be sufficient to bring about plastic deformation, demonstrating the need to generalise this theory to include plastic deformation. However, it should be noted that it seems probable that in the case of the auger filler, build-up is formed via plastic deformation

which occurs primarily as a result of an externally applied load from the auger. Surface forces would then potentially determine the adhesive forces acting between the build-up and the tube surface following the removal of the external load from the auger. Maugis and Pollock [31] were able to demonstrate experimentally that following two bodies coming into contact under the influence of an external load P and generating a contact radius r, the adhesive force generated is dependent upon load applied, surface force and the mode of separation. Separation can be ductile (F_d), brittle (F_b) or a composite of both mechanisms with the contact radius reducing gradually followed by a sudden brittle separation (F_m) (see Figure 2-12). Figure 2-12 shows the three modes of adherence (adherence = pull off force).

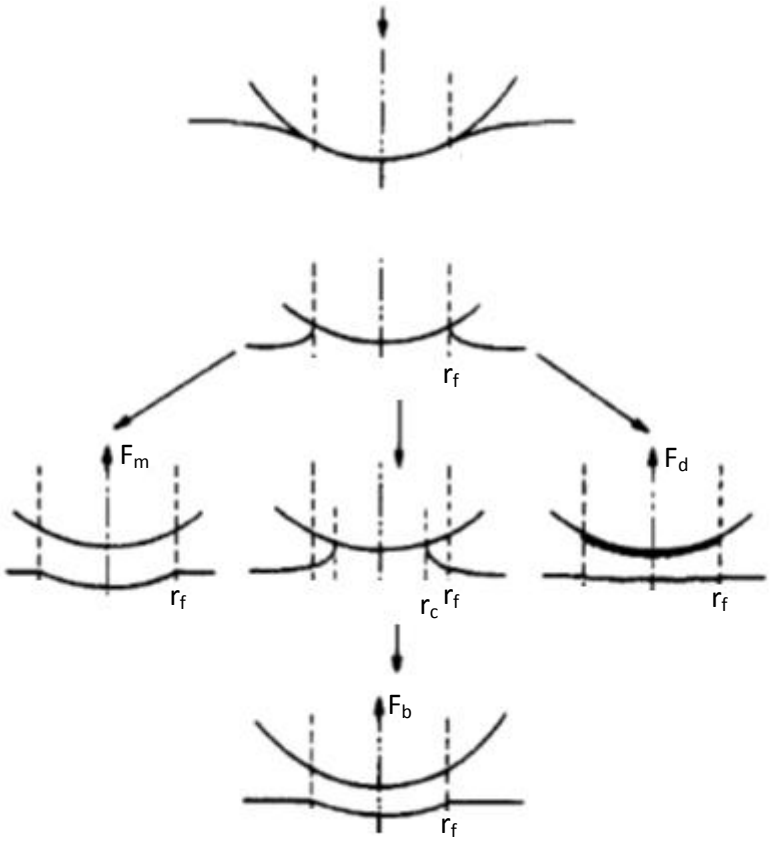

Figure 2-12: Schematic of the three modes of contact failure observed by Maugis and Pollock, during unloading contact area was observed to be constant until F_d or F_m was reached. In the case of brittle failure this was followed by a reduction of the contact from r_f to r_c [31].

The three modes of detachment were differentiated based upon the degree to which the contact radius is reduced prior to detachment. F_m is defined by separation without reduction of

the final contact area r_f and brittle/adhesive failure of the contact. F_b is defined by reduction of r_f to r_c prior to detachment with brittle/adhesive failure of the contact. F_d is defined as cohesive/ductile failure of the contact. F_d was only observed at high values of ω_A (580 mJm^{-2} and 2680 mJm^{-2} in Figure 2-10) and F_m was greater than F_b in all cases.

Figure 2-15 shows the conditions for the existence of each of the three modes of separation as a function of relevant material properties and applied loads.

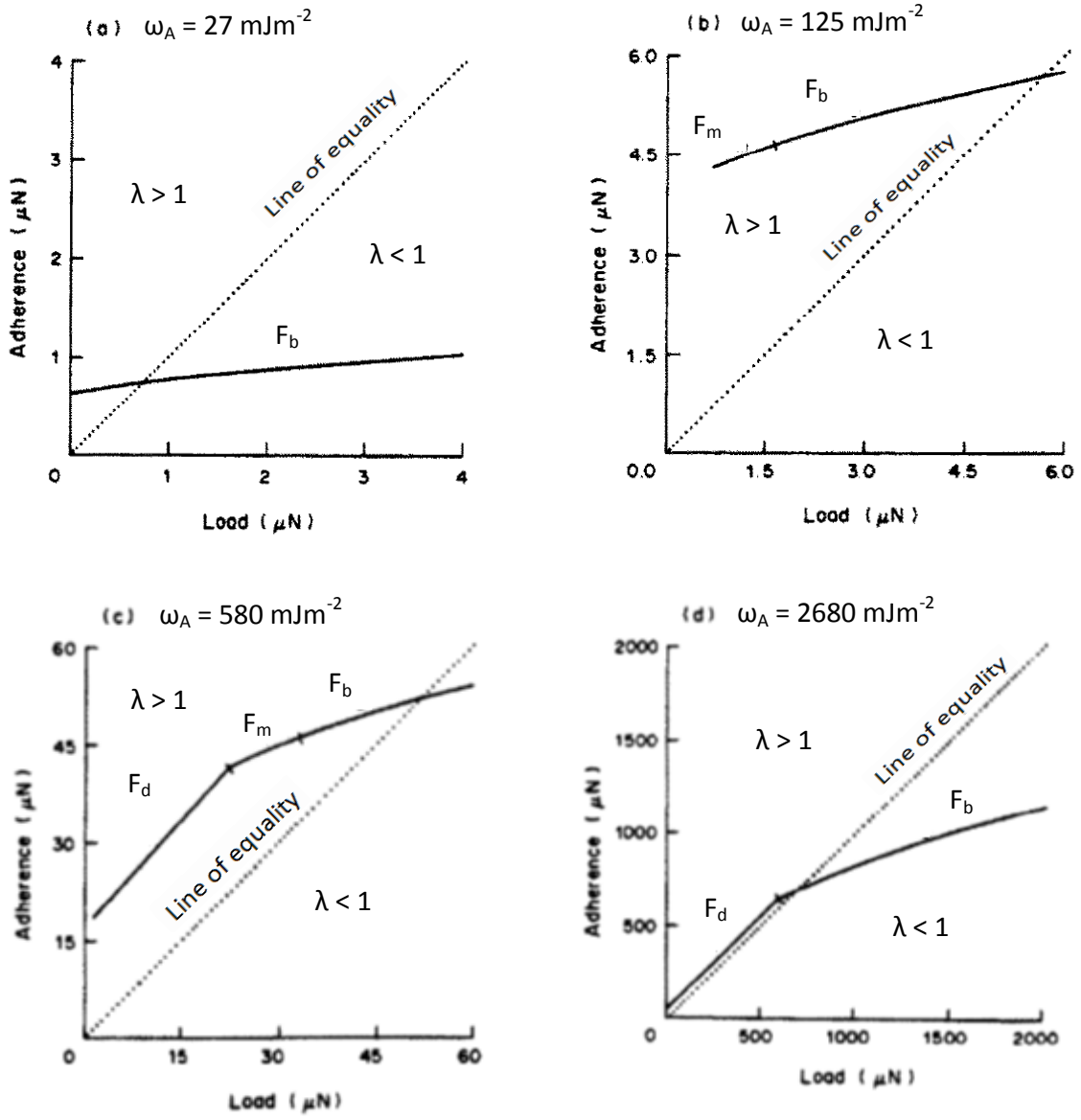

Figure 2-13: Predicted adherence force as a function of the maximum applied load for gold contacted by a rigid sphere of radius 3 μm, for four values of ω_A (27 mJm^{-2}, 125 mJm^{-2}, 580 mJm^{-2}, 2680 mJm^{-2}, where λ = Adherence / Load). Lines annotated with F_b, F_m and F_b to indicate the mode of contact failure.

Maugis and Pollock [31] proposed Eq. (2-39) for the ductile separation of two particles, which predicts that in the absence of a externally applied load P with units of force the thermodynamic work of adhesion is proportional to the square of the contact radius. This is in contrast to Eq. (2-36) which predicts that the thermodynamic work of adhesion will be proportional to the cube of the contact radius. This then allows for the differentiation of plastic and elastic deformation based upon power relationships.

$$-F_d = P + 2\pi\omega_A R = \pi r^2 H \quad \textbf{(2-39)}$$

$$-F_b = \frac{3}{2}\pi\omega_A R \quad \textbf{(2-40)}$$

$$-F_m = (6\pi\omega_A K'' r^3) - (\pi r^2 p_m) \quad \textbf{(2-41)}$$

where H is the plastic hardness of the material related to the yield strength via Eq. (2-42), R particle radius and r is the contact radius, ω_A is the thermodynamic work of adhesion with units of Joules per meter squared and p_m is the mean pressure at defined by Eq. (2-44).

$$H = 3Y \quad \textbf{(2-42)}$$

$$\frac{1}{K''} = \frac{3}{4}\frac{1-\vartheta^2}{E} \quad \textbf{(2-43)}$$

$$p_m = \frac{P_l}{\pi r^2} \quad \textbf{(2-44)}$$

$$P_l = P + \sqrt{6\pi r^3 K'' \omega_A} \quad \textbf{(2-45)}$$

where P_l is the effective applied load including surface forces.

In summary the key finding of Maugis and Pollock's work was Eq. (2-39) which describes the plastic failure of a contact, showing that in this case adhesive forces depart from those predicted by Johnson *et al.* [36] for elastic failure of a contact *i.e.* Eq. (2-40). Maugis and Pollock found that plastic failure of the contact occurred when $\boldsymbol{\omega_A}$ was high (see Figure 2-13). However, it also seems logical that plastic failure of the contact would occur in the case that a material's yield stress reduces below the adhesive stress acting across the contact.

2.6.3 Van der Waals Forces

The adhesive forces acting between plastically deforming particles can be linked to van Der Waals forces, which are the shifting electrostatic attractive and repulsive forces acting between molecules within a particles surface. Lifshitz [41] and Hamaker [42] stated that an estimate of van der Waals forces F_{vdW} can be arrived at by defining the contact zone between two particles as two parallel circular plates of diameter x separated by a distance h_s (see Eq. (2-46)):

Lifshitz: $\mathbf{F_{vdW}} = \frac{\mathbf{h\omega}}{\mathbf{32\pi h_s^3}} x^2$ Hamaker (for h_s < 150 nm): $\mathbf{F_{vdW}} = \frac{\mathbf{M}}{\mathbf{24\ h_s^3}} x^2$ (2-46)

where F_{vdW} is van der Walls force, hω is the Lifshitz–van der Waals constant and M is the Hamaker constant with both constants having units of Joules and h_s is separation distance and x is the contact zone diameter.

In both cases the constants are material dependent. Eq. (2-46) clearly shows the strong dependency of van der Waals force on the geometry of the contact, both in terms of its size acting through the x term and the separation between contacting surfaces acting via h_s. It follows therefore that for van der Waals forces to increase either the contact has to become larger or the separation has to become smaller and thus any plastic deformation of the contact will result in an increase in van der Waals force.

2.6.4 Real Contact Area

An important fact to consider in the area of particle adhesion is that real surfaces tend not to be perfectly smooth and in fact if surfaces were perfectly smooth, van der Waals force would act to hold them together with extremely high forces. This fact can be suitably illustrated by substituting typical values into the Lifshitz [41] and Hamaker [42] forms of Eq. (2-46) (h_s = 1 Å = 1 x 10^{-10} m, x = 1 m, M = 1 x 10^{-19} J and hω = 1 x 10^{-20} J) giving value of F_{vdW} of 99 MN and 4187 MN

which clearly are not typically observed. This is explained by the fact that the adhesive forces acting between the surfaces of particles, metallic surfaces, layers of build-up or some other object depend directly upon the surface area existing between them. This topic has been studied extensively in the area of polymer tribology where it has been determined that surfaces are not perfectly smooth, but are covered with asperities of varying height. If we consider two rough surfaces moving toward one another, initially the contact area will be that which exists between asperities with maximum height. As they move into increasing intimate contact under the influence of an applied load asperities of reducing height will come into contact. The overall area of the spots associated with the contacts existing between these asperities is known as the real contact area (RCA) and in many cases is significantly smaller in magnitude than the macroscopically observed contact area. In some cases, nano-scale asperities exist within micro scale asperities and therefore to definitively assess RCA, a two level model is required. This then allows for the accurate measurement of RCA as a function of an applied load, allowing for the determination of the adhesive forces between two contacting surfaces [43].

For model systems such as non-porous metallic particles the plastic deformation of asperities within a particles surface and the deformation of the whole particle will be driven by the yield stress of the metal. However, if we now consider a hollow metallic sphere the deformation of the asperities will be driven by the yield stress of the metal, but the deformation of the whole particle will also be influenced by the thickness of the particles structure. Therefore if two such hollow spheres are brought into contact they may deform with little adhesive force being generated between them due to a lack of RCA being generated between them.

2.6.5 Build-up as a form of Particle Agglomeration

Build-up involves the transformation of a powder into a solid and coherent, non-porous mass and thus can be considered as a particle agglomeration process similar to tableting, roller

compaction, high shear *etc.* Agglomeration processes can be classified into two categories; dynamic and pseudo static. Plastic deformation tends to promote agglomeration in both situations: in dynamic forms of agglomeration this will occur due to the dissipation of energy during particle-particle impact events leading to a low probability of rebound and thus a greater probability of the particles remaining adhered. In pseudo static forms of agglomeration such as tableting, plastic deformation will lead to the creation of increased contact area which in turn will lead to larger adhesive forces [44]. Rumpf *et al.* [45] stated that the adhesive force acting between two plastic deforming spheres is proportional to the applied force and the ratio of the van der Waals pressure to the plastic yield pressure of the sphere as per Eq.(2-47).

$$F \approx \frac{p_{vdW}}{p_{pl}} F_a \qquad \textbf{(2-47)}$$

where F is adhesive force, F_a is an applied force, p_{pl} is plastic yield pressure of the sphere and p_{vdW} is van der Waals pressure.

$$p_{vdW} = \frac{h\omega}{8\pi^2 {h_s}^3} \qquad \textbf{(2-48)}$$

where hω is the Lifshitz–van der Waals constant with units of Joules and h_s is the separation distance.

With the adhesive force acting between particles prior to plastic deformation considered to be negligible, it should be noted that van der Waals pressure increases as the separation distance h_s reduces and thus materials with a low plastic yield pressure will tend to give rise to large values of adhesive force F per unit of applied force, both because of their low value of plastic yield pressure and because of the consequentially larger value of van der Waals pressure.

The strength of agglomerates manufactured via deformation of plastic binder particles relies on both the adhesion of plastic binder to the surface of the powder particles and the cohesion within the plastic binding substance. In the case that a high amount of binder is present within

a formulation a matrix is built within which the powder particles are embedded, the tensile strength of the agglomerate will then become independent of the adhesive forces between the binder and particle surface, due to the presence of a binder continuous phase. According to Dopfer *et al.* [39] this leads to the physical stability of said agglomerates being dominated by their internal porosity and the plastic yield pressure of the binder. However, experimental evidence in support of this statement is lacking and the statement may not apply to formulated/micro structured materials such as fibre reinforced composites. However, if it is assumed that this relationship applies to build-up forming detergent powder blends, with the resultant build-up being an agglomerate of the particles within the blend, it follows that there may be a critical fraction of build-up forming primary particles above which physically stable build-up is formed.

2.6.6 Influence of Moisture on the Adhesion of Amorphous Plastic Particles

Detergent particles typically contain surfactants such as alkyl ethoxy sulphates (see Figure 2-14) or linear alkylbenzene sulfonate (see Figure 2-15) at levels between 8 and 50 % w/w. These materials are water soluble and amorphous and as such their mechanical properties are highly dependent upon moisture content, due to water's ability to plasticize such materials. When water enters the amorphous structure of a surfactant the glass transition temperature is reduced and as a result its mechanical properties will degrade. Palzer [46] and Haider *et al.* [47] have shown this to be true for the rheological and mechanical behaviour of amorphous water soluble food powders. Therefore it seems probable that, for a given detergent powder, increasing moisture content will lead to a reduction in yield stress and a higher probability of build-up formation. However, it should also be noted that a reduction in yield stress may reduce the stress required to remove build-up. And thus build-up formation may not always impact the reliable operation of the packing equipment.

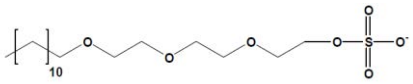

Figure 2-14: Alkyl Ethoxy Sulphate (AES).

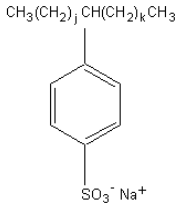

Figure 2-15: Linear Alkylbenzene Sulfonate (LAS).

2.7 Factors Affecting Agglomerate Particle Strength

For build-up to have a significant impact on the operation of an auger filler it must not only form, but must also be of sufficient strength to withstand the forces placed upon it by the auger's flights. Based upon this knowledge it may be possible to formulate a detergent powder in such a way as to ensure it forms weak frangible build-up unable to exist on the tube surface.

Significant work has been performed in the area of wet granulation towards the goal of predicting the agglomeration of particles in the presence of a binder. Iveson and Lister [48] produced the regime map shown in Figure 2-16. The map is based upon the hypotheses that the regime within which a granulator is operating can be defined in terms of two dimensionless parameters:

I. Deformation number De, where ρ_g is granule density, U_c is impact velocity and Y_g is dynamic yield stress.

II. Maximum saturation number s_{max}, where w is the ratio of liquid to solid on a mass basis, ρ_s is the density of the solid particles, p_l is the density of the liquid binder and e_{min} is the minimum granule porosity reached at a set of operating conditions.

In the crumb regime, a loose crumb is formed by a formulation too weak to generate granules which are unable to survive impact events. This leads to small numbers of large granules constantly breaking and reforming [49].

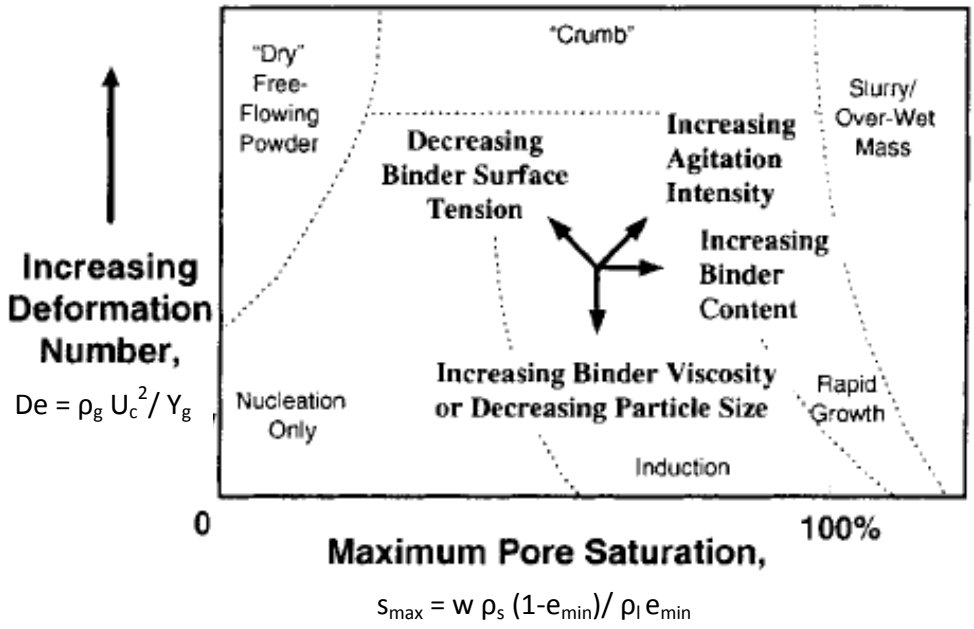

Figure 2-16: Effect of variables on a formulation's position within a granulation regime map [48].

In the case of auger filler build-up no liquid binder is present, however, in many cases detergent powders contain soft plastic particles similar to those studied by Samimi *et al.* [14] and strong particles such as sodium sulphate. In this case it is possible that the plastic particles will act as a fluid binding the strong particles together to form build-up. In this case it may be possible to form a crumb type build-up. This system would require soft low yield stress plastic particles and large strong particles, with a low concentration of the plastic material acting in a similar manner to a lack of binder in Figure 2-16.

2.8 Tablet Strength Measurements

To aid in the differentiation of powders with differing mechanical properties potentially leading to differing tendencies to form build-up during auger filling, measurements of tablet strength

have been made via diametric compression tests. Diametrical compression tests are also known as the diametrical tensile test, Brazilian disc test, indirect tensile test, or compact hardness test. The test induces a tensile stress acting in the transverse direction versus the compressive applied stress. The diametrical compressive test has become widespread in its use partly because it enables the use of a simple disc shaped specimen, in this case a tablet, to measure the force required to initiate tensile failure of a material [51].

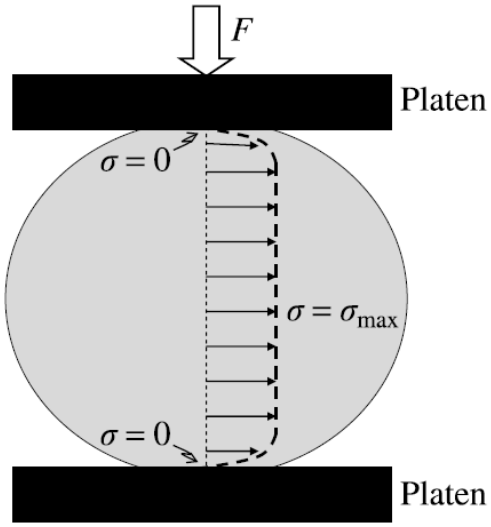

Figure 2-17: Illustration of a tablet diametrical crushing test [50].

To avoid effects associated with tablet size and shape Eq. (2-49) has been used, this was done to avoid effects shown in Figure 2-18 where tablet size and shape affect the value of tablet breaking force, but do not affect tablet strength on a stress basis [50].

$$Tablet\ strength = \frac{2F_t}{\pi D_t t} \quad \textbf{(2-49)}$$

where F_t is tablet breaking force, D_t is the diameter of the tablet and t is the thickness.

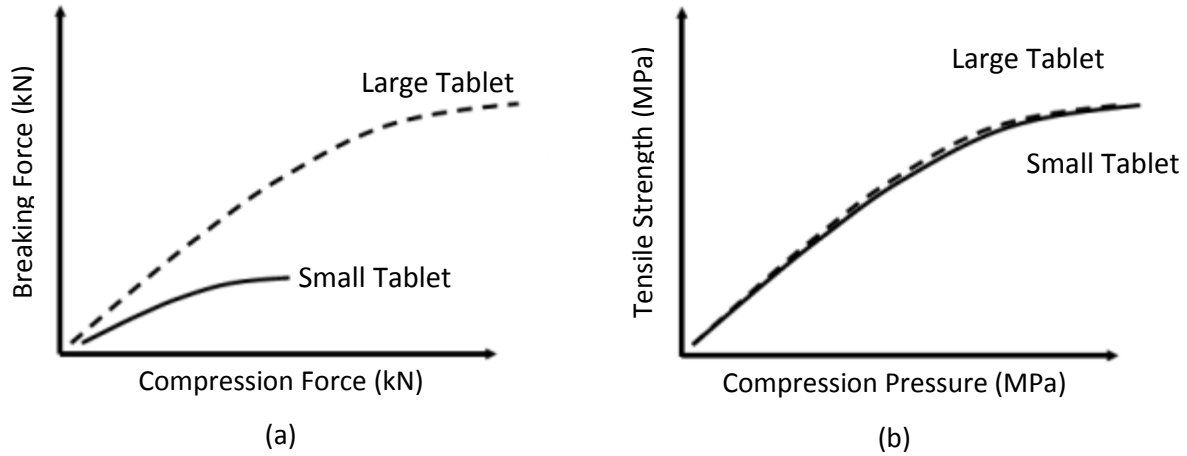

Figure 2-18: Diametric compression experiments (a) breaking force as a function of compression force, (b) tensile strength as a function compression pressure [50].

When using Eq. (2-49), it is important to consider that it is derived from the work of Hertz [32], who developed a mathematical expression describing the stress states of elastic two dimensional discs under diametric compression with elastic point loading. Hertz's [32] expression assumes that the maximum stress within the disc occurs in the centre of the disc and is tensile, acting perpendicular to the applied compressive force and is the stress which leads to the fracture of the disc [51]. Because of these considerations care should be taken when applying Eq. (2-49) to tablets which do not deform entirely by elastic deformation, do not deform entirely within a two dimensional plane or do not fail via tensile fracture as tablet geometry effects may have some influence upon the tablet strength values calculated.

Since the purpose of tablet strength measurements made in this thesis is characterisation of powders it seems wise to consider the manner in which a powder's mechanical properties influence the strength of the tablets they form:

- Contact area: plastic deformation will tend to generate more contact area between particles per unit of applied pressure and thus will tend to gain more strength per unit strain [50].

- In the case that the two halves of a tablet separate with particle-particle contacts failing via ductile separation according to Eq. (2-39), tablets of low plastic hardness will fail at low stresses. This potentially explains why soft polymers such as Poly (ethylene oxide) tend to form weak tablets [50].
- Contact flattening: Procipio *et al.* [51] showed via 2D Finite Element Modelling (FEM) with experimental validation that plastic deformation of compacts during diametric compression leads to stress concentrations at points located away from the compact centre, with consequential off centre crack propagation. These stress concentrations will tend to lead to premature failure of the tablet and thus lower values of tablet strength than would otherwise be the case.

In this thesis, measurements of tablet strength have been made of tablets of low porosity, removing the effects associated with the evolution of contact area during compression. In this case, it is proposed that for soft low yield stress powders, low tablet strengths will tend to be associated with the low yield stress material from which the tablet is formed.

2.9 Literature Review Conclusions

The build-up of laundry detergent powders in auger fillers and other similar systems is an area of powder handling currently missing from the literature. However, if we consider that auger filler build-up formation involves a powder becoming a smeared solid and coherent film adhered to the tube surface, it then seems reasonable to consider that other similar situations such as the adhesion of plastic particles to surfaces, the formation of tablets or the attrition of particles in small clearances/gaps will be relevant.

2.9.1 Literature Review Summary

A review of the literature in the area of uniaxial compaction has shown that it may be possible to determine parameters informative of the plastic yield stress of particles. This would be

achieved via the use of uniaxial compaction with the data resulting from said compaction analysed via the Heckel, Kawakita and Adams models.

Comments made by Duncan-Hewitt [27] regarding the impact of shear forces on particle-particle contact area suggests that the high levels of shear in the auger may lead to a larger contact area than if forces were applied to particles via normal forces alone.

The work of Roberts and Row [20] suggests that soft plastic particles of low yield stress are likely to exhibit strain rate dependent behaviour and given the high rotation speed of the auger it seems probable that high strain rates will exist within the auger fillers. However, it is possible that data generated at low strain rates within a laboratory environment could be correlated with the high rate behaviour that powders exhibit in the augers. This leads to the conclusions that work must be performed to determine if testing at high strain rates is required in order to enable the prediction of auger filler build-up from data generated at laboratory scale.

The work of Crutchley and Bridgwater [29] and Calvert *et al.* [30] in the area of the attrition of particles within small clearances/gaps leads to the conclusion that, the plastic particles which form build-up should experience large stresses on the MPa scale which are a function of the ratio of their size to the magnitude of the auger/tube clearance.

A review of literature in the area of particle adhesion and in particular the work of Maugis and Pollock [31] has shown that in the case of a ductile failure of a contact (see Figure 2-12) the force required to remove a particle from a surface is defined by Eq. (2-39), which would predict that under the influence of an externally applied load P a particle of low plastic hardness plastic H, will generate a large contact area which will act via r (the radius of the contact) to increase - F_d. However, we must also consider that since H=3Y, particles of low yield stress Y will have low values of plastic hardness which act to reduce the adherence force F_d. Leading to the conclusion

that soft plastic particles of low yield stress may fail to strongly adhere to surfaces, however, it is currently unclear how this would influence build-up formation since large adhesive forces may not be required.

$$-F_d = P + 2\pi\omega_A R = \pi r^2 H \quad \textbf{(2-39)}$$

where F_d is the pull off force for a ductile separation, P is an applied load with units of force, ω_A is the thermodynamic work of adhesion with units of Joules per meter squared, R is particle radius, r is contact radius and H is hardness with units of pressure.

A brief review of work performed in the area of polymer tribology has shown that large adhesive forces resulting from van der Waals force which exist between all perfectly smooth surfaces are in practice mitigated via surface roughness or real contact area (RCA). RCA will tend to increase with an increasing load and thus it is not only the deformation of the particle which must be considered when studying adhesion but also the deformation of surface asperities.

It has been concluded that the formation of auger filler build-up is a form of particle agglomeration involving the plastic deformation. This leads to the conclusion that work performed in other areas of particle agglomeration involving plastic deformation *e.g.* tableting, roller compaction, high shear agglomeration *etc.* may have led to findings which are transferable to build-up formation. Specifically this review has concluded that for a given powder increasing moisture content will lead to a reduction in yield stress and potentially a higher probability of build-up being formed. In a blended powder containing soft particles able to act as a plastic binder, and hard particles which are not, there may be a critical value of plastic particle volume fraction. Below this value, any build-up formed may have a weak 'crumb-like' structure which is unable to survive in an auger filler.

A brief review of tablet strength measurements has also been conducted which has led to the theory that for soft low yield stress powders forming tablets of near zero porosity said tablets will also be weak and of low yield stress, with Eq. (2-49) used to remove effects associated with tablet geometry / size.

2.9.2 A Literature Review Based Hypothesis for the Mechanisms by which Auger Filler Build-up is formed

Based upon literature published in these areas it is then possible to formulate a hypothesis which can then be tested via an experimental investigation. This hypothesis would be that:

1. As a powder is conveyed through an auger a small proportion of the agglomerate particles will pass through the auger / tube clearance and within this clearance they will experience stresses which are a function of the ratio of their size to the magnitude of the clearance.
2. Agglomerate particles which form build-up do so because they have sufficiently low yield stress and thus undergo a sufficiently large amount of plastic deformation to enable their adhesion to the tube surface.
3. To allow for the measurement of plastic yield stress within a time frame which would be feasible for industry, uniaxial compactions will be performed with subsequent application of the models proposed by Heckel [17], Kawakita and Ludde [18] and Adams [19].
4. Powder moisture content may have a significant influence upon whether auger filler build-up is formed. However, as moisture content is a less fundamental measurement versus measurement of a powder's mechanical properties via the Kawakita b^{-1} parameter, moisture content measurements will not be specifically investigated as a means of predicting auger filler build-up. Additionally from an industrial perspective, in

the event that build-up formation could be prevented via control of powder moisture content, this would be more challenging and costly to implement than potential alternatives such as larger auger/tube clearances, due to the need to modify a large number of powder storage facilities.

3. Experimental Methods and Materials

3.1 Introduction

The purpose of this chapter is to introduce the experimental methods and equipment used in the generation of the results presented in this thesis. The justification for the selection of each technique is discussed, with reasons given for the specific design of each method. The final section of this chapter information will be given which describes the laundry detergent powders which will be used for the bulk of the experiential work undertaken.

3.2 Auger Filler Experiments

To determine the extent to which a powder does or does not build-up, each powder was run at least once through an Auger Filler to deliver a minimum of 1000 fills (3000 revolutions) or until the formation build-up led to the auger filler tripping due to high current drawn by its drive. The Auger Filler (see Figure 3-1 and Figure 3-2) used in these experiments was a semi-automatic filler manufactured by ALLFILL International Ltd and was of a clutch break design (model number; S10, Serial number: 10503). Clutch break auger fillers operate with the drive running constantly connecting to an auger via an electromagnetic clutch break system, at the start of fill cycle the clutch is energized and the auger begins to rotate. At the end of fill cycle the clutch is de-energized and the break is energized returning the auger almost immediately to a stationary condition. The duration of a fill cycle is determined via an encoder on the auger shaft and based upon a number of revolutions entered into the auger fillers control panel. Auger rotational speed is varied via a rheostat and data from the encoder is used to output an RPM value on the control panel.

Unless otherwise stated during auger filler build-up experiments the filler setup was as follows:

- 3 revolutions per fill

- Approximate volume per fill: 27 cm^3 (approximately 10 to 20 g per fill depending upon bulk density).
- Auger speed: 840 rpm in the clockwise direction, time for 1 fill 0.21 seconds.
- One second between fills
- Spinner plate / tube clearance: 8 mm
- #16 auger tooling :
    - Auger diameter: 24.5 mm
    - Straight funnel internal diameter: 25.1 mm
    - Auger tube wall clearance: 0.3 mm (see Figure 1)
    - Pitch: 31.7 mm
- Material of construction: Stainless steel
- Surface Finish:
    - Auger: Mirror polished
    - Straight funnel: Smooth
- Agitator type: flat blade running counter clock-wise during fills only at 20rpm.

The purpose of the agitator is to feed powder into the auger and prevent rat holing in the hopper. As well as the auger, the agitator has a tendency to build-up and so to minimize this issue the running of the agitator was limited to during fills only.

Manual measurements of the torque required to turn the auger were taken at regular intervals using a deflecting needle torque wrench (Manufacturer; Torqueleader, Model number; ADS 25, Full measurement range: 0 to 27 Nm). Filling was stopped and measurements were made by attaching the wrench to a nut on the base of the spinner plate and turning the auger counter clockwise with the electrical supply to the filler isolated and the clutch plate and brake disengaged.

The test method employed was as follows:

- Start with Auger filler in empty and clean.
- Tighten nut on base of spinner plate to >5 Nm to ensure no further tightening during experiment and measure torque required to turn auger (0.5 Nm).
- Transfer powder to hopper using a plastic scoop.
- Start the filling of powder from the auger filler into an appropriately sized receptacle.
- At Intervals of 2 to 4 minutes filling is paused and the following recorded:
    - The torque required to turn the auger.
    - The outside surface temperature of the tube taken using a digital thermometer with a Nickel Chromium thermocouple.
    - The total mass of powder discharged by the auger filler using a Sartorius Signum 2 industrial weigh scale, capacity 7.0 kg.
- To reduce the mass of powder required per experiment, filled powder was returned to the auger filler's hopper at intervals of approximately 4 minutes.

It could be argued that recycling powder may influence the results of an experiment. However, build-up is believed that:

I. The agglomerate particles which go on to form build-up are a small fraction of the bulk powder (<1% w/w), and do as they pass through the auger/tube clearance where large stresses are experienced.

II. The remainder of the bulk powder experiences low stresses within the larger volume existing between the auger's flights.

It then seems reasonable that a powder's tendency to form build-up will not be significantly impacted by recycling of powder during build-up experiments. In section 6.2 of this thesis an experimental validation of this hypothesis can be found. Also experiments conducted in order to develop this test method will be discussed in Chapter 5 and section 6.2 of this thesis.

Figure 3-1: Exterior of pilot plant auger filler fully assembled with auger installed within collection funnel.

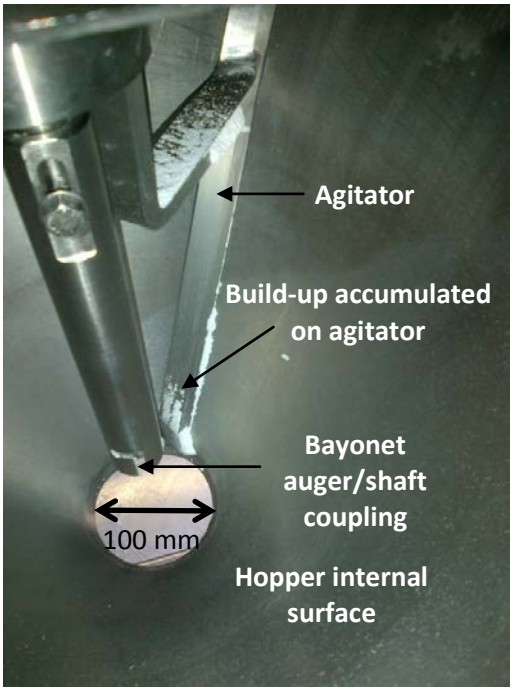

Figure 3-2: Interior of pilot plant auger filler showing agitator showing build-up accumulated at slow speed. The auger was removed from bayonet connection post operation of the filler to enable removal of the powder from the hopper.

3.3 Screw Tester Experiments

A second similar case to the auger filler has also been considered for powder build-up, this item of equipment is known within P&G as the screw tester (see Figure 3-3). It is a bespoke one off item of equipment developed internally within P&G and was originally designed to reproduce build-up within screw conveyors within P&G's agglomerate manufacturing processes. The most significant and relevant difference between the screw tester and the auger filler are as follows:

1. The screw tester is significantly smaller than the auger filler and thus the powder requirements per experiment are approximately one 10^{th} that of the auger filler experiments (0.5 to 1.0 kg versus 5 to 10 kg in the case of the auger filler).

2. The screw in the screw tester is mounted horizontally whereas the augers filler's auger is mounted vertically. This leads to the screw tester running less than 100% full and build-up typically forming along the base of screw (see Figure 3-5).
3. The rotational speed of the screw tester screw is lower than that of the auger filler with RPM values of 75 in the case of the screw tester versus 840 in the case of the auger filler test method.
4. As can be seen in Figure 3-4 the geometry of the screw tester's screw is significantly different to that of the auger filler auger which has a constant pitch. The open region towards the back of the screw is designed to allow for the feeding of powder into the less open section towards the exit of the screw. Also the auger's diameter is 24.5 mm whereas the screw tester's screw diameter is 31.5 mm and the clearance between the screw and its housing is 0.1 mm compared to 0.3 mm in the auger filler.

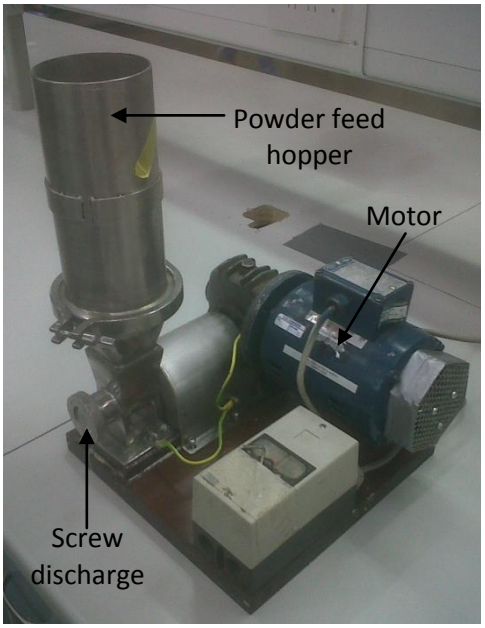

Figure 3-3: The screw tester

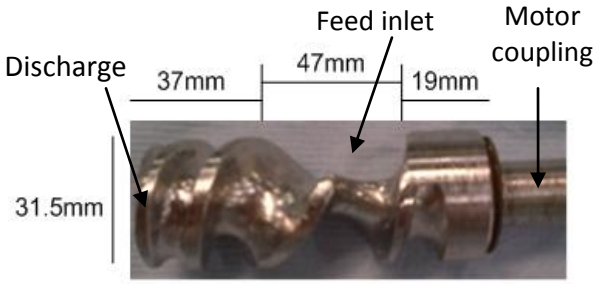

Figure 3-4 The screw tester's screw*

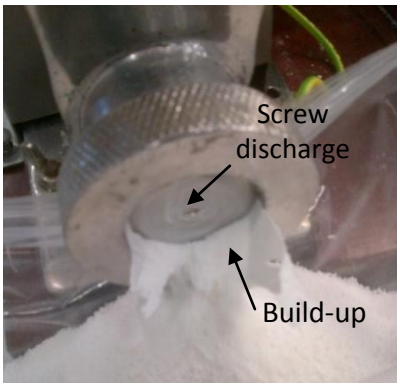

Figure 3-5: The screw tester, during an experiment with powder and build-up leaving via the screw discharge.

* A video of the build-up formation shown in Figure 3-5 can be found on the CD accompanying this thesis

Screw tester experiments were performed by filling the screw tester with the desired quantity of powder, 0.5 kg for low bulk density spray dried powder and 1.0 kg for higher bulk density agglomerates and extrudates. The screw tester was then run until all powder held within it had exited the screw. Any build-up formed was then scraped from the screw's housing and its mass was recorded. In this case build-up is defined as material which adhered to the screw's housing including material which subsequently detached and fell out of the screw as can be seen in Figure 3-5.

3.4 Moisture measurements

All of the powders tested in this study are used in the manufacture of laundry detergents and have varying moisture contents due to both the variability inherent in the manufacturing process and the conditions under which they are stored. It is reasonable to expect that the moisture content of the powder might have an effect on the mechanical properties which may then impact their tendency to generate build-up.

3.4.1 Infra-Red Heat Balance

To assess the level of moisture, each powder was tested with an Infra-Red heat balance (Mettler Toledo HB43-S Halogen). The balance heated 2.0 ± 0.1 g of powder to 160 ˚C for 5 minutes. The method used for this measurement is the standard P&G procedure used globally throughout P&G laundry detergent business and described by Hassall [2]. Thus results could be related directly to those made in other work within P&G. This method has been developed and used over many years, the temperature of 160 °C is used because it is above that required to evaporate both free and chemical bound moisture within the powder. 5 minutes is long enough to ensure the entire sample has been heated to 160 °C and that the moisture is completely eliminated from the sample [2].

This technique has a disadvantage in that it involves heating to a high temperature at which mass changes other than those attributed solely to drying may also occur, though no melting or combustion was observed for any of the powder tested. Also this technique fails to discriminate between free and chemically bound moisture. For example water of hydration in inorganic materials such as sodium carbonate would have a different effect on the mechanical properties of a particle than free moisture held within an organic binder.

3.4.2 Equilibrium Relative Humidity (eRH)

To assess the level of free moisture existing within each powder, equilibrium relative humidity (eRH) was measured using AW-DIO Water Activity Station probes with a Hygrolab 3 bench-top display unit. eRH is the value of relative humidity which a material can be placed in with no exchange of moisture occurring between the sample and the air within the sealed sample holder. This process is dominated by free moisture within the powder, as within the sealed volume of the sample holder (145 cm^3) it can be assumed that only a negligible mass of moisture is introduced with the air. This is due to the large difference in density between a powder and air under ambient conditions. This in turn means that eRH measurements are equal to the relative humidity of the air surrounding the powder during storage, prior to testing.

To measure the eRH of a powder a sample is placed inside a plastic sample container, which was in turn inserted into a thermally insulated block to prevent temperature changes in the sample during measurement. The sample is then covered with a water activity probe preventing moisture ingress from the surrounding environment, the probe then continues to measure relative humidity until equilibrium is reached, the RH value was then recorded as the eRH (all measurements were taken at 21 ± 3 ˚C). eRH values should only be used to compare powders of the same formulation at different moisture contents and is not valid for a comparison of powders with differing formulations, other than to assess the extent to which a powder is at

equilibrium with its surroundings. For example if a powder has an eRH of 10 % and is exposed to an RH is 30 % this indicates that the powder will go on to absorb ambient moisture.

3.4.3 eRH versus Infra-Red Heat Balance

In summary eRH measurements should be used to determine how close a sample of powder is in equilibrium with its surroundings, while the level of moisture in a powder as measured via the Infra-Red Heat Balance method can be used to determine the level of water present with a sample. Assuming the purpose of these measurements is to determine the likelihood of a powder undergoing plastic deformation and as a result forming build-up, the mass of moisture is likely to be more informative. However, it should be noted some of the inorganic materials present within some detergent powders such as zeolite, will not be completely anhydrous at 160 ˚C. That said it is probable that liquid present within the water soluble organic materials will act as a plasticiser reducing yield stress, while the water present in non water soluble materials such as zeolite may have little or no impact upon a particle's mechanical properties.

3.5 Uniaxial Compaction

Uniaxial compactions were performed within a cylindrical close fitting compression tableting die with an internal diameter of 31 mm. The die was placed between the plattens of an Instron 4469 Universal Testing machine fitted with a 50 kN load cell with a resolution of ± 1.35 N. For each compaction a mass of powder was weighed accurately using an analytical balance (Manufacturer: AND, Model HF-300OG). For each compaction the powder was transferred to the compaction die, the die was then gently shaken to create an even powder bed and the punch was lowered slowly to avoid damaging the agglomerate particles prior to compaction. The powder was then compacted to a force of 45 kN at a speed of 5 mm/min, the initial bed height was determined from the punch position at the start of loading. One or more of the compaction models proposed by Heckel [17], Kawakita and Ludde [18] and Adams [19] was then

applied using a Microsoft Excel spread sheet. Excluding the results presented in Chapter 4 (where only one repeat was performed per powder tested), results are quoted as the mean of 3 to 5 repeats with the standard error of the measurements quoted as the error.

Following comments made by Denny [11], to reduce the influence of die wall friction upon measurements obtained low values of initial powder bed aspect ratios have been used. These values were achieved via the use of a die with a 31 mm internal diameter containing 4.00 g of powder yielding aspect ratios between 0.1 and 0.4, unless otherwise indicated. Typically detergent powders have geometric mean particle sizes within the range 300 μm to 700 μm; significantly greater than the critical 50 μm quoted by Nordstrom *et al.* [12] above which it was observed that no significant particle rearrangement occurred. Also in some cases detergent powders can be of particularly low plastic yield stress [14]. For these reasons vibration pre-compaction has not been used prior to compaction as it was felt that this may lead to plastic yielding prior to uniaxial compaction. Also as recommended by Denny [11] internal lubricants have not been used and powder samples were characterised prior to compaction to determine both particle size and moisture content as these parameters are believed to affect the mechanical properties of the powders tested.

3.6 Diametric Tablet Compression

Following each uniaxial compression test the tablet formed was removed from the die and its thickness was measured using callipers to an accuracy of ±0.01 mm. Values of tablet strength were then determined using a Vankell VK200 tablet hardness tester which measures the strength of tablets via diametric compression of horizontally positioned tablets. This strength is then converted to units of pressure using Eq. (2-49). Figure 3-6 shows a failed tablet, formed from a powder which generated auger filler build-up, showing contact flattening (see section 2.8).

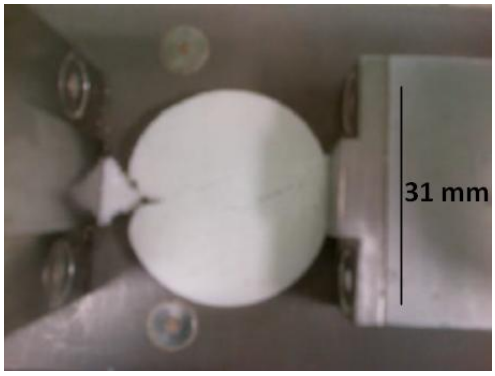

Figure 3-6: A failed tablet formed from of a build-up forming agglomerate (AG2 Batch 1).

$$Tablet\ strength = \frac{2F_t}{\pi D_t t} \tag{2-49}$$

Where F_t is tablet breaking force, D_t is the diameter of the tablet and t is the thickness.

3.7 Density Measurements

The density of a powder can be measured via a number of methods. The method used is typically dictated by the density measurement required: bulk, tapped, envelope or absolute. In this investigation bulk density, tapped density and absolute densities have been measured. Bulk density is defined as the mass of a powder occupying a given volume divided by that volume *e.g.* the bulk volume Figure 3-7.

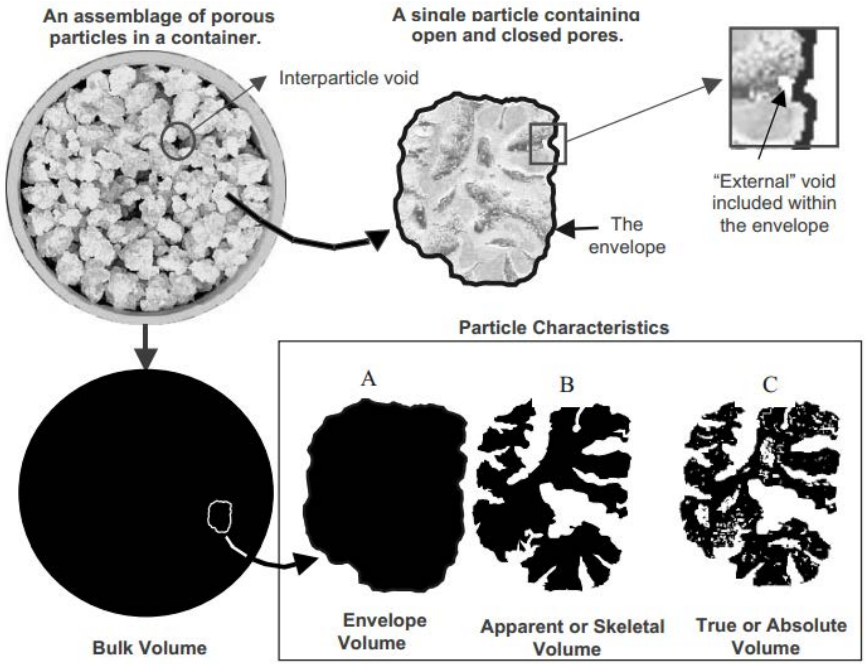

Figure 3-7: Various types of particle volume, volume A is the envelope volume, B is A minus the volume of open pores, and C is B minus the closed pore volume [52].

The absolute density of the powder is defined by the absolute volume (see volume C in Figure 3-7) which is the volume occupied by the solid fraction of a particle.

3.7.1 Bulk density measurements

Measurements of bulk density were performed using a re-pour density cup. This method is designed to measure the freshly poured non-compacted density of the powder. Measurements were made by placing an excess of powder into the upper hopper of a re-pour density cup. The orifice is then rapidly opened allowing the powder to fall under gravity into the receiving vessel or cup. The top surface of the powder is then scraped flat using a spatula to give a well defined volume of powder within the cup. The cup is of a calibrated volume therefore the mass of powder within the cup can be measured allowing for the determination of the bulk density.

3.7.2 Absolute density

The measurements of absolute density were made using an AccuPyc helium gas pycnometer. A sample of known mass was placed within a chamber of known volume, the chamber was then evacuated prior to helium being admitted and subsequently expanded into a reference chamber again of known volume. The difference in pressure from before and after is measured and then used to calculate the sample volume. Dividing the sample volume by its mass then gives the gas displacement density. Helium is used as it is known to be readily diffusible into small pores [52].

3.8 Testing for Cationic Sulphate ($CatSO_3$) Test Method

For various reasons during the course of the work detailed in this thesis it has been desirable to determine the amount of surfactant within either a sample of powder or a sample of build-up. As the vast majority of surfactants within P&G's detergent powders are cationic and contain sulphate ions (See Figure 2-14 and Figure 2-15) this has been achieved via the use of the $CatSO_3$ test method detailed in Appendix 2 supplied by Procter and Gamble, Technical Centres

Newcastle Innovation Centre, Analytical Test Department, who have performed all testing for $CatSO_3$ presented in this thesis.

3.9 Surfactant Content

Many of the powders discussed in this thesis are commercially sensitive and because of this it is not possible to discuss their formulation in detail. However, to give some indication of a given powder's formulation the surfactant content will be quoted on a mass fraction basis. Surfactants are organic materials with amorphous structures and density comparable to that of water *i.e.* specific gravity ~ 1 and thus adding increasing level of surfactant to a powder formulation will typically lead to a reduction in absolute density.

3.10 Scanning Electron Microscope Images

All scanning electron microscope (SEM) images presented in this thesis were obtained using a Hitachi table top Microscope, quasi-SEM TM-1000. This can achieve magnifications from 50 to 10,000X with a fixed accelerating voltage of 15 kV under a vacuum of 0.1 Pa.

3.11 Indentations

To gain additional understanding of both the mechanical and adhesive properties of tablets and build-up, indention experiments were performed using a Micrometrics TA-XT2 Texture Analyser, and a 2.00 mm diameter stainless steel indenter. Figure 3-8 is an SEM image of the indenter.

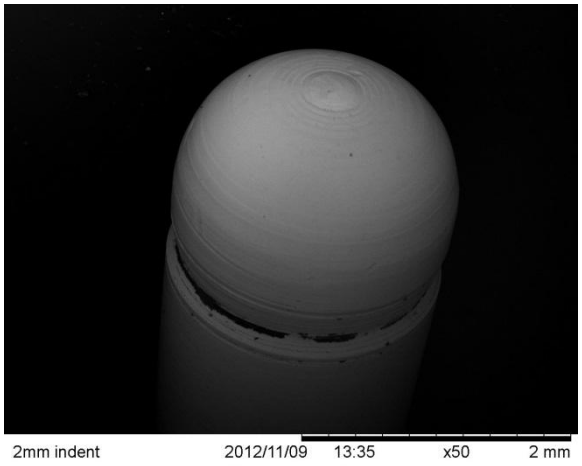

Figure 3-8: SEM image of a 2.00 mm stainless steel indenter at x 50 magnification.

Samples were attached to an SEM stub using an adhesive pad, the stub was then attached to a 1 kg mass again with an adhesive pad (see Figure 3-9). This was done to ensure the sample remained in place as the indenter retracted. Indentations were performed by applying a 1.0 N compressive load to the sample at a velocity of 0.1 mm/min; the load was then maintained for 10 seconds and then removed at a velocity of 5.0 mm/min. This process takes the sample into compression and then tension (see Figure 3-10 and Figure 3-11), this process is characterised by two parameters: pull-off force and maximum indentation depth.

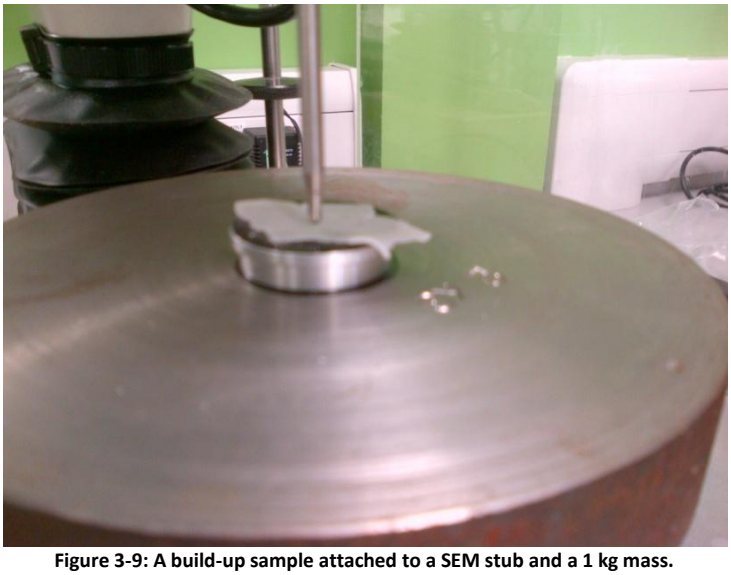

Figure 3-9: A build-up sample attached to a SEM stub and a 1 kg mass.

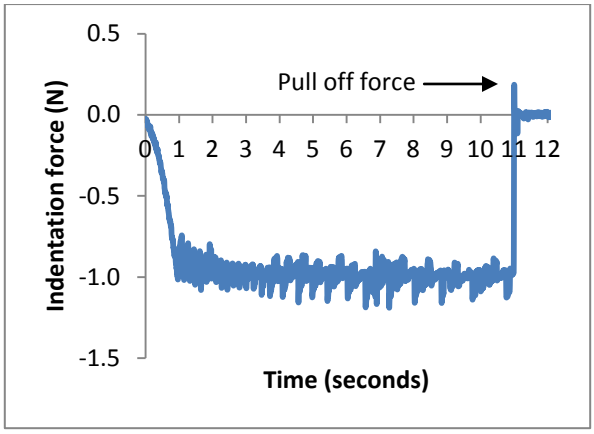

Figure 3-10: Variation in indentation force with time.

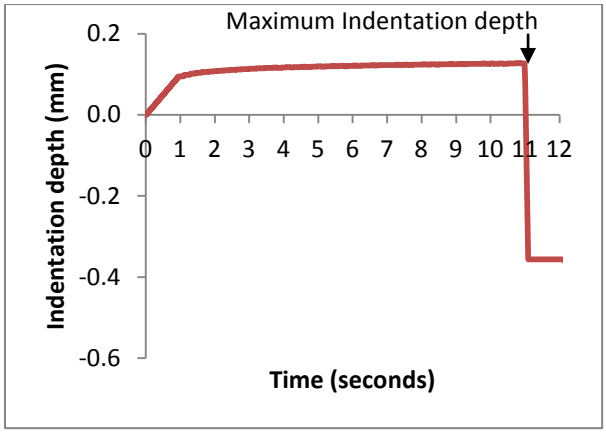

Figure 3-11: Variation in indentation depth with time.

The oscillations in indentation force seen in Figure 3-10 are due to the indentation depth varying in order to control indentation force at an approximately constant value of -1.0 N.

3.12 Particle Size Measurements

Measurement of particle size were made using a Rotap RX-29-10 sieve shaker (serial number: 19515) fitted with seven or more sieves selected in order to give sieve sizes distributed across the powder particle size distribution. For example in Chapter 6 sieves of 100, 150, 250, 425, 600, 710, 1180 µm were used. For each measurement the sieves were shaken for a 5 minute period.

3.13 Materials

The experimental work discussed in this thesis primarily involves powders manufactured and used by P&G in laundry detergent formulations, either commercially or within R&D prior to becoming commercially available. Most of the powders used contain significant levels of surfactant and are made via one of two manufacturing processes:

I. Spray drying

II. High shear agglomeration

In both cases powders typically have a geometric mean agglomerate particle size of around 400 to 500 μm and D_{10} and D_{90} around 100 μm and 1000 μm respectively. These numbers are important because they impact both the mechanical properties of the powders which then affect their behaviour within the manufacturing process and the consumer perception of the powder during its commercial use.

A key difference between powders made via the two methods is that, spray drying tends to give rise to powders which are of low bulk density and high porosity [57, 58]. High shear agglomeration will tend to generate agglomerate particles of near zero initial porosity and thus higher bulk density. Because of this high shear agglomeration typically gives rise to powders with a bulk density approximately twice that of the spray dried powders. Powders made via high shear agglomeration also generally contain higher levels of surfactant than the spray dried powders and often appear to be more plastic and less friable than the spray dried powders [53].

4. Materials Characterisation

An initial hypothesis describing the processes involved in build-up formation was proposed in section 2.7; a key conclusion was that plastic yield stress will be a factor in determining if a powder will form build-up. To gain some perspective regarding the yield stresses of the detergent powders manufactured by P&G within the detergent industry, confined compactions of a wide range of powders were performed. The goals of this study were to:

- Identify powder with the lowest failure strengths and in doing so determine which powders have the greatest potential to form build-up.
- Determine the best method for analysis of compaction data. The Heckel model was discounted from this comparison based upon findings of Denny [11], Yap *et al.* [15] and Samimi *et al.* [14] who found that significant curvature within experimental data led to a poor fit to the linear Heckel model. Also the Heckel model requires measurements of absolute density in order to determine relative density B, which would have significantly increased the time taken to complete this experimental study.

Procter and Gamble (P&G) add powders with a wide range of mechanical properties to their detergent finished products ranging from soft surfactant containing powders to hard crystalline materials such as Sodium Percarbonate and Sodium Sulphate. Figure 4-1 shows stress strain curves for Spray Dried Powder 1, High Shear Agglomerate 1 and Sodium Percarbonate measured via uniaxial compaction. Spray Dried Powder 1 and High Shear Agglomerate 1 were manufactured in full scale manufacturing plants and are used to deliver surfactant into laundry detergent formulations. Sodium Percarbonate is a non surfactant containing inorganic powder, used to add peroxide bleach to laundry detergent formulations. As it is manufactured outside of P&G, the details of the manufacturing process are unknown. Table 4-1 gives geometric mean

particle sizes measured via gravimetric sieving, and target surfactant contents for Spray Dried Powder 1, High Shear Agglomerate 1 and Sodium Percarbonate.

Table 4-1: Particle size and surfactant contents for powders shown in Figure 4-1

	Geometric mean particle size (µm)	Target surfactant content % w/w
Spray Dried Powder 1	494	18
High Shear Agglomerate 1	473	24
Sodium Percarbonate	650	0

The large difference in the shape of the two curves gives some indication of the differing mechanical properties, showing that Sodium Percarbonate is the strongest material, undergoing the smallest degree of deformation per unit stress. The spray dried powder is the weakest, showing the highest level of deformation per unit stress. However, from the stress strain curve alone it is not possible to determine if compaction is occurring via plastic deformation, brittle fracture or a combination of the two processes. Sodium Percarbonate is known to be crystalline under ambient conditions [54], and based on comments made by Denny [11] it seems probable that Sodium Percarbonate will be compacted by brittle fracture, followed by plastic deformation.

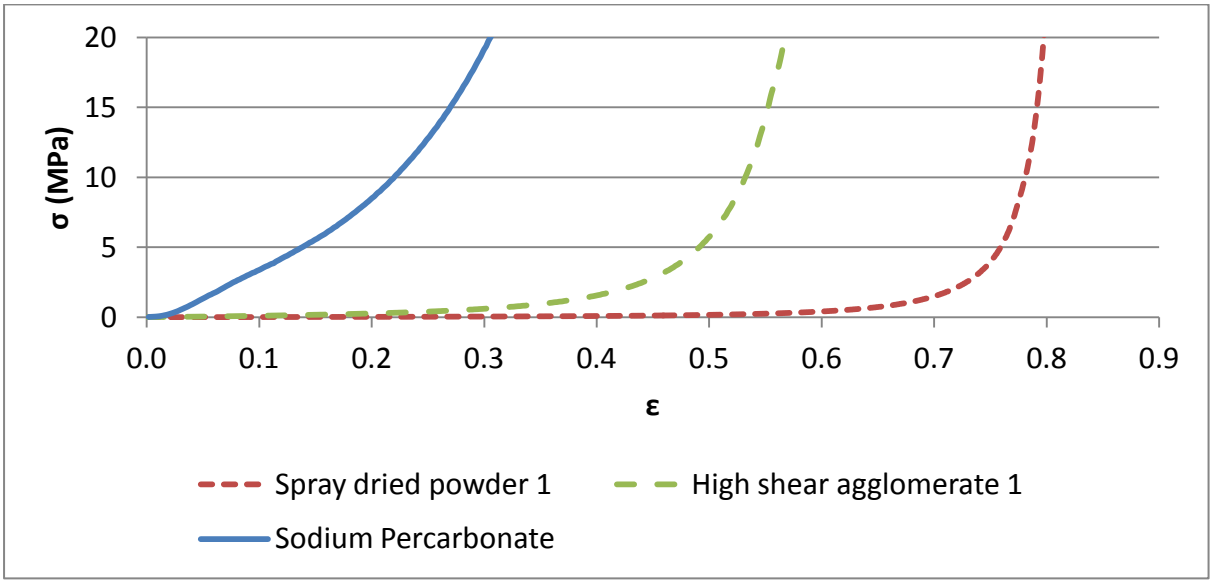

Figure 4-1: Stress strain curves for three Procter and Gamble powders

Figure 4-2 shows Kawakita plots for the powders shown in Figure 4-1. As the Kawakita model Eq. (2-6) is linear, a key issue when applying the model is the degree of linearity within the data selected for analysis. In this case data within ranges of stresses have been selected for analysis based upon two considerations.

I. The linearity of the data, as there seems little value in applying a linear equation to non-linear data.
II. The assumption that most of the plastic deformation occurs within the early part of the compaction process. For example, in the case of the spray dried powder, data above 10 MPa would not be considered for analysis due to the level of strain at this point in the compaction.

As can be seen in Figure 4-2 Sodium Percarbonate shows a clear departure from linearity in the lower portion of the stress range possibly relating to a transition from brittle fracture to plastic deformation. This lack of linearity is in line with comments made by Kawakita and Ludde [18] that the model works best for soft and fluffy powders and in this case is potentially related to a transition from brittle fracture to plastic deformation. However, that said experimental data was found to be linear between 10 to 20 MPa. Both the spray dried and high shear agglomerate show a high degree of linearity between 0.5 and 5 MPa, above 5 MPa a small degree of curvature is observed. Figure 4-3 show that the model gives an excellent fit to the experimental data across a reasonably wide range of applied stresses.

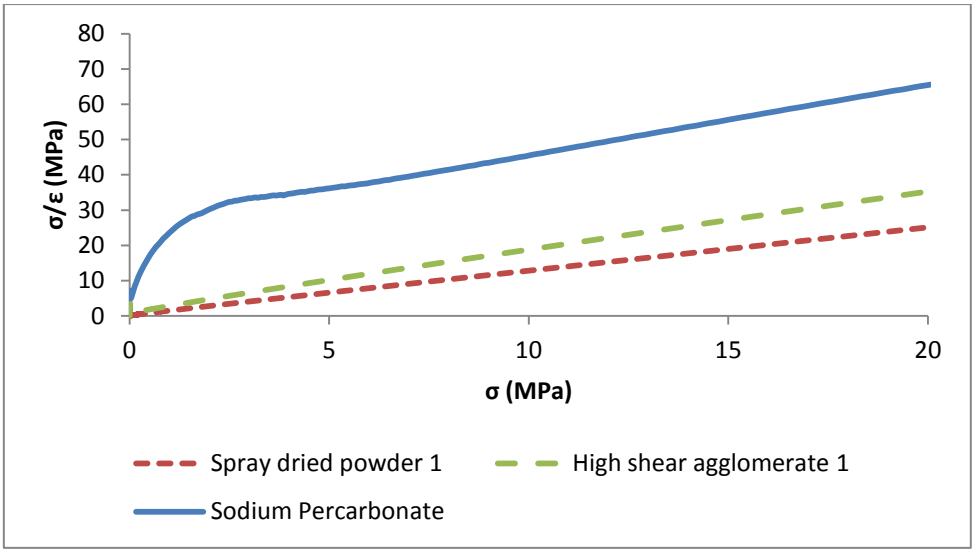

Figure 4-2: Kawakita plots over the full force range for three Procter and Gamble detergent powders

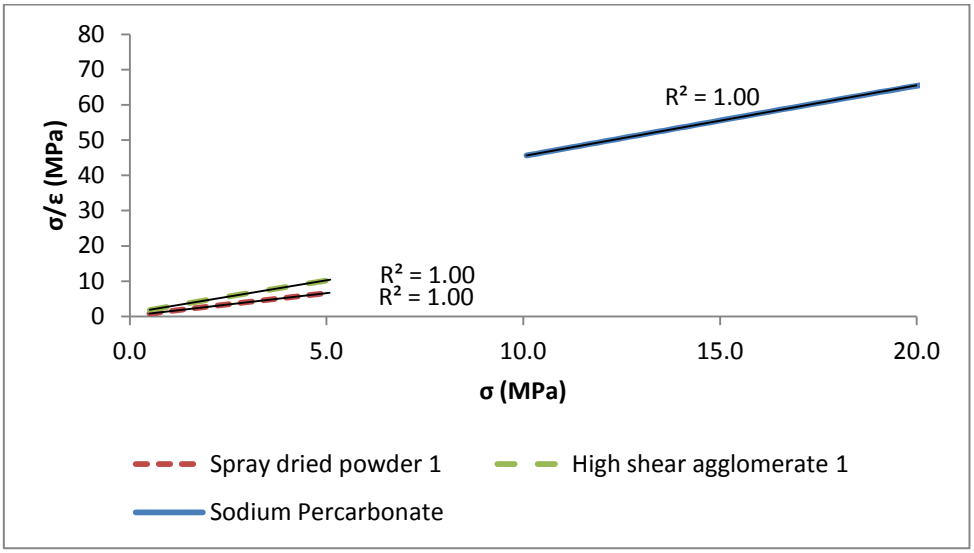

Figure 4-3: Kawakita plots showing the fit of the model to the experimental data for three Procter and Gamble detergent powders

Figure 4-4 shows Adams plots for the powders shown in Figure 4-1. As stated by Yap *et al.* [15] at very high values of ε_N the plot should become linear; all three powders behave in this way. However, for the high shear and spray dried surfactant containing powders at very high values of ε_N this relationship appears to break down.

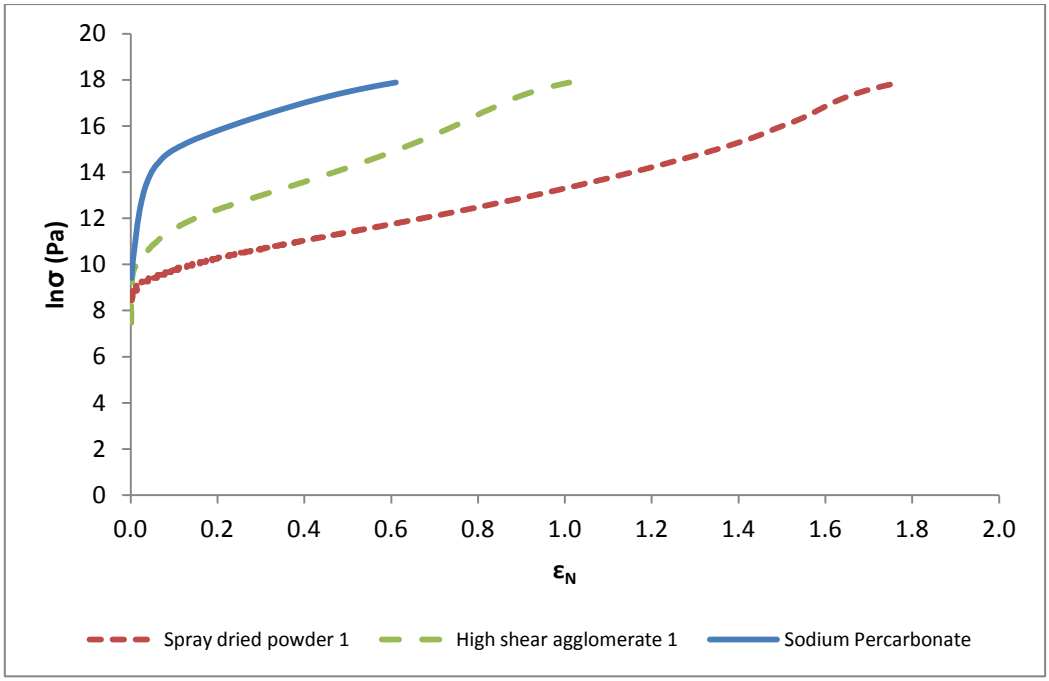

Figure 4-4: Adams plots for three Procter and Gamble powders

Figure 4-5, Figure 4-6 and Figure 4-7 show the experimental data and theoretical predicted data for the three powders shown in Figure 4-1. The theoretical prediction has been generated based on a fitting of data between values of ε_N between 0 and 0.6 using Eq. (2-25). In all three cases the prediction shows deviation from the experimental data at low stresses and good fit at higher stresses.

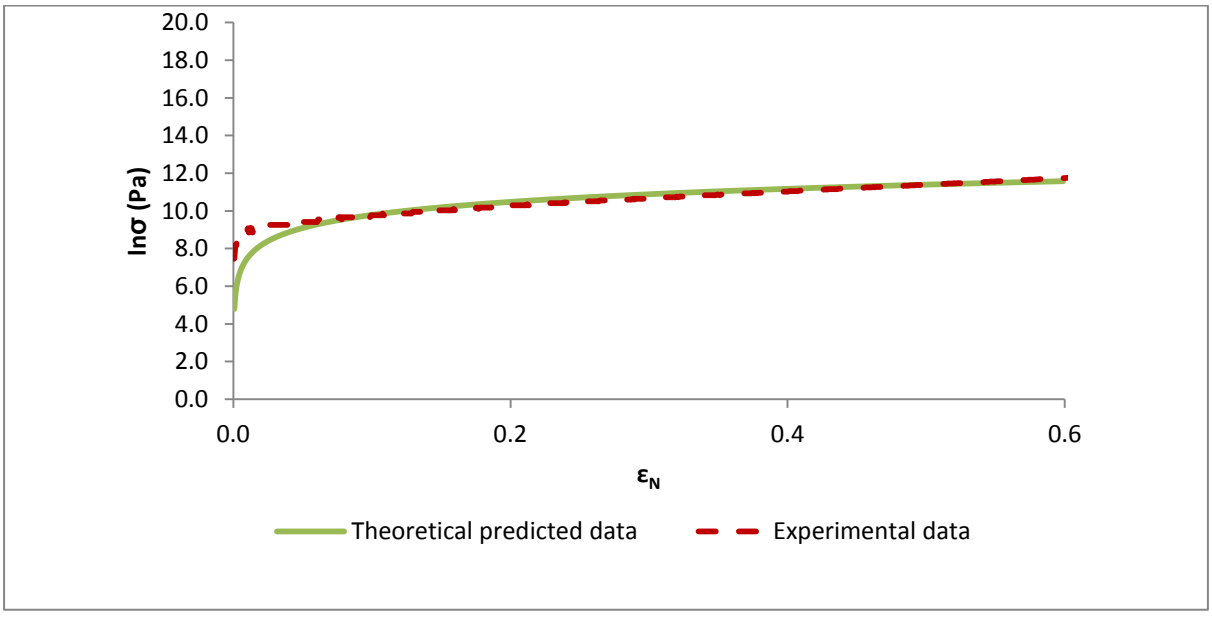

Figure 4-5: Adams plot for spray dried powder 1, showing the fit of the model to the experimental data.

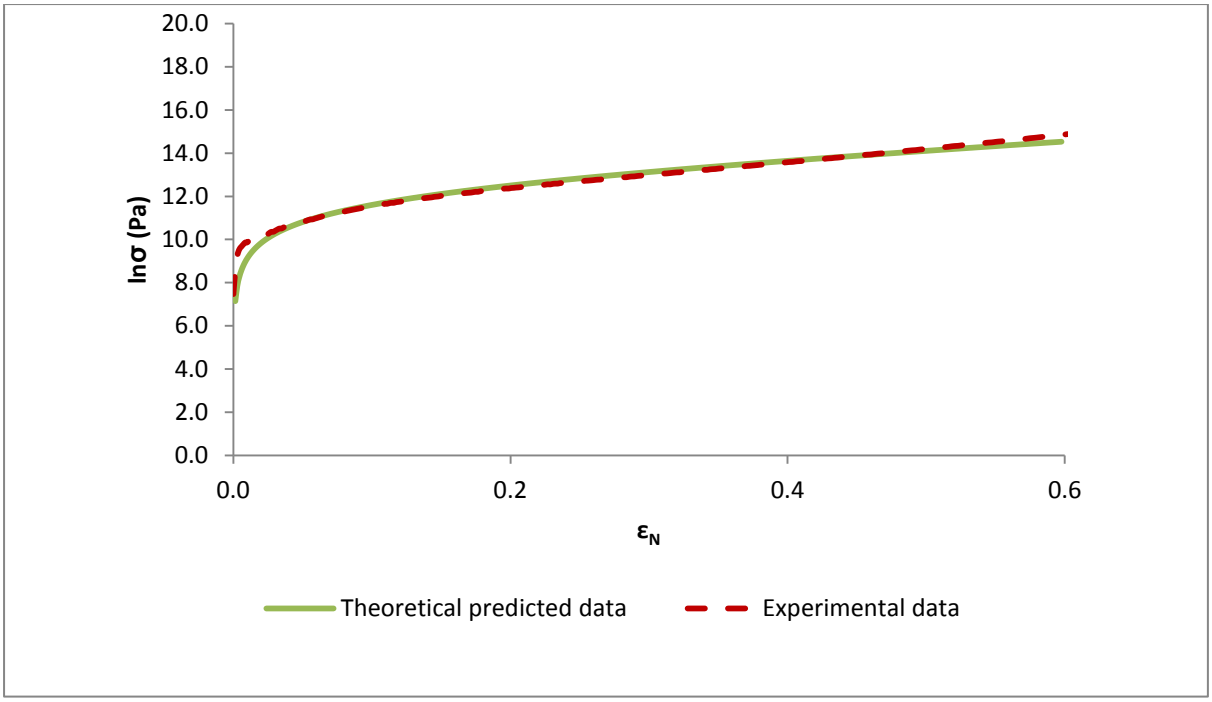

Figure 4-6: Adams plot for high shear agglomerate 1, showing the fit of the model to the experimental data.

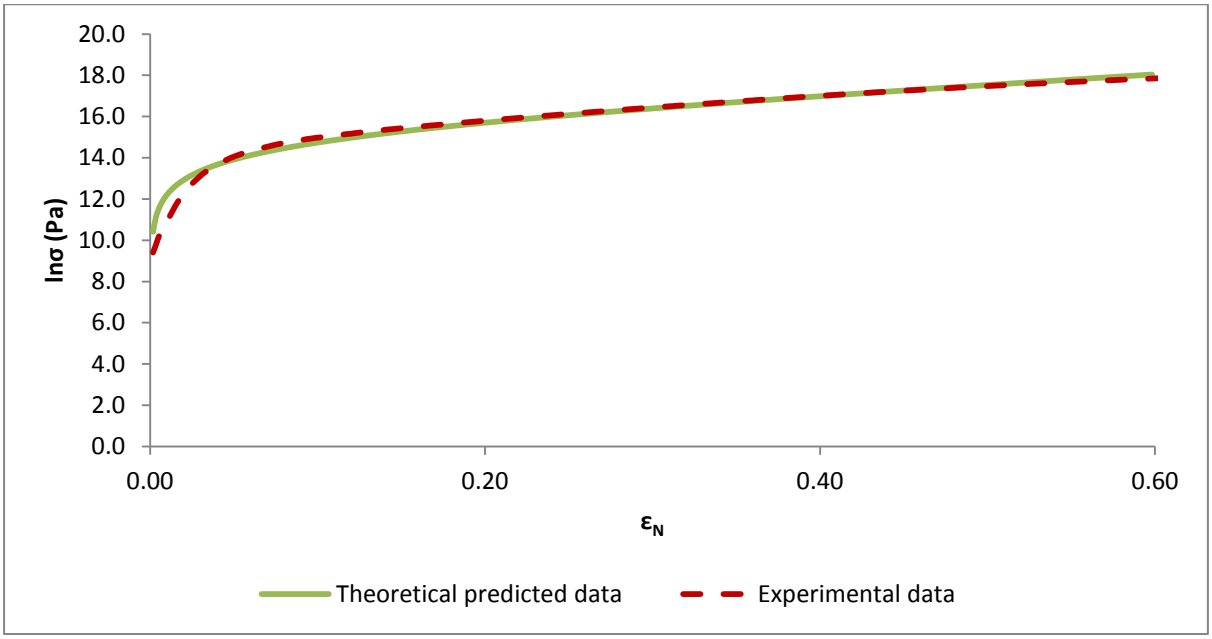

Figure 4-7: Adams plot for sodium percarbonate, showing the fit of the model to the experimental data.

An alternative to use of the Kawakita and Adams models is the density-stress compaction curve analysis approach developed for spray dried ceramic agglomerates by Lukasiewicz and Reed [55]. They determined that such a plot showed three approximately linear regions (see Figure 4-

8), with compaction within each region occurring via a different mechanism and the points denoting the transitions between regions denoted as yield pressures and joining pressures.

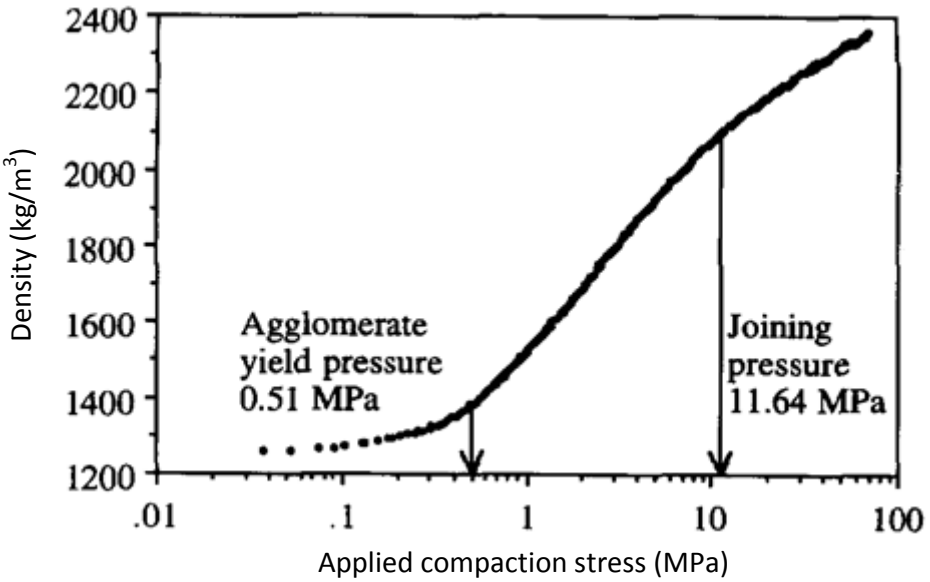

Figure 4-8: Density-stress compaction curve for agglomerated alumina powder pressed to 70 MPa in a lubricated die [56].

Within the region below the yield pressure, compaction occurs via rearrangement. Between the yield pressure (defined as the onset of deformation) and the joining pressure, deformation and crushing occur. At the joining pressure, compaction then moves into the third region where deformation of primary particles is occurring [56].

Compaction curves for Spray Dried Powder 1, High Shear Agglomerate 1 and Sodium Percarbonate can be seen in Figure 4-9, Figure 4-10 and Figure 4-11. Yield pressures and joining pressures were determined by fitting linear equations to each section of the three compaction plots and then calculating the point at which the lines intersect. In all three cases yield pressures were indentified. Joining pressures were identified for Spray Dried Powder 1 and High Shear Agglomerate 1 surfactant containing powders. However, in the case of Sodium Percarbonate a joining pressure could not be identified. This is potentially due to the high resistance to compaction seen for this powder or the lack of primary particle, leading to a joining pressure not being obtained.

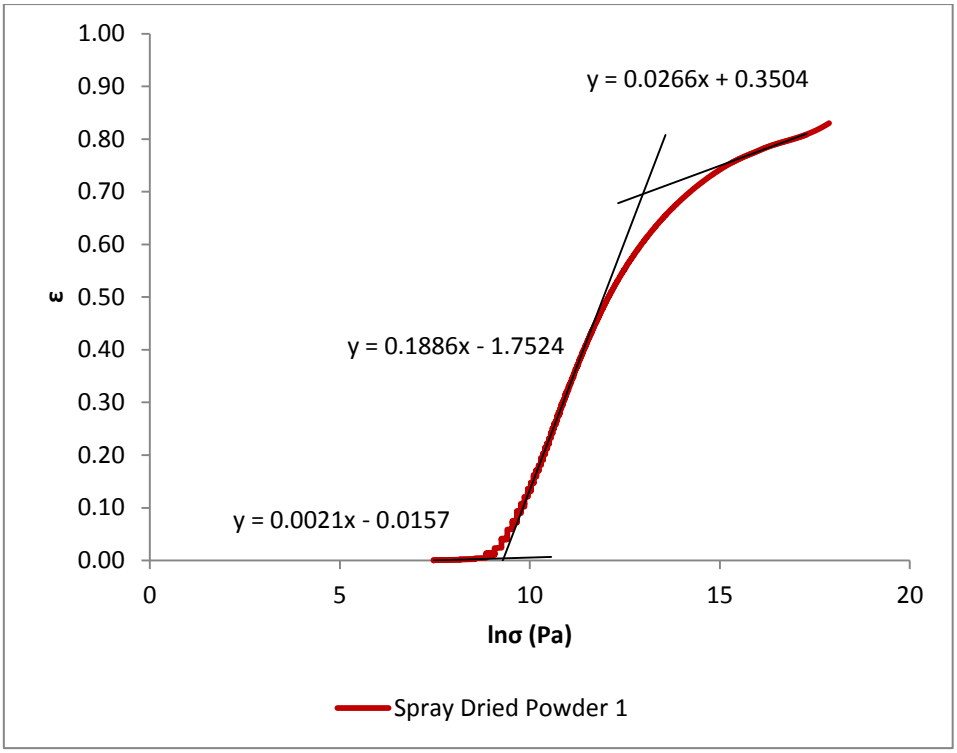

Figure 4-9: Strain-stress compaction curve for Spray Dried Powder 1.

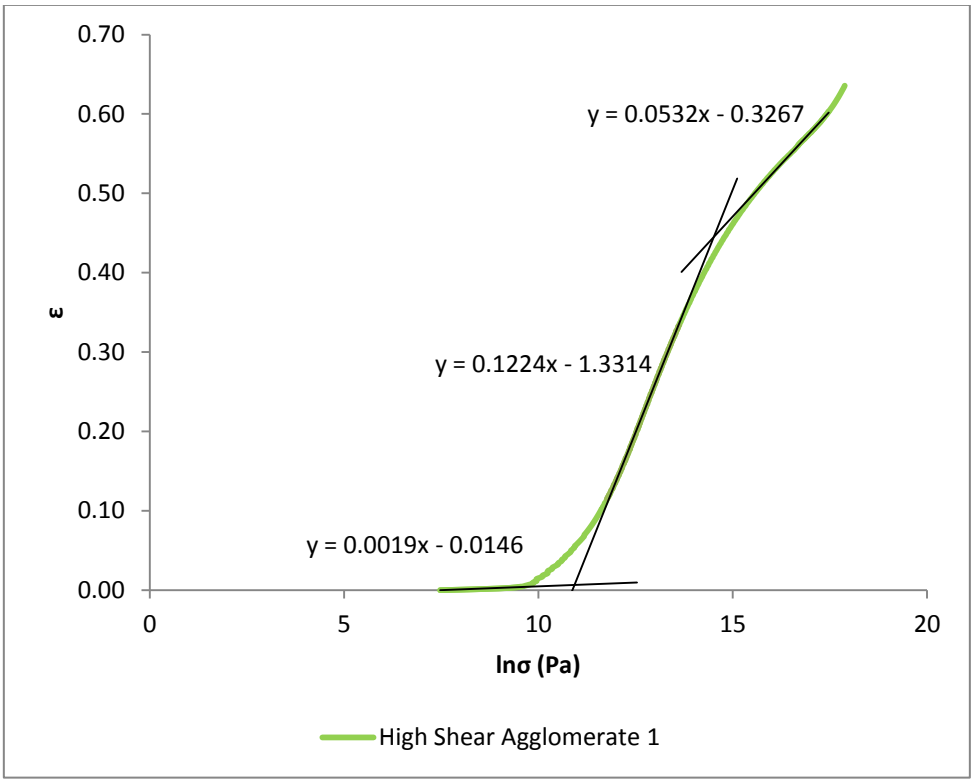

Figure 4-10: Strain-stress compaction curve for High Shear Agglomerate 1.

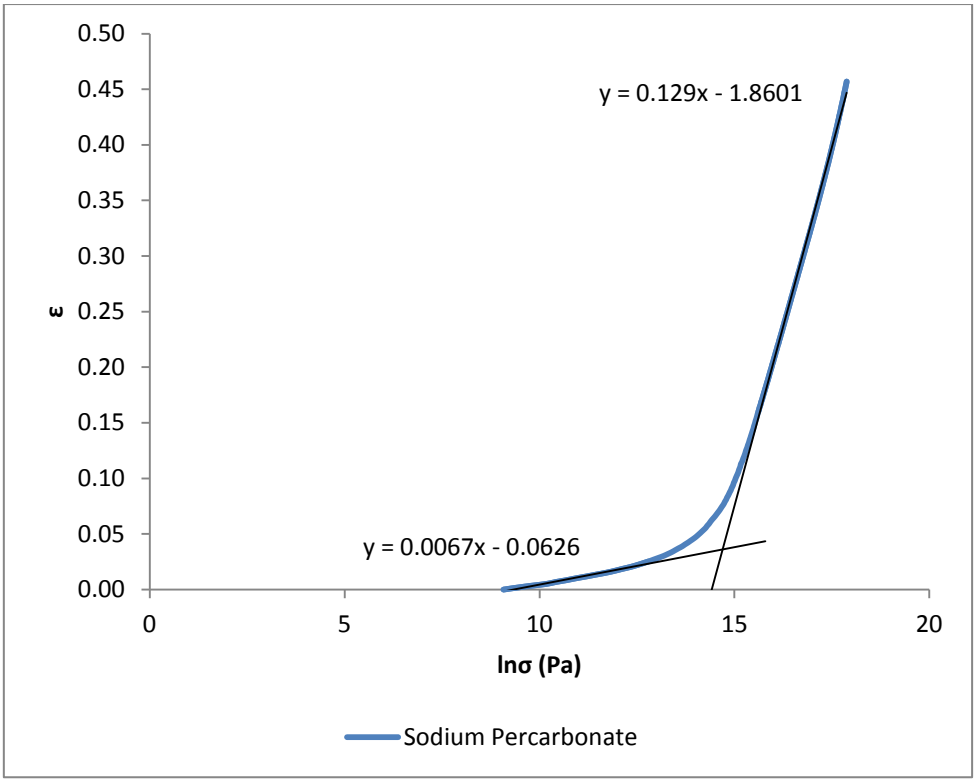

Figure 4-11: Strain-stress compaction curve for Sodium Percarbonate.

Table 4-2 gives parameters derived from fitting Eq. (2-6), Eq.(2-25) and compaction curves analysis to experimental data. The Adams τ_0' and Kawakita b^{-1} and yield pressures parameters rank the two powders in the order which would be expected from the stress stain curves shown in Figure 4-1. However, on the basis that:

I. The Kawakita model gave a better fit to the experimental data versus Adams over the range of data points studied.

II. The Kawakita model has a simpler form versus Adams, making it simpler to apply and draw conclusion from.

III. The compaction curve analysis method has no clear advantage over analysing data via the Kawakita model.

It will be the Kawakita model which shall be used for the remainder of this chapter.

Table 4-2: Kawakita b^{-1} and Adams τ'_0 parameters derived from the experimental data presented in Figure 4-1.

	a	b^{-1} (MPa)	α'	τ'_0 (MPa)	Yield pressure (MPa)	Joining pressure (MPa)
Spray Dried Powder 1	0.78	0.15	0.0	0.18	0.01	0.43
High Shear Agglomerate 1	0.53	0.50	3.8	0.90	0.06	2.02
Sodium Percarbonate	0.50	12.75	4.8	19.55	2.42	NA

Table 4-3 gives Kawakita a and b^{-1} parameters for a range of powders typically added to P&G's finished detergent powder products, see Appendix 3 for the corresponding stress strain and Kawakita plots. For the surfactant-containing powders Kawakita plots were found to linear between 0.5 MPa and 5.0 MPa, non-surfactant containing powders were found to be linear between 10.0 and 20.0 MPa with R^2 values greater than 0.99 in all cases.

Table 4-3: Kawakita parameters for P&G detergents powders, based on data between 0 and 10 MPa

Powder	Surfactant Containing	Aspect ratio	a	b^{-1} (MPa)
Spray dried powder 1	Yes	0.39	0.78	0.15
Spray dried powder 2	Yes	0.40	0.75	0.41
Spray dried powder 3	Yes	0.34	0.73	0.44
Spray dried powder 4	Yes	0.32	0.74	0.35
Spray dried powder 5	Yes	0.30	0.70	0.63
Spray dried powder 6	Yes	0.25	0.72	0.89
High shear agglomerate 1	Yes	0.19	0.53	0.50
High shear agglomerate 2	Yes	0.20	0.54	0.53
High shear agglomerate 3	Yes	0.20	0.43	0.45
High shear agglomerate 4	No	0.20	0.54	1.37
Extrudate 1	No	0.32	0.55	1.47
Sodium carbonate	No	0.16	0.50	5.91
Citric Acid	No	0.17	0.51	7.31
Sodium Percarbonate	No	0.16	0.50	12.8
Sodium Sulphate (fine grade)	No	0.11	0.48	12.0

The b^{-1} parameters presented in Table 4-3 show that the surfactant-containing powders manufactured via spray drying and high shear agglomeration are weaker than the non-surfactant-containing powders. This is perhaps unsurprising given that the surfactants used in the manufacture of these powders are either liquid or soft waxy solids at room temperature and

thus they would not be expected to enhance the strength of an agglomerate particle they are added to. The spray dried powders have the highest 'a' parameters, which reflects the fact that the 'a' parameter is related to the initial bed voidage [10] and thus this will be a reflection of the internal porosity typically found within spray dried detergent agglomerate particles [2, 57]. Also the internal porosity present with the spray dried powders leads to them having significantly lower bulk densities than the non-porous high shear agglomerates, reflected in the higher aspect ratios quoted in Table 4-3 versus the other powders tested.

For the strong non-surfactant-containing non-agglomerated powders higher levels of curvature were observed in the Kawakita plots versus those obtained for the surfactant-containing powders (see Figure 4-12 and Figure 4-13). This may be because these stronger powders undergo brittle fracture during compaction, with curvature arising from weak particles fracturing early in the compaction process and smaller stronger particles fracturing later and at higher stresses, leading to powders becoming harder to compact at high value of stress and strain.

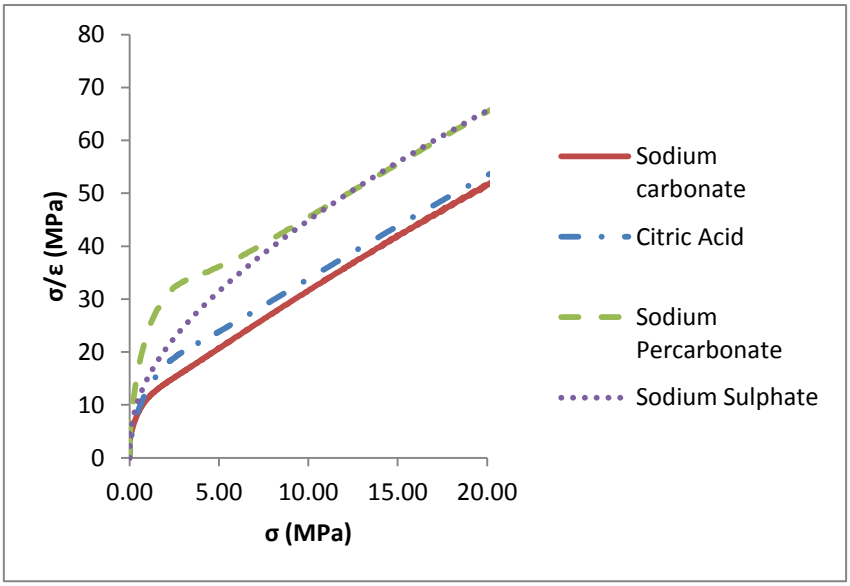

Figure 4-12: Kawakita plots for strong non surfactant containing powders

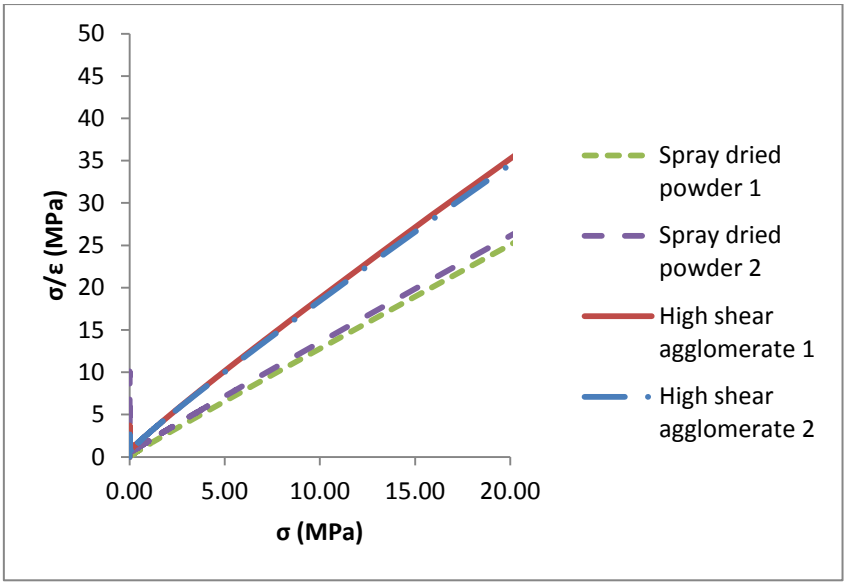

Figure 4-13: Kawakita plots for weak surfactant containing powders

4.1 Conclusions

Data presented in this chapter leads to two conclusions:

I. The Kawakita model appears to be able to yield parameters which reflect the mechanical properties of the powders tested.

II. If we assume that weak particles are more likely to form build-up than strong particles then it seems likely that it will be the surfactant-containing agglomerate particles which are typically responsible for build-up formation. However, because the mode of failure has not been determined it is possible that all agglomerate particles may not have failed exclusively via plastic deformation. This leads to the conclusion that some of the powders tested may have contained weak, brittle agglomerate particles which would not form build-up.

5. Initial Experimental Investigation

To determine the nature of build-up, in terms of its structure and composition and to determine if the literature based hypothesis stated at the end of Chapter two was likely to be valid, an initial investigation was performed. The specific goals of this investigation were to:

- Determine if differences can be identified in the manner in which two laundry detergent finished products (Ariel and Bold) build-up during auger filling.
- Determine how the build-up of a finished product (Ariel) is affected by filling under different process conditions, *e.g.* auger rotational speed, auger/tube clearance, spinner plate/tube clearance (see Figure 1-4).
- Determine if differences in finished product build-up formation reflects in compaction analysis results. It should be noted here that samples of Ariel and Bold detergent powder will be used in this chapter. These powders are complex powder blends containing a large number of powders blended together with small amounts of liquid surfactant sprayed on to them. Because of this complexity it will be a key objective of this chapter to determine if it is possible to predict auger filler build-up using compaction analysis of these complex materials or alternatively if simpler powders must be used in order to gain understanding regarding build-up formation which can then be reapplied to the more complex detergent finished products.
- Assess the structure of any build-up samples via SEM imaging and $CatSO_3$ analysis and in doing so confirm if it is the surfactant or non surfactant-containing powders which form build-up.

Ariel and Bold contain powders formed of both agglomerates and unagglomerated primary particles. For clarity all references to particles made within this chapter refer to the

macroscopically observed particles e.g. secondary particles in case of the agglomerated powders, and primary particles in the case of the non-agglomerated materials.

5.1 Initial Auger Filler Test Method

The auger filler experiments performed in this initial investigation were carried out, prior to the development of the experimental method described in section 3.2. The parameters used for the experiments discussed in this chapter were:

- Three revolutions per fill
- Two seconds between fills
- Auger rotational speed 840 RPM unless otherwise stated.
- Agitator type: flat blade running counter clock-wise during fills only at 20 RPM.
- Spinner plate / tube clearance: 8.0 mm
- The augers used are shown in Table 5-1:

Table 5-1: Dimensions of #16 and #22 auger tooling

Auger #	Auger diameter (mm)	Tube internal diameter (mm)	Auger/tube clearance (mm)	Pitch (mm)
#16	24.5	25.1	0.3	31.7
#22	34.3	35.5	0.6	38.0

- Material of construction: Stainless steel
- Surface Finish:
    - Auger: Mirror polished
    - Straight funnel: Smooth

The frequency at which powder was recycled to the hopper was 5 minutes or every 135 fills. In all cases 10 kg of powder was used. Figure 5-1 shows torque data for the packing of Ariel and Bold detergent powders, during the experiment torque measurements were made to an

accuracy of ±0.5 Nm which assumes that any rise in torque due to the presence of build-up will be at least 1 Nm. In the case of the Ariel detergent powder the experiment finished when the filler tripped with the final torque measurement taken after this event.

5.2 Build-up of Ariel and Bold Detergent Powder

To assess the ability of two formulated laundry detergent finished products to build-up during auger filling, samples of both Ariel and Bold laundry detergent were passed through the auger filler. Both powders were made via the manufacturing process shown in Figure 1-2. At the end of the Ariel auger filler experiment shown in Figure 5-1, the surface of the tube was found to be coated with build-up, at the end of the equivalent experiment for Bold detergent powder no build-up could be found on the tube surface. This finding points strongly to the conclusion that the rise in torque shown in Figure 5-1 is the consequence of build-up forming on the tube surface.

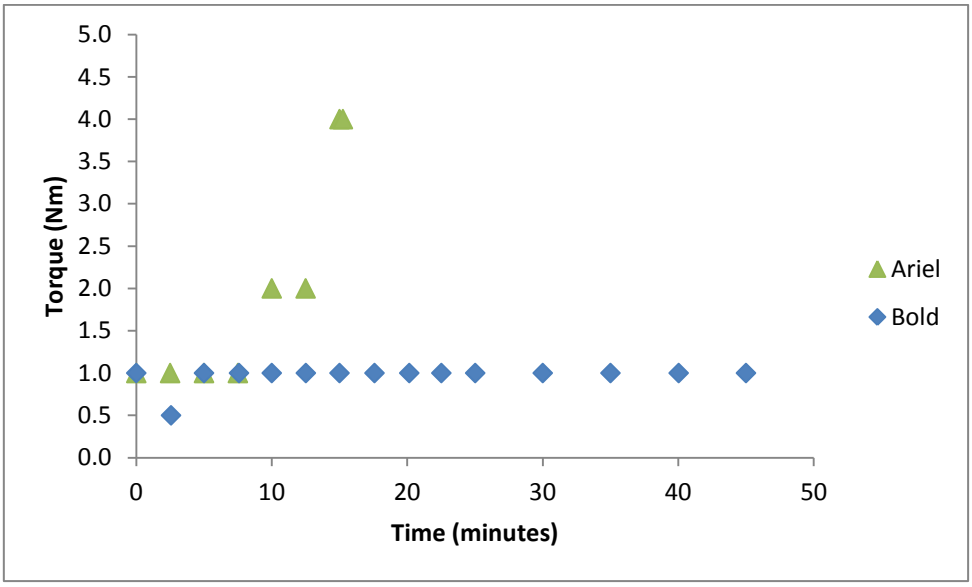

Figure 5-1: Auger filler build-up experiments for Ariel and Bold laundry detergents @ 840 rpm with #16 auger tooling.

5.3 Build-up of Ariel Detergent Powder Using #16 and #22 auger tooling

Figure 5-2 shows a comparison of the torque data generated in Figure 5-1 with Ariel detergent powder and #16 auger tooling with auger filling of Ariel detergent powder with #22 auger tooling.

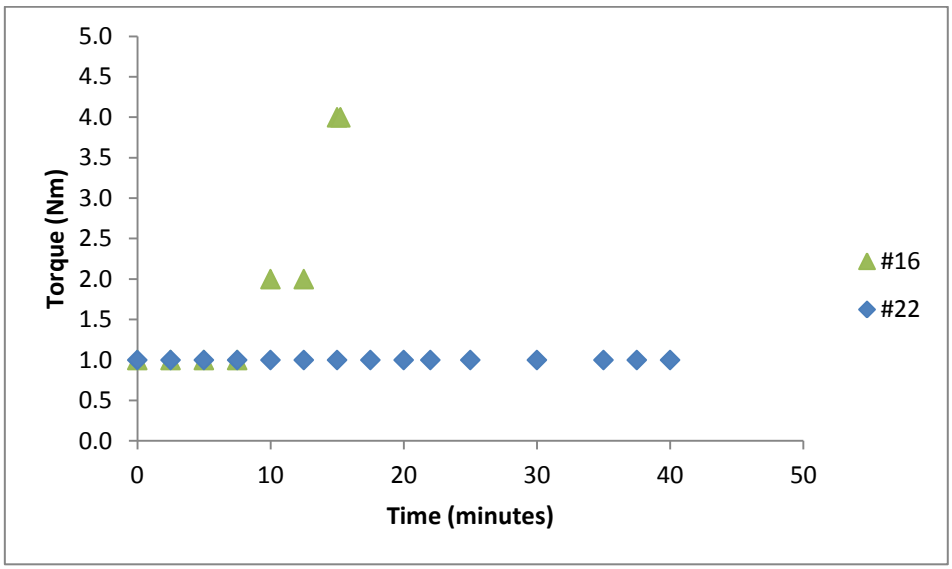

Figure 5-2: Auger filler torque data recorded during the filling of Ariel Detergent powder with #16 and #22 augers @ 840 rpm.

This comparison clearly shows that filling with the #16 tooling resulted in a sudden increase in torque leading to the filler tripping due to high current drawn. Filling with #22 tooling did not result in any measurable rise in torque. Images produced at the end of the experiments shown in Figure 5-2 can be seen in Figure 5-3 and Figure 5-4 clearly showing significantly more build-up was formed during the filling with #16 auger tooling.

Figure 5-3: Build-up on tube surface after the auger filling of Ariel detergent powder with a #16 auger.

Figure 5-4: Build-up on tube surface after the auger filling of Ariel detergent powder with a #22 auger.

It is clear that moving between the #16 and #22 augers had a significant effect upon the formation of build-up in the auger. To arrive at a possible reason for this we must consider the hypothesis stated in section 2.7:

- Build-up is formed due to stresses particles experience as they pass through the auger/tube clearance.
- The stresses particles experience are a function of the ratio of the particle size to the magnitude of the clearance.

It then seems reasonable to suggest that this difference in build-up formation may be the result of the auger/tube clearance being 0.3 mm for the #16 tooling and 0.6 mm for the #22 tooling. As the same powder was used in both cases the stress particles experience will be lower in the case of the #22 tooling and thus build-up will be formed more slowly. However, if we must also consider that Ariel is a blended powder comprised of agglomerated and non-agglomerated particles of differing size and mechanical properties and thus it is possible that increasing the clearance changed the nature of the particles entering the clearance.

5.4 Build-up of Ariel Detergent Powder at Varying Auger Rotational Speed

Figure 5-6 and Figure 5-5 show auger torque data generated during the auger filling of Ariel detergent powder at auger rotational speeds of 400, 700 and 840 RPM. Torque data has been plotted versus time and fills performed to illustrate the fact that changing auger rotational speed does not significantly impact filling rate. This is because the time take for the auger to rotate, 0.21 seconds at 840 RPM and 0.45 seconds at 400 RPM, is relatively small versus the delay between fills 2.00 seconds.

In the case of the 700 and 840 RPM data the experiment finished when the auger filler tripped due to high current. In the case of the 400 RPM data the auger continued to run, but with lumps

of build-up leaving the auger in a manner similar to that shown in the video titled 'Pilot Plant Auger Filler Build-up' found within the CD accompanying this thesis.

From the torque data generated at the three RPM values shown in Figure 5-5 and Figure 5-6 we can see that reducing auger rotational speed did prevent the auger tripping, but did not prevent the formation of build-up. This suggests that the deformation of particles as they pass through the auger/tube clearance is not significantly impacted by auger rotational speed, within the range studied.

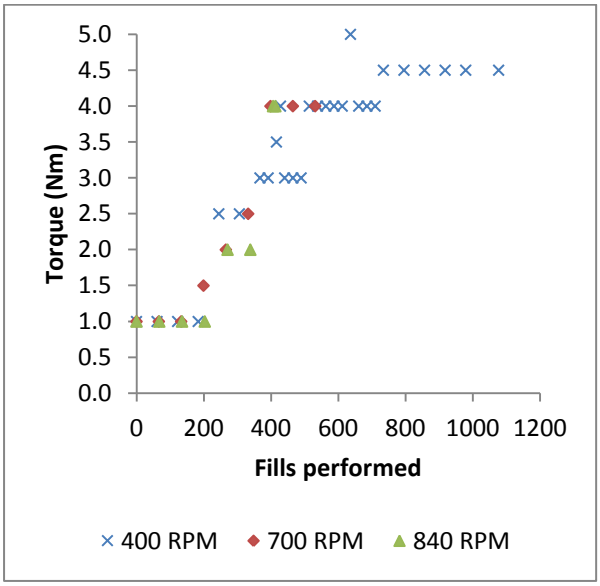

Figure 5-5: Auger torque data recorded during the filling of Ariel Detergent powder with #16 auger tooling at 400, 700 and 840 RPM as a function of fills performed.

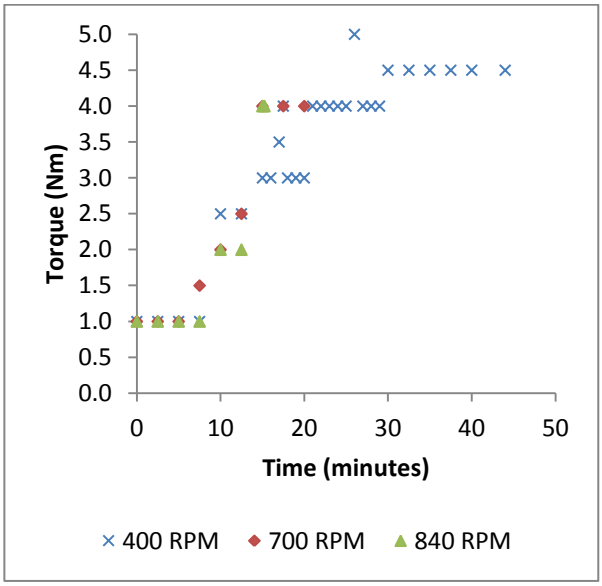

Figure 5-6: Auger torque data recorded during the filling of Ariel Detergent powder with #16 auger tooling at 400, 700 and 840 RPM as a function of time.

5.5 Build-up of Ariel Detergent Powder at Varying Spinner Plate Gap

Figure 5-7 shows torque data generated during the auger filling of Ariel detergent powder at 840 RPM with #16 auger tooling and spinner plate gaps of 9.0 and 7.5 mm. 7.5 mm was selected as the smallest possible spinner plate gap with smaller values leading to jamming events within 5 fills. These events were clearly different to build-up formation as they involved the sudden compaction of the entire bulk within the auger into a single coherent mass as opposed to the slower formation of a film on the tube surface associated with build-up formation. The 8.5 Nm torque reading at the end of the experiment with the 7.5 mm spinner

plate gap, was recorded following the powder within the auger becoming compacted due to build-up effectively reducing the spinner plate gap.

The two experiments shown in Figure 5-7 show little difference in the rate of torque rise associated with build-up formation compared to the differences previously seen when moving between #16 and #22 auger tooling. This is perhaps unsurprising when we consider that varying the spinner plate gap will tend to lead to changes in forces acting upon the entire bulk powder and not preferentially affect particles at the tube surface, as would be the case if auger/tube clearance is varied. The slightly more rapid rise in torque with the larger spinner plate gap is potentially related to differences in flow rate through the spinner plate gap, reflecting 4.2 kg being filled with the 7.5 mm spinner plate after 10 minute versus 4.4 kg with 9.0 mm spinner plate gap.

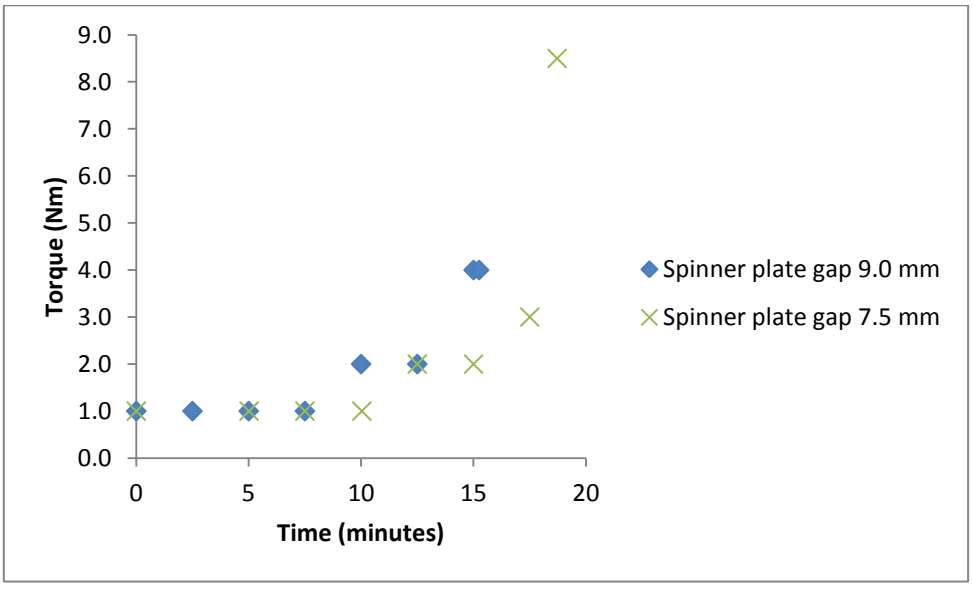

Figure 5-7: Auger filler torque data recorded during the filling of Ariel Detergent powder with 9.0 and 7.5 mm spinner plate gaps at 840 RPM.

5.6 Conclusions of Initial Auger Filler Experiments

While a means of tracking build-up formation via real time online torque measurements would be desirable, auger filler build-up experiments conducted as part of this investigation have shown that it is possible to track the formation of build-up using manual torque measurements.

Also during the investigation four parameters were varied:

I. Powder formulation *i.e.* Ariel and Bold.
II. Auger tooling *i.e.* #16 and #22.
III. Auger rotational speed *i.e.* 840, 700 and 400 RPM.
IV. Spinner plate gap *i.e.* 9.0 and 7.5 mm.

The results of this investigation have shown that changing powder formulation or auger tooling can significantly affect the formation of auger filler build-up while changes in auger rotational speed and spinner plate gap changes have much smaller impacts on build-up formation. These finding support the hypothesis that auger filler build-up is formed as result of particles passing through the auger/tube clearance. Also the experiments with #16 and #22 auger tooling support the theory that increasing the clearance and thus the ratio of the magnitude of the clearance to the particle size reduces the stress particles experience and thus reduces the rate of build-up formation.

5.7 Characterisation of Ariel and Bold Detergent Powder

To determine if it is possible to predict the formation of build-up based on laboratory scale measurements samples of Ariel and Bold detergent powder were characterised via gravimetric sieving and uniaxial compaction.

5.7.1 Particle Size Analysis

Figure 5-8 and Figure 5-9 show particle size distributions for Ariel and Bold detergent powders. The powders have broadly similar distributions with Bold containing a slightly higher level of particles <250 μm, potentially resulting from the presence of sodium sulphate particles within Bold. Comparing Ariel's particle size distribution with that of the #16 and #22 auger/tube clearances it can be seen that the #16 auger's 300 μm clearance is close to the mode particle size for the powder, suggesting that this would lead to a greater level of stress at the tube surface than was the case of the #22 clearance of 600 μm. However, because Ariel is a blend of powders with different particle sizes it must also be considered that the powders response to stress will not be constant with particle size and this may be more significant than the reduction in stress due to the large clearance.

Comparing the particle size distribution of Ariel and Bold in Figure 5-8 and Figure 5-9, Bold contains slightly more fine particles, reflecting in the D_{10} values quoted in Table 5-2, however, clearly both powders contain significant amounts of particles around 300 μm and thus it seems unlikely that the differences seen during the auger filling of the two detergent powders can be explained via particle size measurements. Thus it seems probable that the mechanical properties of the particles within the detergent powders must be different in some way leading to the differences in build-up formation seen during auger filling.

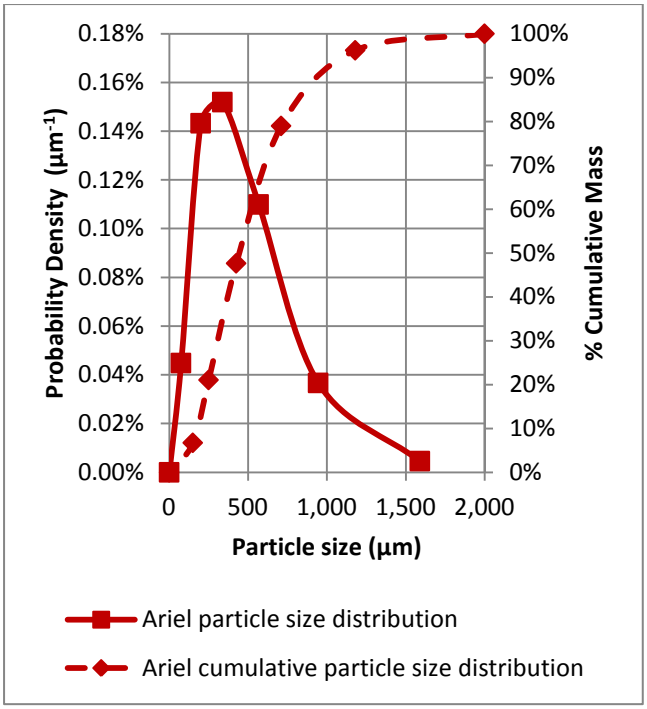

Figure 5-8: Particle size distribution and cumulative particle size distribution generated via gravimetric sieving for Ariel detergent powders.

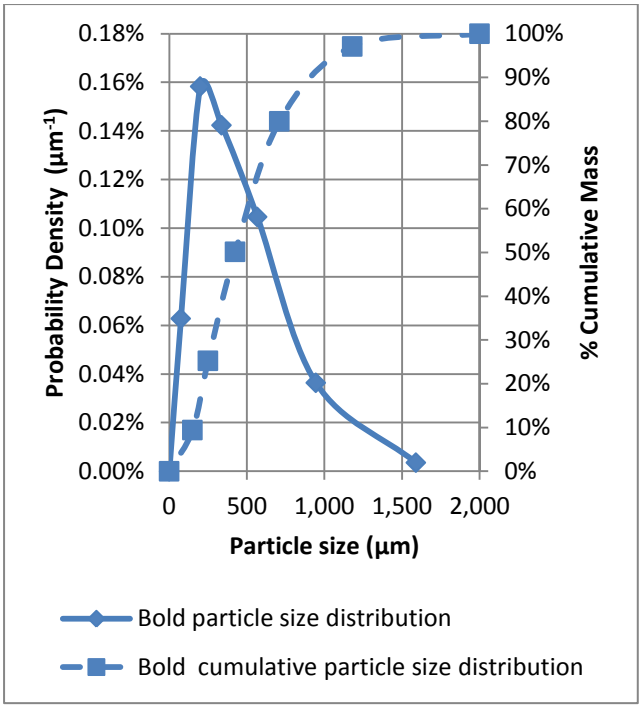

Figure 5-9: Particle size distribution and cumulative particle size distribution generated via gravimetric sieving for Bold detergent powders.

Table 5-2: Particle size measurements for Ariel and Bold detergent powders

	Ariel	Bold
D_{10} (µm)	175	150
D_{50} (µm)	440	425
D_{90} (µm)	925	910

5.7.2 Uniaxial Compaction

To gain some understanding of the mechanical properties of the two detergent powders uniaxial compactions were performed. These were conducted as described in section 3.2.3, but with a 25.4 mm die and 2.0 g of powder per compaction. Figure 5-10 shows typical stress strain curves for Ariel and Bold detergent powders. These plots show that the Ariel and Bold detergent powders have similar compaction profiles which are inconsistent with the large difference in their tendency to form build-up shown in Figure 5-1.

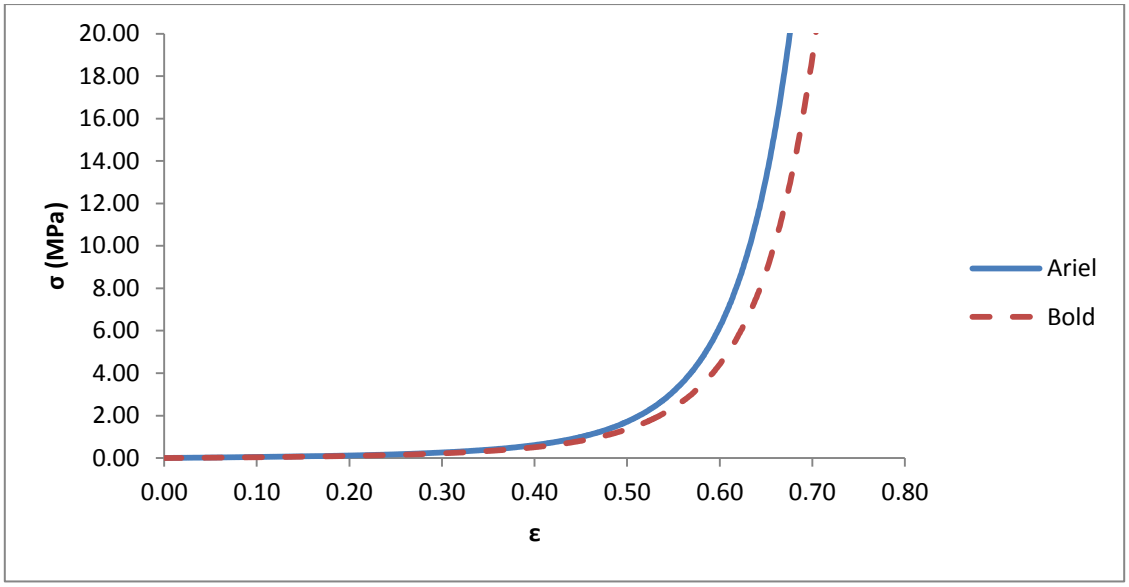

Figure 5-10: Stress strain curves for Ariel and Bold detergent powders.

As can be seen from the data plotted in Figure 5-11 Kawakita plots for Ariel and Bold are linear between 0.5 and 5.0 MPa, with a good fit to the experimental data achieved in all cases leading to R^2 greater than 0.99 in all cases. Table 5-3 gives the results of uniaxial compaction experiments performed with Ariel and Bold detergent powders, all results are the mean of three repeats and quoted in conjunction with standard errors. b^{-1} and 'a' parameters were determined using compaction data between 0.5 and 5.0 MPa. However, the results show that both powders have very similar mechanical properties as defined by the b^{-1} Kawakita parameter, suggesting that the processes via which these complex blended detergent finished products form build-up are more complex than can be reproduced via uniaxial compaction.

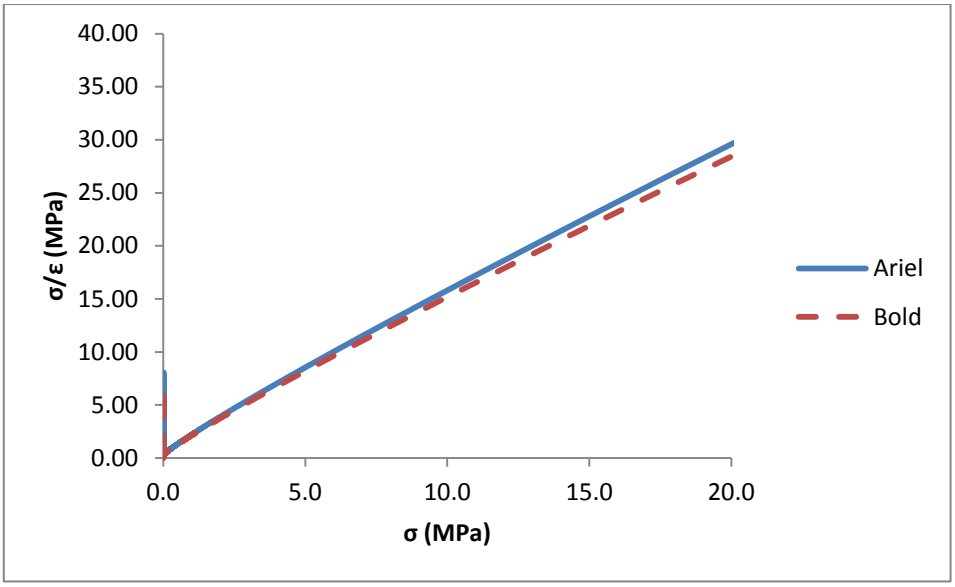

Figure 5-11: Kawakita plots for Ariel and Bold detergent powders.

Table 5-3: Results of Ariel & Bold compaction analysis

	b^{-1} (MPa)	a	Tablet strength (MPa)
Ariel	0.37 ± 0.02	0.62 ± 0.01	1.35 ± 0.01
Bold	0.37 ± 0.01	0.59 ± 0.02	1.93 ± 0.01

Tablet strength data presented in Table 5-3 shows that Bold formed tablets of higher strength than Ariel, however, the testing of a greater number of powder's will be needed in order to determine if this is related to the powders tendency to form build-up. From Figure 5-8 and Figure 5-9 it is clear that the Bold detergent powder contains more particles below 250 µm than Ariel. Also the data presented in Figure 5-1 was generated using auger tooling with a 300 µm clearance and thus fine particles below 300 µm present in the Bold detergent powder may play a role in preventing Bold from forming build-up.

5.8 Chemical Analysis of Ariel Detergent Powder Build-up

Compaction analysis results presented in section 4.2 indicated that the weakest particles typically found within a blended detergent formulation are those which contain surfactant. Assuming that these powders fail via plastic deformation, this suggests that surfactant containing powders are the primary cause of build-up formation. To provide further evidence

for this a sample of Ariel build-up collected at the end of the auger filler experiment shown in Figure 5-2, and two samples of Ariel Detergent powder were tested for $CatSO_3$.

$CatSO_3$ is defined as the percent by mass of cationic surfactant sulphate head groups (see Figure 2-14 and Figure 2-15) present within a given sample of powder. Table 5-4 show the results of this testing, the two repeats for the Ariel Detergent Powder show that the test method is able to give a value accurate to within ± 0.01% w/w. A comparison of the build-up $CatSO_3$ content with that of the Ariel detergent powder shows that the build-up contained significantly more surfactant than the powder blend from which it was formed indicating that the formation of build-up from the Ariel detergent powder involves a segregation process with soft low yield stress surfactant containing particles preferentially forming build-up. However, the Ariel powder contained two surfactant containing powders and thus more work is needed to determine if one or both of these powders led to the formation of the build-up.

Table 5-4: $CatSO_3$ content of Ariel detergent powder and build-up.

Sample	% $CatSO_3$ w/w
Ariel Detergent Powder Repeat 1	2.56
Ariel Detergent Powder Repeat 2	2.55
Ariel Build-up	3.96

From the knowledge gained here it is clear that, the formation of build-up does not involve the entire bulk but preferentially involves surfactant containing powders. For this reason, work following this initial investigation will focus on single component unblended powders, as their reduced complexity and more homogeneous particle properties makes the prediction of build-up formation more realistically obtainable.

5.9 Scanning Electron Microscope (SEM) Image of Ariel Detergent Powder Build-up

To further investigate the nature of the build-up formed by the Ariel detergent powder an SEM image of a sample of Ariel detergent powder build-up was generated. This image can be seen in Figure 5-12 with an optical image of the virgin powder generated using a Veho VMS-004D - 400x Optical USB Microscope presented in Figure 5-13 for comparison. Figure 5-12 shows that in contrast to the virgin powder build-up is a film of material with fine particles (possibly attrition products) on its surface. The film shows little sign of the particulate structure of the material from which it was formed, which is consistent with the hypothesis that for particles to form build-up large amounts of plastic deformation are required. This also suggests that the formation of build-up can be considered a form of pressure agglomeration similar to tableting, roller compaction, extrusion *etc.* However, it should also be noted that the build-up also appears to contain some particles embedded which have not undergone significant plastic deformation, the origin and role of these particles is unclear.

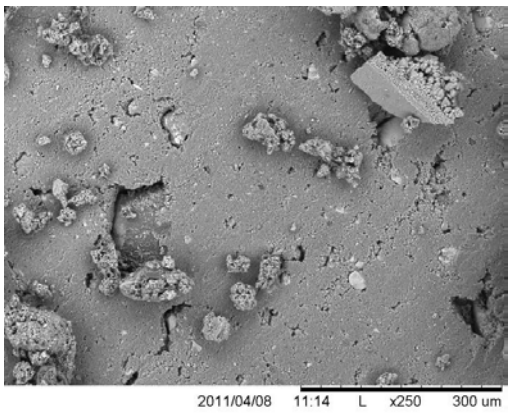

Figure 5-12: SEM image of Ariel detergent powder build-up.

Figure 5-13: Optical microscopy image of virgin Ariel detergent powder

5.10 Conclusions

This initial investigation of auger filler build-up has led to the following conclusions:

I. The auger filler test method employed in this investigation has differentiated between the ability of Ariel and Bold Detergent powders to build-up, with Ariel building-up rapidly leading to the auger filler tripping due to high current after only 15 minutes. Bold could be packed for 45 minutes with no build-up observed on the internal surface of tube.

II. The auger filler test method has also shown that the nature of build-up formation changes greatly when filling with #16 or #22 auger tooling, but is relatively insensitive to changes in auger rotational speed and spinner plate gap. The reduced level of build-up seen with the #22 auger tooling vs. the #16 tooling may be related to a large auger/tube clearance.

III. Particle size data showed that both powders contained large numbers of particles close to the #16 tooling's auger/tube clearance, suggesting that large stresses will be experienced by particles as they pass through the clearance. In the case of particles able to form build-up, this will lead to large degrees of plastic deformation and the formation of build-up. Other particles may undergo fracture, elastic deformation or smaller degrees of plastic deformation.

IV. Uniaxial compaction testing was performed but failed to illustrate differences between Ariel and Bold despite the fact that Ariel built-up rapidly during auger while Bold failed to form build-up. It is believed that is due to the complex nature of Ariel and Bold which are manufactured via the blending of a large number of powders with a wide range of mechanical properties and particle sizes. Differences between Bold and Ariel will be revisited in Chapter 9, where the finding of the intervening chapters will be utilised to

better understand why these two powders differed so widely in their tendency to form build-up.

V. Chemical analysis of the build-up produced by the Ariel detergent powder showed that the build-up contained significantly more surfactant than was present in the powder feed into the auger. This leads to the conclusion that build-up formation involves segregation mechanisms not replicated during uniaxial compaction.

6. Linking Macro and Laboratory Scale Measurements to Develop an Auger Filler Build-up Operating Space Model

The objectives of this investigation were to:

I. Determine which powder(s) within the Ariel detergent powder filled in Chapter 5 caused the finished blended powder to build-up.

II. Develop a standard test method for macro scale auger filler build-up testing.

III. Determine the repeatability of this test method and whether recycling of powder during the experiment impacts the result obtained.

IV. Determine the powder characteristics which lead to this formation of build-up.

6.1 Determining the Root Cause of Ariel Detergent Powder Build-up

The initial experimental investigation detailed in Chapter 5 showed that it was possible to determine and differentiate between the tendencies of two blended detergent powders to form build-up via the use of macro/pilot plant scale auger filler experiments. It was also shown that the build-up formed by the Ariel detergent powder blend contained significantly more cationic surfactant than the powder fed into the auger filler. As the powder blend contained two cationic surfactant contained powders it was unclear which was responsible for the formation of build-up in the auger filler. To confirm which of the two cationic surfactant containing powders was primarily responsible for the build-up formation seen during the auger filling of the Ariel detergent powder, samples of these two cationic surfactant powders were obtained. These powders will be referred to as SD1 and AG1, with the prefix SD indicating a powder manufactured by spray drying and AG indicating a powder manufactured by agglomeration, in the case of continuous high shear agglomeration. It was not possible to obtain samples of the powder batches used in the manufacture of the Ariel and Bold powders studied in Chapter 5 and because of this some compromises had to be made:

- SD1 is a spray dried powder and during this investigation was made at pilot plant scale, whereas the Ariel detergent powder was manufactured at full manufacturing plant scale.
- AG1 was made at the same scale and with the same equipment as the powder contained within the Ariel detergent powder blend tested in Chapter 5, however, was sourced from a different batch of production.

For reference the Ariel and Bold powders tested in Chapter 5, contained 48% w/w SD1 and in the case of Ariel 12% w/w AG1 and in the case of Bold 10% w/w AG1. Also Ariel contained no fine grade sodium sulphate while Bold contained 8% w/w which will be shown in Chapters 7 and 8 to influence build-up formation.

6.2 Further Development of the Auger Filler Test Method

In this section of the thesis the macro scale auger filler test method employed in Chapter 5 will be further developed using SD1 and AG1 as convenient subjects for this investigation to enable resolution of the question raised in section 6.1.

6.2.1 An Initial Auger Filler Experiment

An initial experiment was performed where 10 kg of AG1 was processed with the auger filler running constantly at 840 RPM (i.e. without pausing every three revolutions). This experiment ended when all the powder in the auger filler's hopper had passed through the auger. At the end of this experiment while significant build-up was observed on the tubes internal surface the torque required to turn the auger was 1.0 Nm. This showed that the assumption made in Chapter 5 that any rise in torque resulting from the presence of build-up on the tube's surface, would be at least 1.0 Nm was incorrect. Results will be presented in section 6.5 which explain why the rise in torque associated with the filling of AG1 is smaller than was the case in Chapter 5 with Ariel. All build-up was then removed from the auger filler and the torque required to turn

auger was assessed, taking care to turn the auger as slowly as is feasible. This showed that the torque required was 0.5 Nm, showing that during the filling of AG1 torque had risen from 0.5 Nm to 1.0 Nm.

Build-up was observed to leave the auger filler while the auger was turning and powder flowed through the auger leaving via the spinner plate. However, if the auger was made to rotate while powder was absent and the tube surface was coated with build-up, no build-up was observed to leave the auger. This leads to the conclusion that when build-up leaves the auger it is due to fresh build-up displacing that which already exists, rather than the auger acting to scrape or push build-up downwards towards the spinner plate. However, it must be considered that build-up leaves the auger exclusively via the spinner plate and thus the movement of the auger must influence this process forcing build-up to be displaced in the direction of the powder's downwards movement.

Also the observation that build-up forms while the auger is constantly rotating suggests that build-up is formed during the steady state operation of the auger and not exclusively during the auger rapid ramp to full speed during fill cycles.

Ten measurements of build-up thickness were made using Vernier callipers and samples of build-up which had left the auger filler via the spinner plate gap. The measurements had a mean value of 0.41 mm with a standard deviation of 0.11 mm. This result is perhaps surprising given that the auger/tube clearance is 0.3 mm. A potential explanation for this is that, as build-up is generated within the auger/tube clearance, build-up outside of the auger/tube clearance becomes displaced. Outside of the auger/tube clearance, build-up is not constrained by the auger. It is then possible for a degree of accumulation to occur, leading to build-up outside of the auger/tube clearance being of greater thickness than the clearance within which it was originally formed.

6.2.2 The Repeatability of the Auger Filling of SD1 and AG1

Macro scale auger filler testing of SD1 and AG1 was performed using the test method detailed in section 4.1. The following measurements were made:

I. Torque required to turn the auger manually.

II. Tube external surface temperature.

III. Mass of powder filled.

This then allows for the plotting of torque, temperature and average mass per fill vs fills performed, where fills performed per unit time was constant with time. The recording of measurements of tube surface temperature and mass of powder filled further ensures that the formation of build-up is detected in all cases, as if the build-up formed was of a particularly soft low yield stress nature, it is possible that a detectable rise in torque may not occur. Fills performed was selected as the parameter to plot measured variables against, as it seems reasonable to assume that if the interval between fills was increased build-up would form more slowly. Cumulative mass filled was also discounted as this would be influenced by powder bulk density and thus would be a less effective measure of the work done by the auger.

During the filling of AG1, lumps of build-up were observed to fall out of the auger and at the end of the experiment the internal surface of the tube was found to be completely covered with a soft, plastic film of build-up. During the filling of SD1 no build-up was observed and at the end of the experiment the internal surface of the tube was found to be entirely clean. Figure 6-1 and Figure 6-2 show plots of torque and tube external surface temperature vs. number of fills performed, for the auger filling of AG1 and SD1.

The auger filler experiments were performed using samples of SD1 and AG1 with repeats performed in both cases, using the same powder sample for both the initial and repeat

experiment. This was done to enable an assessment of the repeatability of the test method and secondly to determine if the experimental results were affected by the recycling of powder through the auger filler. Figure 6-1 and Figure 6-2 show the results of these repeats. In the case of the auger filling of AG1 (see Figure 6-1) an increase in torque and temperature occurred while in the case of SD1 this did not occur (see Figure 6-2). The results presented in Table 6-1 show that AG1 built-up with an associated rise in torque and tube surface temperature, and a drop in average mass filled (see Figure 6-3) in both the initial and repeat experiments. Average mass filled is the mass of powder collected within a period of time, divided by the number of fills performed during that period of time. SD1 showed none of these effects in either initial or repeat experiments. This shows that the test method is repeatable and can be used to differentiate the ability of powder to build-up.

Table 6-1: Experimental results for the auger filling of AG1 and SD1.

	Torque (Nm)		Tube Surface Temperature (˚C)		Average mass filled (g/fill)	
	Starting value	Ending value	Starting value	Ending value	Starting value	Ending value
AG1	0.5	1.0	22.2	29.4	18.2	16.3
AG1 (repeat)	0.5	1.0	21.8	29.4	18.5	15.8
SD1	0.5	0.5	15.2	15.8	11.3	11.6
SD1 (repeat)	0.5	0.5	21.7	19.3	10.9	10.9

Figure 6-1 shows the raw data from which the data relevant to AG1 presented in Table 6-1 was generated. Both the temperature and torque data show a period following the start of the experiment where values remain constant. This is then followed by an increase in both temperature and torque. During this experiment an attempt was made to measure torque values to the nearest 0.25 Nm. However, differences between the initial and repeat experiment show that results are only repeatable to the nearest 0.5 Nm (see torque values recorded at 480 fills in Figure 6-1). Because of this in future experiments values will be measured to the nearest 0.5 Nm.

Comparing the results obtained in Figure 6-1 and Figure 6-2 for AG1 and SD1 it seems likely that the build-up formed by the finished blend Ariel detergent powder in Chapter 5 was primarily caused by AG1. However, given that during the auger filling of Ariel in Chapter 5 torque values rose to values higher than the 1.0 Nm reached during the auger filling of AG1, it seems probable that the build-up generated by Ariel was not purely AG1. This suggests that the formation of build-up in powder blends such as Ariel is more complex than in the simpler case of AG1. Potentially in the case of Ariel, powders such as SD1 may embed into the build-up formed initially by AG1 and in doing so increase the strength of the build-up, leading to an increase in torque. Results informative of this phenomenon will be presented in section 6.5.

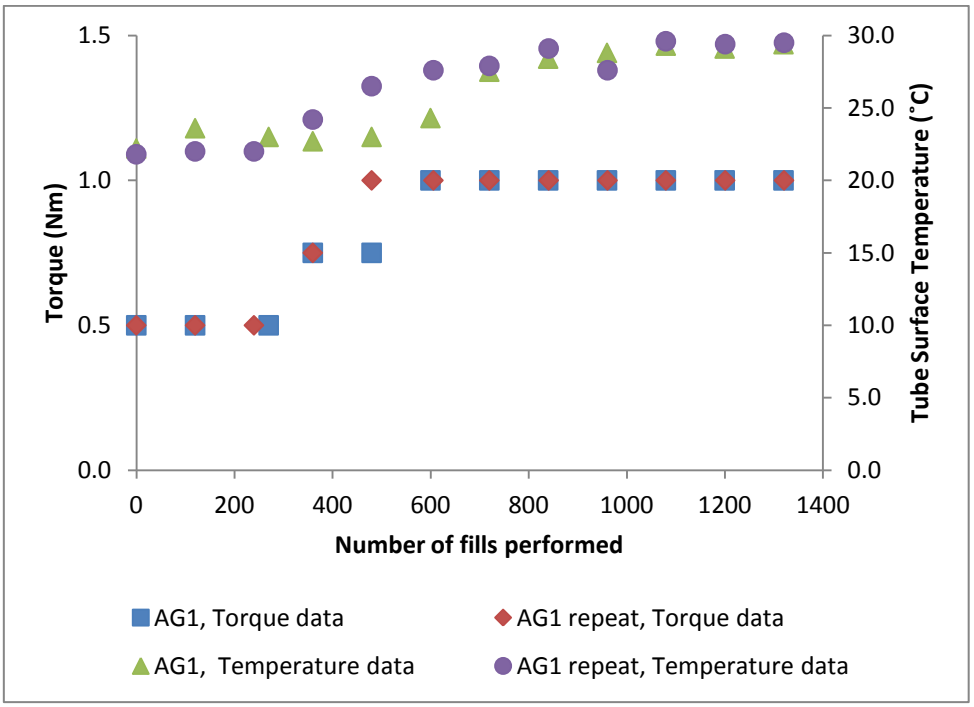

Figure 6-1: Torque and tube surface temperature readings collected during the auger filling of AG1

The tube surface temperature data presented in Figure 6-1, has poor repeatability in terms of the number of fills associated with the initial rise in temperature, with the rise coinciding with the rise in torque for the repeat experiment but not in the case of the initial experiment. This may be because the tube's surface is not completely covered with build-up at the time the initial rise in torque occurred. This suggests that torque better reflects the overall level of build-up

present, giving better repeatability than tube surface temperature which reflects only the temperature at the point the thermocouple is attached.

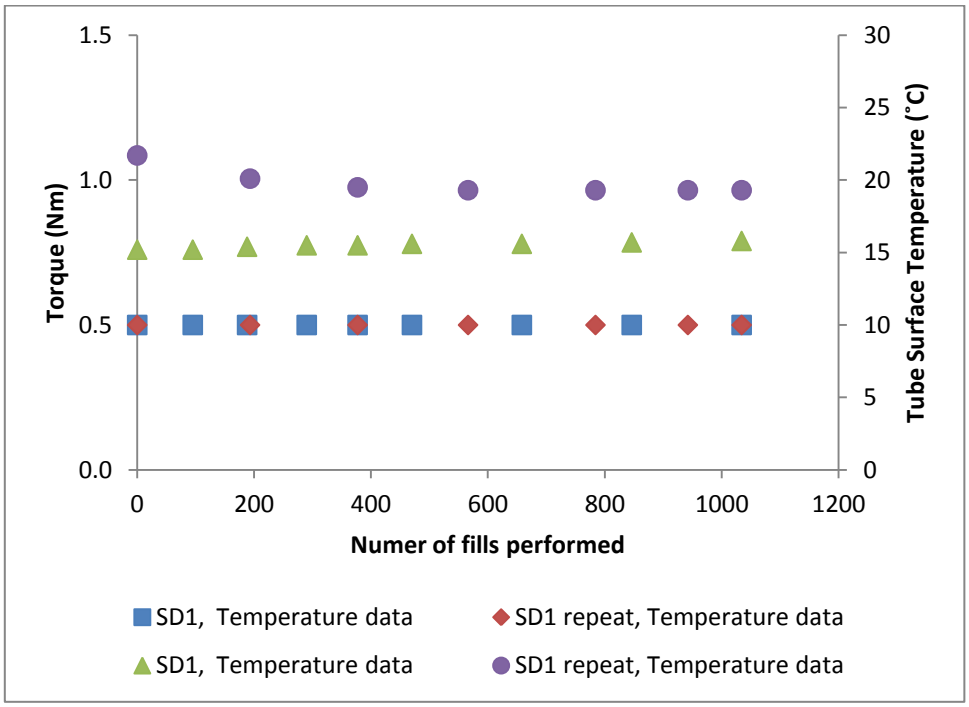

Figure 6-2: Torque and tube surface temperature reading collected during the auger filling of SD1

Figure 6-3 and Figure 6-4 show plots of average mass filled versus fills performed for the auger filling of SD1 and AG1, with the lower bulk density of SD1 (see values quoted in Table 6-2) giving rise to lower average mass filled values. Average mass filled was calculated by dividing the mass filled within a given period of time (5 to 10 minutes) by the number of fills performed during the same period of time. A comparison of Figure 6-3 and Figure 6-4 shows that for AG1 the average mass of powder filled reduced during filling, which did not occur during the filling of SD1. This leads to the conclusion that as build-up forms the volume within the auger available for powder flow reduces and thus the average mass per fills reduces as build-up forms.

There appears to be a reasonably high degree of variability in the absolute values of average mass filled values between the repeats performed for both SD1 and AG1. However, in both AG1 repeats a clear trend can be seen towards decreasing average mass filled values which cannot be seen in either of SD1 experiments. Therefore, if it is the existence of a trend towards

reducing average mass filled values resulting from build-up formation and not the absolute numbers which is of interest the data can be said to have good repeatability.

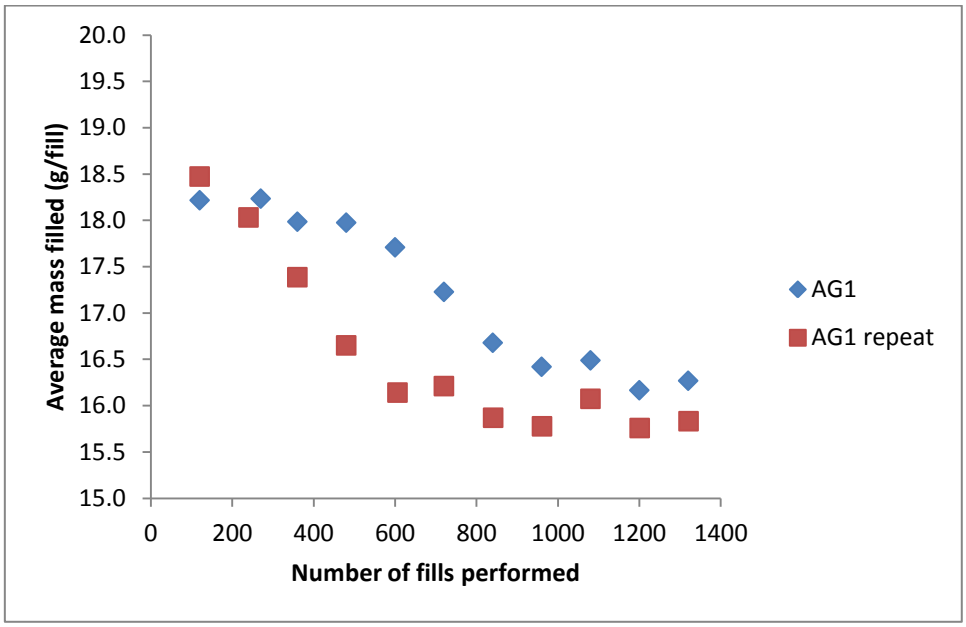

Figure 6-3: Variation in average mass filled for the auger filling of AG1

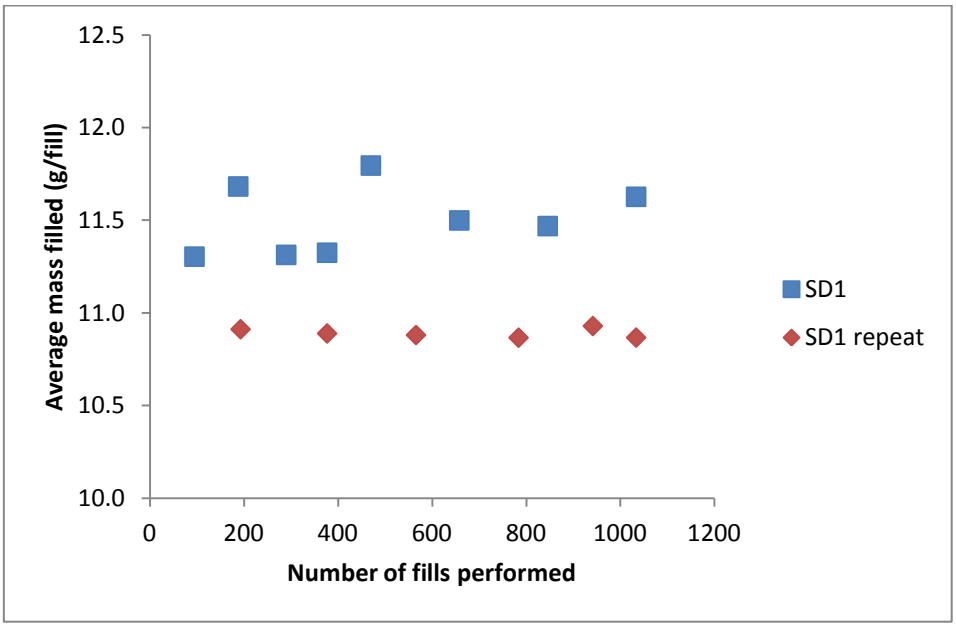

Figure 6-4: Variation in average mass filled for the auger filling of SD1.

If it is assumed that the auger's capacity reduction on a per fill basis is equal to the 23 mm^2 annular cross sectional area existing between the auger and the tube, multiplied by three times (three auger revolutions per fills) auger's pitch length (31.7 mm), a theoretical volume reduction

of 2223 mm^3 is arrived at. If the actual volume reduction is then determined using AG1's bulk density (782 kg/m^3) we arrive at values 2430 mm^3 and 3453 mm^3 for the initial and repeat experiments respectively. These values are of similar magnitude to the theoretical value, with the additional effect of build-up acting to reducing the spinner plate gap potentially accounting for the difference between the theoretical and actual values. This then supports the hypothesis that as build-up is formed and thus covers an increasingly large fraction of the tube surface this leads to a gradual reduction of the augers gravimetric output.

Standard deviations could not be calculated to complement the average mass filled values plotted in Figure 6-3 and Figure 6-4, because, average mass filled values are based upon the mass collected after a given period of time divided by the number of fills performed over the same period of time.

Figure 6-5 shows a plot of average mass per fill vs tube surface temperature, the plots shows that for both repeats tube surface temperature and average mass per fill are strongly correlated which supported the conclusions that trends observed in both measured parameters arose from a single cause *i.e.* the formation of build-up on the tube surface.

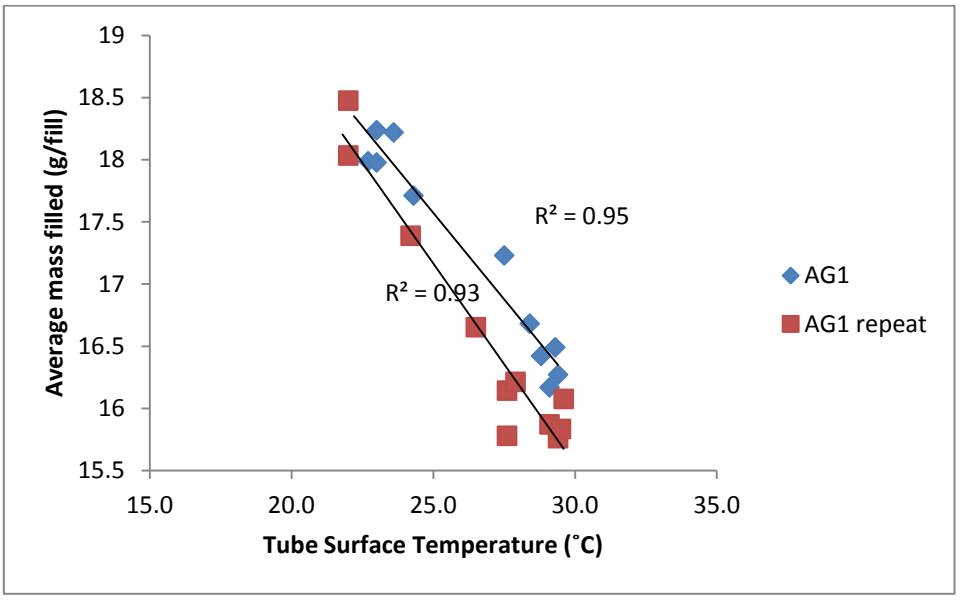

Figure 6-5: Average mass filled versus tube surface temperature for the auger filling of AG1

6.3 Characterisation of AG1 and SD1

The auger filler experiments discussed in section 6.2, showed that AG1 was able to form build-up during auger filling while SD1 did not. In this section the two powders will be characterised with the goal being to determine the powder characteristics which lead to powders forming build-up.

6.3.1 Physical properties of SD1 and AG1

Table 6-2 gives the results of some initial characterisation experiments, showing that AG1 contained a relatively high moisture content compared to SD1 and higher surfactant content which may explain the lower absolute density. AG1 has a relatively high moisture and surfactant content relative to SD1 which may have contributed to AG1 tendency while SD1 did not, although more work will be required to determine if this is the case. Agglomerate particle size data presented in Table 6-2, Figure 6-6 and Figure 6-7 shows that AG1 was finer than SD1 with a narrow span, however, clearly both powders contained many agglomerate particles similar in size to the auger filler clearance (300 μm) and thus differences in agglomerate particle size alone seem unlikely to be sufficient to explain the large difference in build-up formation seen in the auger filler experiments. Density measurements reflect the high levels of internal porosity typically found within spray dried powders such as SD1 and absent in the case of detergent powders made via high shear agglomeration such as AG1. However, while it is probable that this may lead to SD1 being weaker than AG1 and thus undergoing higher levels of deformation per unit stress (see Figure 6-8) it is currently unclear how this would affect the ability of a powder to form build-up.

Table 6-2: Physical characteristics of AG1 and SD1

	AG1	SD1
% Surfactant content w/w	24	18
Moisture content % w/w	6.1 ± 0.1	2.9 ± 0.0
% eRH	45.3 ± 0.3	35.1 ± 0.2
D_{10} (µm)	175	200
D_{50} (µm)	325	625
D_{90} (µm)	800	1100
Bulk Density (kg/m^3)	782	358
Absolute density (kg/m^3)	1829	2041

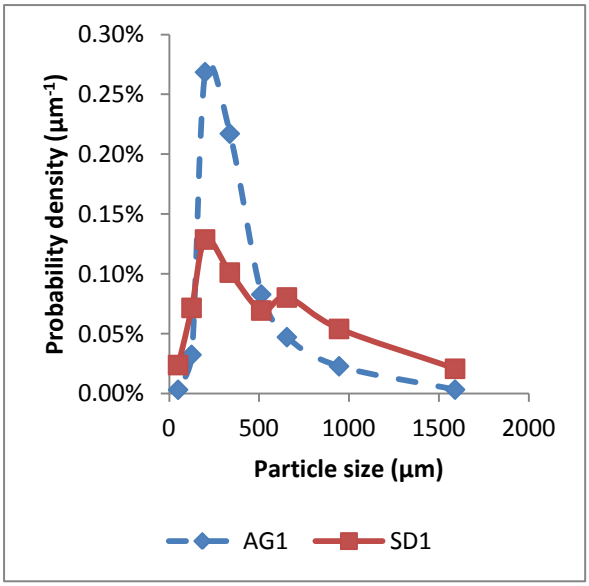

Figure 6-6: Agglomerate particle size distribution for AG1 and SD1

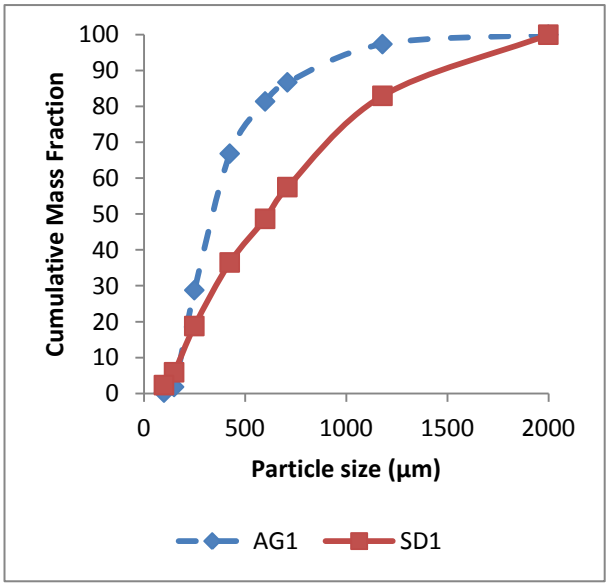

Figure 6-7: Cumulative Agglomerate particle size distribution for AG1 and SD1

6.3.2 Uniaxial Compaction of SD1 and AG1

Stress strain plots for compactions of SD1 and AG1 can be seen in Figure 6-8, the results show that SD1 has higher levels of strain than AG1 for a given level of applied stress, implying that SD1 is weaker than AG1.

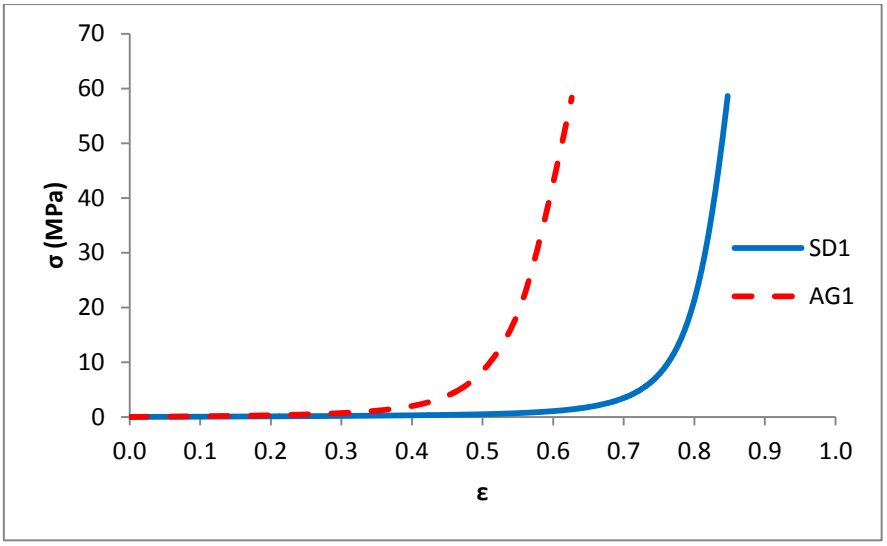

Figure 6-8: Stress strain plots for SD1 and AG1

The powder bed height and tablet thickness data for compaction of AG1 and SD1 are presented in Table 6-3. Final powder bed height was adjusted to remove the influence of equipment deflection using force displacement data generated in the absence of powder. The data shows that most of the deformation of the powder bed during the compaction was plastic leading to the conclusion that analysis of compaction data will be informative of plastic deformation.

Table 6-3: Bed height and elastic recovery parameters for compactions of SD1 and AG1.

	SD1	AG1
Initial bed height (mm)	13.0	6.0
Final bed height (mm)	1.99	2.24
Final bed height adjusted to remove equipment deflection (mm)	2.61	2.86
Tablet thickness (mm)	2.65	2.92

Figure 6-9 shows the first 5.0 MPa of the uniaxial compactions of AG1 and SD1, plotted to show the relationship defined by Kawakita and Ludde [18] (see Eq. (2-6)). Data below 5.0 MPa was selected for analysis based upon the assumption that no significant agglomerate particle rearrangement based compaction occurred during the compactions. An inspection of the data

presented in Figure 6-9 shows the majority of the data with this range is linear with some deviation during the initial compaction of the powder bed, in the case of AG1 this has little or no effect upon the fitting of the data to the Kawakita relationship illustrated by the 0.99 R^2 obtained. In the case of SD1 an R^2 value of 0.81 was obtained, to improve the R^2 value obtained data below 0.5 MPa was excluded from the analysis allowing for an R^2 of 1.00 which is deemed to be acceptable.

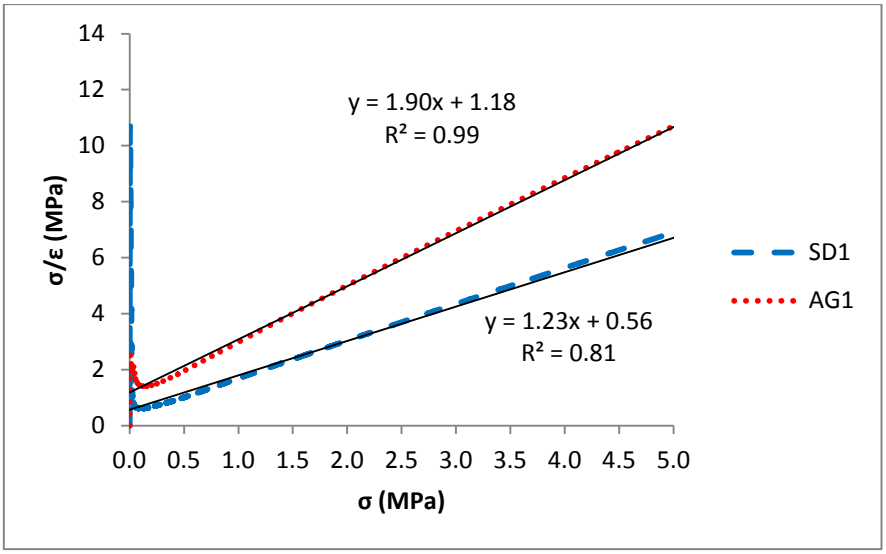

Figure 6-9: Kawakita relationships for uniaxial compactions of SD1 and AG1

Deviation from linearity in the early portion of the Kawakita plot has previously been observed by many others for example Samimi *et al.* [14] and Yap *et al.* [15] both observed these phenomena. Many possible explanations such as a transition from elastic to plastic deformation have been suggested. Regardless of the underlying cause of the lack of linearity, there is little value in applying the linear Kawakita model to such strongly non-linear data. Therefore, data below 0.5 MPa will be excluded in order to obtain a good fit with the experimental data.

Figure 6-10 shows data extracted from compactions of SD1 and AG1 for natural strains of 0 to 0.6, plotted to show the relationship first identified by Adams *et al.* [19]. In both cases the Adams model was fitted to the experimental data using a solver function to determine the values of α' and τ'_0 which gave the optimum fit to the experimental data throughout the full data range. A natural strain of 0.6 was found to give an associated stress of 0.40 MPa in the case of SD1 and 3.96 MPa in the case of AG1, indicating that a similar region was analysed similar to that studied via the Kawakita model. As can be seen in Figure 6-10 it was not possible to fit experimental data to the relationship proposed by Adams *et al.* [19] Eq. (2-25) across the full range of stresses studied. However a good fit was achieved between natural strains of 0.2 and 0.6.

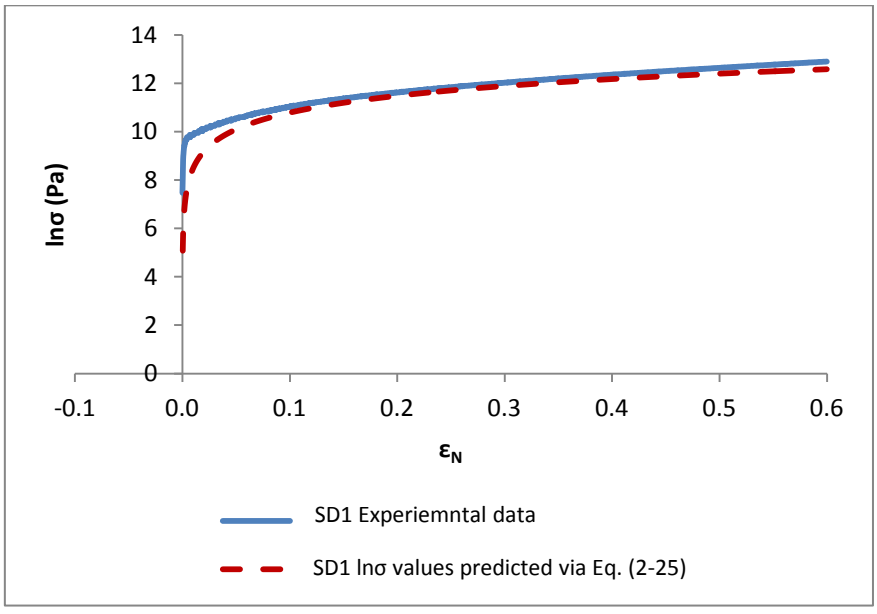

Figure 6-10: The Adams relationship for a uniaxial compaction of SD1

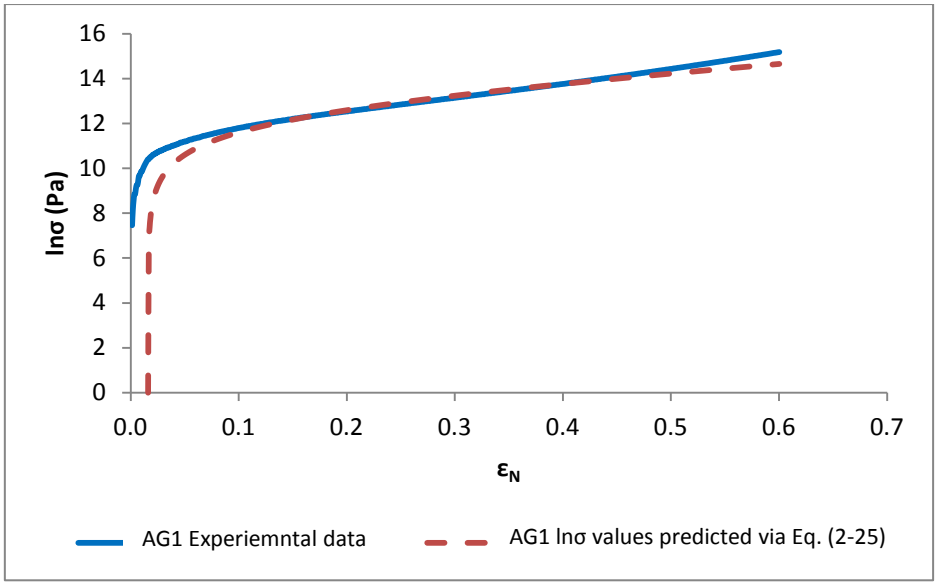

Figure 6-11: The Adams relationship for a uniaxial compaction of AG1

An attempt was also made to fit the Adams model to experimental data between ε_N values of 0.2 and 0.6 excluding the final terms in Eq. (2-25) which will tend towards zero at high value of ε_N, however, while this approach did allow for a good fit to be achieved within the linear region of the plot between ε_N values of 0.2 and 0.6 a poorer fit versus that shown in Figure 6-10 was achieved in the low stress region of the plot.

Figure 6-12 shows Heckel relationships for SD1 and AG1, values of relative density B were determined using the powder's absolute density (determined by helium pycnometry) and the in die powder bed's bulk density, measured throughout the compaction using force displacement data. The graphs show that experimental data contains significant curvature across a wide range of stresses as is common for this form of analysis [11], this is problematic as the Heckel model (Eq. (2-3)) is linear. As previously discussed both powders underwent elastic deformation in the high stress region of the compaction and thus it seems likely that the curvature observed in the high stress region is a result of the compact's bulk density approaching its absolute density and as a result deforming primarily by elastic deformation. The curvature in the lower stress region of the plot may result from many phenomena such as agglomerate particle

rearrangement or the plastic yield of the agglomerate particles, however, as with the curvature observed with the Kawakita plots in Figure 6-9 it may simply be an artefact of the models description of the powder bed's compaction.

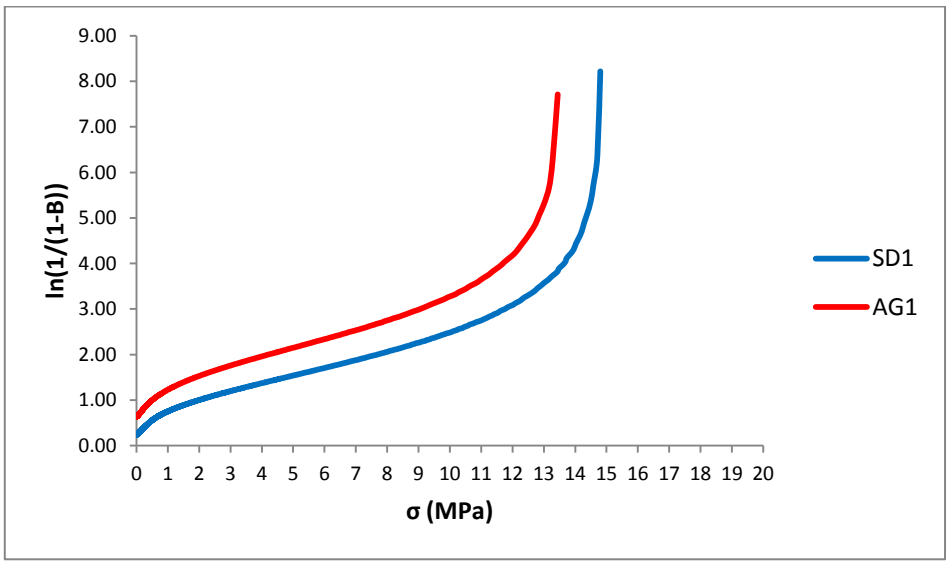

Figure 6-12: Heckel relationships for uniaxial compactions of SD1 and AG1.

There are two regions of the plot which could be considered to be linear: 0 to 0.5 MPa and 5 to 8 MPa. As can be seen in Figure 6-13 values of intercept and gradient have been extracted from these regions allowing for the calculation of Heckel A and K parameters. This shows that the region selected significantly affects the values of the Heckel A and K parameters.

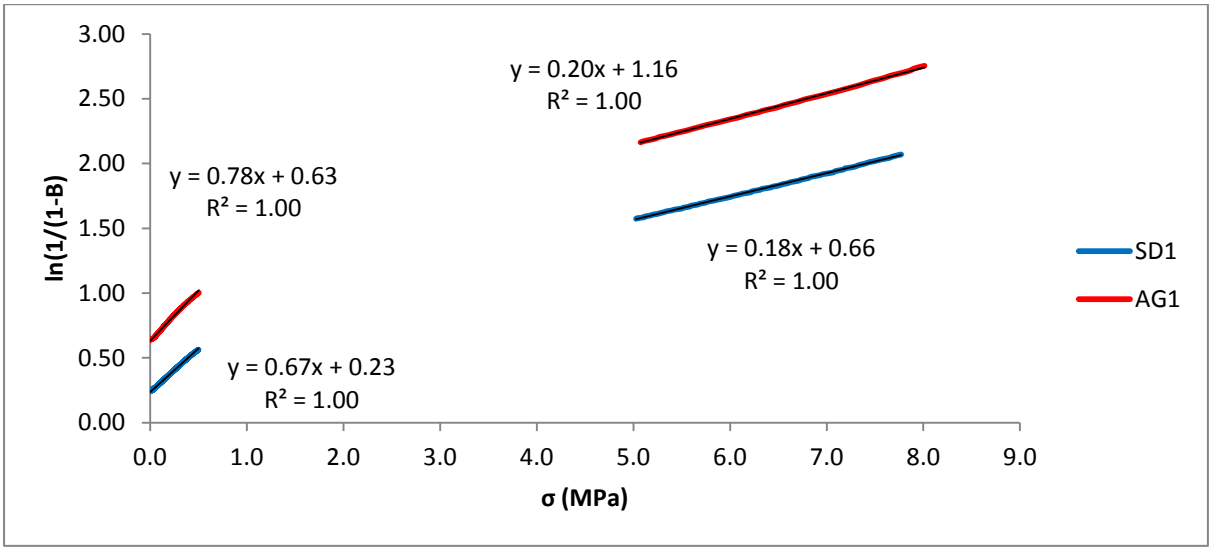

Figure 6-13: Heckel relationships for uniaxial compactions of SD1 and AG1 below 0.5 MPa and between 5 and 8 MPa.

Three uniaxial compactions of AG1 and SD1 were performed, and the data was analysed based upon the findings of the first compaction. It was found that:

- The Kawakita model gave a good fit to experimental data provided that data between 0.5 and 5.0 MPa was analysed reflecting in R^2 being above 0.99 in all cases.
- Due to the Adams model not relying on experimental data being linear, it was possible to apply the model over a wide range of natural strains (0 to 0.6). The model fitted the experimental data reasonably well between natural strains of 0.2 and 0.6 but not below 0.2.
- The Heckel model gave a good fit to experimental data provided that data between either 0 and 0.5 MPa or 5.0 and 8.0 MPa reflecting in R^2 being above 0.99 in all cases. However, between these regions experimental data was non-linear and it is unclear which linear region would yield the most representative data. Given the limited range of stresses over which R^2 values greater than 0.99 were obtained the Heckel model will not be used for the remainder of this thesis.

Excluding the early regions of both the Kawakita and Adams plots both gave a good fit to experimental data over a wide range of stresses and thus both could potentially be used. Additionally many authors have shown that a strong correlation exists between the Kawakita b^{-1} parameter and Adams τ'_0 parameter [9, 14, 15 & 19]. Therefore, given the simpler form of the Kawakita model, making comparisons between powders easier and simpler it will be this model which shall be used primarily for the remainder of this thesis.

Parameters extracted from uniaxial compactions of SD1 and AG1 are presented in Table 6-4 and Table 6-5, with initial aspect ratios being 0.4 in the case of SD1 and 0.2 in the case of AG1. Table 6-4 gives parameters known to be related to the failure stresses of the agglomerate particles within the compaction die. In all cases AG1's b^{-1}, τ'_0 and K^{-1} parameters between 5 and 8 MPa

are greater in magnitude than those extracted for compactions of SD1. The deviation from this trend in the case of the K^{-1} parameter derived from data between 0 and 0.5 MPa suggests that this data may be a particularly poor measure of the agglomerate particles failure stresses.

Given that auger filler build-up experiments concluded that AG1 was able to form build-up while SD1 did not and the data in Table 6-4 suggests that SD1 has a lower failure stress than AG1, it is clear that the parameters in Table 6-4 alone will not be sufficient to enable predictions of their ability to form build-up, possibly because SD1 is not failing via pure plastic yielding.

Kawakita 'a' parameters presented in Table 6-5 reflect the high levels of internal porosity typically present within spray dried powders such as SD1 and the lack of internal porosity typically present within powders made via high shear agglomeration such as AG1. Adams α' parameters suggests that more friction was present within the die during the compaction of the AG1 versus SD1. However, it is unclear how friction would influence the b^{-1}, τ'_0 and K^{-1} values presented for AG1 in Table 6-4 (see Chapter 7 for a more detailed investigation of aspect ratio effects).

Table 6-4: Mean values of the parameters of bulk compaction models

	Kawakita b^{-1} parameter (MPa)	Adams τ'_0 parameter (MPa)	Heckel K^{-1} parameter (MPa)	
Data range analysed	σ between 0.5 and 5 MPa	ε_N between 0 and 0.6	σ between 0 to 0.5 MPa	σ between 5 to 8 MPa
AG1	0.47 ± 0.03	0.91 ± 0.11	1.15 ± 0.05	3.69 ± 0.04
SD1	0.24 ± 0.02	0.48*	1.24 ± 0.07	5.29 ± 0.02

Table 6-5: Mean values of the parameters of bulk compaction models

	Kawakita a parameter	Adams α' parameter	Heckel A parameter	
Data range analysed	σ between 0.5 and 5 MPa	ε_N between 0 and 0.6	σ between 0 to 0.5 MPa	σ between 5 to 8 MPa
AG1	0.52 ± 0.01	3.81 ± 0.10	0.63 ± 0.01	0.94 ± 0.12
SD1	0.76 ± 0.01	0.01*	0.23*	0.66 ± 0.01

*Standard error less than 0.01

6.3.3 Diametric Tablet Strength Measurements

Following uniaxial compactions of SD1 and AG1 to a final compaction stress of 58 MPa, diametric tablet strength measurements were made. The results of these experiments are presented in Table 6-6. Values are the mean of three repeats quoted with standard errors. In the case of AG1 plastic contact flattening and a clear fracture of the tablet was observed similar to that shown in Figure 3-6. In case of SD1 neither contact flattening nor fracture of the tablets were observed. The large stress used in forming these tablets suggests that they will be of very low or zero porosity, which is confirmed by the porosity data shown in Table 6-7.

These results show that AG1 compacted into tablets which were weaker than those formed by SD1. This also suggests that while the Kawakita b^{-1} parameters presented in Table 6-4 shows that SD1 has a lower failure stress than AG1, following the application of a pressure which is sufficiently large to remove its porosity, SD1 compacts into a material which is stronger than AG1. This is potentially explained by SD1 being comprised of weak porous agglomerate particles which compact into a hard compact. While AG1's particles are stronger than SD1's, AG1's particles are weak in comparison with particles which could be considered to be strong/hard and thus AG1 compacts into a weak/soft compact. AG1's behaviour is common for weak/soft polymeric materials such as Poly(ethylene oxide) [50] which may reflect AG1's higher surfactant content, 24% w/w versus 18% w/w in case of SD1.

Table 6-6: Diametric Tablet Strength measurements for AG1 and SD1, performed following compaction to 58 MPa.

	Tablet Thickness (mm)	Tablet Strength (N)	Tablet Strength (MPa)
AG1	2.93 ± 0.01	57 ± 1	0.39*
SD1	2.70 ± 0.03	312 ± 12	2.35 ± 0.09

*Standard error less than 0.01

Table 6-7: Tablet porosity data for AG1 and SD1

	Tablet density (kg/m^3)	Absolute density (kg/m^3)	Porosity
AG1	1770	1829	3 %
SD1	1923	2041	6 %

It is proposed that AG1's low tablet strength reflects its soft plastic nature, which also reflects in its ability to build-up via compaction into a soft plastic material able to adhere to the auger filler. Conversely SD1 compact into a harder material which is unable to adhere to the tube surface reflecting the lack of build-up formed by SD1.

6.3.4 Scanning Electron Microscope (SEM) Images

Figure 6-14 and Figure 6-15 show SEM images of AG1 and SD1, clearly both powders contain agglomerate particles with a wide array of shapes and sizes. However, in the case of SD1 pores can be seen which demonstrate the porous nature of SD1.

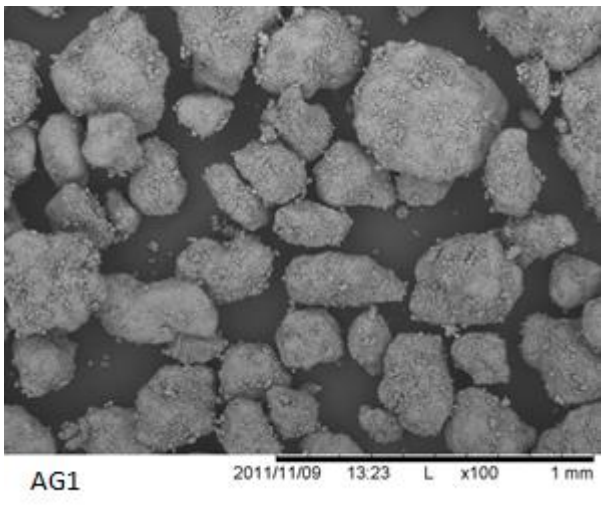

Figure 6-14: An SEM image of AG1

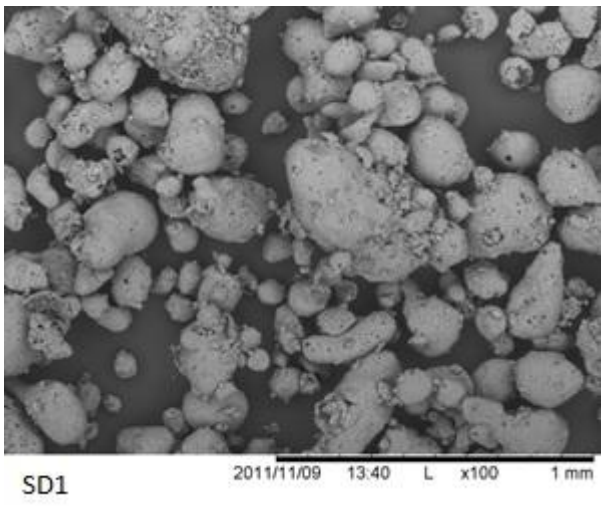

Figure 6-15: An SEM image of SD1

Figure 6-16 shows a sample of build-up collected during the auger filling of AG1, as was previously shown for the build-up of Ariel detergent powder the samples appear to be non-porous, with no identifiable sign of the agglomerate particles remaining.

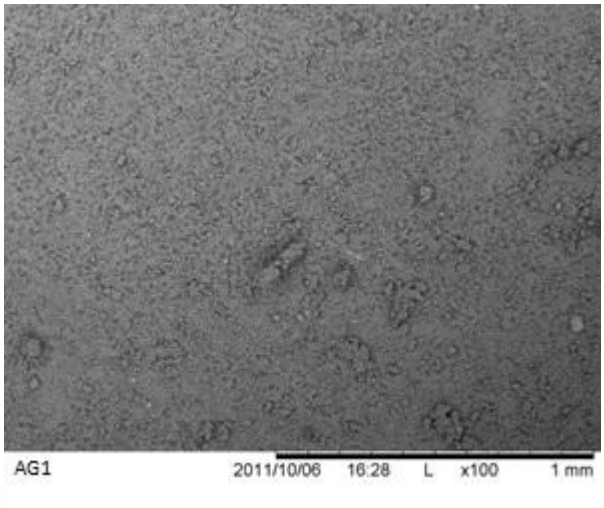

Figure 6-16: Auger filler build-up generated by AG1

Figure 6-17 and Figure 6-18 show SEM images of the fracture planes of compacts formed from SD1 and AG1, both images show that the agglomerate particles within the compact have undergone a large degree of plastic deformation and appear to be agglomerated into a single mass.

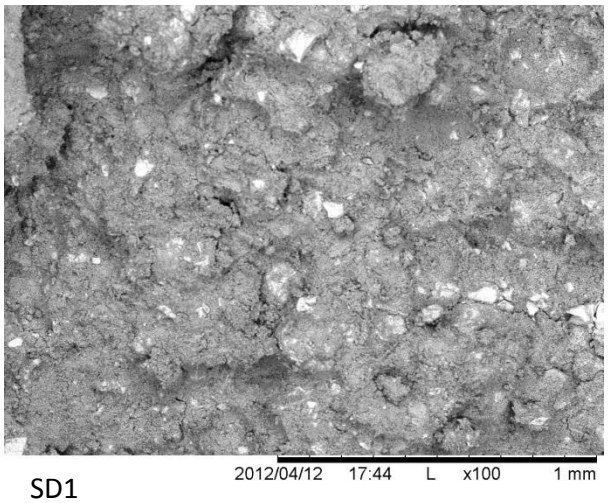

SD1

Figure 6-17: An SEM image of SD1's compact's fracture plane

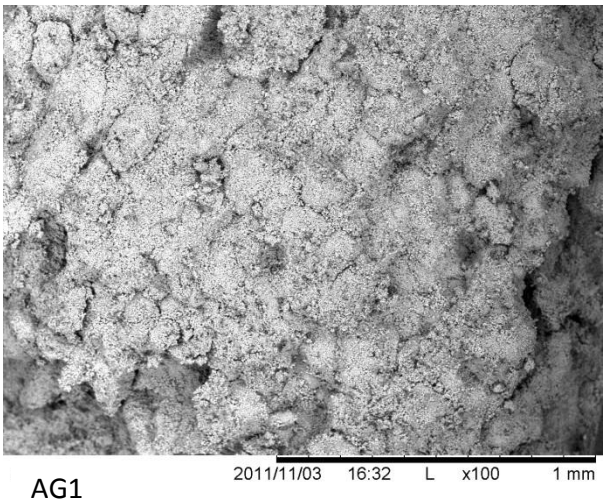

AG1

Figure 6-18: An SEM image of AG1's compact's fracture plane

6.4 Conclusions Derived from Auger filling and Characterisation of SD1 and AG1

The auger filling of AG1 and SD1 showed that:

I. AG1 was able to form build-up while SD1 was not.

II. AG1 was passed through the auger filler with the auger filler running continuously and also with the auger performing three revolutions at intervals of one second. In both cases build-up was formed suggesting that build-up is not primarily formed due to the auger's rapid acceleration from a stationary to rotating state.

III. Repeats of auger filler experiments performed with both powders showed that results obtained from auger filling were highly repeatable. The two repeats with both AG1 and SD1 were performed using the same sample of powder showing that recycling powder has no significant impact upon the results obtained.

IV. Auger filling of AG1 showed that it was possible to repeatably detect the formation of build-up using three separate measurements: manual torque measurements, tube temperature and mass per fill.

Laboratory scale characterisation experiments led to the following conclusions:

I. SD1 has a lower failure stress than AG1, which is believed to be related to SD1's highly porous structure which is common for spray dried powders.

II. Following compaction to a stress of 58 MPa, SD1 and AG1 formed compacts of low porosity (3% in case of AG1 and 6% in the case of SD1). SD1 formed tablets six times stronger than AG1 (2.4 MPa in the case SD1 and 0.4 MPa in the case of AG1).

Two hypotheses are proposed for SD1 failing to form build-up during auger filling experiments:

a. SD1's porous structure leads to it shattering rather than plastically deforming as it passes through the auger filler's 0.3 mm auger/tube clearance.

b. While both SD1 and AG1 are plastic materials able to form coherent tablets of low porosity, the material from which SD1 is formed is harder than that of AG1 which reflects in its higher tablet strength. This then leads to the SD1 agglomerate particles having hard surfaces which will develop lower real contact areas when brought into contact with the tube surface. In addition this leads to the conclusion that SD1 will compact into a harder material than AG1, less able to adhere to the auger filler's tube's internal surface via the generation of only small real contact areas.

It should be noted that these two hypotheses are not mutually exclusive and both may be occurring at the time.

6.5 Testing of Blends of AG1 and SD1

In this section of the thesis blends of SD1 and AG1 will be tested. The results generated will then be used to gain a better understanding of the interactions which may exist between powders within blends and the impact this has upon auger filler build-up formation.

6.5.1 Macro Scale Auger filling of Blends of AG1 and SD1

Auger filling of Ariel detergent powder in Chapter 5 led to a rise in torque plateauing at 4.5 ± 0.5 Nm, this powder contained both surfactant containing powders AG1 and SD1. Auger filling with AG1 and SD1 in section 6.2 showed that the AG1 powder was able to form build-up while SD1 did not, however, the build-up formed by the AG1 powder led a rise in torque plateauing at 1.0 ± 0.25 Nm significantly lower than that arising from the build-up formed by the Ariel detergent powder. Characterisation of the AG1 and SD1 powders in section 6.3 showed that SD1 compacted into a material significantly stronger than that formed by AG1, this suggests that if a blend of AG1 and SD1 were auger filled the build-up generated may lead to a rise in torque to values greater than 1.0 Nm.

To determine if this initial hypothesis is correct three blends of AG1 and SD1 were prepared, by mixing for 30 seconds in a Forsberg twin shaft paddle mixer. The paddle mixer is known to impart a high level of shear to the powder blend and achieve good mixing with a period of time considerably shorter than 30 seconds [58]. For each blend 10.0 kg of powder was prepared at the ratios of AG1 to SD1 quoted in Figure 6-19. These powders were then passed through the auger using the standard test method developed in section 6.2.

As can be seen in Figure 6-19 the blends with highest levels of AG1 and SD1 behaved in a manner similar to that of the pure AG1 and SD1 powder packed in section 6.2 of this thesis. However the 1:1 bend AG1:SD1 generated build-up which led to a rise in torque plateauing at 2.5 ± 0.25 Nm. This suggests that although SD1 is not able to build-up when filled in its pure form in the presence of a sufficient quantity of a build-up forming powder such as AG1 it is then able to influence the properties of the build-up, leading to higher torque values and a higher probability of the filler tripping due to high torque drawn by the auger filler's motor.

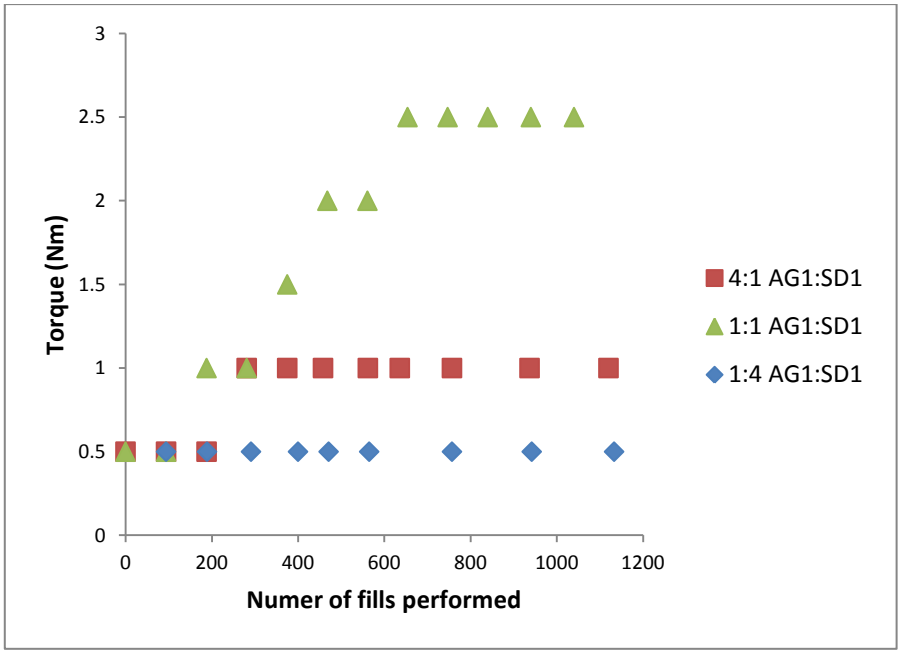

Figure 6-19: Torque data generated during the auger filling of blends of AG1 and SD1.

6.5.2 Uniaxial Compaction and Tablet Strengths for Blends of AG1 and SD1

Figure 6-20 shows Kawakita plots for blends of SD1 and AG1 (samples taken prior to auger filling), as was found with pure samples of SD1 and AG1 the Kawakita model provided a good fit to experimental data within the range 0.5 to 5 MPa, with R^2 values greater than 0.99 in all cases. Examination of the values in Table 6-8, Figure 6-21 show that neither the b^{-1} parameter nor tablet strength vary linearly with blend composition and remain approximately constant until some critical concentration of SD1 is reached.

The results presented in Figure 6-22 show that a transition from non-build-up forming powders to build-up forming powders occurs between tablet strengths of 0.46 and 0.90 MPa. This is possibly because, for powders to form build-up, they must not only contain agglomerate particles of low failure stress resulting in a low b^{-1} parameter, but must also fail plastically reflecting in an inability to form a strong tablet. This theory is supported by other weak plastic materials such as Poly (ethylene oxide) lacking the ability to form strong tablets [50]. However, more work is required to confirm that this would also be true for a wide variety of powders and or powder blends.

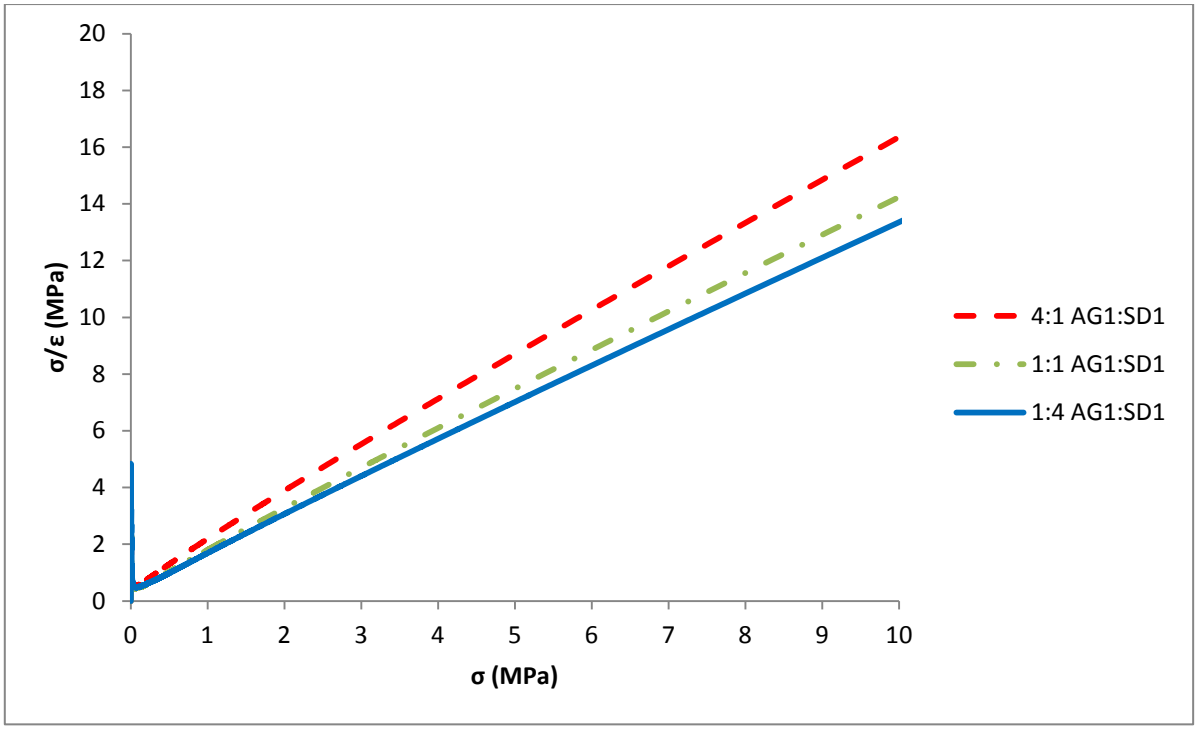

Figure 6-20: Kawakita plots for uniaxial compaction of three blends of AG1 and SD1.

Table 6-8: Kawakita parameters and tablet strengths for pure and blended powders containing AG1 and SD1

Blend w:w AG1:SD1	a	b^{-1} (MPa)	Tablet Strength (MPa)	Maximum auger filler torque (Nm)
1.0:0.0	0.52 ± 0.01	0.47 ± 0.03	0.39*	1.0 (build-up observed)
0.8:0.2	0.60 ± 0.01	0.32 ± 0.01	0.33 ± 0.01	1.0 (build-up observed)
0.5:0.5	0.70 ± 0.01	0.24 ± 0.01	0.46 ± 0.02	2.5 (build-up observed)
0.2:0.8	0.75*	0.23 ± 0.01	0.90 ± 0.03	0.5 (no build-up observed)
0.0:1.0	0.76 ± 0.01	0.24 ± 0.02	2.35 ± 0.09	0.5 (no build-up observed)

*Standard error less than 0.01

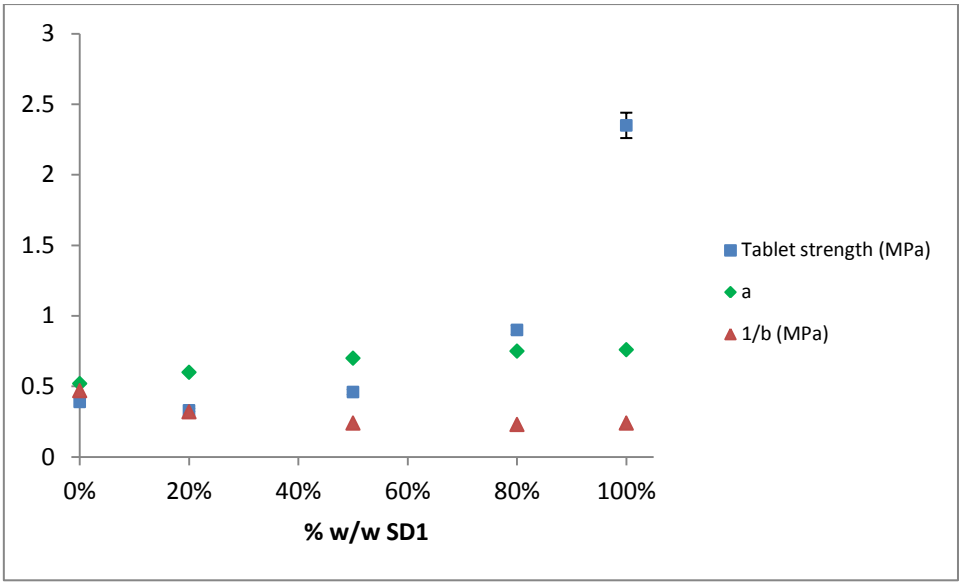

Figure 6-21: Tablet strengths and Kawakita a and b^{-1} parameters as a function of SD1 content

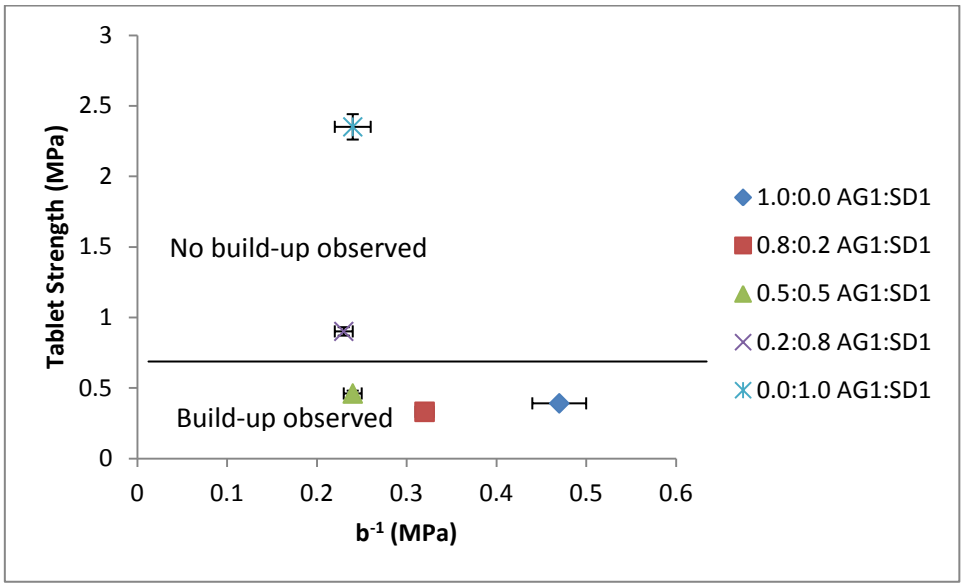

Figure 6-22: Tablet strengths and Kawakita b^{-1} parameters for blends of AG1 and SD1.

Figure 6-23 and Figure 6-24 are SEM images of build-up collected during the filling of blends of AG1 and SD1 (see Figure 6-19). As was shown previously with a sample build-up formed using a pure sample of AG1, the build-up is solid and continues with no clear sign of the agglomerate particles from which it was formed remaining.

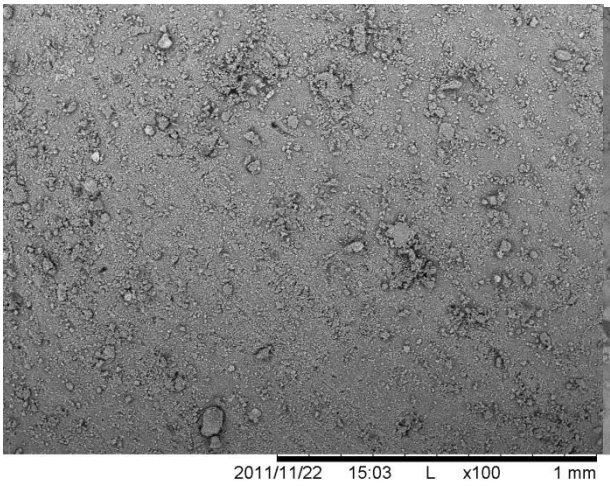

Figure 6-23: A SEM image of build-up produced from a 4:1 blend of AG1 and SD1

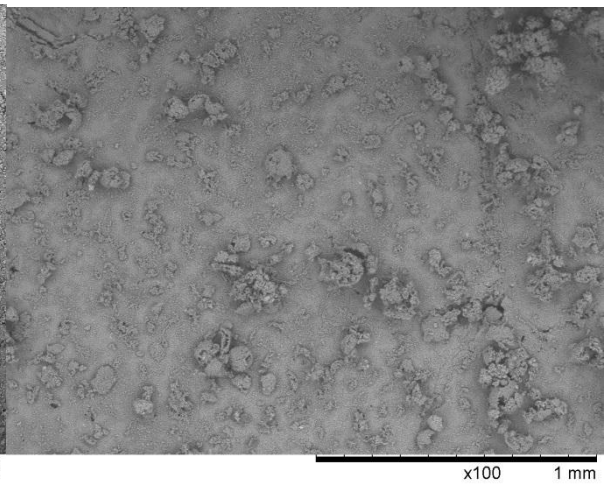

Figure 6-24: A SEM image of build-up produced from a 1:1 blend of AG1 and SD1

6.5.3 A Hypothesis Regarding Build-up Formation and Adhesive Forces

In section 2.9, the hypothesis was proposed that build-up is formed as a result of the stresses experienced by agglomerate particles as they pass through the clearance between the auger and tube. In the case of the blend comprising 1 part of AG1 to 4 parts of SD1 it seems unlikely that no AG1 agglomerate particles passed through the auger filler's 300 µm auger/tube clearance and thus a number of AG1 agglomerate particles must have experienced the stresses which lead to the pure AG1 powder forming build-up.

$$F \approx \frac{p_{vdW}}{p_{pl}} F_a \qquad \textbf{(2-47)}$$

where F is the adhesive force acting between two plastic deforming spheres, F_a is an applied force, p_{vdW} is Van der Waals pressure and p_{pl} is the plastic yield pressure of a sphere.

$$-F_d = P + 2\pi\omega_A R = \pi r^2 H \qquad \textbf{(2-39)}$$

where F_d is the pull of force in the case of a ductile separation, P is an externally applied load, ω_A is thermodynamic work of adhesion with units of Joules per meter squared. R is the radius of the agglomerate particle, r is the contact radius and H is plastic hardness which is considered to be three times the plastic yield stress.

Eq. (2-47) shows that low values of plastic yield pressure will lead to greater values of adhesive force, due to an increase in contact area arising from the plastic deformation of agglomerate particles and a reduction in separation distance leading to an increase in p_{VdW}. However, Eq. (2-39) shows that while plastic deformation will lead to an increase in contact area and thus an increase in adhesive force, a reduction in plastic hardness will lead to a reduction in adhesive force per unit of contact area. Based upon this knowledge the following hypothesis is proposed where adding increasing levels of SD1 to a blend of AG1 and SD1 increases the plastic hardness of the build-up formed resulting in an increase in the adhesive force acting between the build-up and the tube surface, an increase in torque *i.e.* the 1:1 blend. However, if a sufficiently large amount of SD1 is added the hardness of the build-up then reaches a point where build-up is no longer able to adhere to the tube surface *i.e.* the 1:4 blend, where high plastic hardness leads to lack of contact area being formed and a lack of adhesion.

6.6 Auger Build-up Testing for a Wide Range of Detergent Powders

Testing of AG1 and SD1 showed that AG1 formed build-up during auger filling while SD1 did not, despite SD1 having a lower failure stress than AG1, it is proposed that this could be explained by the porous nature of SD1 leading to it undergoing fracture during both uniaxial compaction and auger filling. SD1 also formed tablets six times stronger than AG1, following compaction to 58 MPa. It is proposed that this reflects the softness of the material from which AG1 is formed relative to SD1, which in the auger filler leads to AG1 creating substantial contact areas between itself and the tube wall and thus forming build-up.

Based upon these results it is now proposed that the powder characteristics which will determine if a powder is able to form build-up are:

I. Agglomerate particle failure stress as measured via the Kawakita b^{-1} parameter.

II. Tablet strength measuring following compaction to 58 MPa to ensure low porosity.

III. Agglomerate particle size in relation to the magnitude of the auger / tube clearance.

To confirm this hypothesis 12 powders were selected for testing via:

I. Auger filling.

II. Uniaxial compaction.

III. Diametric tablet compression.

IV. Gravimetric sieving to determine agglomerate particle size.

In this section of the thesis, powders have been selected in order to give a suitably wide range of mechanical properties, however the powders tested were commercially sensitive and thus it is not possible to give full formulation details apart from the following details.

- Table 6-9 gives the surfactant contents of the powders tested in this section of the thesis and SD1 and AG1 batch 1 tested in the previous section.

Table 6-9: Surfactant contents of powders tested.

Powder	Target Surfactant content % w/w
SD1	18
AG1 Batches 1 & 2	24
AG2 Batches 1 & 2	26
AG2 Batches 3 & 4	24
AG3 Batches 1 & 2	24
AG4 Batch 1	25
AG4 Batch 2	21
AG5	45
AG6	25
AG7	23

- AG1 and AG2 have very similar formulations with the only difference being the surfactant binder, leading to AG2 being typically weaker than AG1 [58].

- AG3 was selected on the basis that unlike AG1 and AG2 it contained a significant amount of relatively large (geometric mean agglomerate particle size 300 μm) un-milled sodium carbonate primary particles (see Figure 6-26) which typically only partially agglomerate due to their large size [58]. Thus it may be expected that this powder may exhibit phenomena different to AG1 and AG2 during auger filler build-up formation. AG3 also has complex blended surfactant binder which is believed to lead to it yielding stronger agglomerate particles than AG1 and AG2 for the same moisture content.
- AG4 was selected on the basis that its surfactant binder contains a smaller head group compared to the binders in AG1 and AG2 which based upon P&G's historic experience would lead to stronger agglomerate particles and thus potentially lower levels of build-up formation [59].
- AG5 was selected on the basis that it contained the same surfactant binder present in AG4, but at a significantly higher level (45% w/w), which would typically lead to its agglomerate particles being weak. However, it also contained primary particles which are known to be particularly fine and lead to AG5's agglomerate particles being relatively strong despite its high binder content.
- AG6 was selected on the basis that all other agglomerates tested were manufactured within Lodige high shear granulators with subsequent drying in a fluidised bed. However, AG6 was manufactured within a twin axial Forberg paddle mixer which may reasonably be expected to lead to impact both its structure (see Figure 6-28 and Figure 6-29) and thus its mechanical properties. AG6 also has a particularly complex formulation making it a good test of the models ability to predict build-up formation.
- AG7 was selected on the basis that it is known to contain particularly strong agglomerate particles and thus would not be expected to form build-up during auger filling.

Table 6-10 gives measured moisture contents and agglomerate particle size data. Values of moisture content are the mean of five repeats, eRH values are the mean of three repeats. In both cases values are quoted in conjunction with standard errors.

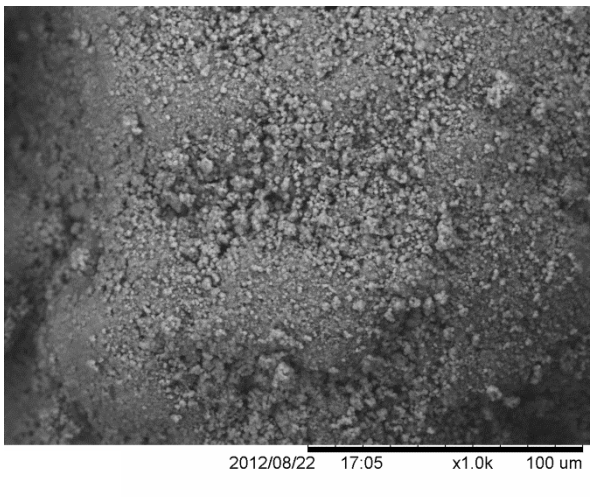

Figure 6-25: An SEM image of AG1 Batch 2 at 1000 x magnification

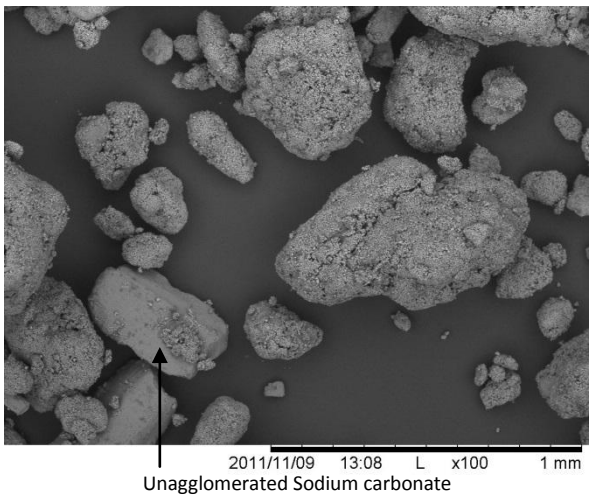

Figure 6-26: An SEM image of AG3 Batch 1 at 100 x magnification. See Figure 6-27 for a higher magnification image of the unagglomerated sodium carbonate primary particle.

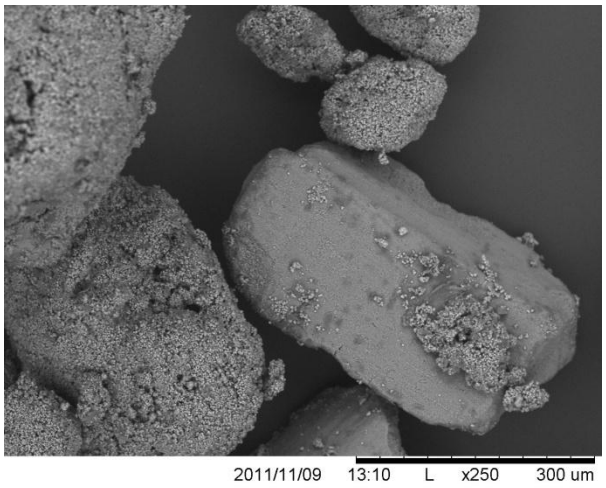

Figure 6-27: An SEM image focused upon the unagglomerated sodium carbonate particle within AG3 Batch 1 at 250 x magnification, showing a lack of primary particles and binder confirming that it is not an agglomerate.

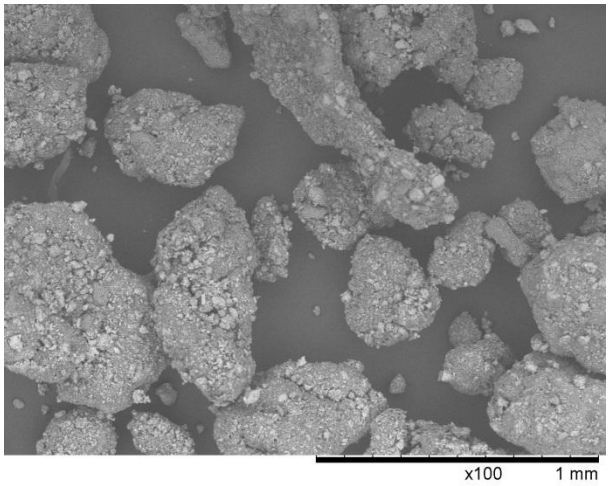

Figure 6-28: An SEM image of AG6 at x 100 magnification

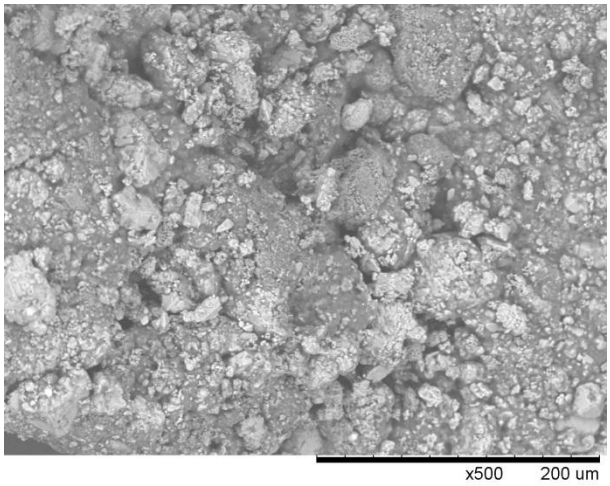

Figure 6-29: An SEM image of AG6 at x 500 magnification

Table 6-10: Moisture content and agglomerate particle size data

Powder	Batch	% Moisture w/w	eRH %RH	Geometric mean particle size (μm)	Span
SD1	NA	2.9*	35.1 ± 0.3	770	2.2
AG1	Batch1	6.1 ± 0.1	45.4 ± 0.5	368	1.6
	Batch2	5.3*	27.9 ± 0.1	439	1.8
AG2	Batch1	4.7*	38.3 ± 0.3	486	1.6
	Batch2	4.8*	35.5 ± 0.3	772	1.5
	Batch3	5.0*	40.3 ± 0.1	596	1.9
	Batch4	4.1 ± 0.1	36.1 ± 0.5	384	2.0
AG3	Batch1	10.5 ± 0.2	61.7 ± 0.2	347	3.6
	Batch2	5.8 ± 0.1	19.4 ± 0.3	495	1.6
AG4	Batch1	6.8 ± 0.2	36.4 ± 0.1	538	1.5
	Batch2	7.0 ± 0.2	20.0 ± 0.2	490	1.8
AG5	NA	2.5*	27.7*	443	1.3
AG6	NA	1.9 ± 0.1	15.7 ± 0.6	552	1.3
AG7	NA	8.5*	2.6 ± 0.2	487	1.4

*Standard error less than 0.1

6.6.1 Uniaxial Compaction Testing

The mechanical properties of the powders listed in Table 6-10 were characterised via uniaxial compaction, with subsequent application of the Kawakita model. In each case 4.00 ± 0.03 g of powder was used to ensure a low aspect ratio and thus minimise the influence of friction at the die walls upon the experimental results. In each case stress strain curves were plotted (see Figures 6-36, 6-38, 6-40 and 6-42) and then converted to Kawakita plots (see Figures 6-37, 6-39,

6-41 and 6-43) which were then used to identify regions of the plots within which the Kawakita model gave a fit to the experimental data enabling R^2 values greater than 0.99 in all cases.

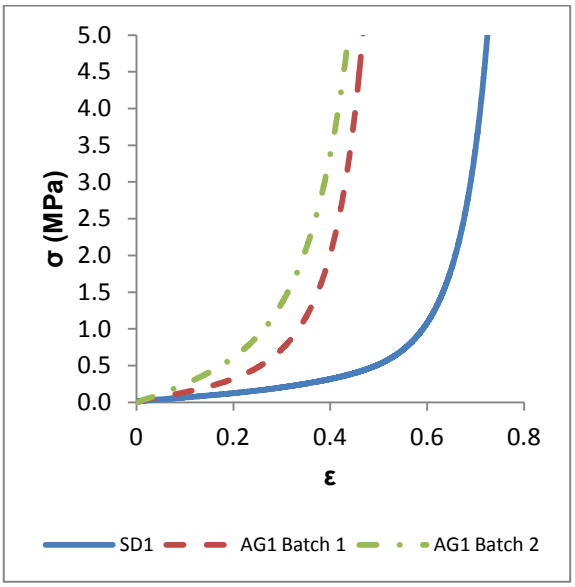

Figure 6-30: Stress strain plots for SD1, AG2 Batch 1, AG2 Batch 2

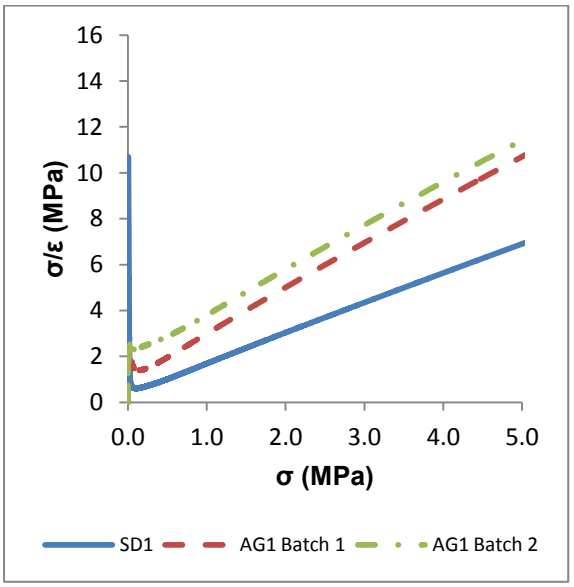

Figure 6-31: Kawakita plots for SD1, AG2 Batch 1, AG2 Batch 2

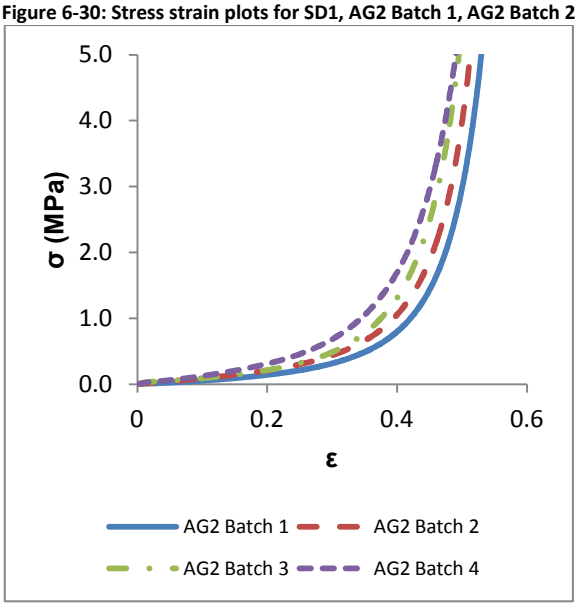

Figure 6-32: Stress strain plots for AG2 Batches 1 to 4.

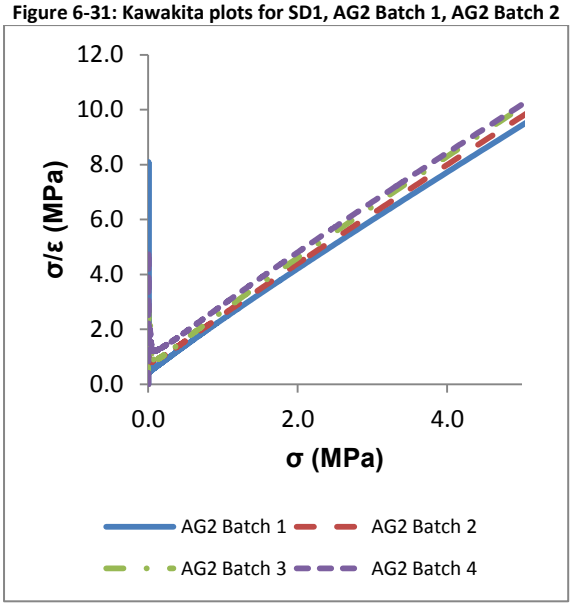

Figure 6-33: Kawakita plots for AG2 Batches 1 to 4.

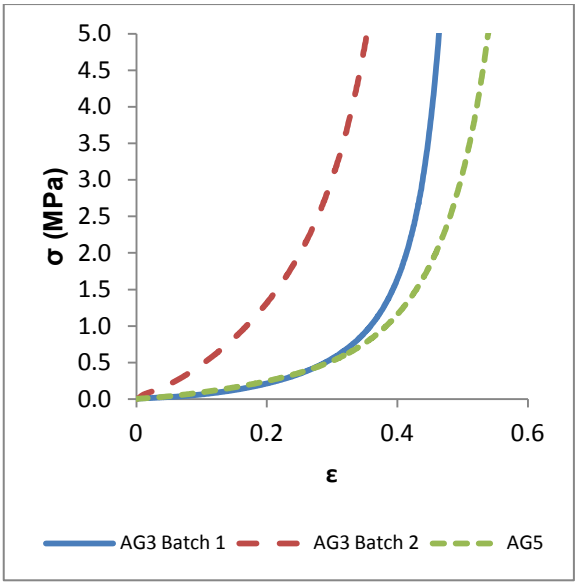

Figure 6-34: Stress strain plots for AG3 Batches 1, 2 and AG5

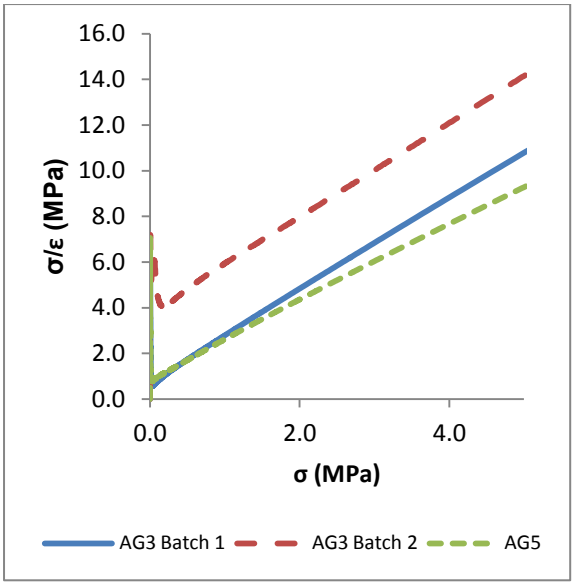

Figure 6-35: Kawakita plots for AG3 Batches 1, 2 and AG5

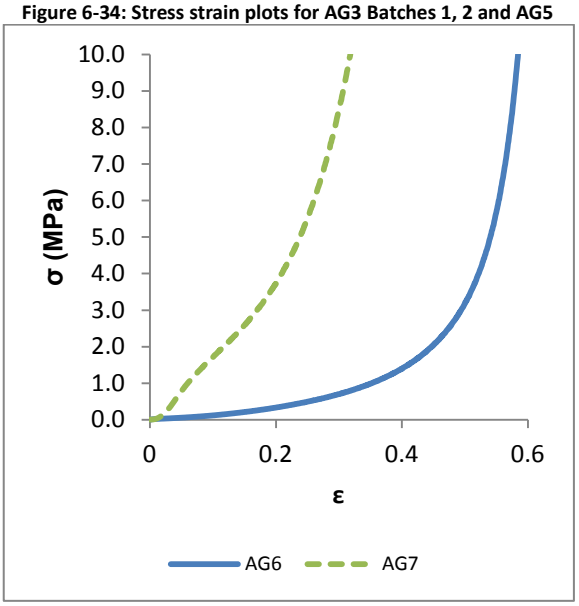

Figure 6-36: stress versus strain for AG6 and AG7

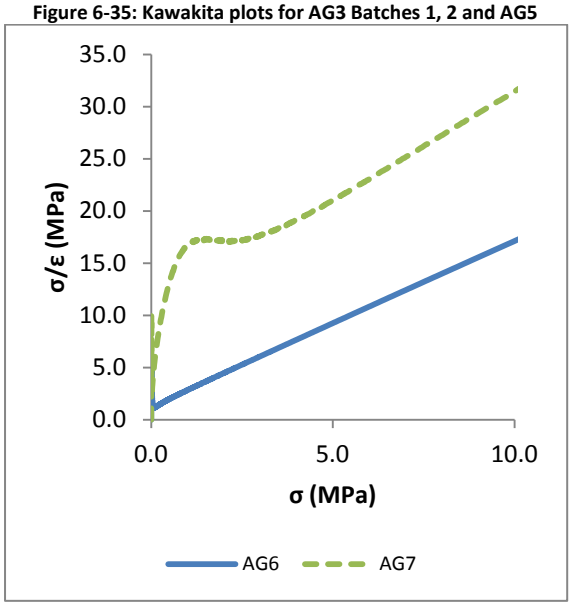

Figure 6-37: Kawakita plots for AG6 and AG7

The regions within which the model enabled a good fit to experimental data are listed in Table 6-11, these regions were also selected on the basis that they were within the regions of the plots where substantial changes in strain per unit stress occur and much of plastic deformation may reasonably be expected to occur. This would not be that case if for example data between 20 and 40 MPa has been used where the powder bed is of low porosity and only relatively small changes in strain occur and thus the data extracted from these regions of the plots would not be expected to be informative of a powder plastic yield stress.

Table 6-11: Force ranges used to in order to select data which is a good fit to the Kawakita model

Powder	Batch	Stress Range Studied (MPa)
SD1	NA	0.5 to 5.0
AG1	Batch1	0.5 to 5.0
	Batch2	0.5 to 5.0
AG2	Batch1	0.5 to 2.5
	Batch2	0.5 to 2.5
	Batch3	0.5 to 2.5
	Batch4	0.5 to 5.0
AG3	Batch1	0.5 to 5.0
	Batch2	0.5 to 5.0
AG4	Batch1	0.5 to 5.0
	Batch2	0.5 to 5.0
AG5	NA	0.5 to 5.0
AG6	NA	0.5 to 2.5
AG7	NA	5.0 to 10.0

Examination of experimental data showed that curvature in the early part of the compaction process could be avoided by excluding data below 0.5 MPa from the analysis. The exception to this situation was AG7, where it was necessary to exclude data below 5.0 MPa due to the large degree of curvature observed in this region. This may have arisen from a greater degree of fracture or elastic deformation in the early portion of the compaction of AG7 relative to the other powders tested.

6.6.2 An Operating Space Model for Auger Filler Build-up

Table 6-12 gives Kawakita parameters, tablet strengths and build-up observations of the powders tested in this section of the thesis and SD1 and AG1 Batch 1 tested in the previous section. Kawakita parameters and tablet strengths are the mean of at least three repeats and quoted in conjunction with standard errors. During auger filler build-up experiments manual auger torque measurements were made at intervals of 90 to 180 fills, tube build-up onset is defined as the mean of the number of fills associated with the final torque reading of 0.5 Nm and the number of fills associated with the first reading greater than 0.5 Nm typically 1.0 Nm.

The error associated with these values assumes that the major source of error is that associated with the frequency of the torque measurement, and thus is the difference between the fills. This was subsequently confirmed by the repeat experiments depicted in Figure 6-38 and Figure 6-39. Where good repeatability was observed, the major source of error was the uncertainty arising from the measurement frequency and not the accuracy of the individual measurements. In many of the experiments auger filler build-up was observed on the low speed agitator in the auger filler's hopper on the surface facing into the hopper where no small clearance/gap exists. This suggests that this type of build-up formation occurs via a different mechanism to that observed on the tubes internal surface and while this type of build-up formation is not a key focus of the investigation it has been noted for completeness.

Table 6-12: Kawakita parameters, tablet strengths and build-up observations

Powder	Batch	a	b^{-1} (MPa)	Tablet Strength @ 58 MPa (MPa)	Tube build-up onset (fills)	Agitator build-up observed
SD1	NA	0.76 ± 0.01	0.24 ± 0.02	2.35 ± 0.09	None	No
AG1	Batch1	0.52 ± 0.01	0.47 ± 0.03	0.39*	308 ± 120	Yes
	Batch2	0.51 ± 0.01	0.84 ± 0.06	0.50 ± 0.01	636 ± 107	No
AG2	Batch1	0.53 ± 0.01	0.29 ± 0.02	0.21 ± 0.01	47 ± 95	Yes
	Batch2	0.54*	0.33 ± 0.01	0.29 ± 0.02	331 ± 90	Yes
	Batch3	0.52 ± 0.01	0.39 ± 0.01	0.28*	141 ± 95	Yes
	Batch4	0.54 ± 0.01	0.51 ± 0.02	0.47 ± 0.01	141 ± 94	Yes
AG3	Batch1	0.49*	0.40 ± 0.02	0.33 ± 0.01	235 ± 94	Yes
	Batch2	0.49*	1.72 ± 0.08	0.67 ± 0.06	None	No
AG4	Batch1	0.50*	0.72 ± 0.02	0.44*	None	Yes
	Batch2	0.53 ± 0.01	1.26 ± 0.09	0.55 ± 0.02	None	Yes
AG5	NA	0.59*	0.54*	0.69 ± 0.01	None	No
AG6	NA	0.61 ± 0.01	0.52 ± 0.10	1.30 ± 0.15	None	No
AG7	NA	0.47*	4.53 ± 0.19	0.28*	None	No

*Standard error less than 0.01

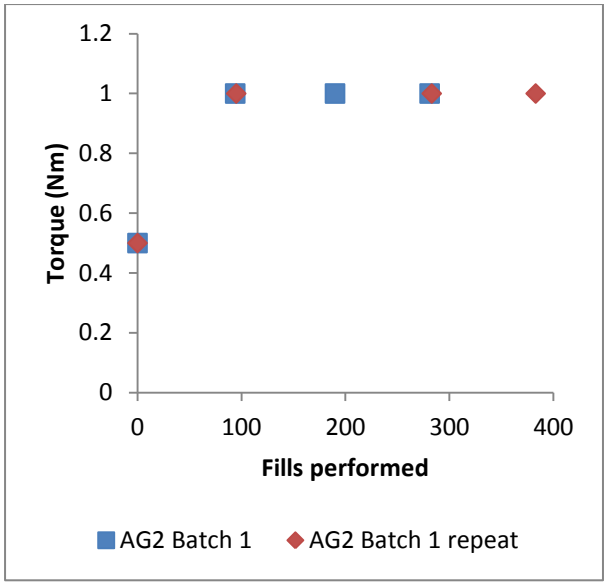

Figure 6-38: Auger filler repeat experiments for AG2 Batch 1

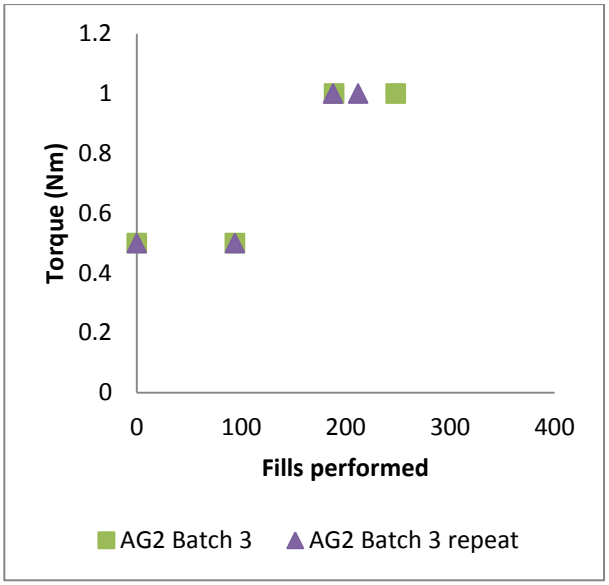

Figure 6-39: Auger filler repeat experiments for AG2 Batch 3

In the case that no rise in torque was detected the experiment was continued for a minimum of 1000 fills and the tube was inspected at the end of the experiment to ensure no build-up had formed. The relevant powder was then classified as non-build-up forming with respect to the tube surface. Tablet strength and Kawakita b^{-1} parameters presented in Table 6-12 are plotted in Figure 6-40, it can be seen from this plot that powders which form build-up on the tube surface have low b^{-1} parameters and low tablet strengths.

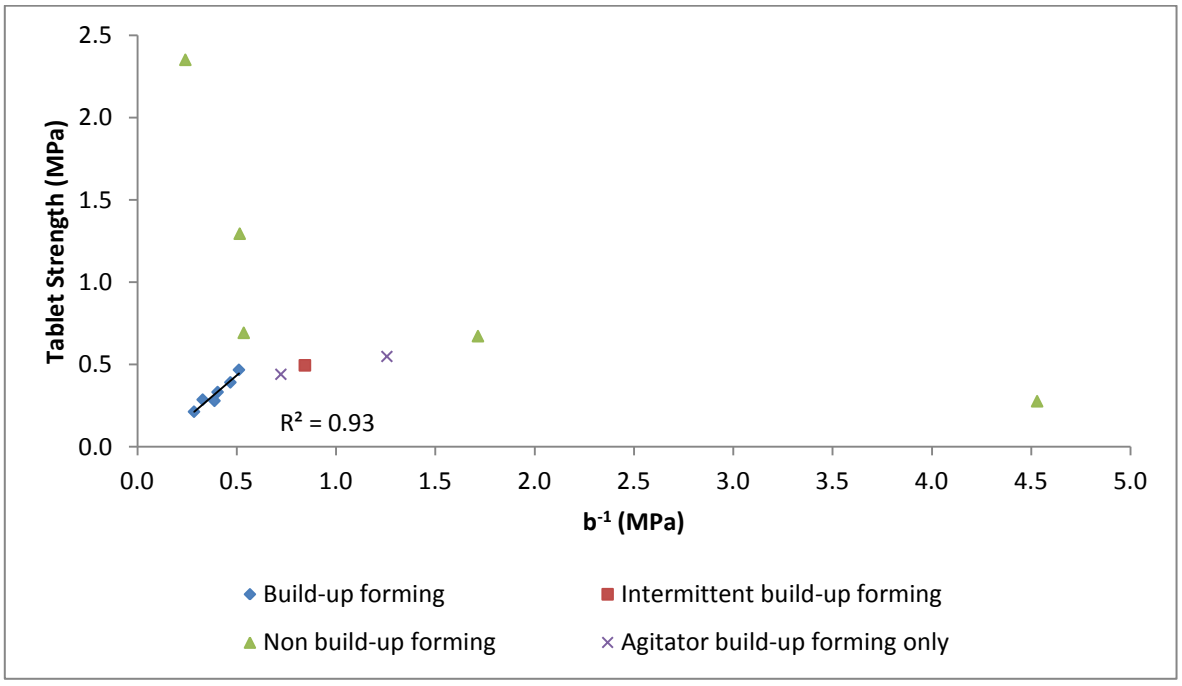

Figure 6-40: An auger filler build-up operating space model

It is known that for powders which compact via plastic deformation the b^{-1} Kawakita parameter is related to the plastic yield stress of the agglomerate particles within the die [10]. From this knowledge it is proposed that the adhesive forces existing between agglomerate particles and the tube surface, resulting from the forces applied to them as they pass through the auger filler's 0.3 mm auger/tube clearance is a function of the agglomerate particles plastic yield stress and thus also for these materials also a function of the b^{-1} parameter.

It is proposed that these powders also had low tablet strengths because there agglomerate particles are formed from soft plastic materials which agglomerated into a solid coherent singular mass during compaction. As these powders formed build-up and had low b^{-1} parameters this suggests that they were of low plastic hardness. Given the plastic nature of these materials it seems probably that the forces holding the agglomerate particles together within their tablets are a function of their ability to undergo plastic deformation and a ductile separation is probable in preference to a brittle separation involving only elastic deformation. Eq. (2-39) describes such a ductile separation and predicts that in the case of a material of low yield stress and thus plastic hardness reduced force per unit contact area will be required to achieve separation. This may also explain the strong correlation between b^{-1} and tablet strength for build-up forming materials ($R^2 = 0.93$) shown in Figure 6-40.

Tube build-up onset and b^{-1} values presented in Table 6-12 are plotted in Figure 6-41 showing that powders with low b^{-1} parameters and thus plastic yield stress (assuming that build-up forming agglomerates fail via plastic yielding) tend to give rise to an increase in torque, due to the presence of build-up earlier during auger filler build-up experiments. Tube build-up onset is characterised as the point at which the presence of build-up on the tube surface leads to an initial rise in torque indicating that build-up is now able to provide a measurable resistance to the augers movement.

Figure 6-41 illustrates the time dependent nature of build-up formation. It seems reasonable to assume that a number of agglomerate particles will pass through the auger fillers auger/tube clearance during each rotation of the auger and a fraction of these agglomerate particles will be transformed into build-up on each occasion. The data presented in Figure 6-41 suggests that this efficiency is inversely proportional to the Kawakita b^{-1} parameter which suggests that agglomerate particles of low yield stress have a higher probability of forming build-up than particles of high yield stress.

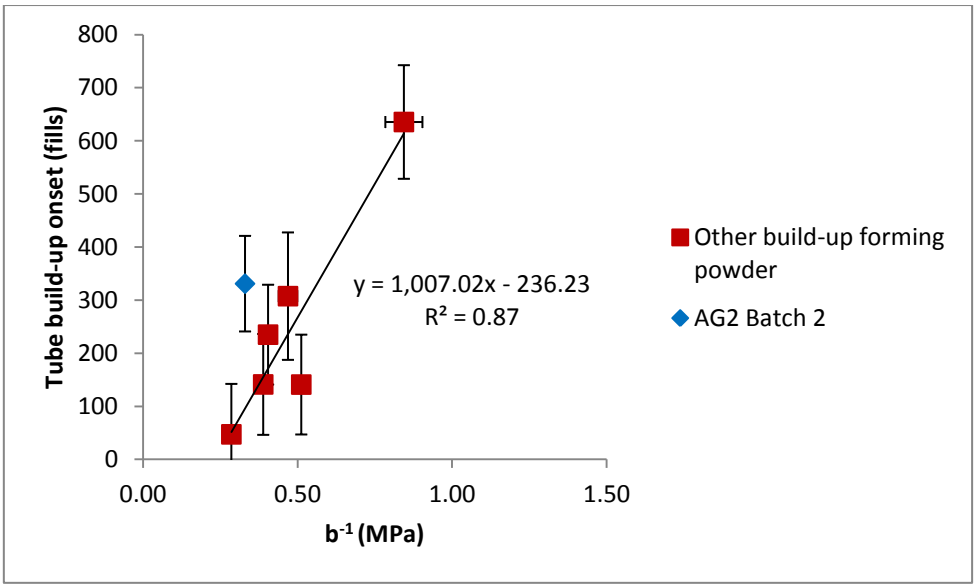

Figure 6-41: Tube build-up on set as a function of b^{-1}

Eq. (2-39) shows that while agglomerate particles of low yield stress will tend to undergo a greater level of deformation in response to a given force, their associated low values of plastic hardness will tend to mean that the work per unit contact area required to remove them from the tube surface will be lower than would otherwise be the case. This suggests that at some low value of plastic yield stress, build-up may be insufficiently strong to enable the build-up to remain adhered to the tube's surface under the influence of the forces acting upon it. However, as can be seen in Figure 6-40 this was not observed to be the case, which suggests that the stresses acting to remove build-up from the tube surface are not sufficiently great to achieve this. This may be explained in a number of ways. Firstly the adhesive force acting between

build-up and the tube surface must be sufficiently great to resist gravity. Secondly the build-up may undergo plastic flow under the influence of the forces exerted upon it from the auger which would tend to dissipate forces prior to them reaching the build-up tube interface.

AG2 Batch 2 was excluded from the correlation presented in Figure 6-41 as it is believed that data collected during its auger filling was significantly influenced by its large agglomerate particle size (geometric mean particle size 772 µm) relative to the other build-up and intermediate build-up forming powders included in this correlation (see Table 6-10). This is supported by the fact that during the auger filling of AG2 Batch 2, build-up was observed to form in a manner different to that observed in other experiments such as the auger filling of AG2 Batch 1. Specifically following build-up being observed to begin to leave the auger filler at 141 ± 47 fills, the auger was then observed to rub against one side of the tube with build-up forming on the opposite side of the tube only. Small rises and falls in temperature and a delayed rise in torque was then observed, as opposed to the more typical behaviour seen with AG1 Batch 1 (see Figure 6-42 & Figure 6-43).

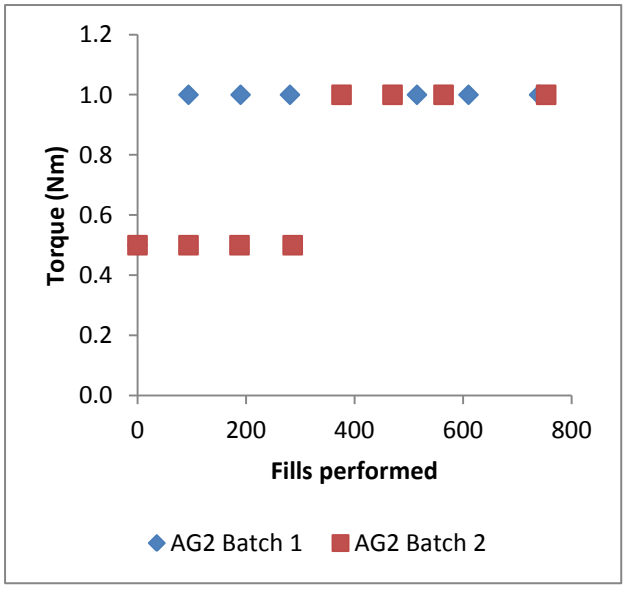

Figure 6-42: Torque data for the auger filling of AG2 Batch 1 and 2

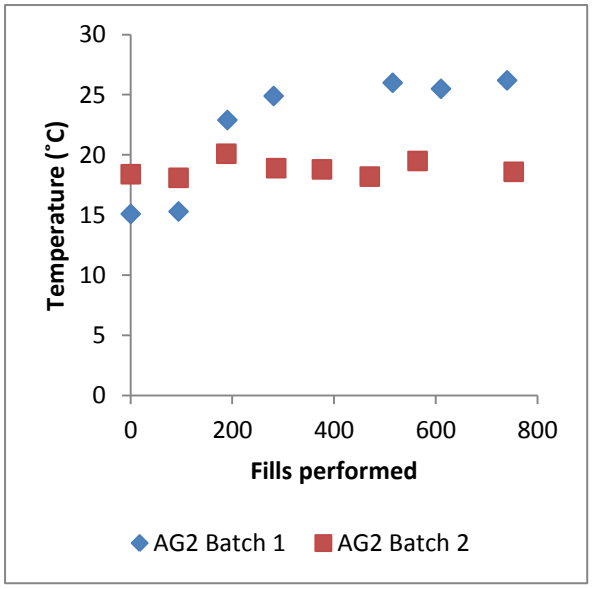

Figure 6-43: Temperature data for the auger filling of AG2 Batch 1 and 2

The final torque values of 1.0 Nm in Figure 6-42 are typical for powders tested in this section of thesis with a value of 1.0 Nm. The only exception to this was torque data generated during the auger filling of AG3 Batch 1 where the final torque value reached after 1128 fills was 3.0 Nm (see Figure 6-44). This is believed to be related to the presence of unagglomerated sodium carbonate primary particles. Pure sodium carbonate was shown to be comprised of strong particles with high b^{-1} values in section 4.2 and are also known to form strong tablets when compacted to high pressures [59]. This suggests that sodium carbonate is a strong plastic material and thus may act to harden build-up formed by AG3 Batch 1.

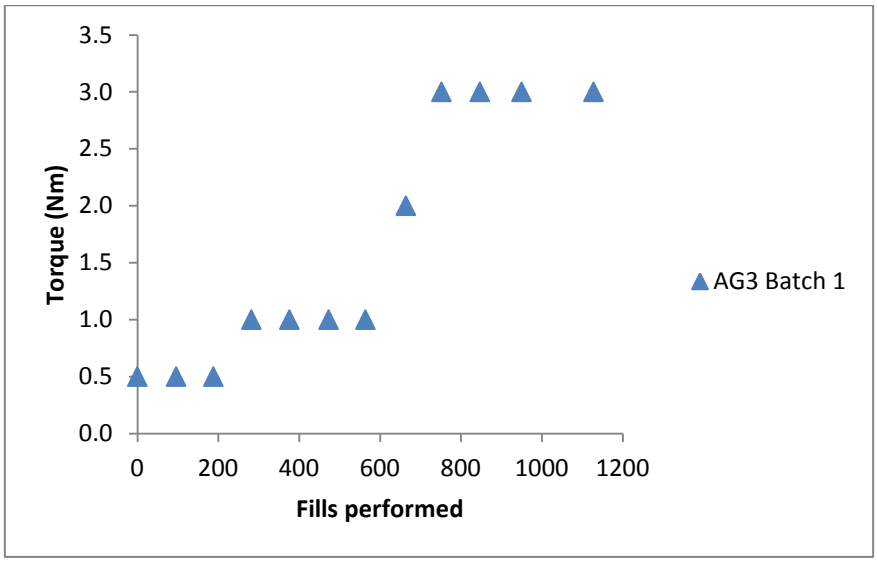

Figure 6-44: Torque data for AG3 Batch 1

6.6.3 Build-up Indentations

To assess the mechanical and adhesive properties of samples of build-up generated during auger filler experiments, build-up indentations were performed and compared with Kawakita b^{-1} parameters presented previously in Table 6-12. Kawakita b^{-1} parameters are presented with associated build-up pull off forces and indentation depths in Table 6-13. It should be noted that this assumes no reduction in the contact area occurred during the withdrawal of the indenter which cannot be definitively proven to be the case. However, a clear indentation was observed to be present following the withdrawal of the indenter and no material was observed to transfer

to the indenter from the build-up sample. This would suggest that the mode of contact failure was brittle and not ductile (see section 2.6.2 for definitions of brittle and ductile separation) and thus this seems a reasonable assumption.

Table 6-13: Build-up Indentations results and Kawakita b^{-1} parameters for six build-up forming powders.

Powder	Batch	Powder b^{-1} (MPa)	Build-up Pull off force (N)	Build-up Indentation depth (mm)
AG1	Batch 1	0.47 ± 0.03	0.12 ± 0.02	0.18 ± 0.02
AG1	Batch 2	0.84 ± 0.06	0.08*	0.10 ± 0.01
AG2	Batch 1	0.29 ± 0.02	0.37 ± 0.03	0.29 ± 0.01
AG2	Batch 2	0.33 ± 0.01	0.40 ± 0.01	0.33 ± 0.03
AG2	Batch 4	0.51 ± 0.02	0.28 ± 0.01	0.23 ± 0.03
AG3	Batch 1	0.49 ± 0.02	0.08 ± 0.01	0.14 ± 0.03

*Standard error less than 0.01

Figure 6-45 shows a plot of powder b^{-1} parameters and build-up indentation depths. The plot shows that powders with lower b^{-1} parameters form build-up with larger indentation depths and thus contact areas. This leads to the conclusion that powders with low plastic yield stresses form build-up with similarly low plastic yield stress and thus plastic hardness.

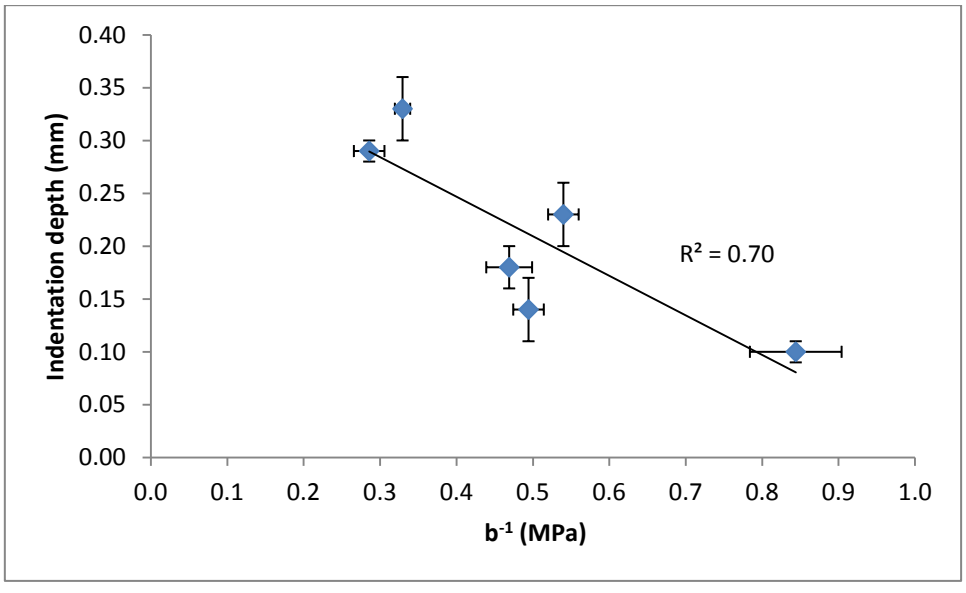

Figure 6-45: Correlation between build-up indentation depth and b^{-1}.

Figure 6-46 shows a clear linear correlation (R^2 = 0.94) between indentation depth and pull off force. This shows that pull of force per unit area is approximately constant[†] and thus the forces acting over the indenter/build-up contact area must also be constant, suggesting that for the samples tested, pull off force is primarily a function of the ability of the build-up sample to deform and generate contact area.

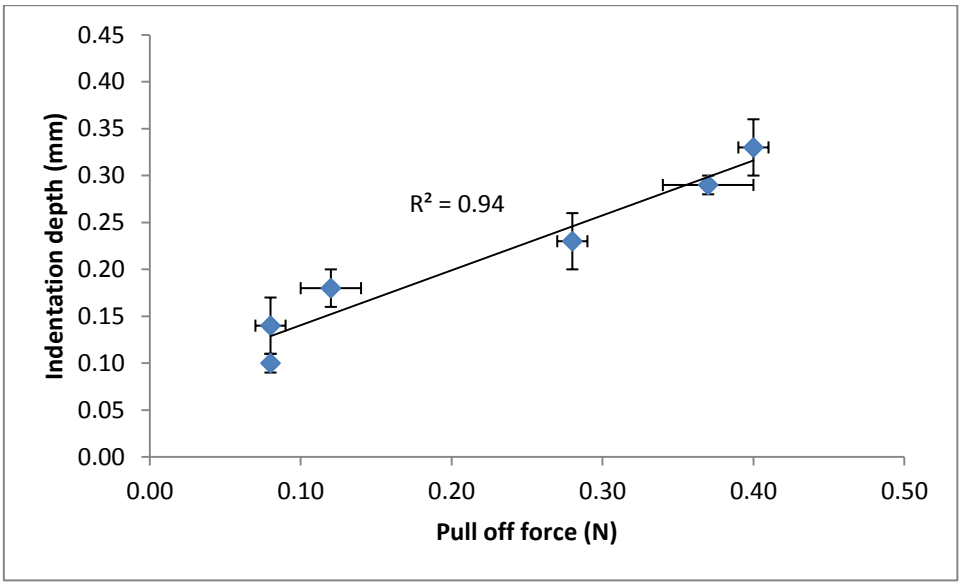

Figure 6-46: Correlation between build-up indentation depth and pull of force.

6.6.4 Build-up Indentation Conclusions

The results presented in this section of the thesis show that:

I. A reasonable correlation (R^2 = 0.70) exists between maximum indentation depth and the relevant powder's Kawakita b^{-1} parameter. This shows that the mechanical properties of the build-up samples can be predicted based upon the Kawakita b^{-1} parameter.

II. A good correlation (R^2 = 0.94) exists between maximum indentation depth and the pull off force, supporting the conclusion that the build-up samples mechanical and adhesive properties are closely related.

[†] Indenter/build-up contact area = 2π x Indenter radius x Indentation depth = a constant x Indentation depth

6.7 Auger Filling of Bisto Gravy Granules

Powders tested in section 6.6 were exclusively for use in detergent powder formulations and thus have similar formulations and physical properties. To determine if the operating space model can predict build-up formation for non-detergent powders, a sample of Bisto gravy granules was obtained. Table 6-14 gives moisture and agglomerate particle size data for Bisto prior to auger filling showing the sample tested had a relativity high moisture content and a large agglomerate particle size with a narrow span.

Table 6-14: Moisture and particle size data for Bisto gravy granules

% Moisture w/w	7.5*
eRH (%RH)	41.3 ± 0.2
Geometric mean particle size (mm)	1.3
Span	0.67

*Standard error less than 0.1

Figure 6-47 and Figure 6-48 are SEM images of Bisto agglomerate particles. From these images it appears that the agglomerate particle are extrudates with a crumb type structure which is beneficial for dissolution [60].

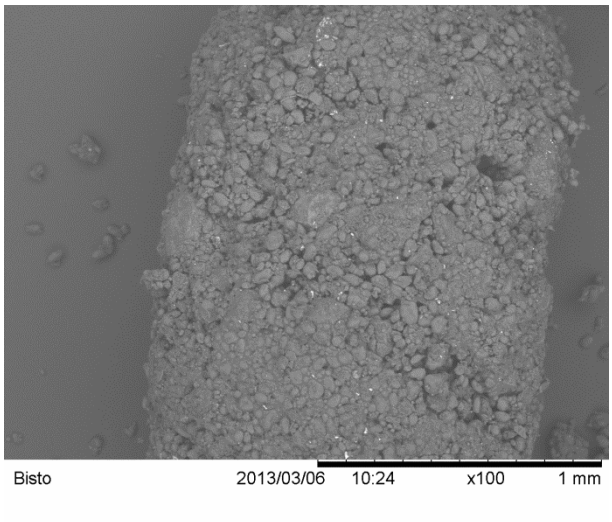

Figure 6-47: Bisto SEM image at x 100 magnification

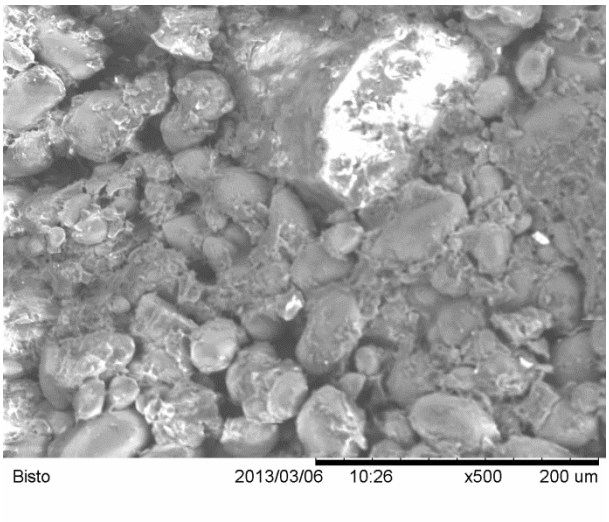

Figure 6-48: Bisto SEM image at x 500 magnification

6.7.1 Uniaxial and Diametric Tablet Compressions

Figure 6-49 and Figure 6-50 shows results of uniaxial compression testing of Bisto. As can be seen from Figure 6-50, a linear region suitable for application of the Kawakita model was found to exist between 0.5 and 2.5 MPa, within this range an R^2 value of greater than 0.99 was obtained.

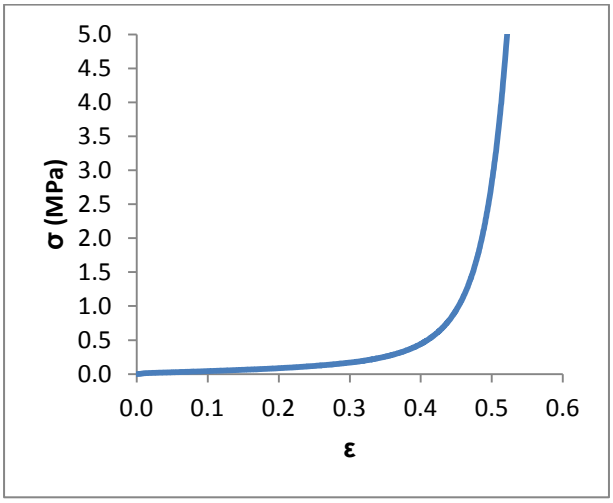

Figure 6-49: Stress versus strain plot for Bisto

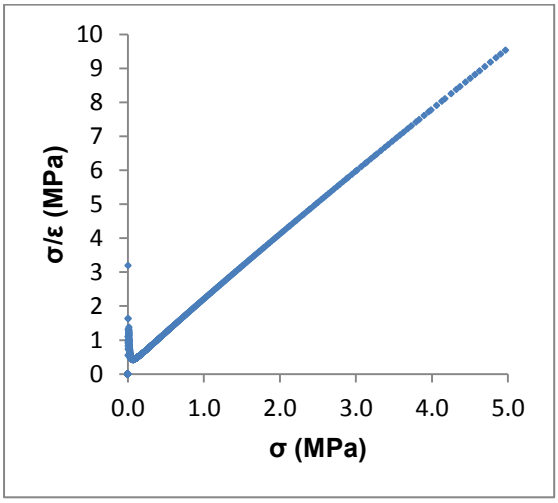

Figure 6-50: Kawakita plot for Bisto.

Table 6-15 gives the results of uniaxial compaction and tablet diametric compression experiments. The results show that Bisto has very low Kawakita b^{-1} parameter and tablet strength which would lead to the conclusion that it should form build-up during auger filling. A comparison of the tablet strength and b^{-1} parameters associated with Bisto and build-up forming detergent powders can be found in Figure 6-51. It can be seen in Figure 6-51 that the values associated with Bisto lie on the same correlation between the b^{-1} parameter and tablet strengths seen previously with build-up forming detergent powders. This suggests that based upon the correlation presented in Figure 6-41 Bisto will not only form build-up but will do so very rapidly.

Table 6-15: Kawakita and tablet strength results for Bisto

a	0.54 ± 0.01
b^{-1} (MPa)	0.13 ± 0.01
Tablet strength (MPa)	0.04*

*Standard error less than 0.01

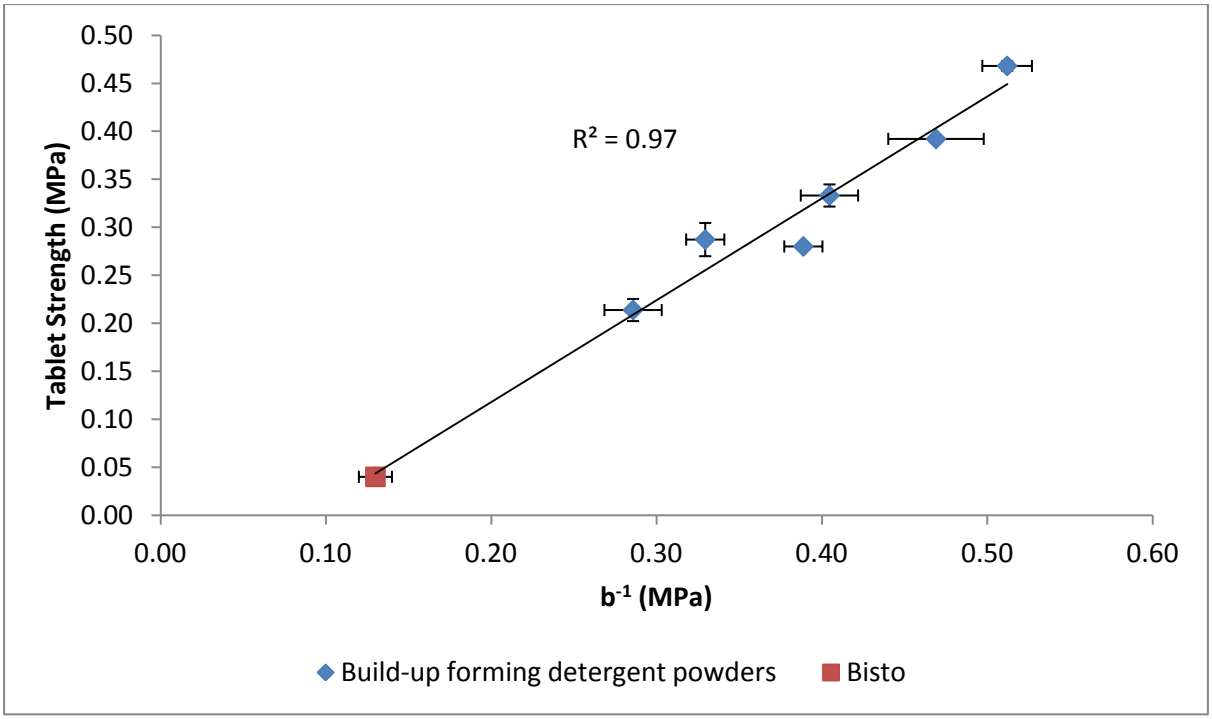

Figure 6-51: Comparison of Bisto with build-up forming detergent powders

6.7.2 Auger Filling of Bisto Gravy Granules

An auger filled build-up experiment was conducted with a 10 kg sample of Bisto to determine if the prediction that it would build-up made in section 6.7.1 of this thesis was accurate. As can be seen in Figure 6-52 the Bisto did form build-up on the tube surface and also on the slow speed agitator as was the case with build-up forming detergent powders. However, in contrast to detergent powders, Bisto also formed build-up on the auger (see Figure 6-53) and the spinner plate.

Figure 6-52: Bisto tube build-up

Figure 6-53: Bisto auger build-up

In addition to this other differences observed between build-up generated by Bisto and detergent powders, no rise in torque was observed during the experiment (see Figure 6-54). Also upon leaving the auger build-up disintegrated leading to an increase in fine particles post auger filling (see Figure 6-55). It should be noted that the temperature rise observed in Figure 6-54 occurred significantly later than the correlation presented in Figure 6-41 would suggest, however, given that the stresses agglomerate particles experience as they pass through the 0.3 mm auger/tube clearances will be a function of their size [29, 30]. As Bisto's geometric mean particle size is 1.3 mm versus 347 µm to 596 µm for the powders included in the correlation presented in Figure 6-41, it is unsurprising that Bisto does not follow the correlation presented in Figure 6-41.

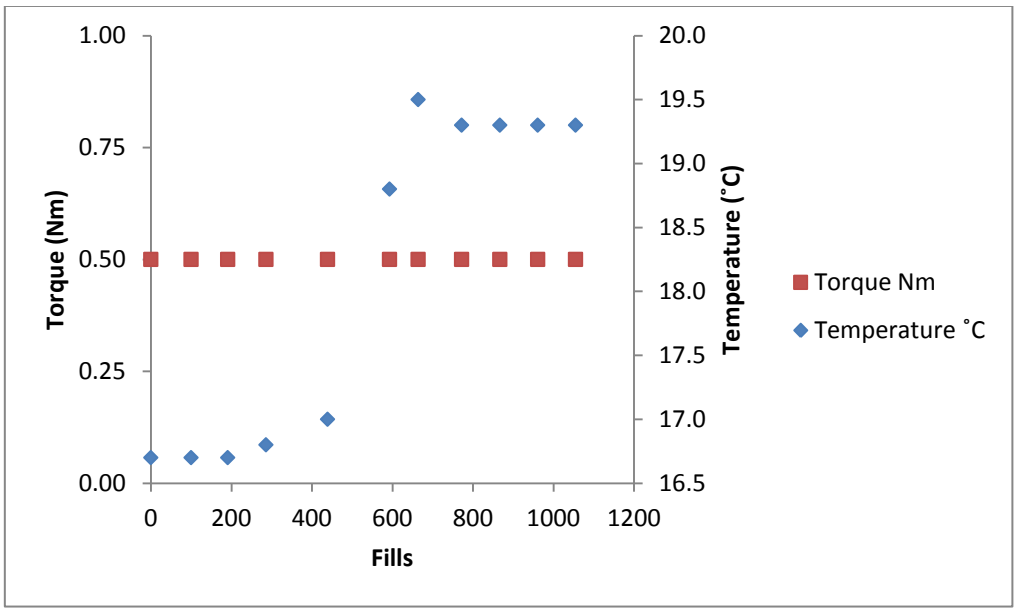

Figure 6-54: Bisto auger filling torque and temperature data

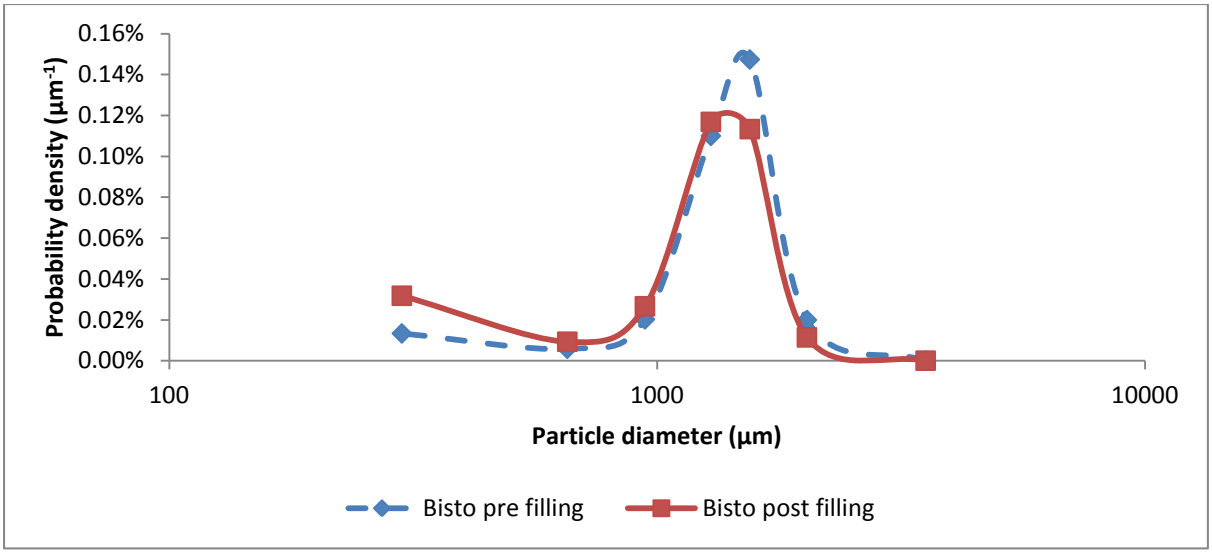

Figure 6-55: Bisto particle size distributions pre and post auger filling

6.7.3 Bisto Auger Filling Conclusions

Characterisation of Bisto showed that it had high moisture content and a relatively large particle size compared to the detergent powders tested earlier in this thesis. Also SEM images suggested that Bisto has a crumb like structure whereas detergent powders typically do not. Uniaxial compaction and tablet diametric compression testing showed that Bisto has a very low b^{-1} parameter and tablet strength leading to the prediction that it would form build-up during auger filling. Auger filling of Bisto showed that it did form build-up during auger filling, but did so with some distinct differences versus build-up formed by detergent powders. However, all the testing of the Bisto Gravy Granules has shown that it is possible to predict the formation of auger filler build-up based on Kawakita b^{-1} parameters and tablet strength measurements.

6.8 Conclusions

The following are the main conclusions to be drawn from the experimental investigation presented in this chapter of the thesis:

1. Auger filler experiments performed with samples of AG1 and SD1 have shown that the test method has good repeatability with measurements of auger torque, tube

temperature and mass per fill being viable methods for the detection of build-up formation.

2. A comparison of macro scale auger filler build-up experiments with uniaxial compaction experiments has shown that only powders with Kawakita b^{-1} parameters of 0.51 MPa or less and tablet strengths of 0.47 MPa or less formed build-up, excluding cases where intermittent and agitator only build-up was formed (see Figure 6-40).
3. Build-up indentation experiments showed that the mechanical properties of the build-up are correlated with the mechanical properties of the powder *i.e.* build-up indentation depths and Kawakita b^{-1} parameters.

7. Development of an Operating Space Model for Screw Tester Build-up

In this chapter of the thesis the following experimental results will be presented and discussed:

1. A series of powders have been tested via the screw tester methodology detailed in section 3.2. These powders have then been tested via uniaxial compaction and diametric tablet compression, as discussed previously in Chapter 6, to determine if an operating space model similar to that shown Figure 6-40 can be generated for the screw tester.
2. Using the same set of powders passed through the screw tester, experiments will be presented which were designed to give a more in depth understanding of the b^{-1} Kawakita parameters and tablet strength, exploring phenomena such as aspect ratio effect.
3. Finally, results derived from indentions into tablets will be explored as an alternative to tablet strength measurement.

7.1 Characterisation of Powders to be Studied

Powders studied in this chapter of the thesis are listed in Table 7-1. All powders were manufactured as part of P&G's ongoing commercial manufacturing processes. AG9 is unusual as in contrast to the other powders listed in Table 7-1, it contains a relatively hydrophobic surfactant with a small head group which is solid at room temperature, allowing for a higher surfactant content.

Table 7-1: Granulation methods and target surfactant contents for powders to be studied in Chapter 7

Detergent Powder	Granulation method	Target Surfactant content % w/w
SD2	Spray drying	17%
SD3	Spray drying	24%
AG2 Batch 5	Lodige high shear granulator	24%
AG8	Medium shear Paddle mixer granulator	27%
AG4 Batch 3	Lodige high shear granulator	25%
AG5 Batch 2	Lodige high shear granulator	45%
AG9	Extrusion with subsequent spheronization	80%

The moisture contents, eRH's and geometric mean particle sizes for powders studied in this chapter are listed in Table 7-2. In case of the moisture contents five repeats were performed, in the case of eRH's three repeats were performed, in both cases the values quoted are means quoted in conjunction with standard errors. With the exception of AG8 and AG9 all powders listed had a geometric mean particle size of approximately 440 ± 40 μm. AG8 has a particularly low geometric mean particle size and AG9 has a particularly high geometric mean particle size. AG2 Batch 5 also has a significantly higher moisture content than the other powders listed in Table 7-2.

Table 7-2: Moisture contents and geometric mean particle sizes for detergent powders to be studied in Chapter 7

Detergent powder	% Moisture content w/w	eRH (%RH)	Geometric mean particle size (μm)
SD2	1.8*	35.7 ± 0.2	480
SD3	2.1*	36.8 ± 0.2	399
AG2 Batch 5	4.2*	35.7*	448
AG8	2.3*	26.9 ± 0.3	280
AG4 Batch 3	3.2 ± 0.1	24.4 ± 0.2	423
AG5 Batch 2	2.2*	18.8 ± 0.2	463
AG9	2.3*	44.6 ± 0.3	979

*Standard error less than 0.1

Particle size distribution for the powders listed in Table 7-1 and Table 7-2 are plotted in Figure 7-4, Figure 7-5 and Figure 7-6, showing that both spray dried powders (SD2 and SD3) and AG8 have bi-modal distributions while all other powders have mono-modal distributions. Figure 7-4 to Figure 7-10 show SEM micrographs of powders studied in this chapter of the thesis. Figure

6-28 showed that AG6 had a poorly agglomerated 'crumb' like structure; this structure can also be seen in larger agglomerate particles present in the SEM image of AG8 shown in Figure 7-7. This supports the argument that this type of agglomerate structure arises due to granulation in a paddle mixer, where stress would be expected to be lower than in a high shear granulator and thus levels of compaction would tend to be lower.

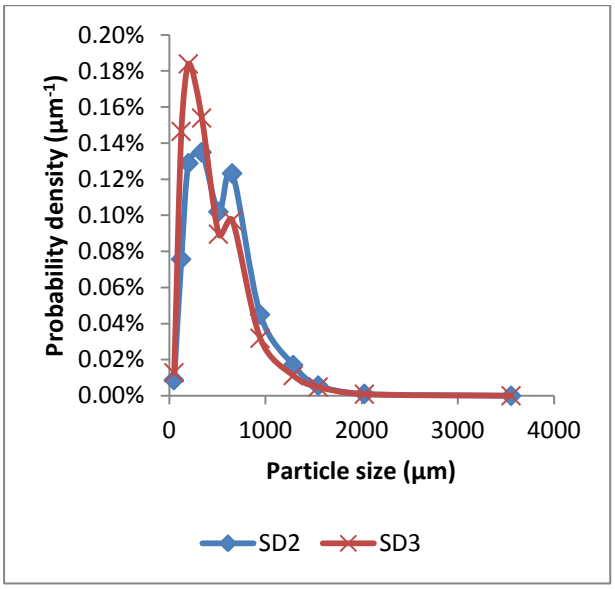

Figure 7-1: Particle size distributions for SD2 and SD3

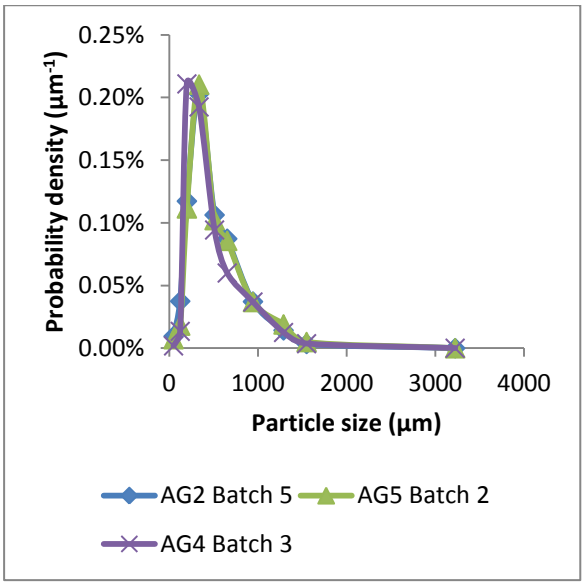

Figure 7-2: Particle size distributions for AG2 Batch 5, AG5 Batch 2 and AG4 Batch 3

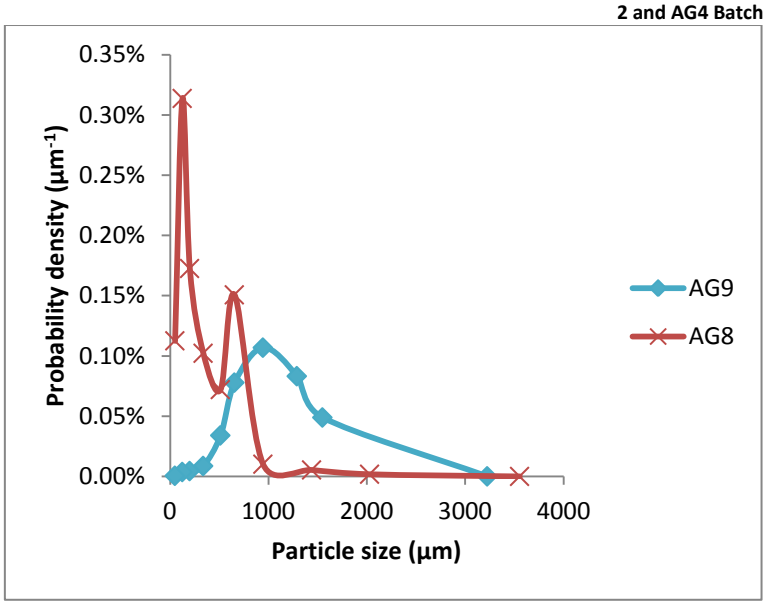

Figure 7-3: Particle size distributions for AG8 and AG9

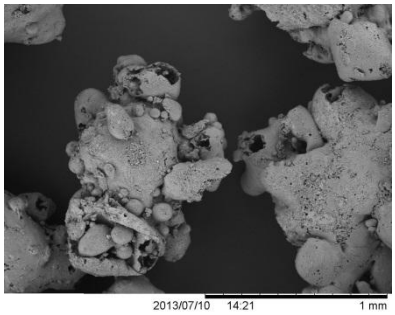

Figure 7-4: SEM micrograph of SD2

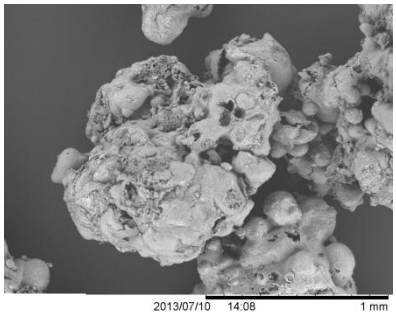

Figure 7-5: SEM micrograph of SD3

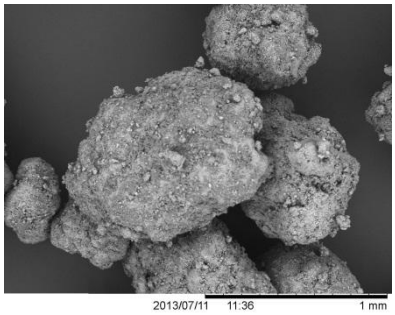

Figure 7-6: SEM micrograph of AG2 Batch 5

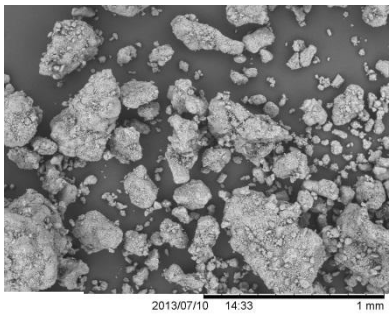

Figure 7-7: SEM micrograph of AG8

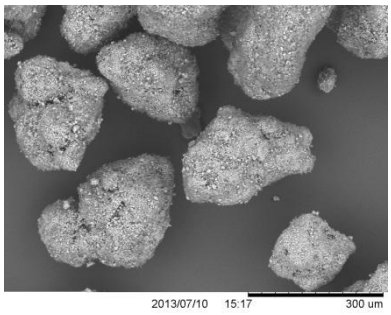

Figure 7-8: SEM micrograph of AG4 Batch 3

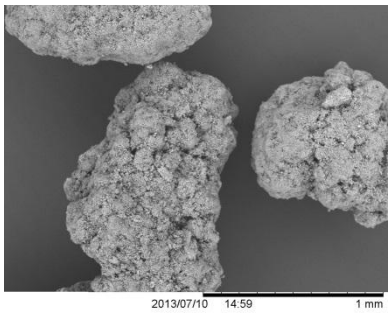

Figure 7-9: SEM micrograph of AG5 Batch 2

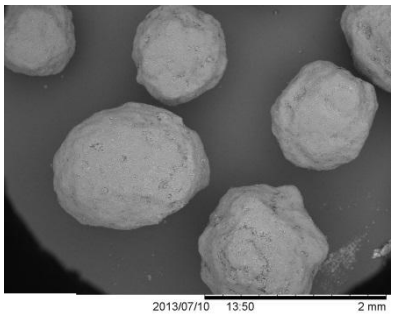

Figure 7-10: SEM micrograph of AG9

Figure 7-4 and 7-5 show SEM images of SD2 and SD3 showing their porous structure which is typical of spray dried detergent powders. Figure 7-10 shows AG9 agglomerate particles which appear in contrast to the other powders to be relatively spherical, which is unsurprising given that they were manufactured by extrusion with subsequent spheronization.

7.2 Uniaxial Compaction Testing

Samples of AG2 Batch 5 and AG5 Batch 2 were characterised via uniaxial compaction with subsequent application of the Kawakita model in order to extract Kawakita 'a' and b^{-1} parameters. In both cases experiments were performed with 4 g, 6 g and 8 g of powder in order

to investigate the effect of initial powder bed aspect ratio, in the case of the experiments performed with 4 g of powder die filling effects were also studied. Two methods of die filling were studied:

1. Fast die filling: performed by rapidly pouring powder from a weigh boat into the die.
2. Slow die filling: performed by transferring powder from the weight boat in small portions using a spatula allowing agglomerate particles to rearrange during die filling, thus reducing the potential for rearrangement during compaction versus fast die filling.

The purpose of these experiments was to determine the potential for experimental results presented previously in this thesis to be influenced by both aspect ratio and die filling effects.

7.2.1 Uniaxial Compaction of AG2 Batch 5 and AG5 Batch 2

Samples of AG2 Batch 5 and AG5 Batch 2 were tested via uniaxial compaction, the purpose of this testing was to determine if the sample of AG5 and AG2 tested in Chapter 6, were sensitive to die filling effects. Table 7-3 and Table 7-4 show Kawakita a and b^{-1} parameters derived from uniaxial compaction experimental results performed using AG2 Batch 2 and AG5 Batch 2. The aspect ratio, b^{-1} and 'a' parameters values are means of three repeats quoted in conjunction with the standard errors of the same three values. Typical Kawakita plots for both powders are shown in Figure 7-11, Figure 7-12, Figure 7-13 and Figure 7-14. In all cases it was found that a region between 0.5 and 2.5 MPa existed which gave a near perfect fit to the Kawakita model with R^2 values above 0.99 in all cases.

Table 7-3: Kawakita parameters for die filling and aspect ratio experiment performed for AG2 Batch 5

Die filling method	Mass tested (g)	Initial aspect ratio	b^{-1} (MPa)	a
Slow	4.00	0.20	0.53 ± 0.01	0.54*
Fast	4.00	0.20	0.50 ± 0.01	0.54*
Fast	6.00	0.29	0.54 ± 0.01	0.52*
Fast	8.00	0.39	0.56 ± 0.03	0.52*

Table 7-4: Kawakita parameters for die filling and aspect ratio experiment performed for AG5 Batch 2

Die filling method	Mass tested (g)	Initial aspect ratio	b^{-1} (MPa)	a
Slow	4.00	0.25	0.92 ± 0.06	0.54 ± 0.01
Fast	4.00	0.26	0.72 ± 0.04	0.56*
Fast	6.00	0.38	0.65 ± 0.02	0.56 ± 0.01
Fast	8.00	0.50	0.73 ± 0.06	0.56*

*Standard error less than 0.01

From the data presented in Table 7-3 and Table 7-4 it can be seen that:

I. In the case of AG2 Batch 5, some small increase in b^{-1} with increasing aspect ratio occurs. However, in the case of AG5 Batch 2 no significant variation in b^{-1} parameter occurred as a function of initial aspect ratio. However, it must be noted that the higher level of error in AG5 Batch 2 b^{-1} parameters may have masked this effect.

II. In the case of AG2 Batch 5 fast and slow die filling methods make little difference to b^{-1}. However, in the case of AG5 Batch 2 a large difference (0.2 MPa) was observed. To statistically test the hypothesis that the two data sets are from different populations, a student t-test [61] was applied which Indicted a 94% confidence of the data sets being from different populations. This supports the hypothesis that the two data sets are from different populations as they are not within 90% confidence intervals.

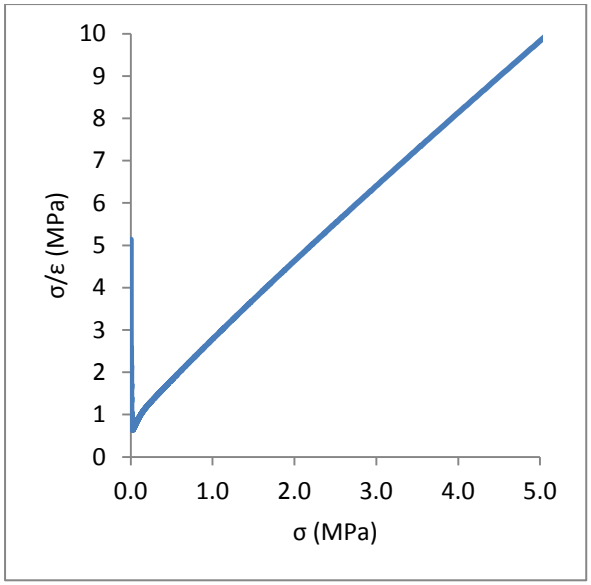

Figure 7-11: Kawakita plot for AG2 Batch 5 performed with 4 g of powder and fast die filling.

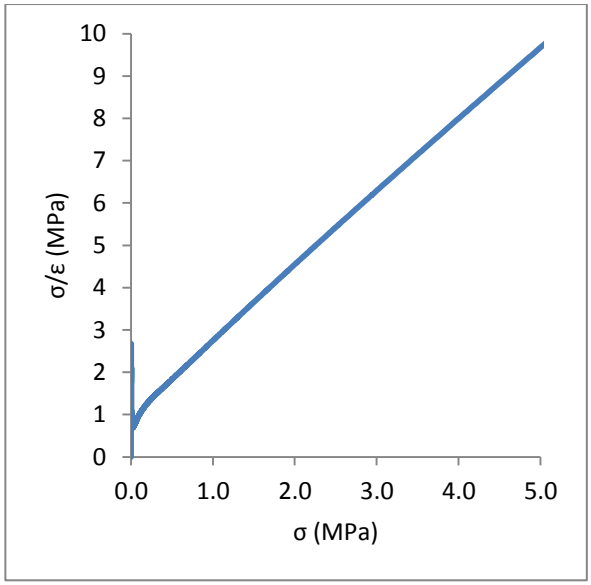

Figure 7-12: Kawakita plot for AG2 Batch 5 performed with 4 g of powder and slow die filling.

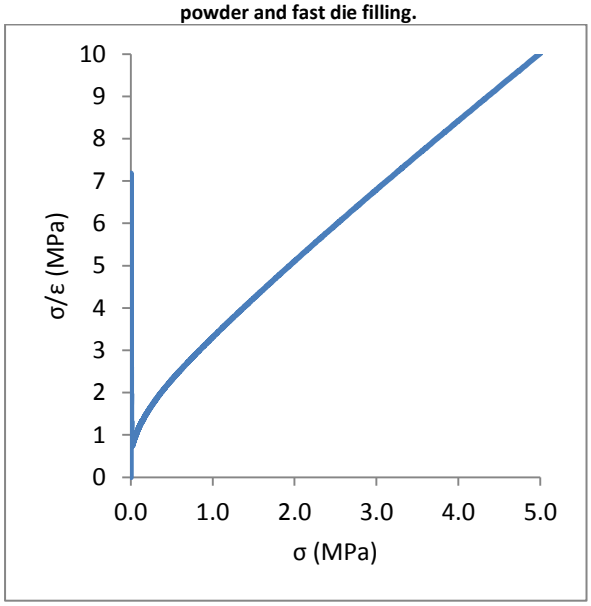

Figure 7-13: Kawakita plot for AG5 Batch 2 performed with 4 g of powder and fast die filling.

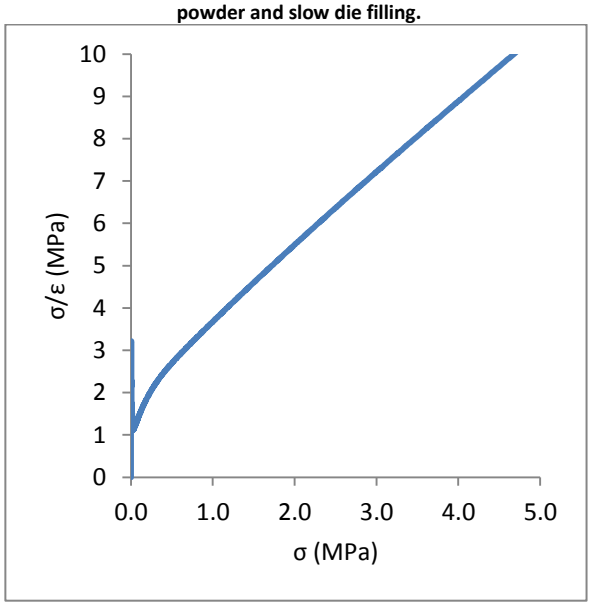

Figure 7-14: Kawakita plot for AG5 Batch 2 performed with 4 g of powder and slow die filling.

7.2.1.1 Fast and Slow Die Filling Methods

The results derived from testing of AG5 Batch 2 with fast die filling led to a lower Kawakita b^{-1} parameters than those derived from the testing with slow die filling. This suggests that in this case the fast method of die filling results in a less dense powder bed within which agglomerate particles have greater freedom to undergo rearrangement versus the denser bed arising from

slow die filling. This hypothesis is supported by the higher 'a' parameter associated with fast die filling and the larger initial aspect ratio, indicating that the initial powder bed created using the fast method was of high inter agglomerate particle porosity. Also it makes logical sense that a powder bed of increased initial porosity would lead to a reduced b^{-1} parameter, as it was shown in section 2.3.2 that b^{-1} can be defined as the stress required to reduce the bed porosity by half.

Comparing the results of fast and slow die filling performed with AG5 Batch 2 with those generated using AG2 Batch 5, it appears that AG5 Batch 2 is more sensitive to fast and slow die filling resulting in differing b^{-1} parameters. Nordstrom *et al*. [12] proposed that a critical particle size existed below which significant rearrangement occurs. The fast and slow die filling results presented in Table 7-3 and Table 7-4 suggest that given the similar particle size distributions of AG2 Batch 5 and AG5 Batch 2, other phenomena must also be influential. For example in addition to particle size it seems likely that the propensity of a powder to undergo particle-particle rearrangement would be influenced by phenomena such as segregation during die filling, particle shape, forces acting between agglomerate particles and the density of the agglomerate particles within the die.

7.2.1.2 Aspect Ratio Effects

b^{-1} parameters for AG2 Batch 5 and AG5 Batch 2 with varying aspect ratio are shown in Figure 7-15. The results presented in Figure 7-15 show that in the case of AG5 Batch 2, b^{-1} values show no significant influence of aspect ratio. In the case of AG2 Batch 5 aspect ratio has a weak influence upon b^{-1} parameters.

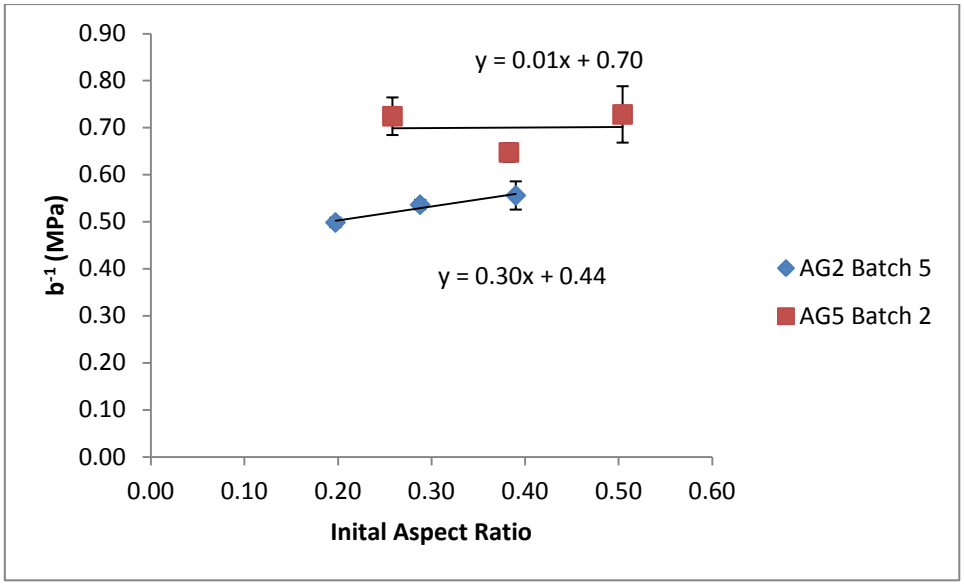

Figure 7-15: Kawakita Aspect ratio results for AG2 Batch 5 and AG5 Batch 2

7.2.2 Uniaxial Compaction of AG4 Batch 3, AG9 and AG8

In section 7.2.1 is was shown that slow die filling gave rise to higher b^{-1} values compared to fast die filling, suggesting that b^{-1} values derived using slow die filling are more closely related to plastic yielding and less sensitive to agglomerate particle rearrangement effects. Because of this, in this section of the thesis slow die filling will be used when investigating aspect ratio effects in order to give a cleaner separation of die filling aspect ratio effects.

Typical Kawakita plots for AG4 Batch 3, AG8 and AG9 are presented in Figure 7-16, Figure 7-17 and Figure 7-18. In the case of AG4 Batch 3 and AG8 a linear region was identified between 0.5 and 2.5 MPa, in the case of AG9 a similar region was identified between 2.5 and 5.0 MPa with R^2 above 0.99 in all cases. The Kawakita 'a' and b^{-1} parameters derived from these experiments with AG4 Batch 3, AG9 and AG8 are presented in Table 7-5, Table 7-6 to Table 7-7.

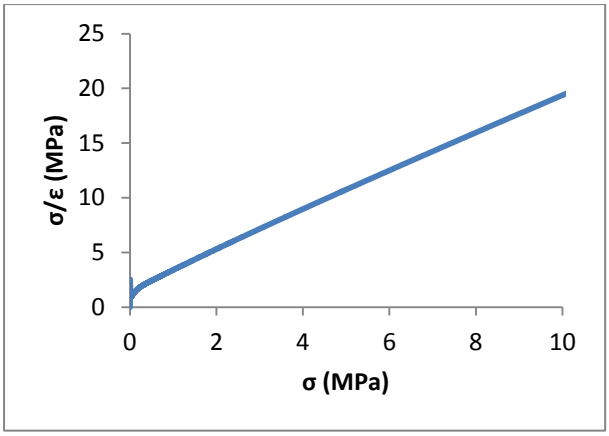

Figure 7-16: Kawakita plot for AG4 Batch 3, using 4 g of powder and fast die filling.

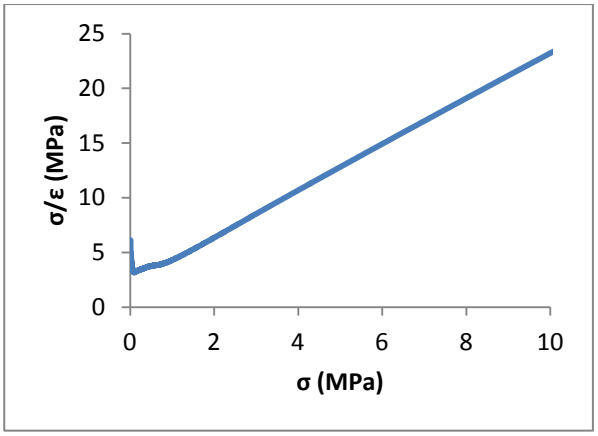

Figure 7-17: Kawakita plot for AG9, using 4 g of powder and fast die filling.

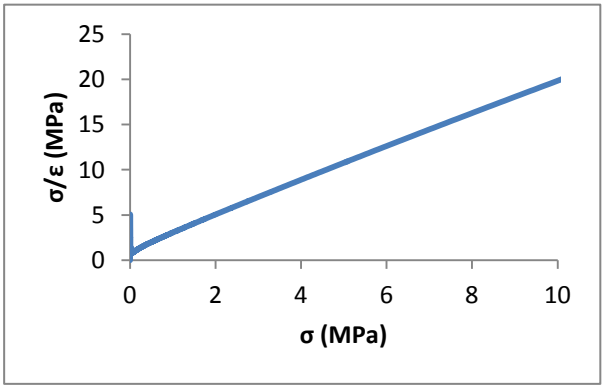

Figure 7-18: Kawakita plot for AG8, performed using 4 g of powder and slow die filling

Table 7-5: Kawakita parameters for die filling and aspect ratio experiment performed for AG4 Batch 3

Die filling method	Mass tested (g)	Initial aspect ratio	b^{-1} (MPa)	a
Slow	4.00	0.18	0.84 ± 0.03	0.52*
Slow	6.00	0.28	0.86 ± 0.04	0.50 ± 0.01
Slow	8.00	0.36	1.06 ± 0.02	0.50 ± 0.01
Fast	4.00	0.19	0.85 ± 0.04	0.52*

Table 7-6: Kawakita parameters for die filling and aspect ratio experiment performed for AG9

Die filling method	Mass tested (g)	Initial aspect ratio	b^{-1} (MPa)	a
Slow	4.00	0.23	0.98 ± 0.02	0.46*
Slow	6.00	0.34	1.06 ± 0.03	0.44*
Slow	8.00	0.45	1.14 ± 0.03	0.44*
Fast	4.00	0.23	0.96 ± 0.01	0.46*

Table 7-7: Kawakita parameters for die filling and aspect ratio experiment performed for AG8

Die filling method	Mass tested (g)	Initial aspect ratio	b^{-1} (MPa)	a
Slow	4.00	0.19	0.49 ± 0.02	0.49*
Slow	6.00	0.29	0.49 ± 0.04	0.48*
Slow	8.00	0.38	0.45 ± 0.01	0.48*

*Standard error less than 0.1

7.2.2.1 Die filling methods

Experiments performed with AG4 Batch 3 and AG9 using both fast and slow die filling methods show that b^{-1} parameters were not sensitive to die filling methods.

7.2.2.2 Aspect ratio effects

Figure 7-19 shows b^{-1} parameters as a function of initial powder bed aspect ratio for AG4 Batch 3, AG9 and AG8. The plot shows that as was shown for AG2 Batch 5 in Figure 7-15, for AG4 Batch 3 and AG9 increasing initial aspect ratio leads to increasing value of b^{-1}.

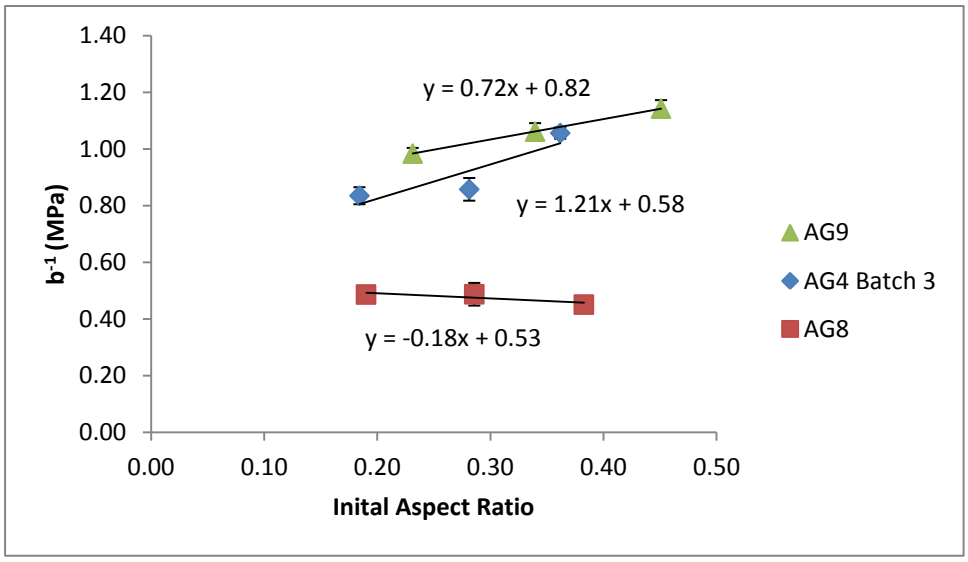

Figure 7-19: b^{-1} parameters determined for three different aspect ratios using slow die filling.

7.2.2 Uniaxial Compactions of SD2 and SD3

Uniaxial compaction experiments were performed with samples of SD2 and SD3 in order to investigate the effect of aspect ratio and in the case of SD2 die filling effect. Typical Kawakita

plots for SD2 and SD3 are shown in Figure 7-20 and Figure 7-21, in all cases a linear region was identified between 0.5 MPa and 2.5 MPa with R^2 values above 0.99 in all cases.

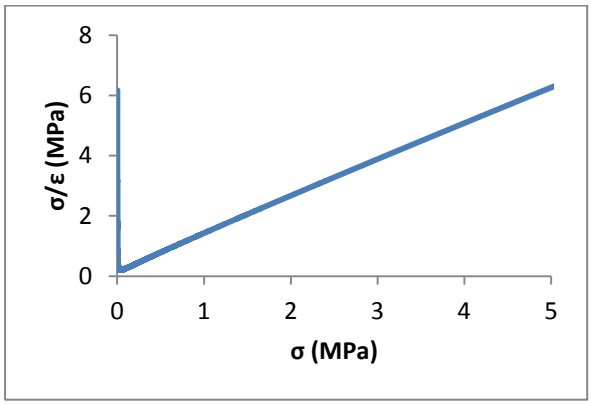

Figure 7-20: Kawakita plot for SD2 performed with 2 g of powder and slow die filling.

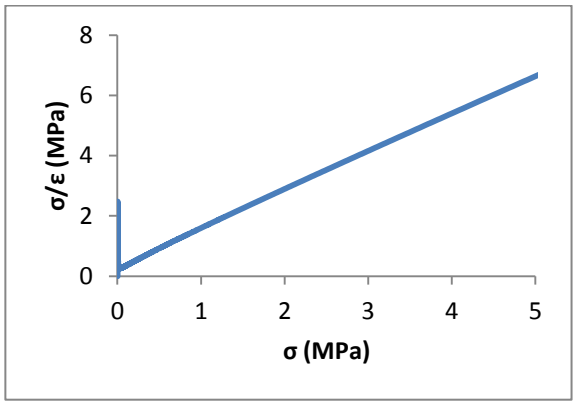

Figure 7-21: Kawakita plot for SD3 performed with 2 g of powder and slow die filling.

Table 7-8 and Table 7-9 give Kawakita a and b^{-1} parameters for SD2 and SD3 as a function of both initial powder aspect ratio and in the case of SD2 die filling method. The initial aspect ratios show that as is typically the case, the spray dried powders SD2 and SD3 are of approximately half the bulk density of the high shear agglomerates (based upon initial aspect ratio values) tested previously in this chapter. SD2 shows sensitivity to the die filling method, however, the variation in b^{-1} is not sufficiently large to influence predictions regarding its ability to form build-up. Both powders show no sensitivity to initial aspect ratio.

Table 7-8: Kawakita parameters for die filling and aspect ratio experiment performed for SD2

Die filling method	Mass tested (g)	Initial aspect ratio	b^{-1} (MPa)	a
Slow	2.00	0.24	0.20*	0.79*
Slow	4.00	0.48	0.17*	0.78*
Slow	6.00	0.73	0.18*	0.79*
Fast	4.00	0.50	0.11*	0.81*

Table 7-9: Kawakita parameters for aspect ratio experiment performed for SD3

Die filling method	Mass tested (g)	Initial aspect ratio	b^{-1} (MPa)	a
Slow	2.00	0.19	0.19 ± 0.03	0.77*
Slow	4.00	0.37	0.15 ± 0.02	0.77*
Slow	6.00	0.58	0.16 ± 0.01	0.76*

*Standard error less than 0.1

Excluding AG5 Batch 2 where experimental error leads to uncertainty regarding the influence of the initial aspect ratio upon b^{-1} parameters, powders with low b^{-1} parameters such as SD1 and SD2 have tended to show little or no influence of initial aspect ratio on b^{-1} parameters.

7.3 Tablet Strength Experiments

For all powders tested in this chapter following uniaxial compactions, tablets were extracted from the die and compressed diametrically to measure their strength as a function of their mass and thus aspect ratio prior to diametric compression. The results of these experiments can be seen in Table 7-10, Figure 7-22, Figure 7-23 and Figure 7-24. The results show that:

- Tablet strengths measured for AG2 Batch 5, AG4 Batch 3, AG8 and SD3 show little or no significant dependency upon aspect ratio.
- For the tablet strengths measured for SD2 and AG5 Batch 2 tablet strength increases with increasing aspect ratio. However, this increase is more significant when moving between low values of aspect ratio.
- Tablet strengths measured for AG9 increase linearly with increasing aspect ratio.

Table 7-10: Tablet strengths for powders tested in Chapter 7

	Mass (g)	Tablet aspect ratio	Tablet strength (MPa)	Fracture observed
SD2	2.00	0.04	0.93 ± 0.07	No
	4.00	0.09	1.52 ± 0.04	Yes
	6.00	0.13	1.67 ± 0.03	Yes
SD3	2.00	0.04	0.16 ± 0.02	Yes
	4.00	0.09	0.20 ± 0.02	Yes
	8.00	0.18	0.26 ± 0.01	Yes
AG2 Batch 5	4.00	0.09	0.59 ± 0.03	Yes
	6.00	0.14	0.54 ± 0.01	Yes
	8.00	0.18	0.57 ± 0.02	Yes
AG8	4.00	0.09	0.76 ± 0.02	Yes
	6.00	0.14	0.85 ± 0.02	Yes
	8.00	0.19	0.81 ± 0.02	Yes
AG4 Batch 3	4.00	0.09	0.82 ± 0.01	Yes
	6.00	0.14	0.71 ± 0.01	Yes
	8.00	0.19	0.86 ± 0.01	Yes
AG5 Batch 2	4.00	0.11	1.13 ± 0.09	No
	6.00	0.16	1.44 ± 0.02	Yes
	8.00	0.22	1.43 ± 0.02	Yes
AG9	4.00	0.14	0.17 ± 0.02	No
	6.00	0.20	0.36 ± 0.01	No
	8.00	0.27	0.50 ± 0.01	No

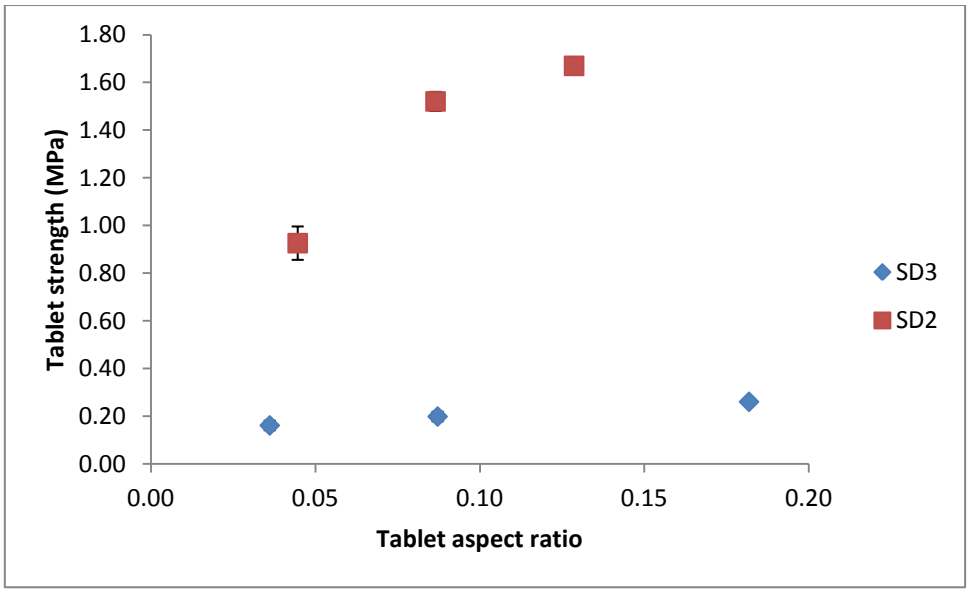

Figure 7-22: Tablet strength data for SD2 and SD3

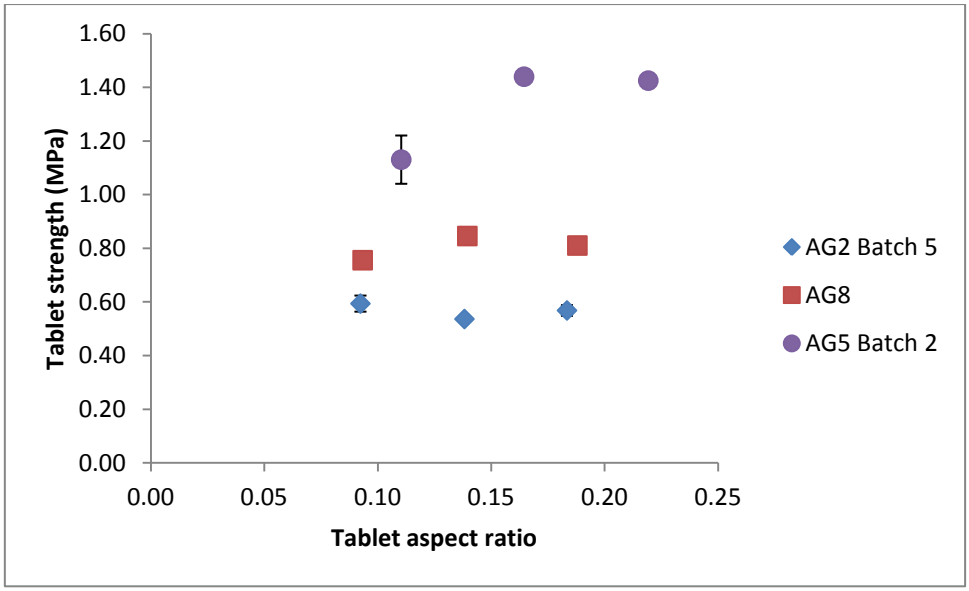

Figure 7-23: Tablet strength data for AG2 Batch 5, AG8, and AG5 Batch 2

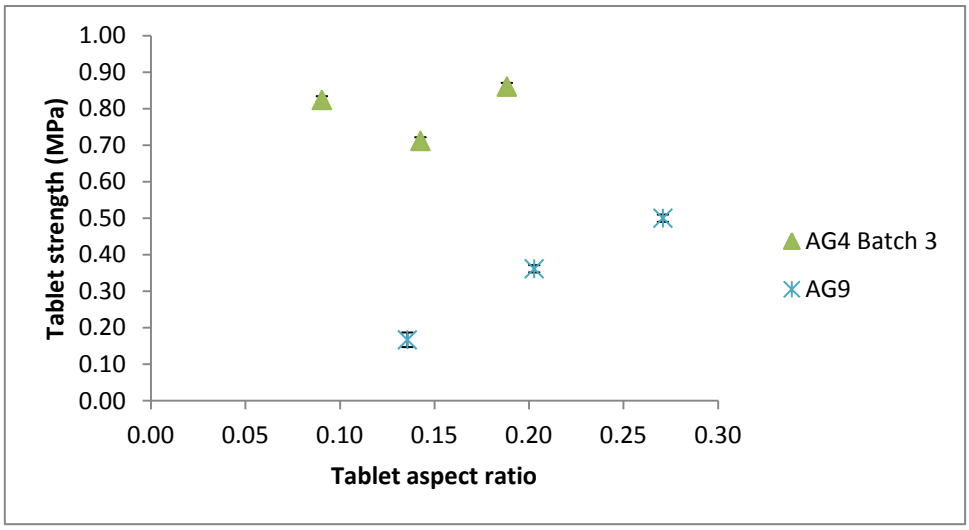

Figure 7-24: Tablet strength data for AG4 Batch 3 and AG9

To determine why tablet strength measurements would vary with tablet aspect ratio (AR_t) it is necessary to start by considering the assumptions made in the initial derivation of the equation used for their calculation i.e. *Eq.* (7-50) presented previously in Chapter two.

$$Tablet\ Strength = \frac{2F_t}{\pi D_t t} \quad \textbf{(7-50)}$$

where F_t is tablet breaking force, D_t is the diameter of the tablet and t is the thickness.

This equation is based on the brittle failure of a two dimensional disc, with all deformation prior to failure being purely elastic, leading to a homogenous force distribution throughout the disc

[51]. Therefore it is possible that variation in tablet strength with tablet aspect ratio arose from a departure from these conditions. More specifically a degree of plastic contact flattening was observed in all cases, indicating that deformation prior to failure was not purely elastic and forces within the tablet may not have been homogenously distributed [51].

However, returning to the data presented in Table 7-10 and plotted in Figure 7-22, Figure 7-23 and Figure 7-24, it is clear that variation in AR_t (defined as the height of the tablet divided by the its diameter) influenced tablet strength measurements only when the failure of the tablet did not lead to observable fracture, specifically:

- SD2 tablets with a AR_t of 0.04
- AG5 Batch 2 tablets with an AR_t of 0.11
- AG9 at all AR_t values

The Vankell VK200 tablet hardness tester records tablet breaking force via the measurement of a peak force with compression ceasing once a peak force has been recorded indicating that yielding has occurred. Therefore if fracture is observed failure of the tablet will have occurred rapidly post yielding i.e. prior to compression ceasing. If fracture is not observed fracture may have initiated but not become visibly observable prior to compression ceasing, indicating that fracture is occurring over a longer period of time i.e. is not rapidly. This leads to the conclusion that Eq. (7-50) may not eliminate the effects of tablet geometry in the case of tablets which do not undergo rapid fracture post yielding.

7.4 A Screw Tester Build-up Operating Space Model

In this section Kawakita b^{-1} parameters (presented in section 7.2) and tablet strengths (presented in section 7.3) will be used in conjunction with screw tester build-up masses (see Table 7-11), to form an operating space model similar to that generated for auger filler build-up in Chapter 6 (see Figure 7-26). In the case of the b^{-1} parameters the values used correspond to

the lowest powder aspect ratio used to minimise the effect of die wall friction. In the case of tablet strengths the values correspond to the highest aspect ratios used, which were selected in order to minimise effects associated with the use of low tablet aspect ratios discussed in section 7.3. Screw tester build-up masses were measured using the method discussed in Chapter 3.

Table 7-11: Screw tester build-up mass, Kawakita b^{-1} parameters and tablet strengths

Powder	Screw tester build-up (g)	Fractional Screw tester build-up w/w	Kawakita b^{-1} (MPa) At the lowest aspect ratio tested, using slow die filling	Tablet strength (MPa) At the highest aspect ratio tested
SD2	1.0	0.20%	0.20*	1.67 ± 0.03
SD3	25.1	5.02%	0.19 ± 0.02	0.26 ± 0.01
AG2 Batch 5	8.5	0.85%	0.53 ± 0.01	0.57 ± 0.02
AG8	2.6	0.26%	0.49 ± 0.02	0.81 ± 0.02
AG4 Batch 3	0.3	0.03%	0.84 ± 0.03	0.86 ± 0.01
AG5 Batch 2	0.0	0.00%	0.92 ± 0.06	1.43 ± 0.02
AG9	0.0	0.00%	0.98 ± 0.02	0.50 ± 0.01

*Standard error less than 0.01

The results presented in Figure 7-25 show that as was previously shown in Figure 6-40 for auger filler build-up alone, powders with both low Kawakita b^{-1} parameters and low tablet strengths form build-up, whilst powders with higher values generate either significantly less build-up or in the case of AG9 and AG5 Batch 2 generate no observable build-up. It should also be noted that for the powders which generated less than 2.0 g of build-up, build-up was found only to the rear of the screw tester in the small section directly behind the powder feed. This suggests that agglomerate particles which build-up in this area of the screw tester may have experienced stresses over longer periods of time, versus agglomerate particles which passed from the feed forwards towards the screw tester exit.

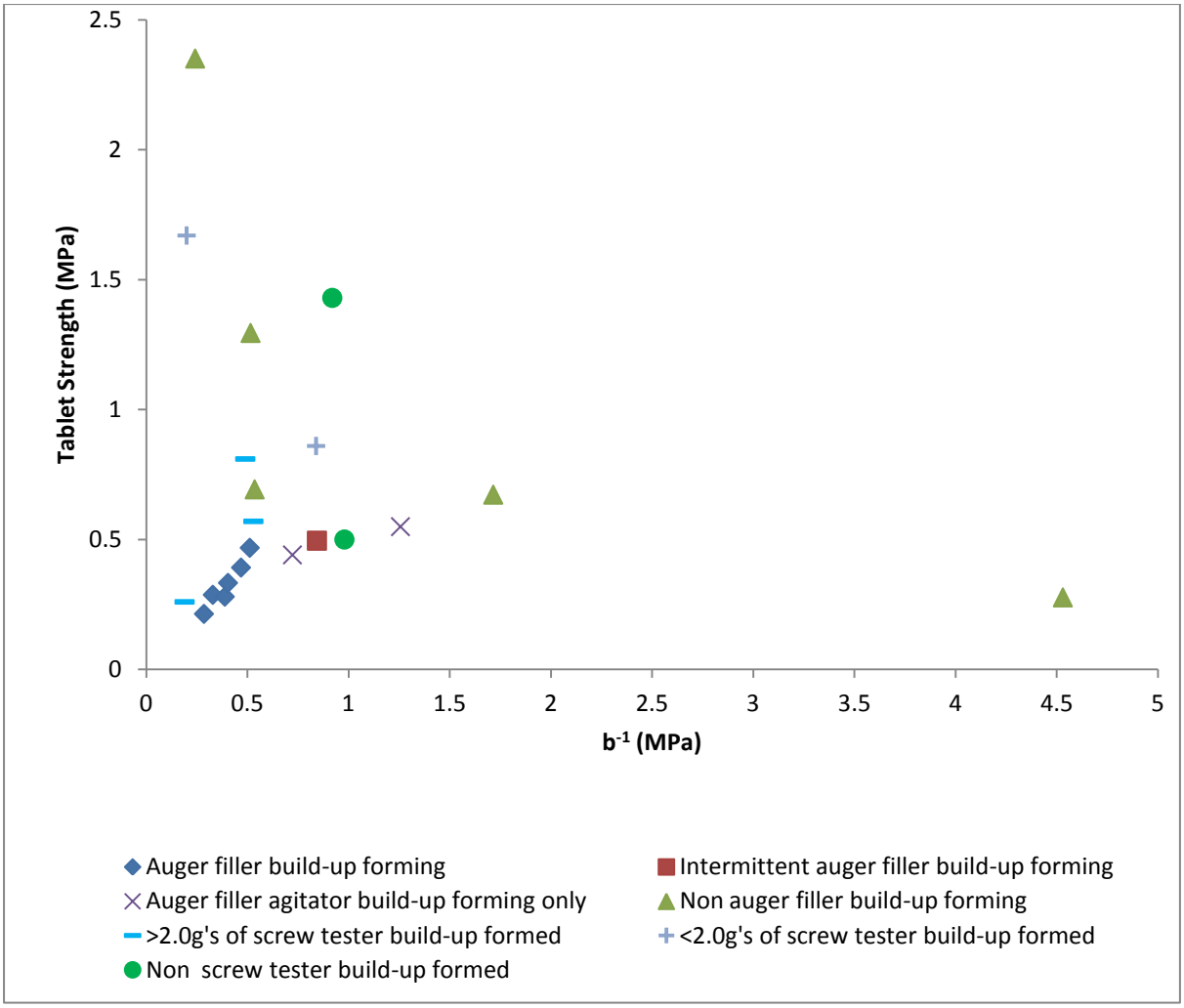

Figure 7-25: An operating space model for the prediction of auger filler and screw tester build-up.

Figure 7-25 shows that:

- Auger filler build-up is formed by powders with Kawakita b^{-1} parameters of 0.51 MPa or less and tablet strengths of 0.47 MPa or less, excluding cases where intermittent and agitator only build-up were formed.
- Screw tester build-up is formed by powders with Kawakita b^{-1} parameters of 0.53 MPa or less and tablet strengths of 0.81 MPa or less. This excludes cases where < 2.0 g of build-up were formed.

From the values presented in Table 7-12 it is clear that the auger filler and screw tester have significantly different values of tip speed and shear rate and thus the similar values of b^{-1} and tablet strength associated with the powders which form build-up within them are perhaps surprising. It is proposed that this similarity results from the fact that they are similar in terms of their clearances, which in all cases were smaller than the geometric mean particle size of the powders tested. In Chapter 8 using sieve fractions of AG3 it will be shown that a powder of sufficiently low b^{-1} parameter and tablet strength will form build-up in such a situation.

Table 7-12: A comparison of the Auger Filler and Screw tester.

	Auger	Screw
Rotational speed (RPM)	840	75
Diameter (mm)	24.5	31.5
Clearance (mm)	0.3	0.1
Tip speed (m/s)	1.1	0.1
Shear rate (s^{-1})	3592	1237

7.5 Tablet Indentation Experiments

As was discussed in section 7.3 there is some uncertainty regarding the exact value of tablet strength for AG9 due to its sensitivity to tablet aspect ratio. However, AG9's high value of b^{-1} means that in this case tablet strength measurements are not required to predict that no build-up will be formed.

It was proposed in Chapter 6 that material with low b^{-1} parameters and high tablet strength *e.g.* SD1, do not form build-up, because their high tablet strength reflects the high strength/hardness of material from which they were formed while their low b^{-1} parameters arose from their porous structures. An issue with this proposal is that powders with high b^{-1} parameters and no evidence of any internal porosity, such as AG9 tested in this chapter and AG7 tested in Chapter 6 have low tablet strengths, possibly because the agglomerate particles within their tablets were not strongly agglomerated. A possible alternative to diametric tablet strength

measurements is the use of indentation into tablets using the method previously used for indentations into samples of build-up in Chapter 6.

Table 7-13: Tablet indentation depths and Kawakita b^{-1} parameters

Powder	Screw tester build-up (g)	Kawakita b^{-1} (MPa) At the lowest aspect ratio tested, using slow die filling	Tablet indentation depth (mm)
AG2 Batch 5	8.5	0.53 ± 0.01	0.09 ± 0.01
AG8	2.6	0.49 ± 0.02	0.06*
AG4 Batch 3	0.3	0.84 ± 0.03	0.06 ± 0.01
AG5 Batch 2	0.0	0.92 ± 0.06	0.03*
AG9	0.0	0.98 ± 0.02	0.03*

*Standard error less than 0.1

The results presented in Table 7-13 show that AG9 has a low indentation depth which in contrast to the tablet strength's measurement in Table 7-11 is now equal to that measured for AG5 Batch 2, reflecting the lack of screw tester build-up formation observed in both cases. Figure 7-26 shows an alternative operating space model for screw tester build-up formatting utilising b^{-1} and tablet indention depth measurements. The results show that powders which formed build-up tended to have low b^{-1} parameters and high indentation depths. This supports the hypothesis that powders which form build-up tend to form soft plastic tablets. This in turn reflects the soft plastic nature of the agglomerate particles and their ability to generate large contact areas under the influence of forces applied to them during screw tester and/or auger filler experiments.

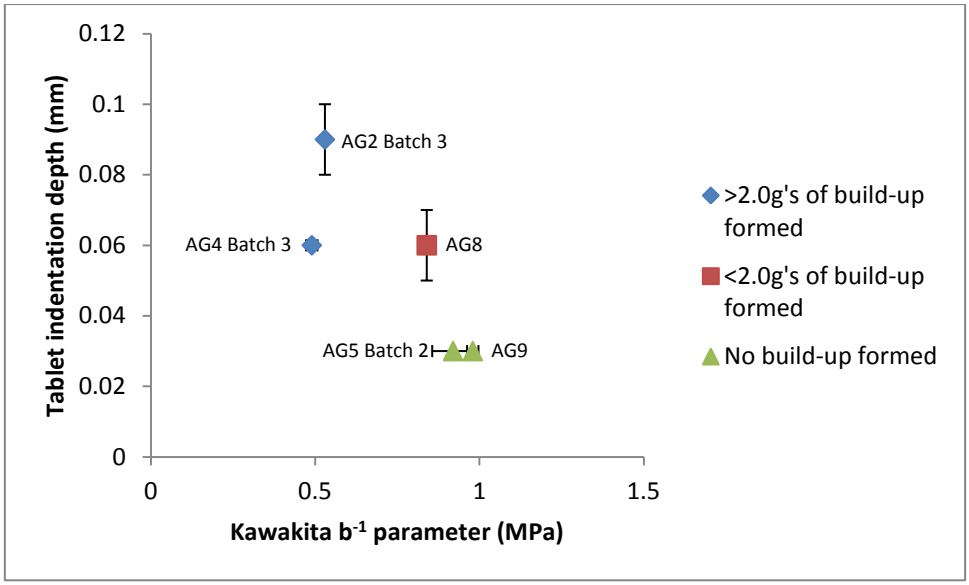

Figure 7-26: A Screw tester build-up operating space model, utilising b^{-1} and tablet indention depth measurements

7.6 Conclusions

The experimental results presented in this chapter have shown that:

- A study on the influence of the initial powder bed aspect ratio on b^{-1} parameters showed that while many of the powders tested showed some sensitivity to initial powder bed aspect ratio, powders which formed build-up *e.g.* AG8 and SD3, showed little or no sensitivity.
- A parallel study of the effects of fast and slow die filling methods showed that only AG5 Batch 2 demonstrated significant sensitivity to die filling effects. The results obtained using fast die filling of AG5 Batch 2 yielded b^{-1} parameters 0.2 MPa lower than those obtained using the slow die filling method. This is believed to result from fast die filling leading to a less dense powder bed, within which agglomerate particles have greater freedom to undergo rearrangement, relative to the denser bed arising from the slow die filling method.

- A study of the impact of tablet aspect ratio on tablet strength measurements showed that SD2 and AG5 Batch 2 and AG9 were sensitive to tablet aspect ratio. However, for all powders excluding AG9 these effects can be avoided by using tablet aspect ratios above 0.15.
- It should be noted that the results generated for AG5 Batch 2 would suggest that the values of tablet strength and b^{-1} quoted in Chapter 6 for AG5 Batch 1 may have been lower than would have been the case if slow die filling and larger tablet aspect ratios had been used.
- Screw tester build-up experiments were then used in conjunction with b^{-1} parameters and tablet strength measurements to develop an operating space model. This model was found to have a similar form to that of the auger filler model presented in Chapter 6. The auger filler and screw tester have many differences, but have relevant clearances of similar magnitudes (0.3 mm and 0.1 mm). This suggests that it may be the magnitude of the clearance which dominates the build-up formation process, and not other parameters such as strain and shear rate.
- Tablet indentations were investigated as an alternative to tablet strength measurements. The results obtained via this method were found to more accurately reflect the non-build-up forming nature of AG9 and AG5 Batch 2.

8. The Influence of Auger/Tube Clearance and Particle Size on Auger Filler Build-up

As discussed in Chapter 2, a hypothesis has been formed that the stresses experienced by agglomerate particles passing through the auger filler is a function of the ratio of the agglomerate particle size to the magnitude of the auger/tube clearance. In Chapter 5 results generated using #16 and #22 augers (clearances 300 and 600 μm) supported this hypothesis. However, the powder used (an Ariel finished detergent powder) was a blend of powders of widely varying agglomerate particle size and mechanical properties e.g. fine grade sodium sulphate, sodium percarbonate, AG1 and SD1. This leads to the conclusion that changing the auger/tube clearance may have altered the nature of the agglomerate particles within the auger/tube clearance, potentially impacting the powder's tendency to form build-up. In Chapter 6, auger filler build-up results generated with AG2 Batch 1 and 2 and the #16 auger showed that the large agglomerate particle size of the AG2 batch 2 powder (geometric mean particle size 772 μm) destabilised the auger and led to build-up forming more slowly than was the case with AG1 Batch 1.

8.1 Blends of Sodium Sulphate and AG2 Batch 3

As was shown previously in Chapter 4, P&G's laundry detergent finished products contain a wide variety of powders including hard crystalline salts such as sodium sulphate. Figure 8-1 and Figure 8-2 show SEM images of fine and coarse grades of sodium sulphate used in this section of the thesis. It seems reasonable to assume that crystalline powders such as sodium sulphate will not form build-up when filled in their pure form. However, it is proposed that when sodium sulphate is blended with a build-up forming powders such as AG2 Batch 3 the presence of sodium sulphate may act to slow or eliminate the formation of build-up. It is proposed that this

process may be sensitive to the particle size of sodium sulphate particles in relation to the auger/tube clearance.

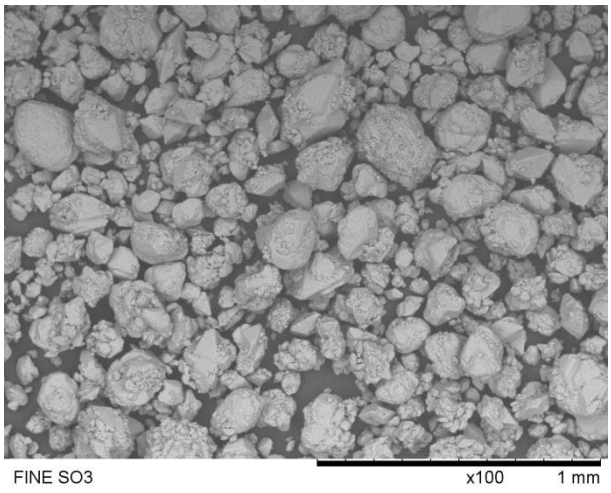

Figure 8-1: An SEM image of sodium sulphate, fine grade

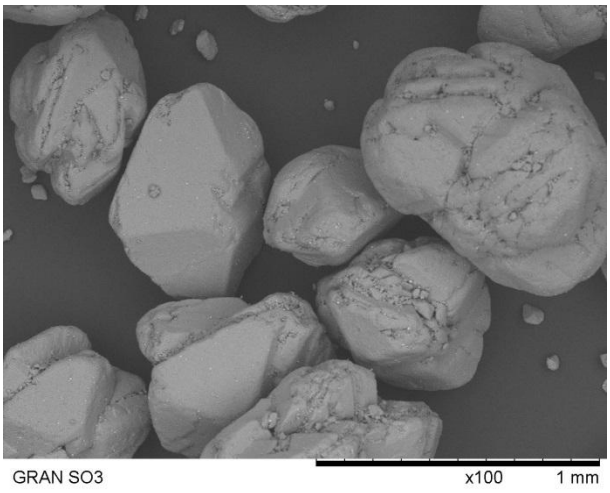

Figure 8-2: An SEM image of sodium sulphate, course grade

Particle size distributions for fine and coarse grades of sodium sulphate and AG2 Batch 3 in relation to the 300 µm auger/tube clearance are shown in Figure 8-3. These powders will be used in this section of the thesis in conjunction with characterisation data generated for AG2 Batch 3 in Chapter 6.

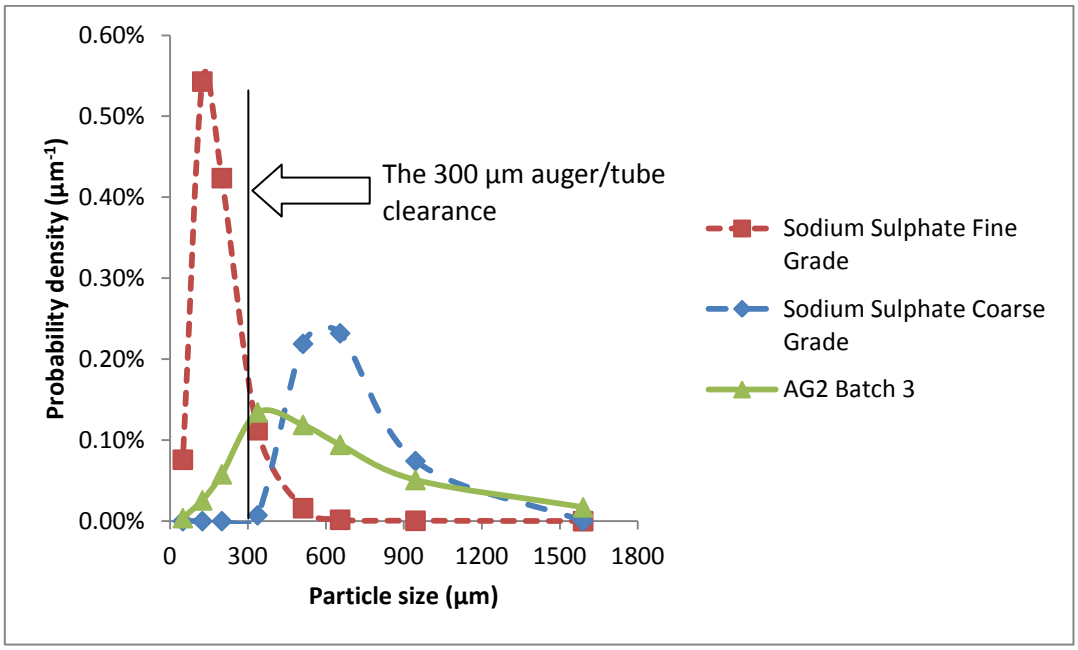

Figure 8-3: Particle size distributions for fine and course grades of sodium sulphate and AG2 Batch 3, in relation to the 300 µm auger/tube clearance.

Figure 8-4 shows torque data recorded during auger filler experiments performed with:

I. AG2 Batch 3

II. AG2 Batch 3 blended with an equal mass of fine sodium sulphate

III. AG2 Batch 3 blended with an equal mass of coarse sodium sulphate

Blends were produced using the same method described for the blends of SD1 and AG1 in Chapter 6. The results include a repeat performed with unblended AG2 Batch 3, presented previously in Chapter 6 showing that the test method is highly repeatable. The results show that the blend containing the fine grade of sodium sulphate did not form build-up, while the blend containing the coarse grade did, but did so more slowly than the unblended samples of AG2 Batch 3.

It is proposed that the particle size differences presented in Figure 8-3 may explain the differences seen during the filling of the two blends of sodium sulphate and AG2 Batch 3 shown in Figure 8-4. This is because the particles with the coarse grade of sodium sulphate are predominantly larger than the auger/tube clearance and thus its particles are unable to prevent the formation of build-up formed by AG2 Batch 3 in the auger filler. In the case of the blends of the fine grade of sodium sulphate and AG2 Batch 3 the sodium sulphate particles are predominantly smaller than the auger tube clearance, and thus they were able to enter the auger tube clearance zone, interfering with build-up formation.

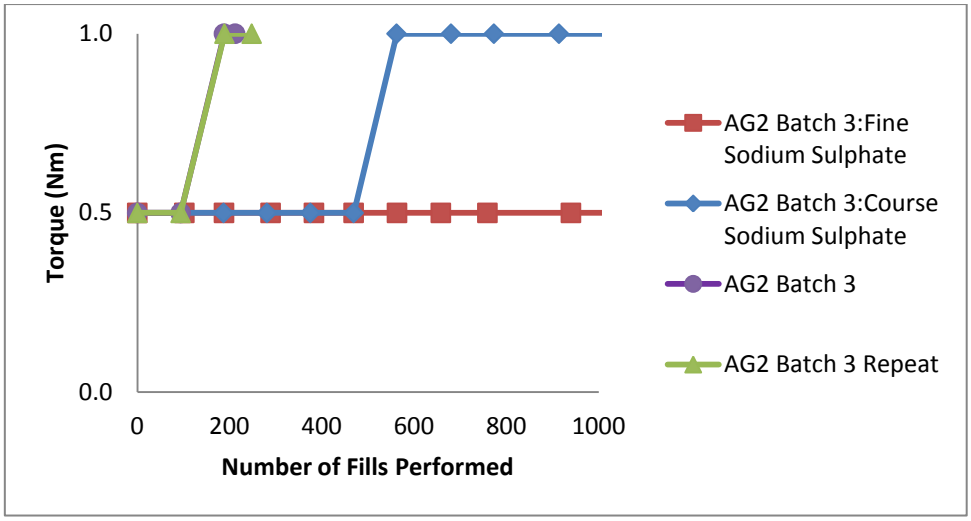

Figure 8-4: Torque data extracted from auger filler experiments performed with both pure AG2 Batch 3 and 1:1 blends w/w with coarse and fine sodium sulphate.

This shows that hard crystalline powders are able to prevent plastic low yield stress powders forming build-up. Given the comparable particle sizes of the fine grade of sodium sulphate and AG2 Batch 3 it seems unlikely that the fine grade of sodium sulphate is able to prevent the formation of build-up by acting as a flow aid, reducing adhesive forces acting between the AG2 Batch 3 agglomerate particles and the tube wall. It is thus proposed that the sodium sulphate particles are able to reduce the cohesion within the build-up formed by AG2 Batch 3 leading to the build-up having a weak 'crumb'- like structure unable to survive on the tube surface.

The delayed rise in torque for the blend containing the coarse sodium sulphate versus the unblended sample of AG2 Batch 3 shown in Figure 8-4 is potentially due to dilution of the build-up forming AG2 Batch 3 agglomerate particles with non-build-up forming sodium sulphate particles. This would then lead to less build-up forming agglomerate particles entering the clearance per unit time. However, it is also possible that while the coarse sodium sulphate particles were not able to enter the clearance they may have acted to obstruct AG2 Batch 3 agglomerate particles entering, again reducing the number of build-up forming agglomerate particles entering the clearance per unit time.

8.1.1 Uniaxial Compactions of AG3 Sodium Sulphate Blends

Figure 8-5 shows typical Kawakita plots for 1:1 blends of AG2 Batch 3 with coarse and fine grades of sodium sulphate. Table 8-1 gives Kawakita parameters extracted from compaction data between 0.5 and 2.5 MPa and tablet strengths measured post compaction to 58 MPa. The values quoted are the mean of four repeats quoted in conjunction with standard errors.

Table 8-1: Kawakita parameters and tablet strengths for blends of AG2 Batch 3 and sodium sulphate

	a	b^{-1} (MPa)	Tablet Strength (MPa)
AG2 Batch 3: Coarse Sodium Sulphate	0.45*	0.37 ± 0.01	0.28 ± 0.01
AG2 Batch 3: Fine Sodium Sulphate	0.42 ± 0.01	0.63 ± 0.03	0.30 ± 0.01

*Standard error less than 0.01

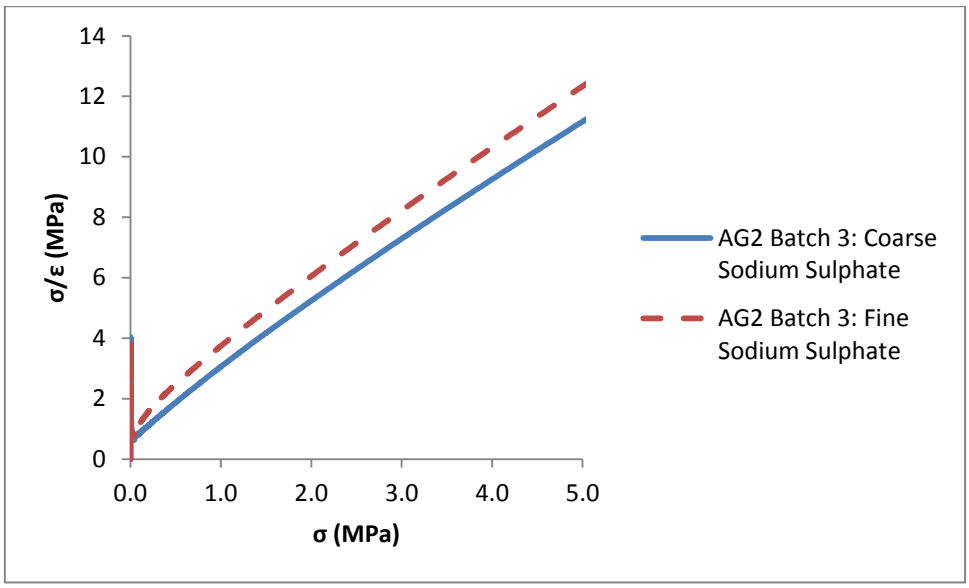

Figure 8-5: Kawakita plots for AG2 Batch 3: Sodium sulphate blends

From the values presented in Table 8-1 it can be seen that:

- In the case of the coarse sodium sulphate blend b^{-1} and tablet strength values, reflecting the fact that build-up was formed.
- For the blend containing fine sodium sulphate, b^{-1} and tablet strength values do not clearly reflect the lack of build-up formation.

- Additionally the b^{-1} value for the fine sulphate blend is low considering the value of 12.0 MPa reported in Chapter 4 for pure fine sodium sulphate.

This suggests that the compaction of these blends was dominated by the weaker AG2 Batch 3 agglomerate particles which were shown to have a b^{-1} of 0.39 MPa in Chapter 6. Additionally considering that in Chapter 6 AG2 Batch 3 had a tablet strength of 0.28 MPa, the results show that sodium sulphate did not act to increase tablet strength, possibly because the sodium sulphate particles were held within a continuous phase formed by plastic AG2 Batch 3 agglomerate particles which then dominated the tablet strength measurements. This leads to the conclusion that as was shown in Chapter 5 with Ariel and Bold, a new methodology for predicting powder build-up is needed in the case of powder blends.

8.2 Build-up of AG3 Sieve Fractions

To explore the effect of agglomerate particle size in more detail a sample of AG3 with a broad agglomerate particle size distribution was obtained. This sample was subsequently sieved manually into three size fractions: 0 to 600 μm, 600 to 1180 μm and 1180 to 4750 μm. Particle size distributions for the three fractions are plotted in Figure 8-6. Table 8-2 gives geometric mean particle sizes measured via gravimetric sieving and equilibrium relative humidities for each sieve fraction, showing that the three size fraction's moisture contents were at equilibrium with one another.

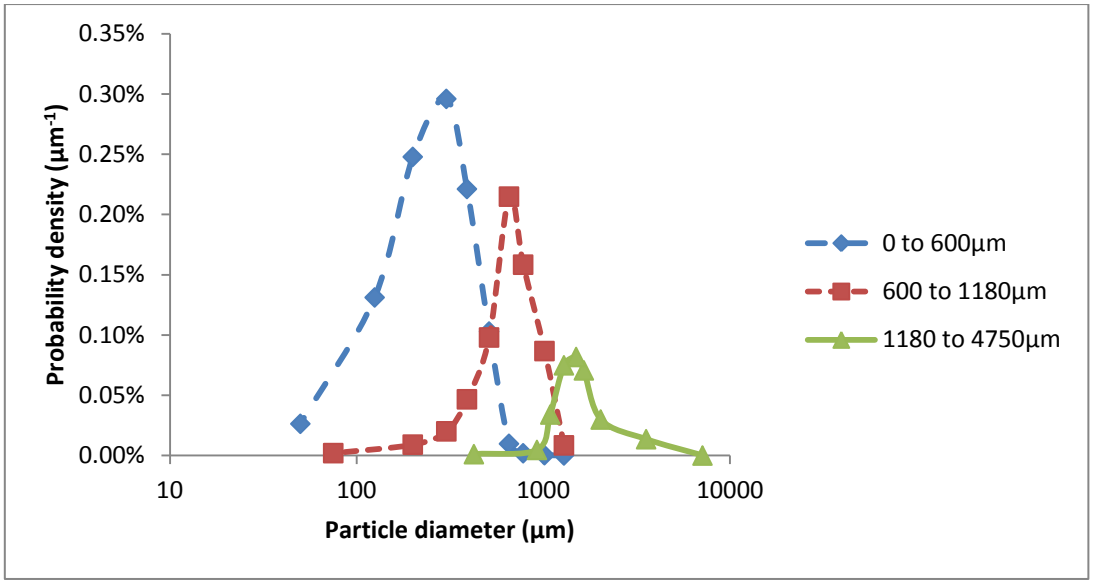

Figure 8-6: Particle size distributions for AG3 sieve cuts

Table 8-2: Particle size and equilibrium relative humidity data for sieve fractions of AG3

	0 to 600 µm	600 to 1180 µm	1180 to 4750 µm
Geometric mean particle size (µm)	257	703	2209
eRH (%RH)	52.6 ± 0.4	50.4 ± 0.4	52.4 ± 0.4

Each of the three sieve fractions were passed through the auger filler using the method developed in Chapter 6 for a minimum of 1000 fills. Results derived from these experiments can be seen in Table 8-3. The results show clearly that only the packing of the largest size fraction resulted in the formation of build-up on the tube surface, however, it should also be noted that unusually no lumps of build-up were observed to fall out of the auger filler following its formation.

This is perhaps surprising given that clearance/gap existing between the auger and tube is 300 µm *i.e.* significantly smaller than 1180 µm. This is in contradiction to the findings of Crutchley and Bridgwater [29] who showed that the stress experienced by particles within a small clearance/gap reduced as the clearance/gap became small versus the agglomerate particle size. This may be because Crutchley and Bridgwater [29] studied the attrition of brittle particles

whereas in this case the deformation of plastic agglomerate particles resulting in build-up formation is being studied.

Table 8-3: Torque and tube surface temperature data for auger filler build-up experiments conducted with AG3 sieve fractions

Size Fraction (µm)	Fills performed	Build-up observed on tube surface	Torque (Nm)		Tube Surface Temperature (˚C)	
			Start value	End value	Starting value	End value
0 to 600	1053	No	0.5	0.5	18.0	18.0
600 to 1180	1000	No	0.5	0.5	17.8	17.3
1180 to 4750	1033	Yes	0.5	1.0	16.3	28.2

For a model system a plastic agglomerate particles' yield stress should not be considered to be dependent upon particle size. However, as was shown by Samimi *et al*. [14] via bulk compaction and Adams τ'_0 parameters (see Figure 8-7) and single particle compressions (see Table 8-4) this cannot be assumed to be true in the case of formulated/micro structured materials.

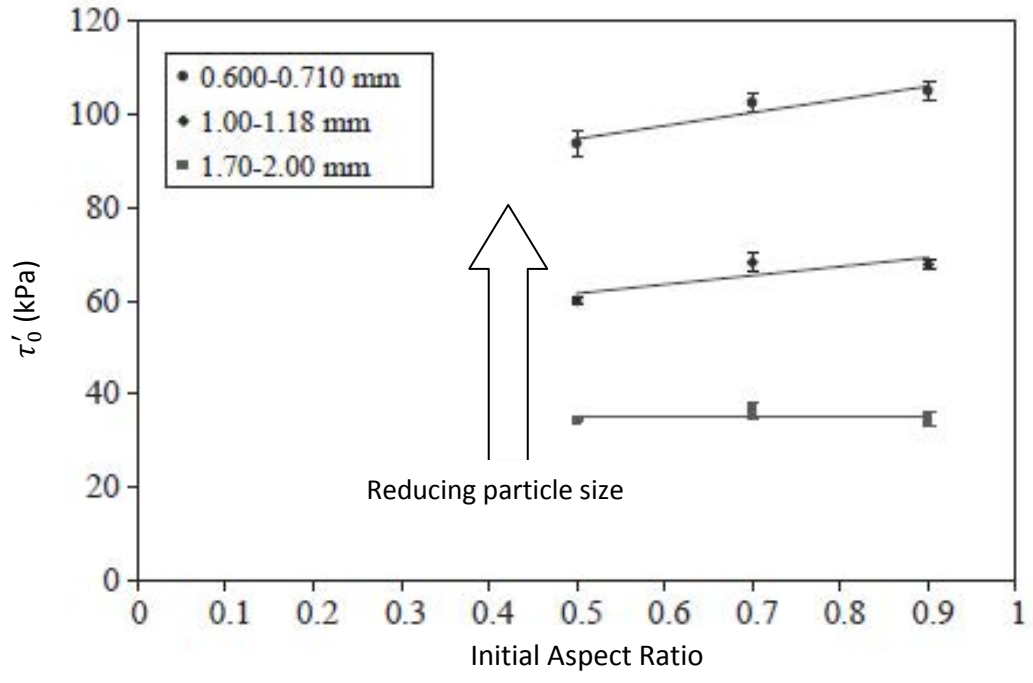

Figure 8-7: Adams τ'_0 parameters derived from bulk uniaxial compactions of soft detergent granules [14]

Table 8-4: Yield stresses of soft detergent granules obtained via single granule compression data [14]

Granule particle size (mm)	Single agglomerate particle yield stress (kPa)
1.70-2.00	297 ± 108
1.00-1.18	405 ± 151

To determine the relationship between particle size and build-up formation for the AG3 size fractions, Kawakita a, b^{-1} parameters as well as tablet strengths have been determined. As can be seen in Figure 8-8, Kawakita plots for the three sieve fractions contain a linear region between 0.5 and 2.5 MPa, within which it was determined that an R^2 value of greater than 0.99 could be obtained.

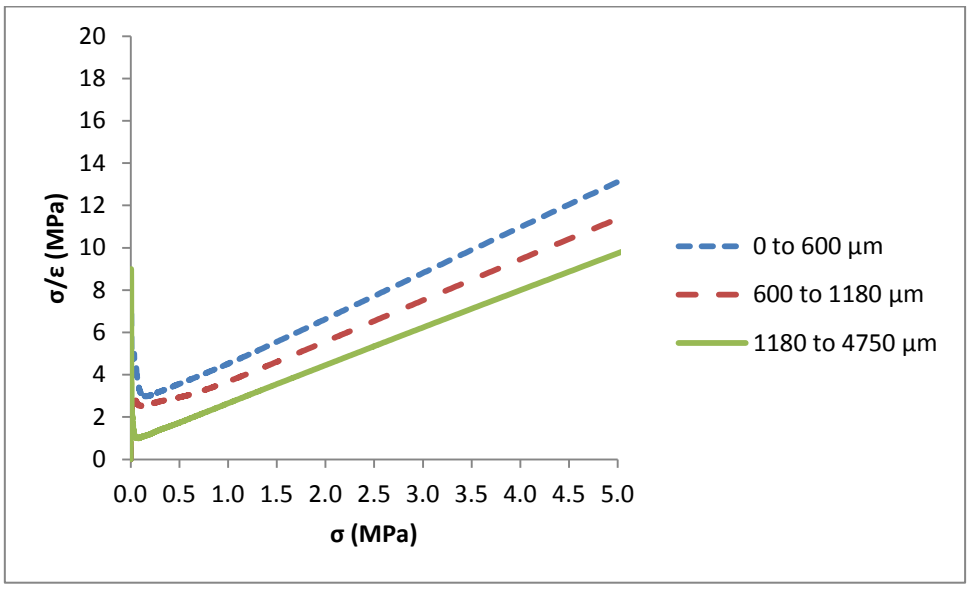

Figure 8-8: Kawakita plots for sieve fraction of AG3

Table 8-5 and Figure 8-9 give tablet strengths as well as Kawakita a and b^{-1} parameters for the sieved fractions of AG3. The results show that:

- Tablet strength is independent of particle size.
- The Kawakita a parameter increases slightly with increasing particle size, indicating the powder bed becomes more porous as the particles within it become larger.
- The Kawakita b-1 parameters reduce significantly with increasing particle size, with only the largest size fraction having a sufficiently low value to be considered consistent with auger filler build-up formation, based upon the results presented previously in Figure 6-40.

Table 8-5: Kawakita parameters, tablet strengths and geometric mean particles size for AG3 sieve fractions

	0 to 600 µm	600 to 1180 µm	1180 to 4750 µm
a	0.48 ± 0.00	0.54 ± 0.00	0.55*
b^{-1} (MPa)	1.16 ± 0.09	1.03 ± 0.03	0.45 ± 0.01
Tablet strength (MPa)	0.18 ± 0.01	0.19 ± 0.01	0.19 ± 0.01
Geometric mean particles size (µm)	257	751	1883

*Standard error less than 0.01

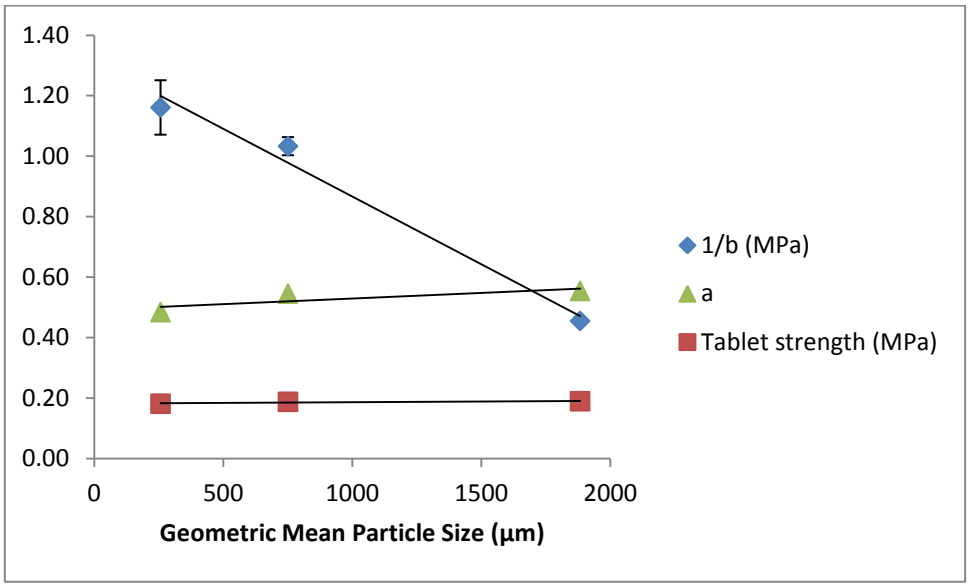

Figure 8-9: Kawakita parameters and tablet strengths as a function of particle size for AG3 size fractions

While all three size fractions have a tablet strength consistent with build-up formation based upon the operating space model generated in Chapter 6 (see Figure 6-40), only the largest size fraction has a b^{-1} consistent with build-up formation. This result is in agreement with the results generated during auger filling and suggests that the operating space model presented in Chapter 6 may be relevant to powder particle sizes larger than the auger/tube clearance.

8.3 Auger Filling of AG2 Batch 4 with Varying Auger Tube clearance and Tube Material of Construction (MoC)

To investigate the potential for reducing or eliminating auger filler build-up via varying the auger/tube clearance, a study was conducted using primarily samples of AG2 Batch 4, but also samples of AG2 Batch 4 with particles greater than 710 µm removed via manual sieving and a

sample of AG1 Batch 2. Particle size distribution for these three powders can see in Figure 8-10 and Figure 8-11. D_{10}, D_{50} and D_{90} values for these powders can be found in Table 8-6, Table 8-7 and Table 8-8. AG2 Batch 4 was selected for the primary subject of this study because samples of AG2 were shown in Chapters 6 and 7 to form build-up, both in the auger filler and in the screw tester.

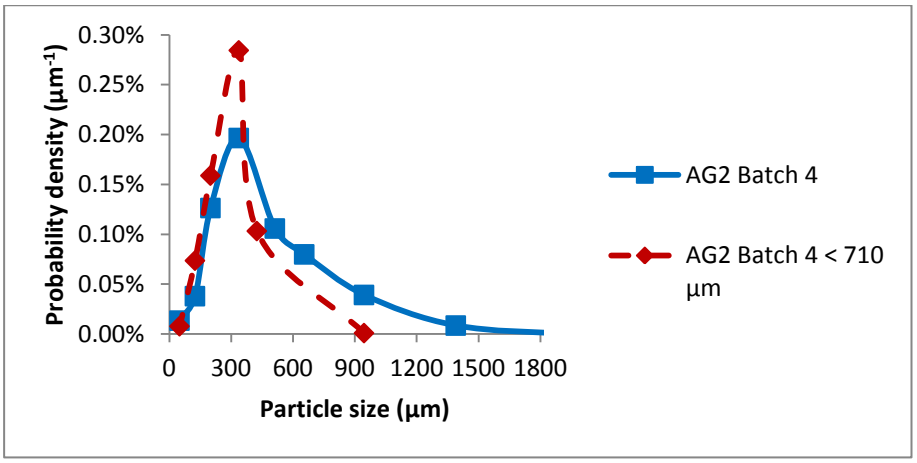

Figure 8-10: Particle distributions for AG2 Batch 2 with and without particle greater than 710 µm

Table 8-6: Particle size data for AG2 Batch 4

D_{10}	200 µm
D_{50}	400 µm
D_{90}	1000 µm

Table 8-7: Particle size data for AG2 Batch 4 < 710 µm

D_{10}	200 µm
D_{50}	340 µm
D_{90}	575 µm

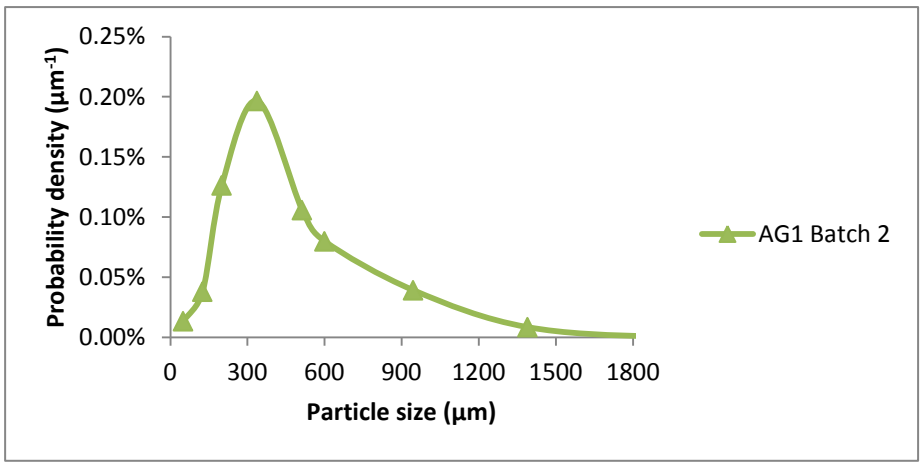

Figure 8-11: AG1 Batch 2 particle size distribution.

Table 8-8: Particle size data for AG1 Batch 2

D_{10}	220 µm
D_{50}	440 µm
D_{90}	1100 µm

Table 8-9: Characterisation data for AG2 presented previously in Chapter 6.

Powder	a	b^{-1} (MPa)	Tablet Strength at 58 MPa (MPa)	% Moisture w/w	eRH %RH
AG2 Batch 4	0.54 ± 0.01	0.51 ± 0.03	0.47 ± 0.01	4.1 ± 0.2	36.1 ± 0.9
AG1 Batch 2	0.51 ± 0.01	0.84 ± 0.11	0.50 ± 0.02	5.3 ± 0.1	27.9 ± 0.2

8.3.1 Auger Filler Build-up Experiments Performed with Varying Auger / Tube Clearances between 0.3 mm and 2.0 mm and Tube Material of Construction (MoC)

Table 8-10 gives the results of auger filler experiments including experiments performed with stainless steel tubes and 0.3 mm auger/tube clearances presented previously in Chapter 6. Auger tube clearance was varied by maintaining auger diameter at a constant value and installing funnels with varying internal diameter. For financial reasons it was not possible to source stainless steel tubes with suitably small differences in internal diameter. To overcome this issue tubes were sourced which were accurately computer numerical control (CNC) machined from cylinders of Ertalyte TX a blended polymer comprising polyethylene terephthalate and a low friction polymer [62]. The supplier of the Ertalyte TX tubes, Quadrant Plastics claims that it has excellent wear properties and significantly lower coefficients of friction than other materials such as stainless steel. This potentially makes Ertalyte TX well suited to applications such as auger filler tubes where a smooth tube surface may act to reduce the shear strength at the interface between the build-up and the tube surface. However, equally it is possible to theorise that as was discussed in section 2.6.4 a smooth material such as Ertalyte TX may be associated with high real contact area formation, due to a lack of surface roughness/asperities which would act to increase the contact area existing between two surfaces [43] as occurs in situations such as smooth/soft rubber racing tyres on a smooth tarmac racing track's surface. This would then potentially increase the likelihood of build-up formation via an increase in adhesive forces.

Tube build-up onset is defined as the mean of the number of fills at which the last auger torque reading of 0.5 Nm was recorded ($f_{0.5}$) and the number of fills corresponding to the first auger torque reading of 1.0 Nm ($f_{1.0}$). The confidence in tube build-up onset is considered to be the difference between $f_{0.5}$ and $f_{1.0}$ divided by two. Tube build-up onset is a measure of the rate of build-up formation, with build-up starting to leave following the rise in torque to 1.0 Nm.

The results presented in Table 8-10 and plotted in Figure 8-12 show that for a single tube MoC and powder, build-up forms more slowly as auger tube clearance increases relative to the powder D_{90}. The results obtained with a 0.3 mm auger/tube clearance, AG2 Batch 4, Ertalyte TX and stainless steel tubes show that, build-up forms slightly more rapidly with the Ertalyte TX funnels. This is potentially because they have a smoother surface lacking surface asperities and allowing for a greater contact area to be formed between the particles and the smooth tube surface. The results generated using a 2.0 mm clearance and AG2 Batch 4 with and without particles greater than 710 µm show that as was shown previously by Crutchley and Bridgwater [29] and Calvert *et al*. [30], the stress and resultant degree of deformation within the clearance are functions of the ratio of the clearance C to the size of the particles within that gap/clearance.

Table 8-10: Auger filler experiments performed with varying auger / tube clearance

Powder	D_{90} (µm)	Auger / Tube Clearance (mm)	Tube MoC	Tube Build-up Onset (fills)	Tube Build-up Observed
AG2 Batch 4	1000	0.3	Stainless Steel	141 ± 47	Yes
AG2 Batch 4	1000	0.3	Ertalyte TX	47 ± 47	Yes
AG2 Batch 4	1000	0.4	Ertalyte TX	48 ± 48	Yes
AG2 Batch 4	1000	0.6	Ertalyte TX	142 ± 47	Yes
AG2 Batch 4	1000	0.8	Ertalyte TX	423 ± 47	Yes
AG2 Batch 4	1000	2.0	Stainless Steel	1032 ± 94	Yes
AG2 Batch 4 < 710 µm	575	2.0	Stainless Steel	No torque rise after 2000 fills	Yes[‡]
AG2 Batch 4	1000	5.0	Stainless Steel	No torque rise after 2000 fills	No
AG1 Batch 2	1100	0.3	Stainless Steel	636 ± 107	No
AG1 Batch 2	1100	5.0	Stainless Steel	No torque rise after 2000 fills	No

[‡] Here the build-up observed at the end of the experiment did not consume the entire clearance and only covered a small fraction of the overall internal tube surface area.

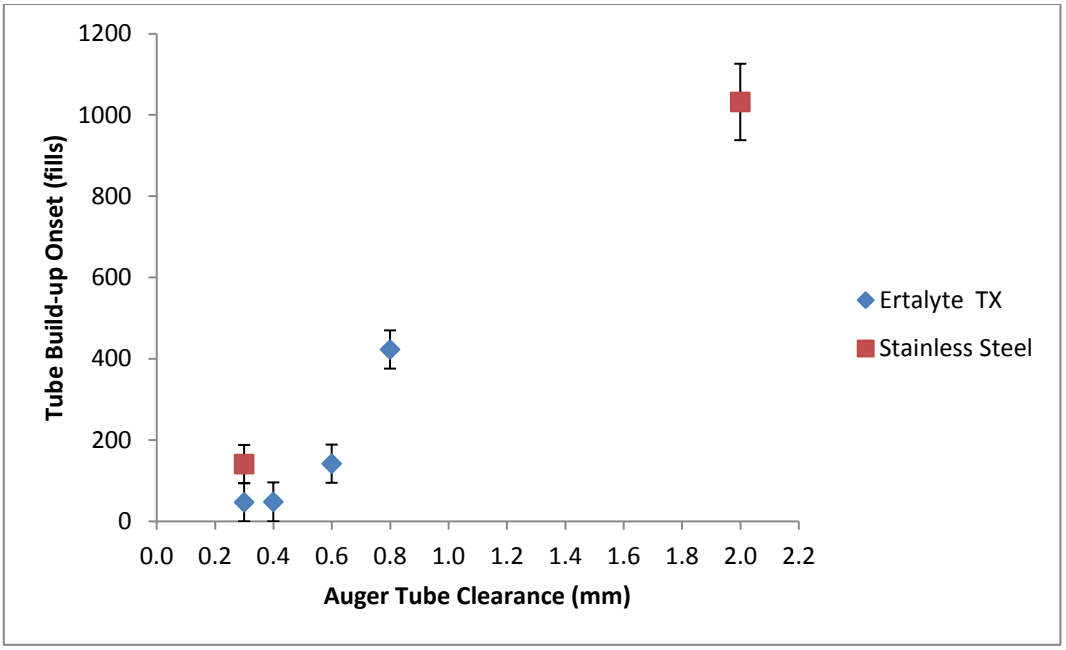

Figure 8-12: Auger filler build-up experiments performed with AG2 Batch 4.

8.3.2 Auger Filler Build-up Experiments Performed with Varying Auger / Tube Clearances between 0.3 mm and 5.0 mm

Calvert *et al*. [30] showed via Discrete Element Method simulations that the forces experienced by particles within a small gap/clearance were a function of the ratio of the clearance C to the powder's D_{90}. While it should be noted that Calvert *et al*. [30] determined D_{90} values based upon a number distribution and D_{90} values expressed here are determined via gravimetric sieving, it seems reasonable to assume that a similar relationship might be observed in both cases. Calvert *et al*. [30] went on to determine that the stresses within the small gap/clearance C reduce to values which might be expected to be outside of the small gap/clearance once C/D_{90} reached a value of 3.5 and thus it might be expected that build-up would not form once this value is exceeded. To enable a simple graphical representation of the build-up formed within the auger filler a build-up index has been used (see Table 8-11), where:

- A build-up index of 1.0 refers to auger torque rising to 1.0 Nm and build-up being observed.

- A build-up index of 0.5 refers to no rise in auger torque being observed but a small amount of build-up being observed.
- A build-up index of 0.0 refers to refers to no rise in torque being observed and no build-up being observed.

Table 8-11: Build-up index as a function of C/D_{90}

Powder	Tube MoC	C (µm)	D_{90} (µm)	C/D_{90}	Build-up Index
AG2 Batch 4	Stainless steel	300	1000	0.3	1.0
AG2 Batch 4	Ertalyte TX	300	1000	0.3	1.0
AG2 Batch 4	Ertalyte TX	400	1000	0.4	1.0
AG2 Batch 4	Ertalyte TX	600	1000	0.6	1.0
AG2 Batch 4	Ertalyte TX	800	1000	0.8	1.0
AG2 Batch 4	Stainless steel	2000	1000	2.0	1.0
AG2 Batch 4 < 710 µm	Stainless steel	2000	575	3.5	0.5
AG2 Batch 4	Stainless steel	5000	1000	5.0	0.0
AG1 Batch 2	Stainless steel	5000	1100	4.5	0.0

The results presented in Table 8-11 and plotted in Figure 8-13 show that no build-up is formed once C/D_{90} exceeds 3.5 which is in good agreement with the findings of Calvert *et al*. [30]. As the results presented by Calvert *et al*. [30] were based upon a number distribution and the D_{90} values presented in Figure 8-13 are based upon a mass distribution, the D_{90} values presented in Figure 8-13 will place greater emphasis on the larger particles and thus should be considered to be conservative in comparison to the results presented by Calvert *et al*. [30].

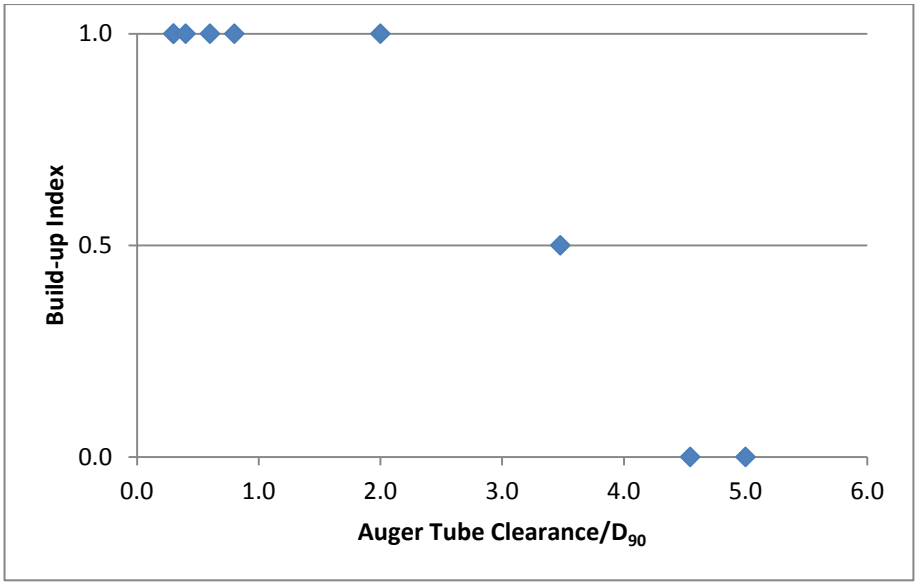

Figure 8-13: Build-up index as a function of the ratio of the auger tube clearance to the relevant powders D_{90}

The count based D_{90c} presented in Table 8-12 were derived from mass distributions used in the calculation auger tube clearance/D_{90} values plotted in Figure 8-13 and were generated based upon the assumptions that:

I. Absolute density is constant with particle size.

II. The volume occupied by particles is equal to that occupied by a sphere.

However, the relevance of number based distributions to build-up formation in the auger filler is questionable, given their lack of sensitivity to the larger particles. Large particles would be expected to have greater influence upon build-up formation versus finer particles, given that they would be expected to be of lower yield stress (based upon the testing of AG3 sieve fractions earlier in this chapter) and would be expected to experience higher stresses, based upon the results presented in Table 8-11.

Table 8-12: Mass based D_{90m} and counted based D_{90c} values for powders tested in Figure 8-13

	Absolute Density (kg/m^3)	D_{90c}	D_{90m}
AG2 Batch 4 < 710 µm	1870	280	575
AG2 Batch 4	1870	220	1000
AG1 Batch 2	1856	360	1100

Also it should be noted the powders simulated by Calvert *et al*. [30] had significantly narrower particle size distribution than those tested here. This leads to a lower sensitivity to differences between mass and number based distributions.

8.4 Auger Filler Build-up $CatSO_3$ Investigation

For powders manufactured via high shear agglomeration and initiated via immersion (as is typical for P&G's surfactant containing agglomerates [59]) it is the case that the mass of binder relative to the mass of the primary particles increases with particle size (see Table 8-13). A possible explanation for this is that for detergent agglomerates, the binder typically is not atomised due to its high viscosity making this impractical. This then leads to a relatively wide variety of binder droplet sizes formed via the action of the moving parts with the granulator which will tend to be large relative to the primary particle size. This then leads to the larger droplets of binder forming larger agglomerates, which then grow more rapidly than the smaller agglomerates due to their lower resistance to deformation. It follows that once the agglomerate size becomes large relative to the binder droplet size, this effect will diminish leading to the binder content becoming constant with particle size [63].

8.4.1 Build-up $CatSO_3$ Content Generated using a 300 μm Clearance

As can be seen from the $CatSO_3$ contents quoted in Table 8-13 AG1 Batch 2, AG2 Batch 4 and AG3 have $CatSO_3$ contents which vary with particle size indicating that surfactant binder content varies with particle size. However, in all cases the degree of variation diminishes with increasing particle size indicating a gradual transition from an immersion to particle-particle size growth mechanism, in the case of AG3 leading to the binder content becoming essentially constant with particle size above a value of approximately 1000 μm. This then leads to the conclusion that the linear variation in b^{-1} with particle size observed for AG3 in Figure 8-9 is not the result of variation in binder content, but some other phenomena such as the ratio of primary particles to

the agglomerate particle size. This assumes that it is the organic binder and not the inorganic primary particles which dominate particle deformation and that particle failure will be initiated at some point(s) of weakness. It follows that as particle size increases and primary particle size remains constant, an applied stress will be distributed over an increasing number of binder bridges between primary particles. This will then increase the number of points at which failure may initiate, increasing the probability of one being weak and reducing the strength of the agglomerate.

Table 8-13: $CatSO_3$ contents of AG1 Batch 2, AG2 Batch 4 and AG3 sieve fraction and build-up samples

Minimum sieve size (μm)	Maximum sieve size (μm)	Sieve fraction geometric Mean (μm)	AG1 Batch 2 % w/w CatSO3	AG2 Batch 4 % w/w CatSO3	AG3 % w/w CatSO3
100	150	122	4.01	4.5	4.46
150	250	194	4.08	4.66	
250	425	326	4.23	4.79	
425	600	505	4.31	4.88	5.02
600	1180	841	4.38	4.97	
1000	1180	1086			5.54
1180	1400	1285			5.53
1400	1600	1497			5.61
1700	2360	2003			5.62
2360	4750	3348			5.64

Figure 8-14 shows that for the three powders tested binder content varies as a logarithmic function of particle size. Logarithmic trend lines were applied on the basis that they gave relatively high R^2 values (0.98), potentially reflecting of the granulation process binder's lognormal droplet size distribution.

The logarithmic functions presented in Figure 8-14 will now be used in conjunction with build-up $CatSO_3$ measurements to gain some understanding of the particle sizes involved in build-up formation. To enable this, build-up samples will be used which in the case of AG1 Batch 2 and AG2 Batch 4 were generated during experiments discussed in Chapter 6 and in the case of AG3 were generated during an experiment discussed previously in this chapter.

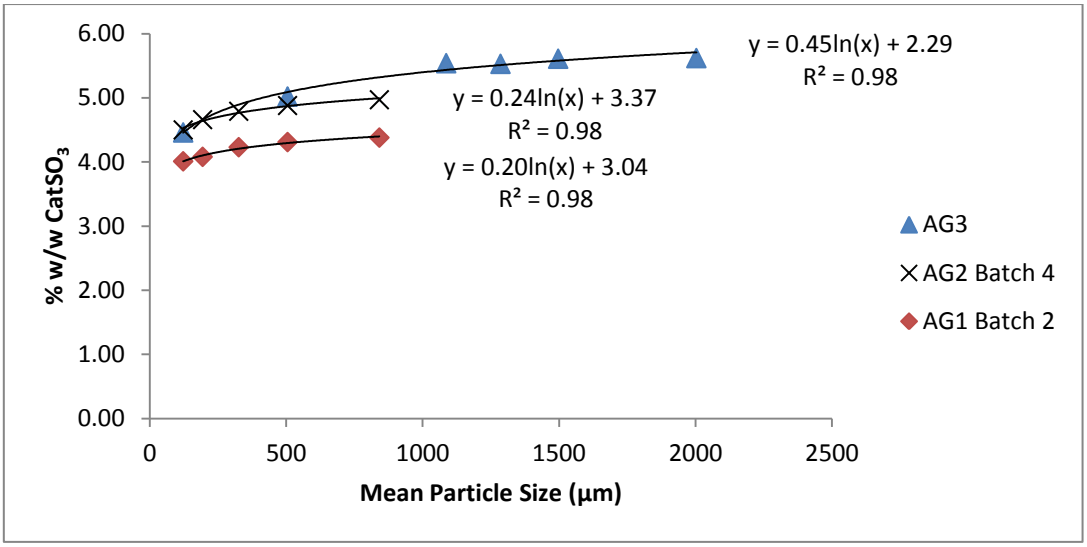

Figure 8-14: Particle $CatSO_3$ content as function of sieve fraction geometric mean particle size

Table 8-14 gives data relating to build-up formed by:

- AG2 Batch 1, AG2 Batch 4 and AG1 Batch 2 in experiments discussed in section 6.6.
- The AG3 1.18 to 4.75 mm sieve fraction used in the experiment discussed in section 8.2.

In the case of AG2 Batch 1 bulk powder $CatSO_3$ was determined via testing of the bulk powder, in all other cases this was determined using the correlations presented in Figure 8-14 and the geometric mean particle sizes measured via gravimetric sieving.

Table 8-14: $CatSO_3$ contents of Build-up and bulk powders presented with data relating to auger filler build-up experiments

Powder	Fills performed	Mass of build-up to leave Auger filler (g)	Build-up % w/w CatSO3	Equivalent build-up particle size (µm)	Bulk powder % w/w CatSO3	Geometric mean particle size (µm)
AG2 Batch 1	1183	32	4.61	NA	4.49	486
AG2 Batch 4	316	6	4.77	341	4.83	444
AG1 Batch 2	2491	7	3.82	49	4.26	439
AG3 1.18 to 4.75 mm sieve fraction	1033	0	5.13	551	5.71	2000

Table 8-14 gives the equivalent build-up particle size calculated using build-up $CatSO_3$ measurements and the correlations presented in Figure 8-14. Surprisingly for samples AG1 Batch 2 and the AG3 sieve fraction equivalent build-up particle size are significantly lower than the

powder's geometric mean particle size. These powders generated significantly lower levels of build-up than AG2 Batch 1 and 4 which have build-up $CatSO_3$ contents much closer to that of the powder. This indicates that the samples of build-up generated spent significantly longer in the auger filler. Clearly the first particles which form a given sample of build-up will encounter an auger/tube clearance of 0.3 mm. However, once build-up has grown to consume the clearance any subsequent particles embedding into the sample of build-up will clearly encounter a significantly smaller clearance. Based upon this knowledge and the results presented in Table 8-14 it is proposed that build-up formation involves two processes:

I. Initially build-up formation involves the weakest particles which based upon the testing of AG3 sieve fractions would be expected to be the larger particles.
II. Once build-up has grown to consume the auger/tube clearance it is then proposed that the small/negligible clearance existing at this time will lead to fine particles embedding into the build-up reducing its $CatSO_3$ content.

This hypothesis would lead to the prediction that as build-up formation reduces the $CatSO_3$ content of the build-up formed will reduce relative to the $CatSO_3$ content of the bulk powder, due to the embedding of fine low $CatSO_3$ particles becoming increasingly dominant. The data presented in Table 8-15 and plotted in Figure 8-15 shows a strong correlation between Bulk Powder $CatSO_3$ – Build-up $CatSO_3$ and Build-up mass per fill, supporting the hypothesis stated above.

Table 8-15: Differences in powder and build-up $CatSO_3$ contents presented with build-up mass per fill.

Bulk Powder $CatSO_3$ – Build-up $CatSO_3$ (% w/w)	Build-up mass per fill (g/fill)
-0.12	0.027
0.06	0.019
0.44	0.003
0.58	0.000

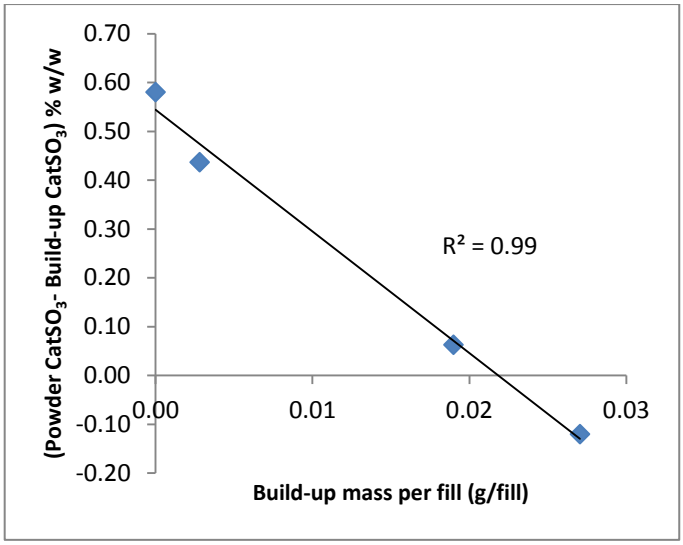

Figure 8-15: Differences in powder and build-up $CatSO_3$ content as a function of build-up mass per fill.

The strong linear correlation presented in Figure 8-15 shows that as the mass of build-up leaving the auger filler reduces the build-up's $CatSO_3$ content reduces. This is consistent with the hypothesis that once build-up consumes the auger/tube it then has increasingly high levels of fine particles embedded into it, due to the negligible auger/tube clearance existing at this time. It should also be said that it is possible that other phenomena may be occurring during build-up formation such as the separation of binder and primary particles, via for example binder being 'squeezed' out the particles. However, if this was the case it then seems logical that build-up samples would contain more $CatSO_3$ than the feed powder, which in most cases has not been observed (see Table 8-13).

8.4.2 Build-up $CatSO_3$ Content Generated using Varying Clearances

In Section 8.4.1 $CatSO_3$ data was used to determine the size of particles forming the auger filler build-up. In this section a similar approach will be used to investigate the influence of auger/tube clearance magnitude upon the build-up $CatSO_3$ content and thus particle size. Table 8-16 gives $CatSO_3$ contents for build-up samples generated during auger filler experiments performed with a range of auger/tube clearances and samples of AG2 Batch 4.

Table 8-16: AG2 Batch 4 Build-up % w/w CatSO3 contents and equivalent particle sizes

MoC	Auger/Tube Clearance (mm)	% w/w $CatSO_3$	Build-up Equivalent Particle size (µm)
Stainless steel	0.3	4.77	349
Ertalyte TX	0.3	4.66	228
Ertalyte TX	0.4	5.04	989
Ertalyte TX	0.4	5.07	1111
Ertalyte TX	0.6	5.07	1111
Ertalyte TX	0.6	5.07	1111
Ertalyte TX	0.8	5.03	952
Ertalyte TX	0.8	5.09	1200
Ertalyte TX	0.8	5.04	989

As can be seen from the data presented in Table 8-16, in the case of the experiments performed with auger/tube clearances of 0.4 and 0.8 mm, repeats were performed using separate samples of build-up. These repeats showed that the variation in values measured was relatively low, versus the difference in % w/w $CatSO_3$ observed when the auger/tube clearance was increased from 0.3 to 0.4 mm. This suggests that this increase in % w/w $CatSO_3$ was not due to error but a change in the processes leading to the build-up's formation.

The results show that experiments performed with larger auger tube clearances give rise to samples of build-up with higher $CatSO_3$ leading to larger equivalent particle size (calculated using the correlation presented in Figure 8-14). This is potentially because the plastic yield stress reduces with increasing particle size and the stress experienced by the particles reduces as the clearances become larger. It then follows that in experiments performed with large clearances only the larger particles are able to form build-up.

8.5 Conclusions

The key conclusions drawn from experimental results presented in the Chapter 8 are as follows:

- When blended with a build-up forming powder such as AG2 Batch 3, the hard crystalline material sodium sulphate has the ability to prevent build-up formation, however, this is only possible when the sample of sodium sulphate has a particle size smaller than the auger tube clearance.
- For the sieve fractions of AG3 tested the yield stress appeared to reduce with increasing particle size. This leads to the largest size fraction forming build-up despite its particle size being significantly greater than that of the auger tube clearance.
- The rate of build-up formation was found to reduce with increasing auger / tube clearance; build-up formation was then found to be eliminated at a value of auger/tube clearance of 3.5 x the powder's D_{90}.
- For a single value of auger/tube clearance (0.3 mm) it was found that the build-up's $CatSO_3$ content reduces relative to the feed powder with reducing build-up per fill (see Figure 8-15). This is believed to result from build-up being initially formed by relatively large low yield stress and agglomerate particles with higher $CatSO_3$ content. Build-up then grows to consume the auger/tube clearance leading to fine low $CatSO_3$ particle depositing into the build-up sample within the now negligible auger/tube clearance.

9. Industrial Case Studies

During the course of this EngD project the findings of the experimental investigations undertaken in previous chapters, have on a number of occasions been used to inform the development of solutions. In this chapter of the thesis a number of case studies will be discussed which illustrate the significant value this project has been able to deliver to P&G's global laundry detergent powder business. Also it should be noted that during the course of this project I have been approached by a number of individuals from UK industry that have experienced problems with auger filler build-up. These individuals have been from companies such as GSK, Premier Foods, Johnson Matthey, Nestle and DuPont, and I was able to give the individuals concerned valuable information which could be used to improve the performance of their auger fillers. I have also passed on the findings of my work to auger filler manufacturers such as All Fill International and Mateer Burt who have found the findings of the work to be broadly in line with their empirical observations.

9.1 Formulation Based Build-up Solutions

Figure 1-2 was previously presented in Chapter 1, and shows the various routes available for the addition of both solid and liquid components. For example a liquid surfactant could be added either into the mixer and then spray dried or could be added as part of a solid agglomerate via one of the solid additive feeders. Similarly a solid material such as sodium sulphate could be added either as part of a spray dried powder or on its own via a solid additive feeder. This would then affect the properties of the final finished detergent powder and potentially the finished powder's tendency to form build-up during auger filling.

Towards the end of the project two new P&G laundry detergent powder formulations were experiencing problems with build-up during auger filling. The fillers were building up rapidly

within one hour of continuous operation and this was resulting in the powders being considered to be 'un-packable' and thus a solution to this problem was needed.

Both of these powders had relatively high levels of liquid added in the continuous mixer.

- The first powder formulation contained a spray dried powder with a high level of surfactant similar to SD3, no other surfactant containing powders and all sodium sulphate delivered within the spray dried powder.
- The second powder formulation contained a relatively high level of AG8 (at 15% w/w), a spray dried powder similar to SD2 (with a lower level of surfactant versus SD3) and again all of the sodium sulphate delivered via the spray dried powder.

The build-up problem with the first powder was resolved by moving 5% w/w of fine grade sodium sulphate (see section 8.1 for particle size data) from the spray dried powder to the solid additive feeders. The powder was then packed on a number of occasions with no build-up problems encountered. It is believed that this resolved the problem via the same mechanism observed in section 8.1, where it was proposed that adding sodium sulphate to a build-up forming powder led to build-up being formed with a weak 'crumb' like structure unable to survive on the tube surface.

The second formulation was then modified to have 5% w/w AG8 and 10% w/w sodium sulphate, on the basis that results generated in Chapter 7 showed that AG8 had a high propensity for build-up formation and increasing the level of sodium sulphate had eliminated build-up formation for the first powder. This new formulation was then packed with no build-up formation observed. Here there are two possible explanations for the elimination which are not mutually exclusive. The higher level of sodium sulphate may have eliminated the build-up formation as occurred with the same first powder, or the reduced level of AG8 may have

eliminated build-up formation via a similar mechanism to that which occurred when AG1 and SD1 were blended in Chapter 6.

9.2 Equipment Modification Based Build-up Solutions

Following the application of the build-up formulation fixes discussed in section 9.1 the question was raised: could the auger filler's auger/tube clearance be increased to a point where the original problematic formulations were considered packable? The clearances used during the work performed in section 9.1 were extremely small to the point where the auger was observed to be rubbing on the tube surface. Based upon the results presented in Chapter 8 it seemed reasonable to assume that a larger clearance would yield a reduction in build-up formation.

To determine if this was possible the following auger fillers within P&G's Cairo laundry detergent plant were fitted with the auger and tubes listed in Table 9-1, yielding a number of clearances C in the range 1.0 to 10.4 mm. Two of the smaller clearances tubes were lined with Ertalyte TX, the larger clearance funnels were all made entirely from Ertalon which was considered to be a more robust material better suited to this application. Machine #25 was fitted with a tube sourced from an existing machine which had been in service for many months and as a result had undergone significant wear.

Table 9-1: Tubes and augers used in the experimental auger/tube clearance trial conducted in P&G Cairo.

Machine #	Tube diameter (mm)	Auger diameter (mm)	Clearance (mm)	Material of Construction
19	83	62.3	10.4	Ertalon
20	78	65.3	6.4	Ertalon
21	73	63	5.0	Ertalon
22	67	63	2.0	Ertalyte TX lined Ertalon
23	65	63	1.0	Ertalyte TX lined Ertalon
24	65	63	1.0	Ertalon
25	69	63	3.0	Badly worn PTFE

Six samples of packed finished product were taken from machine 19 to determine the D_{90} of the powder being packed. Machine 19 was selected on the basis that it had the largest clearance and thus the powder passing through it will experience a lower level of stress than in the case of the other machine and thus the powder will be similar to the feed powder. As can be seen from the data presented in Table 9-2 the D_{90} of the packed powder was 1.05 ± 0.05 mm.

Table 9-2: Cumulative particle size distributions and D_{90}'s determined for six samples of finished product taken from machine 19

Relevant sieve size (µm)	Time sample was taken					
	16:42	16:45	03:45	12:45	19:45	21:55
3350	100	100	100	100	100	100
2350	100	100	100	100	100	100
1700	99	98	98	98	98	99
1180	93	93	91	93	91	93
850	83	83	80	83	80	84
710	76	76	72	75	72	79
425	49	44	43	44	40	47
250	21	15	17	16	13	16
150	7	5	6	5	4	6
D_{90} (µm)	1000	1000	1100	1050	1100	1000

Packing of the second build-up prone powder formulation discussed in section 9.1 was performed for 36 hours. After this time the tubes were removed and inspected to determine if build-up had formed, the results coming from these inspections can be seen in Table 9-3.

Table 9-3: Results of the experimental auger/tube clearance trial conducted in P&G Cairo.

Machine #	Clearance (mm)	Tube material of construction	Build-up observed after 36 hours	C / D_{90}
19	10.4	Ertalon	No	9.9
20	6.4	Ertalon	No	6.0
21	5.0	Ertalon	No	4.8
22	2.0	Ertalyte TX lined Ertalon	No	1.9
23	1.0	Ertalyte TX lined Ertalon	Yes	1.0
24	1.0	Ertalon	Yes	1.0
25	3.0	Badly Worn Polytetrafluoroethylene (PTFE)	Yes	2.9

In Chapter 8 it was shown that once the parameter C / D_{90} exceeded a value of 3.5 build-up formation was eliminated. The results presented in Table 9-3 show that no machines with a C / D_{90} parameters greater than 3.5 formed build-up. However, machine #25 with the badly worn PTFE funnel did contain build-up while having a C / D_{90} value of 2.9. This may be a result of the badly worn internal surface of the tube acting to increase the stress particles experience. Also machine #22 did not build-up, despite having a C / D_{90} value below 3.5. This may be linked to the use of Ertalyte TX lined tube, which may have acted to prevent build-up formation or may have allowed build-up to shear off the tube's surface following its formation. In the case of machine #23 which also had a tube lined with Ertalyte TX, build-up was observed to leave the auger filler on three occasions during the 36 hours of its operation, so this may also have occurred with machine #22 but remained undetected.

9.3 Reapplication to a Rotary Valve

In addition to the problems experienced with build-up in the auger fillers a rotary valve feeding an auger filler (not one including in the study detailed in Section 9.2) was also building up, leading to the need for cleaning three times per shift and interrupting the operation of the downstream auger filler. Figure 1-9 presented in Chapter 1 shows the typical condition of the rotary valve at the point in time cleaning was required. It was then proposed that if the initial clearance of 0.25 mm (0.10 mm at the scraper) was increased to 4.00 mm build-up may be eliminated. This change was made and the valve then remained clean after one week of operation. However, a small amount of powder was able to leak through the value while it was stationary, leading to the need to install a slide gate valve under the rotary valve to act as an isolation point during cleaning activities.

9.4 Reapplication to a Consumer Testing Auger Filler

Within P&G's Newcastle R&D site there is an auger filler which is used for the packing of consumer test powder products. The blended finished powder products packed using this auger filler often contain powders which have been recently developed. In this case the seven powders packed contained between 8 % and 12 % of spray dried powder SD4 (see Figure 9-1) which has a surfactant content of 80 % w/w and anecdotally is very soft and easily deformed.

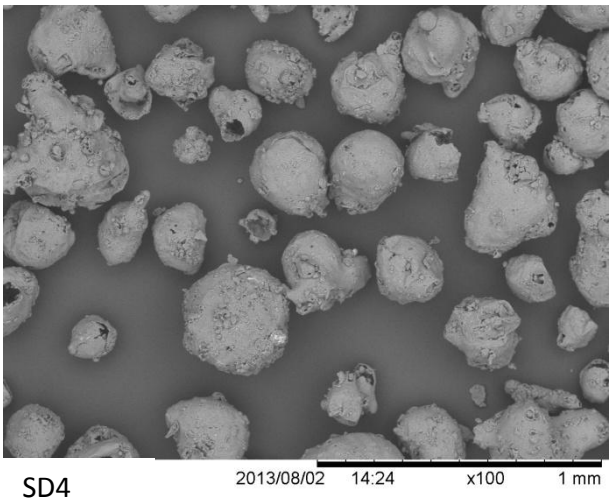

Figure 9-1: SEM image of SD4

To confirm this observation, uniaxial compactions were performed leading to generation of the stress strain and Kawakita plot shown in Figure 9-2 and Figure 9-3. Compressions were performed using 1.00 g of powder which yielded an initial pre compression aspect ratio of 0.2. From Figure 9-2 it is clear that SD4 absorbs a very high level of strain per unit stress confirming the weak/soft nature of SD4. From Figure 9-3 it can be seen that the Kawakita plot is approximately linear between 0.05 and 0.20 MPa ($R^2 > 0.99$). Analysis of the data within this range for three repeats yielded Kawakita b^{-1} values of 0.09 ± 0.01 MPa and 'a' values of 0.99 ± 0.03. Tablet strength measurements were also made using the full capacity of the die (4.00 g of powder) which yielded a post compaction tablet aspect ratio of 0.12. The average tablet strength measured was 0.28 ± 0.06 MPa. The low b^{-1} Kawakita parameters and tablet strength measurements lead to the conclusion that SD4 will build-up rapidly during auger filling and thus

increase the probability that the seven SD4 containing finished products would form build-up during auger filling.

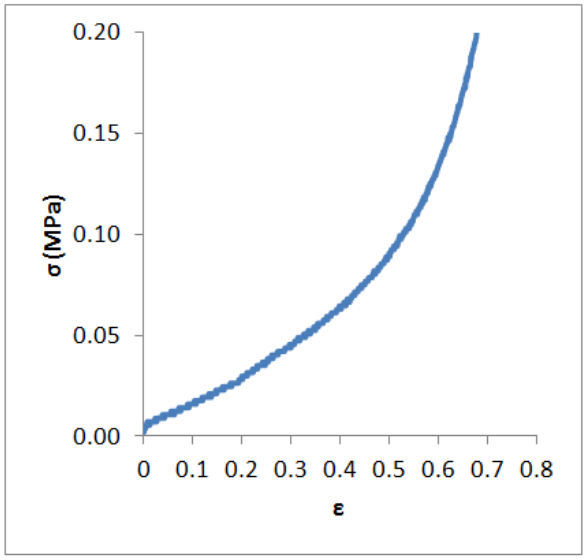

Figure 9-2: Stress strain plot for SD4

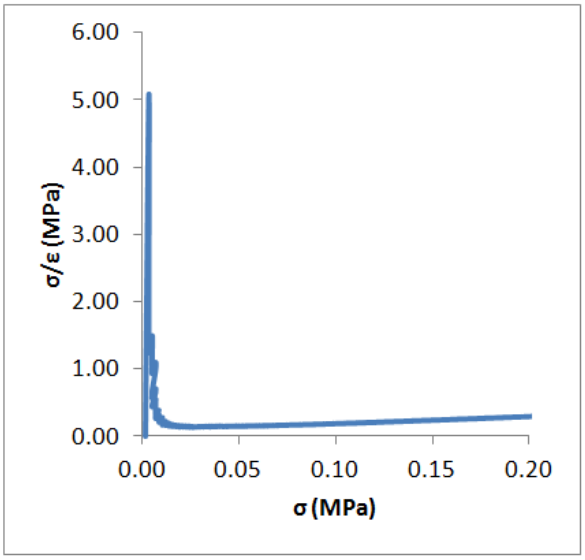

Figure 9-3: Kawakita plot for SD4

To gain understanding of the stresses the seven powders would experience during auger filling, measurements of D_{90} particle size were made via gravimetric sieving (see Table 9-4). These measurements were then used in conjunction with the auger/tube clearance values $C_{0.7}$ and C_{10} quoted in Table 9-5 to determine C/D_{90} values. In Chapter 8 and in Section 9.2 of this chapter C/D_{90} values were shown to enable prediction of the point where a build-up forming powder no longer forms build-up. In all cases excluding the badly worn PTFE tube used in section 9.2, build-up was not formed when C/D_{90} values exceeded 3.5. Therefore based upon the C/D_{90} values quoted in Table 9-4 powder packed using the auger tooling associated with an auger/tube clearance of 10.0 mm will be unlikely to form build-up.

Table 9-4: D_{90} particle sizes for seven SD4 containing finished products

Formulation #	D_{90} (mm)	$C_{0.7}/D_{90}$	C_{10}/D_{90}
1	1.2	0.6	17.1
2	1.2	0.6	17.1
3	1.1	0.6	15.7
4	1.1	0.6	15.7
5	1	0.7	14.3
6	0.9	0.8	12.9
7	1	0.7	14.3

Table 9-5: Auger/tube clerances for two sets of auger tooling.

Auger Tooling	Auger OD (mm)	Funnel ID (mm)	Clearance (mm) C	Build-up Observed
#40 auger and #40 funnel	62.6	64.0	0.7	Yes
#40 auger and #52 funnel	62.6	82.5	10.0	No

Packing of the seven consumer test finished products was performed initially using the auger tooling associated with the 0.7 mm auger/tube clearance. As can been from Figure 9-4, high levels of build-up were observed after packing the seven products. Packing was then repeated using the tooling associated with a 10.0 mm clearance and as can be seen from Figure 9-5 no build-up was observed to form. This shows that powders with the extremely poor mechanical properties can be packing without build-up formation provided that a sufficiently large auger/tube clearance is utilised.

Figure 9-4: Auger and tube after the packing of seven SD4 containing finished products with a 0.7 mm auger tube clearance.

Figure 9-5: Auger and tube after the packing of seven SD4 containing finished products with a 10.0 mm auger tube clearance.

10. Conclusions

10.1 Initial Objectives Restated

The objectives stated at the beginning of thesis were to develop:

I. Macro scale / pilot plant test methods which enable the tracking of build-up generation with time.

II. A means of predicting auger filler build-up based upon the properties of the powder flowing through the auger which is of practical use to industry.

III. Equipment modifications which can then be used to reduce or eliminate powder build-up.

10.2 Objective I

Objective I was addressed in Chapter 6 where a test method was developed which was shown to enable the tracking of build-up formation with time via manual auger torque measurements, tube surface temperature measurements and powder mass per fill measurements. This method was then shown to have good repeatability and was subsequently used extensively throughout the thesis in the fulfilment of objectives II and III.

10.3 Objective II

Objective II was initially addressed in Chapter 6 where it was shown that powders of low Kawakita b^{-1} parameter (< 0.5 MPa) and tablet strength (< 0.5 MPa) formed build-up while powders with higher values did not. The Kawakita b^{-1} parameter is known to be related to failure stress of the particle within the die [10]. In the case of plastic particles the failure stress will be the plastic yield stress. Rumpf *et al.* [45] stated that the adhesive force acting between two plastic deforming spheres is proportional to the applied force and the ratio of the van der Waals pressure to the plastic yield pressure of a sphere as shown in Eq.(2-47).

$$F \approx \frac{p_{vdW}}{p_{pl}} F_a \quad \textbf{(2-47)}$$

where F is adhesive force, F_a is applied force, p_{vdW} is van der Waals pressure defined by Eq. (2-48) and p_{pl} is plastic yield pressure of a sphere.

$$p_{vdW} = \frac{h\omega}{8\pi^2 {h_s}^3} \quad \textbf{(2-48)}$$

where hω is the Lifshitz–van der Waals constant and h_s is separation distance.

From Eq. (2-47) and (2-48) we can say that powders of low plastic yield stress (and it follows low b^{-1} parameter) will tend to form build-up because:

I. Low values of plastic yield pressure will lead to high values of adhesive force.

II. As h_s reduces due to plastic deformation van der Waals pressure p_{vdW} will increase and thus adhesive force will increase.

It is proposed that low tablet strengths are also required for build-up to form because build-up forming agglomerate particles are formed from soft plastic materials which compact to form soft plastic tablets. These tablets are then of low strength, because the soft tablet will fail via ductile separation of contacts, with the tablet providing limited resistance to contact separation due to its low plastic hardness.

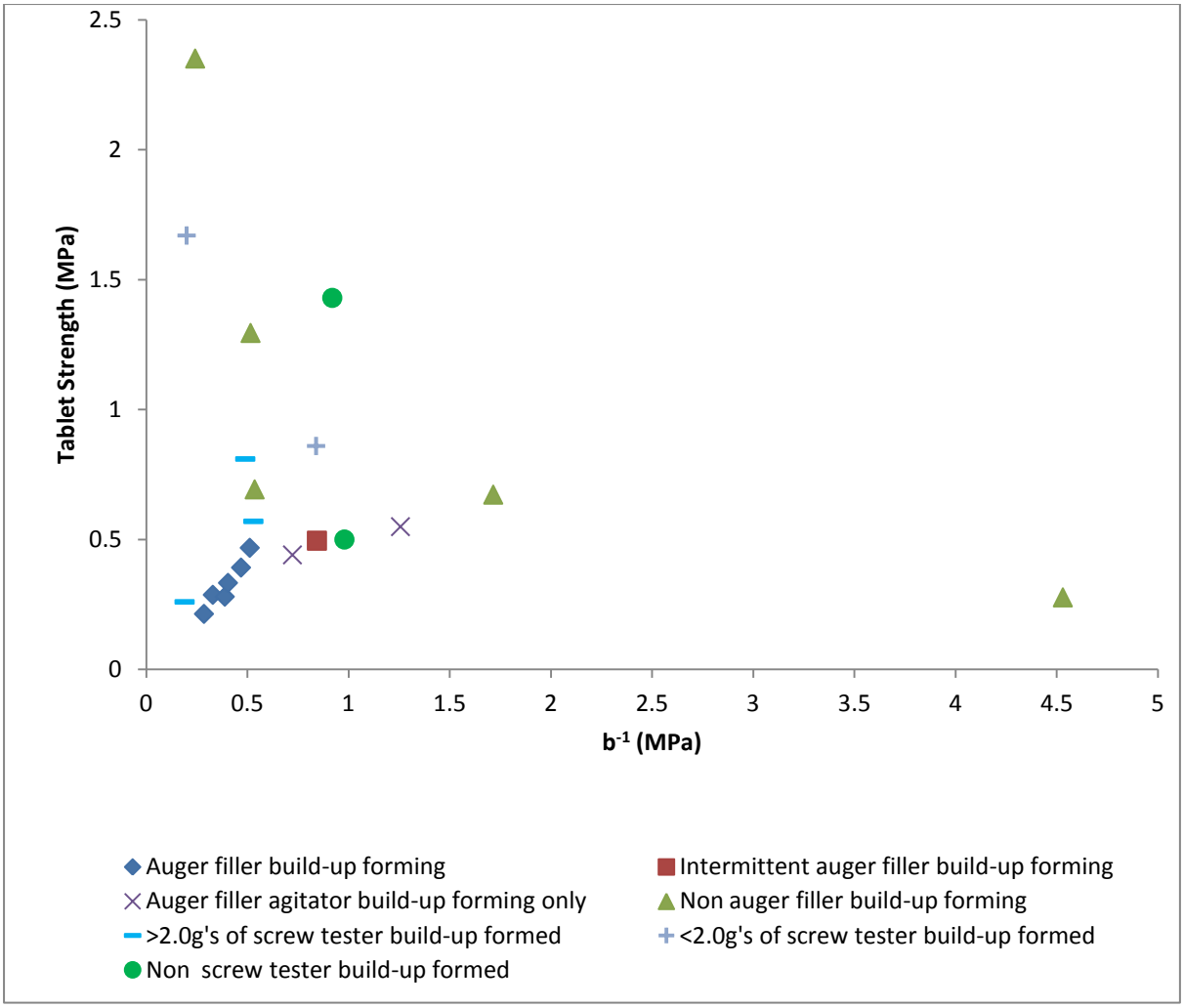

Figure 7-25: An operating space model for the prediction of auger filler and screw tester build-up.

From Figure 7-25 it was then seen that the data generated for the auger filler and screw tester are broadly similar. This shows that despite the fact that the screw tester and auger appear superficially to be different items of equipment, the way in which build-up is formed by the two devices is similar. This in turn suggests that it may be the magnitudes of the relevant clearances (0.3 mm for the auger filler and 0.1 mm for the screw tester) in both items of equipment that are the dominant factors impacting build-up formation.

As stated earlier in this section it is proposed that for the powders studied tablet strength measurements are a measure of the strength of material from which a powder is formed. However, tablet strength measurements made for AG9 and AG7 which have high b^{-1} values are

particularly low, not reflect the strong nature of these agglomerate particles. To address this issue it was proposed that tablet indentation depth measurements could be utilised.

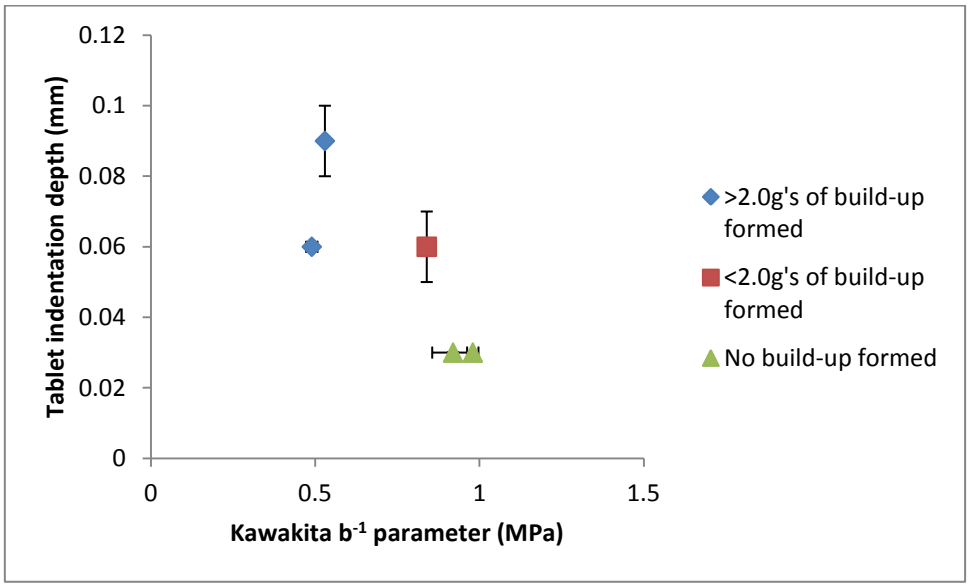

Figure 7-26: A Screw tester build-up operating space model, utilising b^{-1} and tablet indentation depth measurements

As can be seen from the results presented in Figure 7-26 indentation depths were consistently low for both non-build-up forming powders (AG4 Batch 3 and AG9). This supports the hypothesis that the tablet indentation depth more accurately reflects build-up formation than diametric tablet strength measurements.

In Chapter 8 this approach to predicting build-up formation via b^{-1} parameters and tablet strength measurements was applied to sieve fraction of AG3. This testing showed that only the largest sieve fraction 1.18 to 4.75 mm formed build-up which can be seen from Figure 8-9. This was also the only sieve fraction to have a b^{-1} parameter below 0.5 MPa and the only sieve fraction that would be predicted to form build-up.

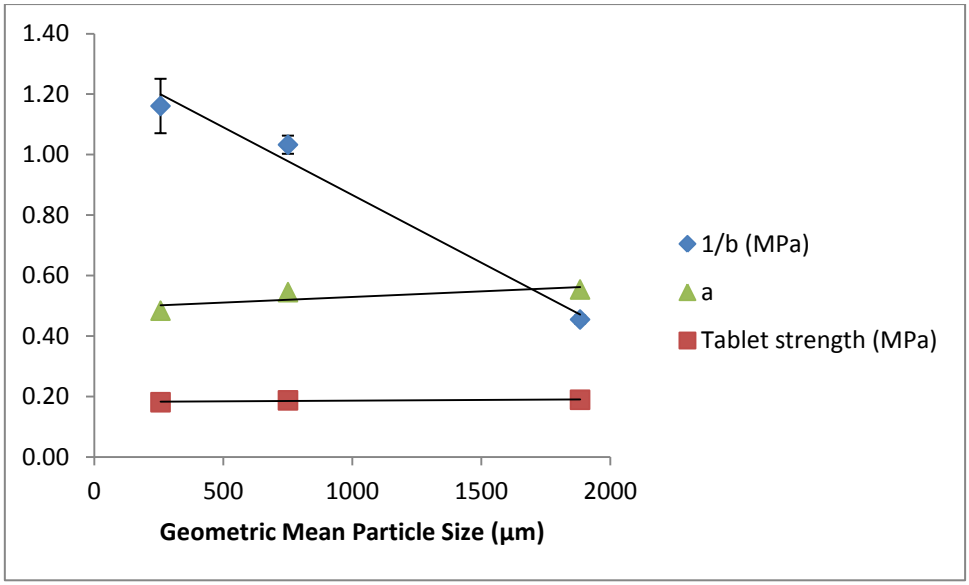

Table 8-5: Kawakita parameters, tablet strengths and geometric mean particles size for AG3 sieve fractions

10.4 Objective III

Crutchley and Bridgwater [29] and Calvert *et al.* [30] showed that the stresses experienced by particles passing through small clearances/gaps were a function of the ratio of the magnitude of the clearance C to the particle size. Calvert *et al.*[30] showed that the larger particles would experience larger stresses and thus the appropriate measure of particle size was the D_{90}. Based upon this knowledge, experiments were conducted upon the basis that the parameter C/D_{90} would give an indication of the stress experienced by particles passing through the auger/tube clearance.

To enable a simple graphical representation of the build-up formed within the auger filler a build-up index has been used (see Table 8-11 and Figure 8-13), where:

- A build-up index of 1.0 refers to auger torque rising to 1.0 Nm and build-up being observed.
- A build-up index of 0.5 refers to no rise in auger torque being observed but a small amount of build-up being observed.

- A build-up index of 0.0 refers to refers to no rise in torque being observed and no build-up being observed.

Build-up formation reduced and then ceased once C/D_{90} rose above 3.5, this figure was in good agreement with the figure quoted by Calvert *et al*. [30] and with results generated over 26 hour period in P&G's Cairo manufacturing plant presented in Chapter 9.

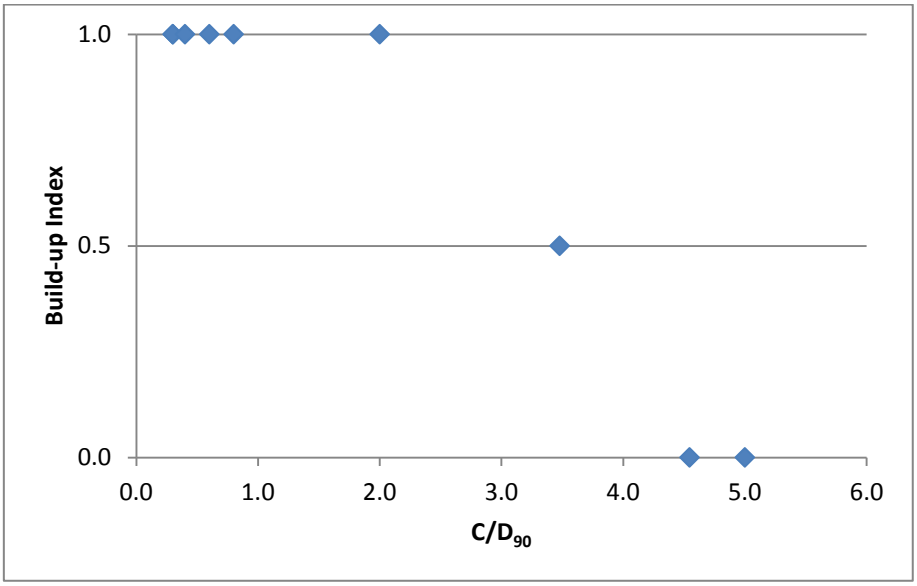

Figure 8-13: Build-up index as a function of the ratio of the auger tube clearance to the relevant powders D90

In Chapter 9 the same approach to build-up elimination was also applied successfully to a rotary valve suggesting that it may be possible to reapply this solution to build-up formation to a wide variety of powder handling operations where low yield stress agglomerate particles have the potential to pass through small clearances.

10.5 Further Work

The following topics are recommended for further investigation.

10.5.1 The Build-up of Powder Blends

While the work presented in this thesis has led to additional understanding of the processes which lead to build-up formation in the case of blended powders (Ariel and Bold in Chapter 5

and AG2 Sodium sulphate blends in Chapter 8), it has not been possible to reliably predict the build-up of blended powders based on laboratory characterisation. For this reason blended powders are recommended for further study, which could involve the development of a laboratory scale test method allowing for the use of variable clearances. This would enable the assessment of the size ratio effects associated with the primary and secondary particles, and the auger/tube clearance.

10.5.2 Temperature Sensitivity Effects

In the detergent powder industry, it is common to pack powders at elevated temperatures in order to avoid costs associated with cooling to ambient after spray drying. This leads to the question of whether powders display a greater tendency to form build-up at high temperatures.

A number of mechanisms can be proposed which would lead to temperature sensitivity effects:

- Agglomerate particle yield stresses may reduce as temperature increases.
- Chemically bound water may be released from materials such as sodium carbonate, which then may act to soften the surfactant within agglomerate particles.
- Materials may pass through a glass transition point, allowing plastic yielding to occur rather than brittle fracture.

Therefore it is recommended that a study be performed to investigate the importance of temperature.

10.5.3 Reapplication to Twin Screw Granulation

The work presented in this thesis has focused on build-up formation in auger fillers, but has also shown that build-up is formed via similar processes in the screw tester (see Chapter 7) and rotary valves (see Chapter 9). It seems logical that build-up would also form in twin screw granulators, however, in this case agglomerate particle size and yield stresses change as

material passes along the length of the granulator. This leads to a more complex situation which is recommended for further investigation.

This investigation could be initiated by determining the yield stress and particle size distribution within various regions of the twin screw granulator, and then relating this information to the quantity of build-up formed and the geometry of the relevant regions of the granulator. The investigation could then proceed to study potential interactions between the granulation of the bulk powder and the formation of build-up at the barrel surface. Here, phenomena such as build-up formation preferentially consuming large agglomerates may influence how agglomerate particle size changes with both time and granulation conditions.

10.5.4 A Multi Variant Fundamental study of Auger Filler Build-up Formation

The thesis has highlighted the lack of underpinning knowledge in this area. For this reason, it is recommended that a fundamental multi-variant study be performed to determine the effects of the following parameters on build-up formation:

I. Primary and secondary particle properties e.g. size, shape, surface roughness, plastic hardness
II. Environmental conditions e.g. atmospheric temperature and humidity
III. Powder flow properties e.g. unconfined yield stress and wall friction angle
IV. Formulation e.g. agglomerate binder/solid ratio, binder viscosity
V. Equipment geometry e.g. auger/tube clearance, auger rotational speed, tube surface finish.

Ideally these parameters would be studied in conjunction with measurements made via an instrumented auger filler or a smaller scale experimental rig. Measurements may include:

I. Auger torque

II. Tube surface temperature

III. Normal and shear stress at the tube surface

IV. Mass flow rate through the auger

V. Spatially mapped agglomerate particle residence times measured by, for example, Positron Emission Particle Tracking.

Appendix 1: Auger/Tube Clearance Shear Rates [§]

Table A1-6: Auger and tube diameters

Auger #	Auger Outside Diameter (mm)	Tube Internal Diameter (mm)	Clearance (mm)
4	6.3	9.5	1.60
5	7.9	11.1	1.60
6	9.5	12.7	1.60
7	11	14.2	1.60
8	12.7	15.8	1.55
9	14.2	17.4	1.60
10	15.8	19	1.60
11	17.4	20.6	1.60
12	19	22.2	1.60
13	20.6	23.7	1.55
14	22.2	25.3	1.55
16	25.3	28.5	1.60
18	28.5	31.7	1.60
20	31.7	34.8	1.55
22	34.8	38	1.60
24	38	41.2	1.60
26	41.2	44.4	1.60
28	44.4	50.7	3.15
30	47.5	54	3.25
32	50.7	57.1	3.20
36	57.1	63.4	3.15
38	60.2	66.6	3.20
40	63.4	69.7	3.15
44	69.7	76.1	3.20
48	76.1	82.4	3.15
50	79.3	85.6	3.15
52	82.4	88.8	3.20

[§]Take from ; Auger and Pump Specifier, Auger Fabrication

Table A1-7: Auger/Tube Clearance Shear Rates

Shear rate (s^{-1})	Rotational speed (min^{-1})									
Clearance (mm)	100	200	300	400	500	600	700	800	900	1000
1.60	21	41	62	82	103	124	144	165	186	206
1.60	26	52	78	103	129	155	181	207	233	259
1.60	31	62	93	124	155	187	218	249	280	311
1.60	36	72	108	144	180	216	252	288	324	360
1.55	43	86	129	172	215	257	300	343	386	429
1.60	46	93	139	186	232	279	325	372	418	465
1.60	52	103	155	207	259	310	362	414	465	517
1.60	57	114	171	228	285	342	399	456	512	569
1.60	62	124	187	249	311	373	435	497	560	622
1.55	70	139	209	278	348	418	487	557	626	696
1.55	75	150	225	300	375	450	525	600	675	750
1.60	83	166	248	331	414	497	580	662	745	828
1.60	93	187	280	373	466	560	653	746	839	933
1.55	107	214	321	428	535	643	750	857	964	1071
1.60	114	228	342	456	569	683	797	911	1025	1139
1.60	124	249	373	497	622	746	870	995	1119	1244
1.60	135	270	404	539	674	809	944	1079	1213	1348
3.15	74	148	221	295	369	443	517	590	664	738
3.25	77	153	230	306	383	459	536	612	689	765
3.20	83	166	249	332	415	498	581	664	747	830
3.15	95	190	285	380	475	569	664	759	854	949
3.20	99	197	296	394	493	591	690	788	887	985
3.15	105	211	316	422	527	632	738	843	948	1054
3.20	114	228	342	456	570	684	798	912	1026	1140
3.15	126	253	379	506	632	759	885	1012	1138	1265
3.15	132	264	395	527	659	791	923	1055	1186	1318
3.20	135	270	404	539	674	809	944	1079	1213	1348

Appendix 2: $CatSO_3$ in Detergent by Hyanine Titration

The below method has been supplied by Procter and Gamble Technical Centres Newcastle Innovation Centre, Analytical Test Department, who also performed all testing for $CatSO_3$ presented in this thesis.

		Keywords: Hyamine 1622 SDS
1	**PRINCIPLE**	
	0.004 N Hyamine is standardised against sodium dodecyl sulphate (SDS) standard using a two-phase titration. The SDS standard solution and a mixed (anionic/cationic) indicator solution are mixed in a water-chloroform system. The complex between the SDS and the cationic dye is red and chloroform soluble. Upon titration with Hyamine 1622 (a quaternary cationic) the red dye-surfactant complex is broken and replaced by a colourless anionic surfactant-cationic titrant complex. A colour change from red to grey in the chloroform layer indicates the end point. If excess Hyamine is added, it complexes with the anionic dye, giving a blue colour to the chloroform layer. Detergent products or their raw materials and intermediates are dissolved in water and an aliquot titrated as described above.	If required, dichloromethane may replace chloroform in this basic procedure. Note that for "after hydrolysis" titrations chloroform must be used.
2	**SCOPE** This method should be used for the determination of Cat SO3 in all SIMPLE water soluble detergent matrices. However, the presence of sodium toluene sulphonate (or sodium cumene sulphonate) at STS:Cat SO3 ratios of 1:1 or greater will introduce a high bias. Other methods are available for the titration of products, raw materials and intermediates requiring special treatment. However, the Hyamine standardisation for all these methods must be performed as described in step 6.12.	
3	**VALIDATION DATA** An average RSD of 0.6% has been obtained by the European plants as of April 94.	
4	**REFERENCES** ISO 2271	

5	**APPARATUS**	
5.1	Automatic burette.	Metrohm Dosimat 645 or equivalent.
5.2	Dispensers.	Any dispenser capable of adding 15 and 20 mL.
5.3	Titration cylinder.	Dimensions: about 25 mm diameter and 200 mm height.
5.4	Magnetic stirrer and stirring bar	Capable of stirring very vigorously in the titration tubes.
6	**REAGENTS AND SOLUTIONS**	
6.1	Hyamine 1622, 0.004 N solution.	P&R Laboratory Supplies Ltd, UK. or equivalent.
6.2	Chloroform (CHCl3) or dichloromethane (CH2Cl2).	Analytical reagent grade. Use only in fume cupboard. CARE-CARCINOGEN, TOXIC
6.3	Dimidium bromide.	Fluka 41785 or equivalent.
6.4	Disulfine blue.	Fluka 76270 or equivalent.
6.5	Sodium dodecyl sulphate (SDS) standard material	Obtain from NTC Analytical. Use only this material to standardise the Hyamine solution. Keep this sample in a sealed bottle all the times. Avoid air contact as much as possible. Re-order this SDS standard at least every six months in order to avoid moisture build up in the standard.
6.5.1	Moisture level Check the moisture level of the standard SDS by Karl Fischer (EM 07042) immediately before using this material in step 6.7.1..	If the moisture level varies more than ± 0.2 % of the stated level, immediately re-order new Standard SDS material from NTC-Analytical. Always use the active content stated on the enclosed sheet supplied by NTC.
6.6	Ethanol	Technical grade
6.7	Sodium Dodecylsulphate, 0.004 N solution	

6.7.1	Weigh, to an accuracy of ± 0.0001 g, exactly X g of the SDS standard sample (6.5) into a 1 L volumetric flask. Dissolve in deionised water and make to volume.	X g is the weight of SDS specified on the instruction sheet supplied with the SDS by NTC Analytical. The normality of this solution is exactly 0.004 N. **Keep this solution no longer than one month**.
6.8	Ethanol, 10 % To 900 mL of deionised water, add 100 mL of ethanol (5.6). Mix well.	
6.9	Sodium hydroxide, 50% While stirring, slowly add 250 g of sodium hydroxide pellets to 250 mL of deionised water.	CARE - Heat is generated. Wear safety goggles and gloves.
6.10	Sulphuric acid (H_2SO_4), 1:4 solution. Whilst stirring and cooling, add 200 mL of concentrated sulphuric acid to 800 mL of deionised water.	CARE - Wear safety goggles and gloves. Never add water to sulphuric acid.

6.11	Mixed Indicator solution	
6.11.1	Mixed indicator stock solution	
6.11.1.1	Weigh, to an accuracy of ± 0.01 g, 1 g of dimidium bromide (6.3) and 0.5 g of disulfine blue (6.4) into separate 100 mL beakers.	
6.11.1.2	Add about 50 mL of hot 10 % alcohol solution (6.8) to each beaker and stir to dissolve.	
6.11.1.3	Transfer the contents of each beaker to the same 500 mL volumetric flask with 10% alcohol solution (6.8) and allow to cool to room temperature.	
6.11.1.4	Make up to volume with 10 % alcohol solution (6.8) and mix well.	
6.11.2	Mixed indicator acidified solution	
6.11.2.1	Add 20 mL of mixed indicator stock solution (6.11.1) to a 1000 mL volumetric flask containing 200 mL of deionised water.	
6.11.2.2	Add 15 mL of 1:4 sulphuric acid (6.10), make up to volume with deionised water and mix well.	This solution is stable for at least 2 months if stored in an amber bottle with ground stopper.
6.12	**STANDARDISATION OF 0.004 N HYAMINE**	The standardisation of the Hyamine normality must be performed at least once a week. It is also essential to perform this standardisation when using a new bottle of Hyamine solution even when this bottle is of the same production batch.
6.12.1	Pipette 20.00 mL of the SDS standard solution (6.7) into a titration cylinder (5.3).	
6.12.2	Add 20 mL of acidified mixed indicator solution (6.11.2). Add a magnetic stirring bar (5.4).	If preferred, the stirring bar may be omitted and the mixture shaken throughly in step 6.12.4.
6.12.3	Add 15 mL of chloroform or dichloromethane (6.2) from a dispenser.	Work in a fume cupboard.

6.12.4	Titrate with the Hyamine solution (6.1) while stirring thoroughly. Add Hyamine rapidly until the upper layer begins to turn red. Continue to add titrant at a moderate rate reducing to dropwise addition as the red becomes less intense. When the top layer becomes grey, stop the stirrer and allow to settle. After separation of the layers, inspect the lower layer for endpoint detection. The endpoint is the change from red to grey in the chloroform layer. A blue bottom layer indicates that the endpoint has been passed. If the endpoint was not reached, restart the stirring and continue adding titrant dropwise until the endpoint is reached.	Stir as vigorously as possible. The vortex should reach down to the bottom of the titration cylinder. A red color indicates that more titrant is needed. Grey indicates that the endpoint has been reached. Blue shows that the endpoint has been passed. Allow at least 30 seconds stirring after each titrant addition. Then stop stirring and allow the phases to settle. If the endpoint is difficult to detect, then the best approach is to record the volume of titrant, add an extra drop of Hyamine and, after stirring, confirm that the lower phase turns blue. If so then the recorded titre is correct. If the lower phase remains grey then a further drop should be added and the colour rechecked.
6.12.5	Record the volume of Hyamine needed to reach the endpoint as mL Hyamine.	
6.12.6	Calculate the normality of the Hyamine solution as follows: $N = \frac{mL\ SDS \times 0.004}{mL\ Hyamine} = \frac{20 \times 0.004}{mL\ Hyamine}$	mL SDS = 20.00 (see 6.12.1) mL Hyamine - see 6.12.5.
6.12.7	Repeat this standardisation at least 3 times involving all analysts who perform Cat SO3 analyses. The results should not differ by more than 0.00002 N. Calculate the average of these 3 determinations to obtain N and mark this on the bottle.	If different analysts percieve different endpoints and therefore find it impossible to agree within 0.00002 N, then each analyst must perform the standardisation in triplicate and calculate his or her own normality. Each analysts value must be recorded on the bottle.
7	**PROCEDURE**	
7.1	**SAMPLE SOLUTION PREPARATION**	

7.1.1	Weigh, to the nearest 0.001 g, about S g of a representative sample into a 400 mL beaker.	S g = $\frac{32}{\%\ \text{Cat SO3 expected}}$ If desired, liquid samples may be weighed directly into the volumetric flask.
7.1.2	Add about 250 mL of hot (60°C) water and stir for 10 minutes.	
7.1.3	Transfer to a 1000 mL volumetric flask with deionised water. Allow the solution to cool to room temperature, make to volume with deionised water and mix thoroughly.	If there is excessive foaming a SMALL amount (a few drops) of ethanol (5.6) may be added.
7.2	**OPERATION**	
7.2.1	Pipette 10.00 mL of the sample solution (7.1) into a titration cylinder (5.3).	
7.2.2	Add 20 mL of acidified mixed indicator solution (6.11.2) from a dispenser and add a magnetic stirrer (5.4).	
7.2.3	Adjust the colour of the sample solution to that of the indicator blank by adding dropwise 1:4 sulphuric acid (if blue) or 50% sodium hydroxide (if pale yellow).	Indicator blank is 10 mL of SDS solution (6.8) + 20 mL of acidified mixed indicator solution (6.11.2).
7.2.4	Add 15 mL of chloroform or dichloromethane (6.2) from a dispenser.	
7.2.5	Titrate the contents of the titration tube as described in steps 6.12.4 and 6.12.5.	Let the volume of Hyamine = T mL.
8	**CALCULATION** $\%\ \text{Cat SO3} = \frac{T \times N \times 80 \times 1000 \times 100}{1000 \times 10 \times S}$ $= \frac{T \times N \times 800}{S}$	T - see 7.2.5 N - see 6.12.6 S - see 7.1.1

Appendix 3: Stress versus Strain and Kawakita Plots for Powders Tested in Chapter 4

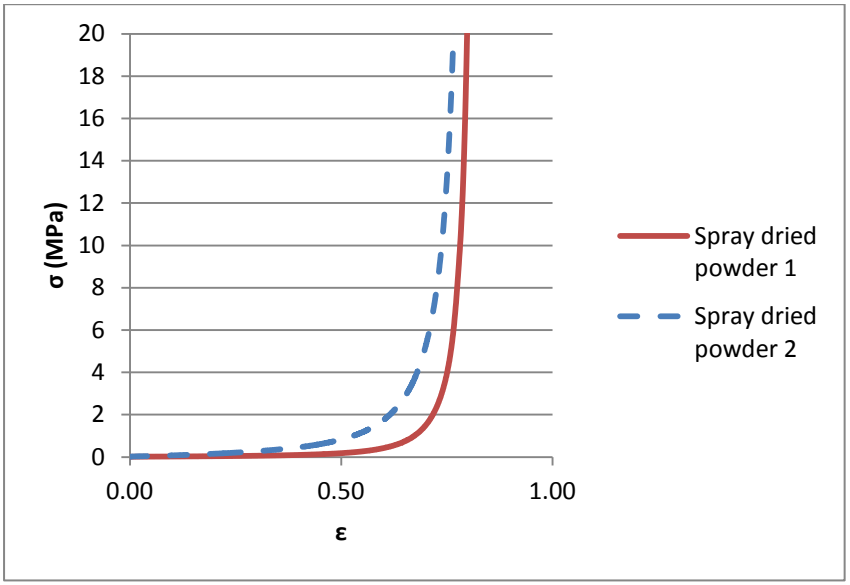

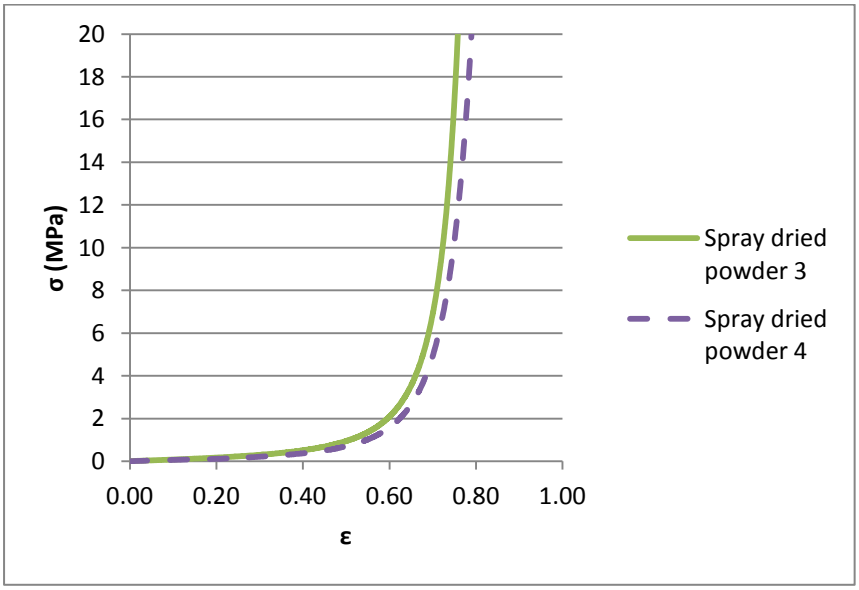

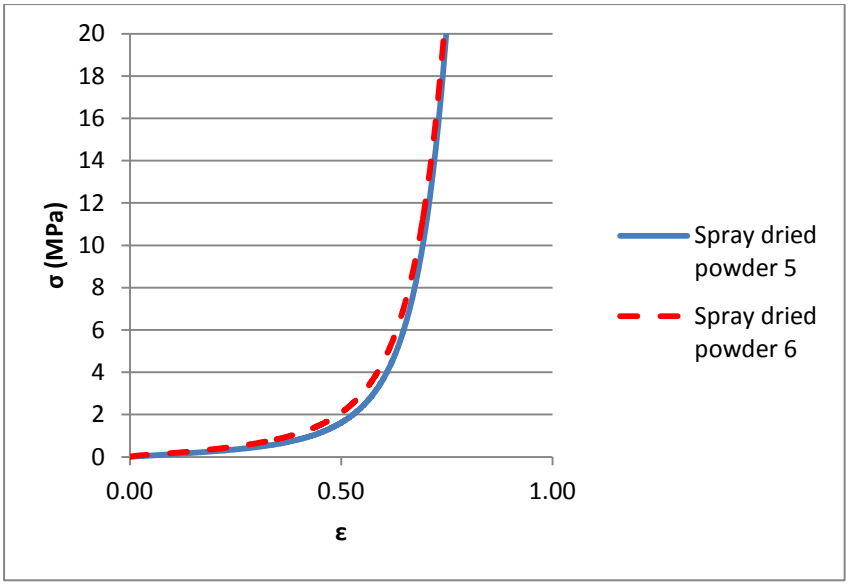
20
18
16
14
12
10
8
6
4
2
0
σ (MPa)
0.00
0.50
1.00
ε
Spray dried powder 5
Spray dried powder 6

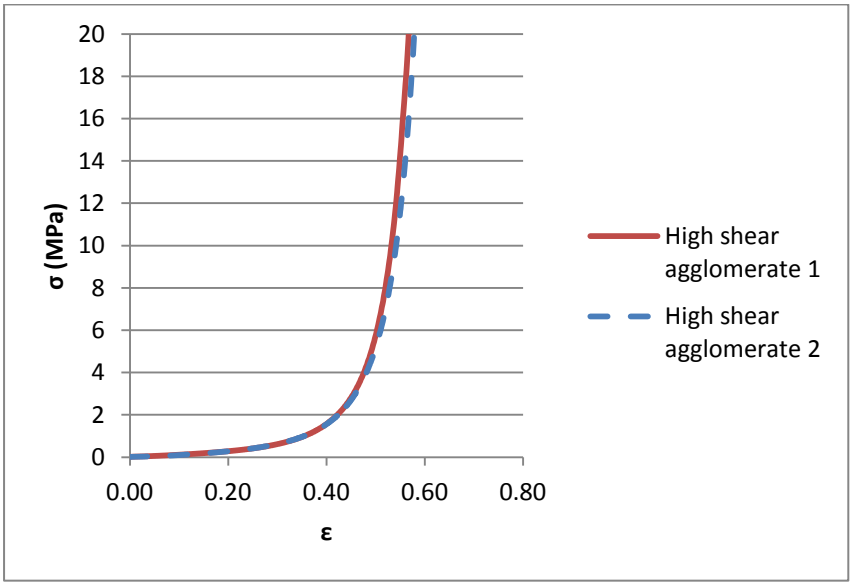
20
18
16
14
12
10
8
6
4
2
0
σ (MPa)
0.00
0.20
0.40
0.60
0.80
ε
High shear agglomerate 1
High shear agglomerate 2

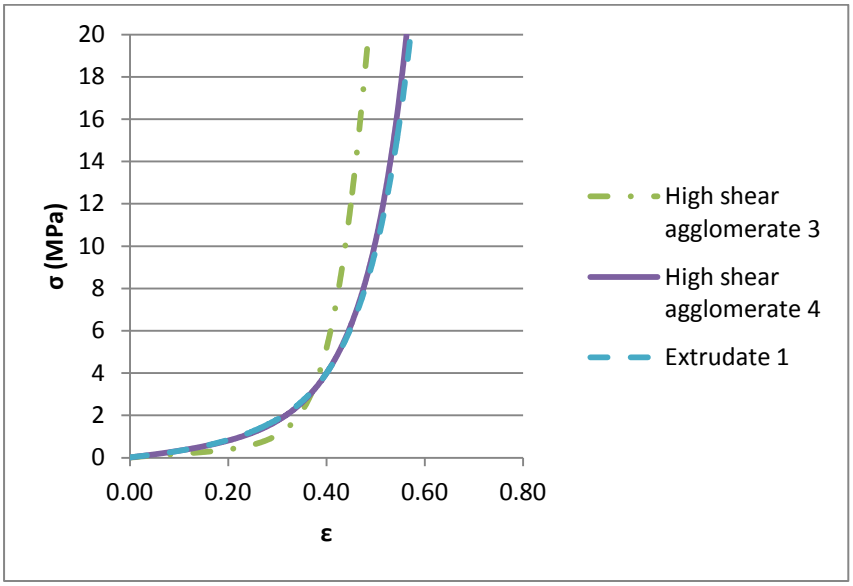
20
18
16
14
12
10
8
6
4
2
0
σ (MPa)
0.00
0.20
0.40
0.60
0.80
ε
High shear agglomerate 3
High shear agglomerate 4
Extrudate 1

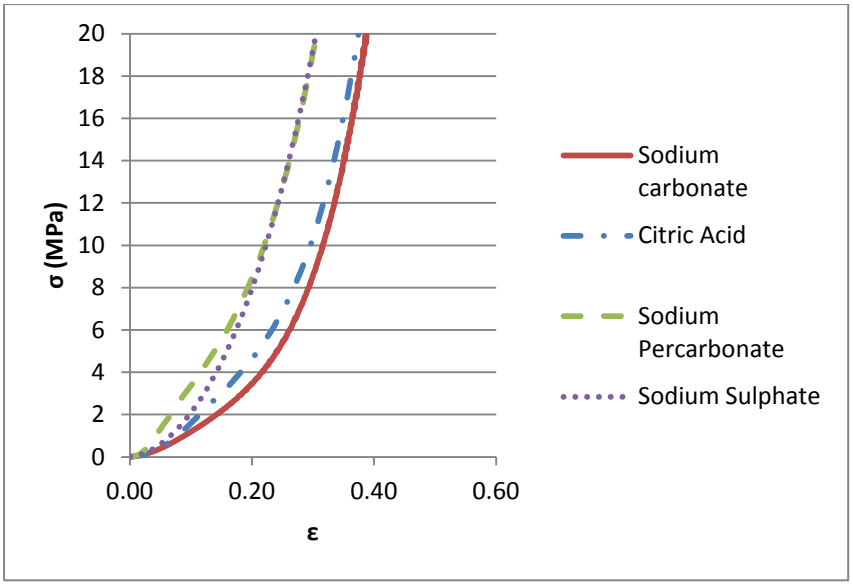
20
18
16
14
12
10
8
6
4
2
0
σ (MPa)
0.00
0.20
0.40
0.60
ε
Sodium carbonate
Citric Acid
Sodium Percarbonate
Sodium Sulphate

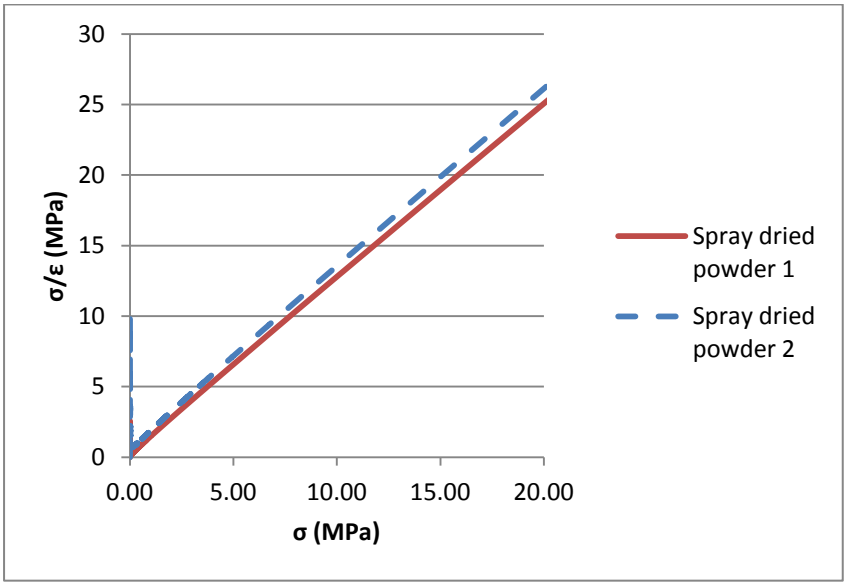
30
25
20
15
10
5
0
σ/ε (MPa)
0.00
5.00
10.00
15.00
20.00
σ (MPa)
Spray dried powder 1
Spray dried powder 2

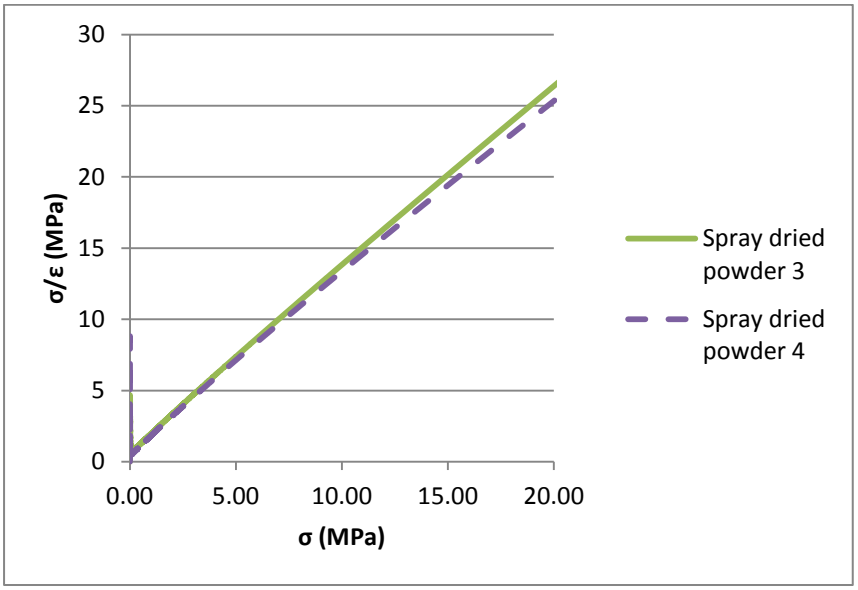
30
25
20
15
10
5
0
σ/ε (MPa)
0.00
5.00
10.00
15.00
20.00
σ (MPa)
Spray dried powder 3
Spray dried powder 4

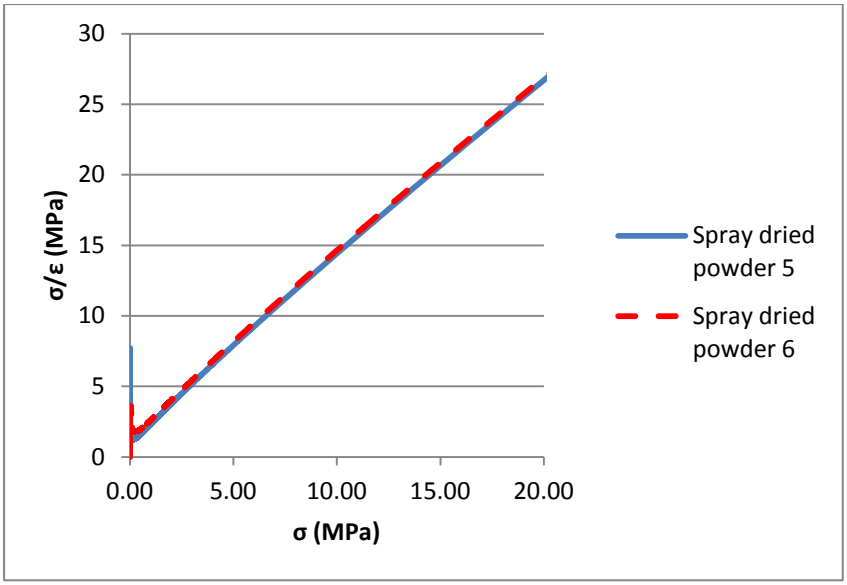
30
25
20
15
10
5
0
σ/ε (MPa)
0.00
5.00
10.00
15.00
20.00
σ (MPa)
Spray dried powder 5
Spray dried powder 6

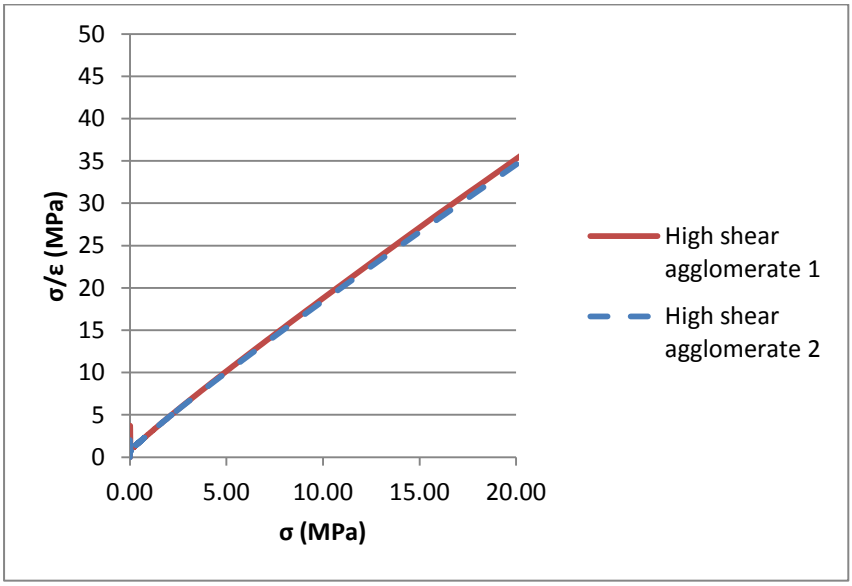
50
45
40
35
30
25
20
15
10
5
0
σ/ε (MPa)
0.00
5.00
10.00
15.00
20.00
σ (MPa)
High shear agglomerate 1
High shear agglomerate 2

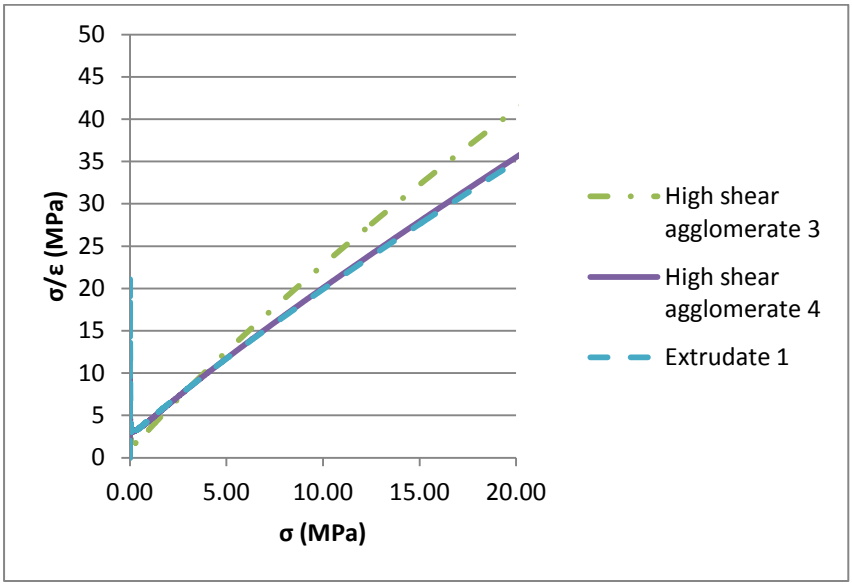
50
45
40
35
30
25
20
15
10
5
0
σ/ε (MPa)
0.00
5.00
10.00
15.00
20.00
σ (MPa)
High shear agglomerate 3
High shear agglomerate 4
Extrudate 1

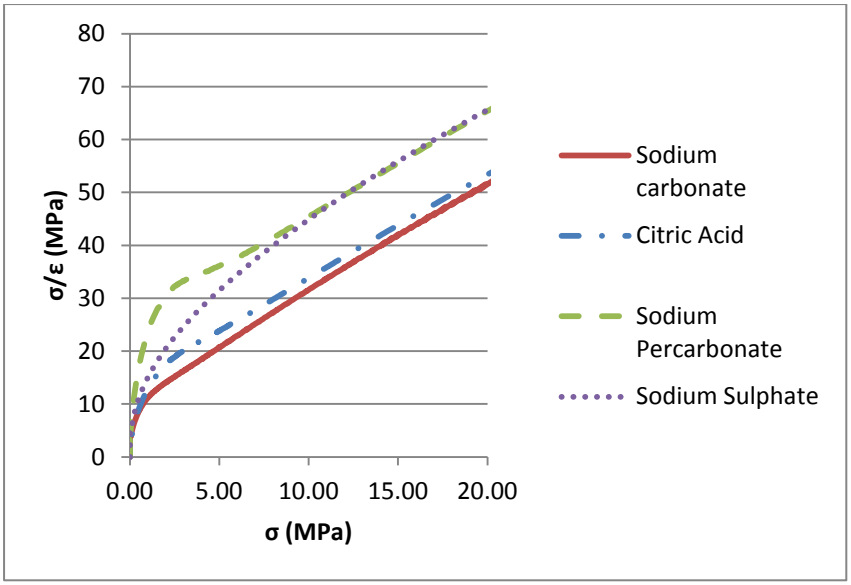

References

1 D. Bajpai, V. K. Tyagi, Laundry detergents: an overview, Journal of Oleo Science, 56, 7 (2007) 327

2 G. J. Hassal, Wall Build-up in Spray Dryers, A thesis submitted to The University of Birmingham UK for the degree of Engineering Doctorate (2011)

3 Coperion K-Tron, Application example: laundry detergent production, Online, Available at: http://www.ktron.com/industries_served/chemical/ (Accessed: 06/08/2013)

4 Mateer Burt Co. Inc., Bespoke P&G 1900 Series Auger Filler, Manual (1995)

5 ALL-FILL International Ltd., FV Weigh Semi 224 V14 Archive Manual – ENGLISH, Manual (2012)

6 R. L. Carr, Evaluating flow properties of solids, Chemical Engineering, 72, 2 (1965) 163

7 L. Scelsi, Personal communication (2012)

8 C. Hewitt, D. Turner, H. Tantawy, W. Caufield, Reapplication of auger redesign, further expanding process operating space, Procter and Gamble, Smart Learning Report (2013)

9 I. Blackmore, M Bradley, A practical guide to rotary valves, Online, Available at: http://www.rotaval.co.uk/40/Technical-Papers/, (Accessed: 29/10/13)

10 M. J. Adams, R. McKeown, Micromechanical analyses of the pressure-volume relationships for powders under confined uniaxial compression, Powder Technology, 88 (1996) 155

11 P. J. Denny, Compaction equations: a comparison of the Heckel and Kawakita equations, Powder Technology, 127 (2002) 162

12 J. Nordström, I. Klevan, G. Alederborn, A particle rearrangement index based on the Kawakita powder compression equation, Journal of Pharmaceutical Sciences, 98, 3 (2009) 1053

13 A. G. Atkins, Y. W. Mai, Review: deformation transitions, Journal of Material Science, 21 (1986) 1093

14 A. Samimi, A. Hassanpour, M. Ghadiri, Single and bulk compressions of soft granules: Experimental study and DEM evaluation, Chemical Engineering Science, 60 (2005) 3993

15 S. F. Yap, M. J. Adams, J. P. K. Seville, Z. Zhang. Single and bulk compression of pharmaceutical excipients: Evaluation of mechanical properties, Powder Technology, 185 (2008) 1

16 E. E. Walker, The properties of powders. Part VI, The compressibility of powders, Transactions of the Faraday Society, 19 (1923) 73

17 R. W. Heckel, Trans. Met. Soc. Density-pressure relationship in powder compaction, Transaction of the Metallurgical Society, AIME, 221 (1961) 671

18 K. Kawakita, K-H. Ludde, Some considerations on powder compression equations, Powder Technology, 4 (1970) 61

19 M. J. Adams, M. A. Mullier, J. P. K. Seville, Agglomerate strength measurement using a uniaxial confined compression test, Powder Technology, 78 (1994) 5

20 R. J. Roberts, R. C. Rowe, The compaction of pharmaceutical and other model materials-a pragmatic approach, Chemical Engineering Science, 42 (1987) 903

21 C. A. Coulomb, Test on the applications of the rules of maxima and minima to some problems of statics related to architecture, Memoirs of Mathematics and Physics, Royal Academy of Sciences, Paris, 7 (1776) 343

22 Auger and Pump Specifier, Auger Fabrication, (2000)

23 M. Watts, Personal communication, (2012)

24 C. Hewitt, D. Smith, A. Ingram, Build-up of powders in auger fillers, 6th International Granulation Workshop, Sheffield, UK, (2013)

25 H. Tantawy, C. Hewitt, A. McGuckin, A. Ashraf Al-Naggar, M. El Askalany, Y. Ali, Lead Site Packing Innovation - Auger redesign and expanding formulation - process operating space, P&G Smart Learning Report (2013)

26 A. P. Green, The plastic yielding of metal junctions due to combined shear and pressure, Journal of the Mechanics and Physics of Solids, 2 (1954) 197

27 W. C. Duncan-Hewitt, Uniaxial compaction modelled using the properties if single crystals, Drug Development and Industrial Pharmacy, 19 (1993) 2197

28 M. Ghadiri, Personal communication (2013)

29 C. C. Crutchley, J. Bridgwater, Particle attrition in small clearances, KONA, 15 (1997) 21

30 G. Calvert, H. Ahmadian, M. Ghadiri, Particle shear and impact (PSI) tester: evaluation of device performance and settings , technical report – covering work done from January to April 2011, Draft 1 – For Comments, Private communication (2011)

31 D. Maugis, H. M. Pollock, Surface forces deformation and adherence at metal microcontacts, Acta Metallurgica, 32, 9 (1984) 1323

32 H. Hertz, Collected works, 1st ed. London: Macmillan (1895)

33 R. S. Bradley, LXXIX. The cohesive force between solid surfaces and the surface energy of solids, The London, Edinburgh and Dublin philosophical magazine and journal of science, 13 (1932) 853

34 R. S. Bradley, The cohesion between smoke particles, Transactions of the Faraday Society, 32 (1936) 1088

35 B. V. Derjaguin, Research on the friction and adhesion, IV, Theory of sticking to smaller particles, Colloid Journal, 69 (1934) 155

36 K. L. Johnson, K. Kendall and A. D. Roberts, Surface energy and the contact of elastic solids, Proceedings of the Royal Society of London, Series A, Mathematical and Physical Sciences 324 (1971) 301

37 D. S. Rimai, L. P. Demejo and R. C. Bowen, Mechanics of particle adhesion, Journal of Adhesion Science and Technology, 8, 11 (1994) 1333

38 B. V. Derjaguin, V. M. Muller and Yu. P. Toporov, Effect of contact deformations on the adhesion of particles, Journal of Colloid Interface Science, 53 (1975) 314

39 D. Tabor, Surface forces and surface interactions, Journal of Colloid Interface Science, 58 (1977) 2

40 V. M. Muller, V. S. Yushchenko and B. V. Derjaguin, On the influence of molecular forces on the deformation of an elastic sphere and its sticking to a rigid plane, Journal of colloid interface science, 77 (1980) 91

41 E. M. Lifshitz, The theory of molecular attraction forces between solids, Soviet Physics, 2, 1 (1956) 73

42 H. Hamaker, The London–van der Waals attraction between spherical particles, Physica 4, 10, (1937) 1058

43 N. K. Myshkin, M. I. Petrokovets, A. V. Kovalev, Tribology of polymers: adhesion, friction, wear, and mass-transfer, Tribology International, 38 (2005) 910

44 D. Dopfer, S. Palzer, S. Heinrich, L. Fries, S. Antonyuk, C Haider, A.D. Salman, Adhesion mechanisms between water soluble particles, Powder Technology, 238 (2013) 35

45 H. Rumpf, K. Sommer, K. Steier, Mechanisms of adhesive force reinforcement in particle adhesion by plastic deformation, sintering and viscoelastic flow, Chemical Engineering and Technology, 48, 4 (1976) 300

46 S. Palzer, Influence of material properties on the agglomeration of water-soluble amorphous particles, Powder Technology, 189 (2009) 318

47 C. Haider, T. Althaus, D. Dopfer, N. Niederreiter, K. Sommer, S. Palzer, Mechanical material properties and their influence on particle deformation and the formation of particle–particle contact points in agglomeration processes, 5th International Granulation Workshop, Lausanne, Switzerland (2011)

48 S. M. Iveson, J. D. Litster, Growth regime map for liquid-bound granules, AIChE Journal, 44 (1998) 1510

49 C. E. Capes, P. V. Danckwerts, Granule formation by the agglomeration of damp powders: Part 1. The mechanism of granule growth, Chemical Engineering Research and Design, 43 (1965) 116

50 C. C. Sun, Decoding powder tabletability: roles of particle adhesion and plasticity, Journal of Adhesion Science and Technology, 25 (2011) 483

51 A. T. Procopio, A. Zavaliangos, J. C. Cunningham, Analysis of the diametrical compression test and the applicability to plastically deforming materials, Journal of Materials Science, 38 (2003) 3629

52 P. A. Webb, Volume and Density Determinations for Particle Technologists (2001) Online, Available at: http://www.particletesting.com/Library/Scientific-Articles.aspx (Accessed: 14/11/13)

53 D. Smith, Personal communication (2010)

54 R. G. Pritchard and E. Islam, Sodium percarbonate between 293 and 100 K, Acta Crystallographica Section B, Structural Science, Crystal Engineering and Materials (2003) 596

55 S. J. Lukasiewicz, J. S. Reed, Character and compaction response of spray-dried agglomerates, American Ceramic Society Bulletin, 57, 9 (1978) 798

56 B. J. Briscoe, S. L. Rough, The effects of wall friction in powder compaction, Colloids and Surfaces, A: Physicochemical and Engineering Aspects 137 (1998) 103

57 J. A. Stewart, Engineering the properties of spray-dried detergent granules, Engineering in the Faculty of Engineering and Physical Sciences. Manchester, University of Manchester, Doctor of Engineering (2008)

58 M. Dodd, Personal communication (2012)

59 D. Smith, Personal communication (2012)

60 P. Sadd, Personal communication (2013)

61 Encyclopaedia Britannica Online, Student's t-test (2015) Online, Available at: http://www.britannica.com/science/Students-t-test (Accessed: 09/10/15)

62 Quadrant Engineering Plastic Products, Ertalyte® TX product data sheet (2011) Online, Available at: http://www.quadrantplastics.com (Accessed: 10/5/2014)

63 M. Hounslow, Personal communication, (2013)